Preparation of Light and Moisture Stable Flexible and Rigid Asymmetrical Polystannanes

by

Jeffrey Pau

BSc, Ryerson University, Toronto, 2015

A dissertation presented to Ryerson University

in partial fulfillment of the requirements for the degree of

Doctor of Philosophy in the program of Molecular Science

Toronto, Ontario, Canada 2020

AUTHOR'S DECLARATION

I hereby declare that I am the sole author of this dissertation. This is a true copy of the dissertation including any required final revisions, as accepted by my examiners.

I authorize Ryerson University to lend this dissertation to other institutions or individuals for the purpose of scholarly research.

I further authorize Ryerson University to reproduce this dissertation by photocopying or by other means, in total or in part, at the request of other institutions or individuals for the purpose of scholarly research.

I understand that my dissertation may be made electronically available to the public.

Preparation of Light and Moisture Stable Flexible and Rigid Asymmetrical Polystannanes

Jeffrey Pau
Doctor of Philosophy – Molecular Science, Ryerson University 2020

ABSTRACT

Theoretical calculations of polystannanes in an all trans-configuration possess a relatively small band gap (~2.8 eV). This is due to the extensive σ-σ overlap of the diffuse 5sp^3 orbitals of Sn atoms in the conjugated Sn-Sn polymer backbone, which leads to a visible σ-σ* transition by UV-vis spectroscopy. The electronic properties of polystannanes suggests that these materials are candidates for semi-conducting intrinsic polymers. However, due to the weak bonding between Sn-Sn atoms and the Lewis acidic nature of Sn centers, polystannanes readily degrade with exposure to daylight and moist atmospheres.

This project demonstrates clear synthetic pathways and designs to stabilize the Sn-Sn backbone. This was accomplished by incorporating functional ligands with Lewis basic heteroatoms such as oxygen or nitrogen moieties which can form a hypercoordinate interaction with the Sn center. Two major types of asymmetrical polystannane systems were investigated: 1) a flexible system where Sn centers are attached to a propyl chain containing either a bulky or small functional donor ligand and 2) a rigid system where the Sn center contain either a hypercoordinate benzyl methoxy ether (*C*,*O*) or benzyl dimethyl amine (*C*,*N*) ligand prepared using a direct approach.

This thesis is broken into three different chapters. Chapter 1 and 3 include all synthetic pathways, characterization and stability testing of both flexible and rigid polystannanes. Chapter 2 describes a high molecular weight (M_w = 60 kDa) film forming, semi-crystalline (T_g = 49.3 °C and T_m = 110.1 °C) flexible asymmetrical polystannane containing a propylhydroxy

ligand that displays exceptional stability to light and moisture (> 9 months). In addition, a tosyl containing polystannane that could function as a macromolecular intermediate was prepared. Substitution of model tosyl stannanes was demonstrated, and substitutions of the tosyl polystannane are ongoing.

ACKNOWLEDGEMENTS

It was a great pleasure to participate in this project and all who made this possible. I gratefully acknowledge Dr. Daniel A. Foucher for his supervision and the opportunity that he gave me to be involved in this project. I also need to thank him for all the valuable discussions and guidance that he has given me. Dr. Daniel A. Foucher has given me great support throughout the entire five years. I am thankful to him in every possible way and wish him all the best in his research, profession and his family.

I would also like to thank Dr. Bryan D. Koivisto and Dr. Russell D. Viirre for their valuable discussions in organic chemistry matters as my committee members for the past four years. I am especially thankful to Dr. Stephen Wylie for his DFT calculations and Dr. Robert Gossage with help editing all the journal articles that were published. I am thankful to the people at the University of Toronto who are instrumental in support of this project, including Dr. Matthew Forbes for mass spectroscopy and Dr. Alan Lough for crystallography.

I would like to extend my thanks to Aman Ullah Khan who was the PhD working in the lab during 2014. Without his teaching and compassion, my laboratory techniques will not be as great as they are today. I must thank everyone that I have met and supervised in KHN202 since 2014. Everyone in different stages have helped me out in many aspects and I am very thankful for their advice and sharing bright thoughts to support me through this journey.

I would like to give a special thanks to Chelsea Cando. It was my pleasure to meet her. We have been through quite a lot together. I wish her always good health and all the best in her future.

Special thanks to my parents, Mary Pau and Ronnie Pau for their support in school and life even though they are back in Hong Kong. Without their support, nothing will work out.

Table of Contents

List of Tables

List of Figures

List of Schemes

List of Abbreviations

Å	Angstrom
C_6D_6	Deuterated benzene
$CDCl_3$	Deuterated chloroform
Da	Daltons
DCM	Dichloromethane
DSC	Differential scanning calorimetry
Et_2O	Diethylether
eV	Electron volts
GPC	Gel permeation chromatography
HCl	Hydrochloric acid
Hex	Hexane
Hz	Hertz
kJ	Kilojoule
n-Bu	*n*-butyl
NMR	Nuclear Magnetic Resonance
Me	Methyl
M_w	Weight average molecular weight
M_n	Number average molecular weight
ppm	Parts per million
T_g	Glass transition temperature
T_m	Polymer Melting Transition Temperature
THF-d_8	Deuterated tetrahydrofuran
σ	Sigma

List of Appendices Figures

INTRODUCTION

1.0.1 Group 14 elements

The elements that comprise Group 14 in the p-block consist of carbon (C), silicon (Si), germanium (Ge), tin (Sn) and lead (Pb). Each of these elements has two electrons in its outermost p orbital: each has the electron configuration ns^2np^2. Group 14 elements tend to adopt oxidation states of (IV) and, for the heavier elements, (II) due to the inert pair effect (tightly bound s electrons).[1,2,3] Despite their adherence to periodic trends, the properties of the carbon family vary greatly. For example, carbon is a non-metal and behaves as such, whereas tin and lead behave entirely as metals. In their elemental solid states, the Group 14 metalloids silicon and germanium act as electrical semiconductors, although silicon is largely non-metallic. Their electrical conductivity can be effectively tuned by introducing traces of Group 13 or Group 15 elements to the Group 14 solid matrix.[4] These semiconductor properties have wide application for circuitry components in the electronics industry, including diodes, transistors, and integrated circuit (ICs) chips.

The dawn of the semiconductor age dates back to the first transistor in 1947-1948 invented by Shockley.[5] The semiconductor industry grew rapidly following the invention of the transistor and after a decade, it already exceeded sales of 100 million dollars (USD). In 1959, the bipolar integrated circuit (ICs) was invented by Kilby of Texas Instruments and Noyce of Fairchild Semiconductor in the US.[5] These ICs were smaller and lighter in weight and could be widely used in a variety of electronic devices, and marked the start of IC era. Due to the ever increasing societal demands, research and development in semiconductor industries grew rapidly during the 1960s to 2000s. New techniques and devices have been developed to upgrade the effectiveness of semiconductors.[5] For example, p-n junctions, two terminal devices (LED, solar cell), and three terminal devices (unijunction transistors) have been established (Figure 1).

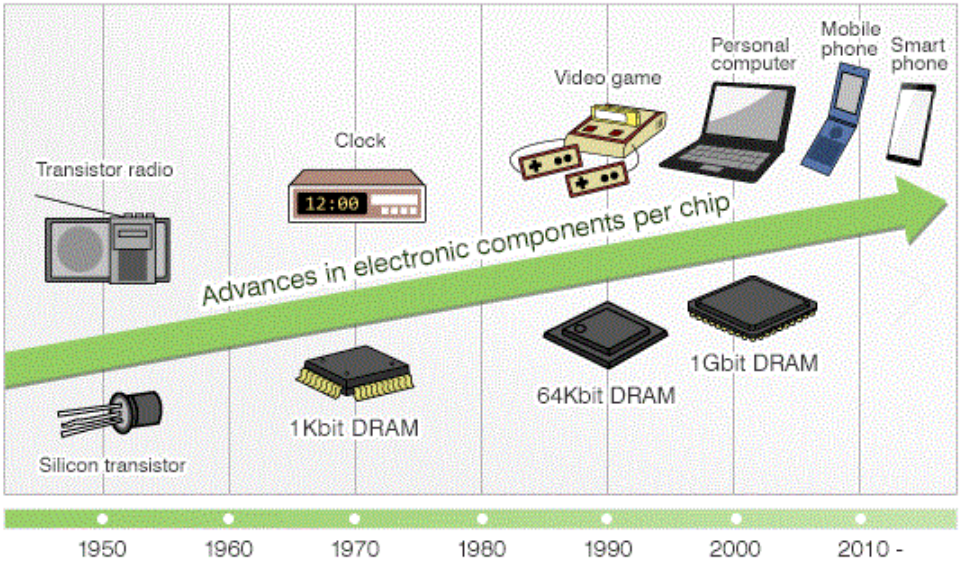

Figure 1. The developments of semiconductor industry from 1950s to 2000s.[6]

Nonetheless, the majority of solid-state semiconductors require extrinsic tuning to amplify their conductive properties. By contrast, conductive polymer wires can either be wholly intrinsic (undoped) or partially doped to a conductive state. Intrinsically conductive polymers (ICPs) were discovered around the mid 20th century during a rapid growth in the semiconductor industry. One of the first ICPs was polyacetylene discovered by Shirakawa in 1970. He demonstrated that polyacetylene possesses different conductivity when in the *cis*- (1.7×10^{-9} S cm^{-1}) and *trans*- (4.4×10^{-5} S cm^{-1}) conformations. Utilizing different reaction conditions afforded control of the morphology of the conjugated polymer, which could be obtained as powder, gel, spongy mass or a film (Scheme 1).[7,8] Doped polyacetylene using molecular halogens enhanced the conduction by 10 orders of magnitude to a value of 10^5 S cm^{-1}. Films can be stretched and processed up to 0.5 cm thickness.[5,9]

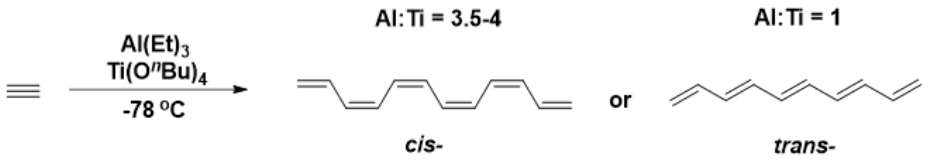

Scheme 1. Controlled reaction condition to make *cis*- or *trans*- polyacetlene.[8]

ICPs possess conductivity similar to that of solid-state semiconductors. One of the advantages of ICPs is that they can be more readily processed than metals. These materials can be transformed into thin orientated films that cover large surfaces with techniques such as a spin-coating or casting of a polymer solution. While many plastics will undergo depolymerisation reactions when exposed to excessive light or heat, these polymers display operating integrity over a wide temperature range and are robust. They possess high elasticity compared to most semiconductors which are brittle.[5] These properties allow ICPs to be shaped into complex, thin multi-polymer architectures and give manufacturers access to printable and bendable electronics.[9,10]

1.0.2 Band Gap Theory – Conductivity: Intrinsic and Extrinsic Semiconductors

Electrons in an isolated atom can only have discrete energy levels (HOMO & LUMO), but when atoms are brought together in the solid-state, these degenerate energy levels will split into many separated levels due to the orbital overlap.[11] Since the levels are so closely separated, they are treated as a continuous band of two different energy states. The lower energy band that is filled with electrons is the valence band and the higher energy band that is unfilled is the conduction band. These two bands are separated by a region of energy that the electrons in the solid cannot hold. This region is the band gap, E_g.[11] Using H_2 as an example, as the number of atoms increases (up to H_{14}), the number of molecular orbitals (both bonding and antibonding) levels increases, but the spread of energies increases slowly and is leveling off for long chains (Figure 2).[11]

Elements with few valence electrons are metallic, whereas those with four or more electrons (e.g. Si, Ge) are expected to adopt a lower coordination structure with a split band where only the lower valence band is filled. This leads to three different types of band gaps – insulator, semi-conductor and metallic conductors (Figure 3).[11,12] For example, a large band gap insulator is diamond, an intermediate band gap semi-conductor is silicon (Si) and low band gap metallic conductor is copper (Cu).

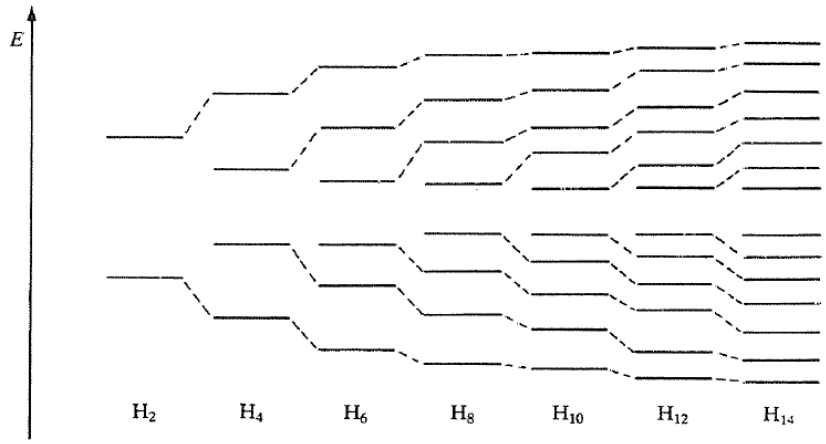

Figure 2. Illustration showing as the number of atoms in the chain increases, the number of molecular orbitals levels also increases.[12]

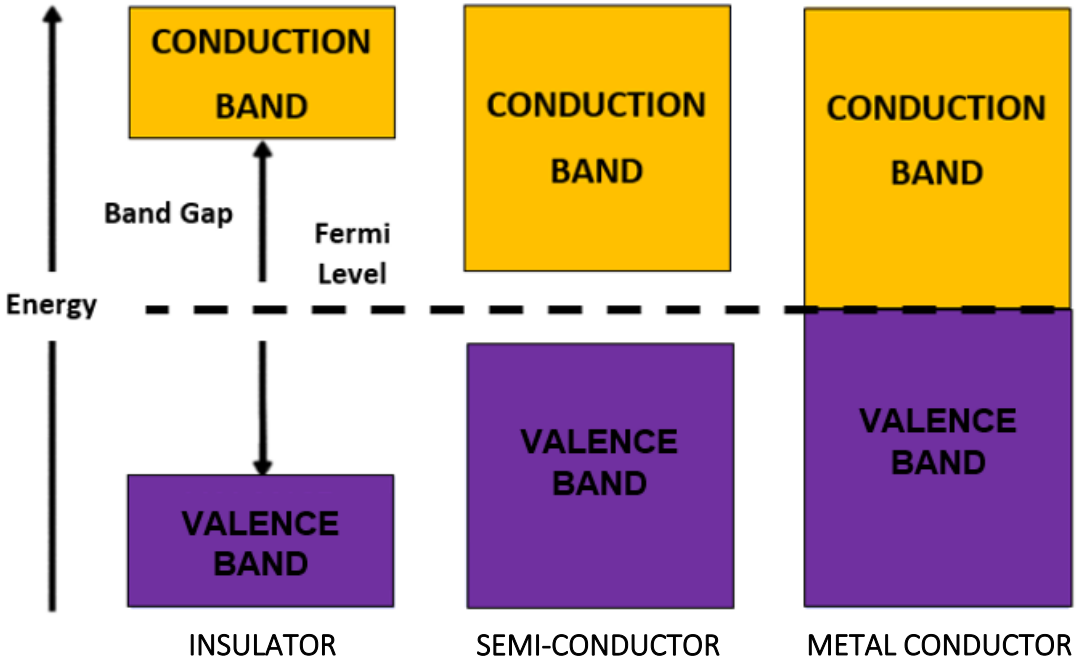

Figure 3. Differences of insulator, semi-conductor and conductor band gaps.

The charge carrying properties of metallic conductors decreases with an increase in temperature. When the temperature rises, the phonons gain energy and the lattice vibrations will be larger.[12] As a result, the displacement of electrons are more scattered, reducing the current by slowing the mobility of the electrons in the lattice.[11,12] By contrast, the conductivity of semi-conductors increases with temperature. Conduction occurs only when electrons are promoted to the conduction band. The resultant current in semiconductors is dependant on the number of available electrons to transport charge (Figure 4).[12]

There are two major types of semi-conductors: intrinsic and extrinsic. An intrinsic semi-conductor is a semi-conductor in its pure state.[12] For every electron that jumps into the conduction band, the missing electron will generate a hole that can move freely in the valence band (Figure 4).[12] The magnitude of the increase in current depends on the band gap and temperature. At any specific temperature, a solid with a small band gap will have more electrons promoted than for a solid with a large band gap. The number of electrons promoted varies exponentially with temperature, so a small change in band gap may have a large effect on the number of electrons promoted and the number of current carriers.[12]

In extrinsic semi-conductors, the band gap is controlled by purposefully adding small impurities to the material in a process known as doping. Doping changes the electrical conductivity and varies the efficiency of the semi-conductor.[12] Unlike intrinsic semi-conductors, the number of holes will not equal the number of electrons displaced. A semi-conductor doped with fewer valence electrons than the bulk is known as a *p*-type, with the fermi level closer to the valence band.[11,12] For example, in a boron doped silicon, the boron center is now electron deficient and gains an electron from the valence band. As a result, electrons in the valence band become mobile. A semi-conductor doped with more valence electrons than the bulk is known as an *n*-type, with the fermi level close to conduction band. Using phosphorus doped silicon as an example, the phosphorus center carries a positive charge. The phosphorus center is now electron rich, and it is willing to give the extra electron into the conduction band (Figure 4). For both cases, the transfer of electron to the bands is how current and conductivity are generated.[12]

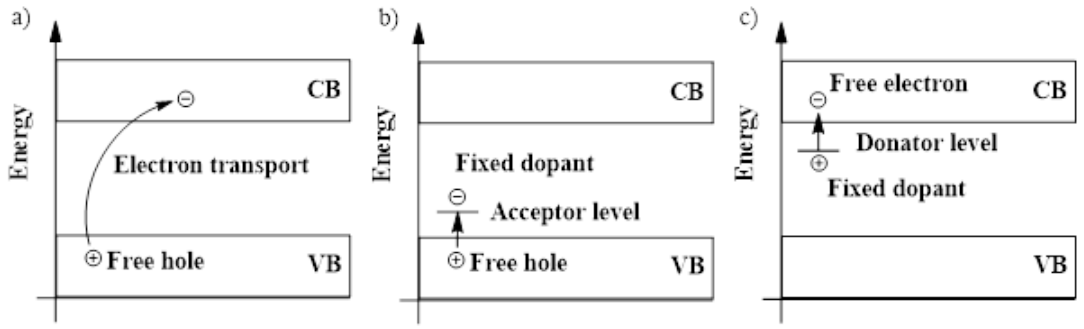

Figure 4. a) Intrinsic semi-conductor b) *p*-type semi-conductor c) *n*-type semi-conductor.

2.0.1 Significance of Group 14 (Sn) & History of Polystannanes

Tin is the chemical element with the symbol "Sn" and atomic number 50. It lies in the 5th period and is located in Group 14 of the periodic table. Elements of Group 14 share an ns^2np^2 valence configuration with the common oxidation states being either (II) or (IV).[13,14,15] Carbon can form multiple bonds with itself or with other elements such as oxygen. The bond energy of a C=C bond is ~ 607 kJ/mol, and consists of both σ- and π-bonds formed through the overlap of sp^2 and 2p orbitals.[15] Carbon double bonds are relatively strong; however, moving down the periodic table, doubly bonded later Group 14 species, E=E dimers (where E = Si, Ge, Sn, Pb) are relatively rare. This leads almost exclusively to singly bonded linear and cyclic material E-E, such as dimers, trimers, oligomers and polymers. These species possess longer bond lengths and as a consequence E-E bonds are considerably weaker than a C-C bond.[15] Moving further down Group 14, stable catenation decreases significantly from carbon to lead. The bonding energy of Si-Si is about 327 kJ/ mol; Ge-Ge (~ 274 kJ/mol) and for Sn-Sn (~ 195 kJ/mol).[16] Tin has three NMR active isotopes (^{115}Sn, ^{117}Sn and ^{119}Sn) each with spin ½. More commonly ^{117}Sn (7.61 %) and ^{119}Sn (8.58 %) nuclei are used for NMR experiments due to their relatively high natural abundance.[6]

The majority of organic and inorganic Sn (IV) compounds possess sp^3 hybridization and adopt a tetrahedral structure, e.g. SnX_4 (Figure 5).[6] The coordination number at tin can be

increased through hybridization to form 5- and 6-coordinated complexes. These hybridized orbitals can accept electrons from ligands to form coordination geometries which are commonly trigonal bipyramidal, square pyramidal or octahedral.[6]

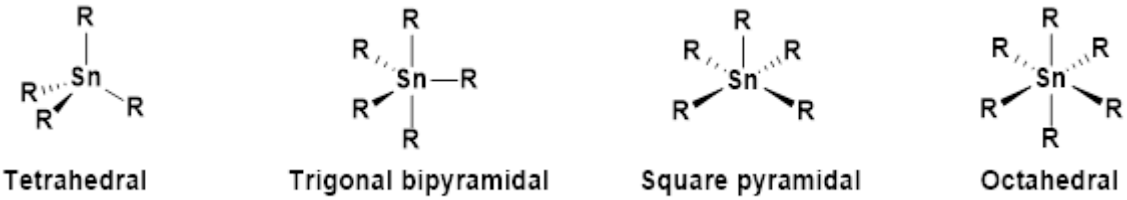

Figure 5. Potential geometry of Sn(IV) compounds.

The bonding chemistry of carbon is of fundamental importance in catenated systems. Polymeric examples of heavier elements of Group 14 have also been discovered during the last 40 years. In the early 1980s, polysilanes with extensive Si-Si bonds were successfully synthesized, giving rise to polymers with unusual electronic and optical properties due to the σ-σ orbital overlap along the silicon backbone.[17,18] The σ-σ* transition in the silicon backbone appears as a strong ultraviolet absorption.[18] Theoretically, the presence of heavier metals in the backbone should lead to greater σ conjugation, a narrower band gap, and more metallic properties. Because of this, interest in tin polymer chemistry arose in the late 1980s to early 1990s. Polystannane materials were successfully prepared using the synthetic approaches previously used for polysilanes and polygermanes (Figure 6) and were estimated to possess a calculated band gap of 2.8 eV.[19] These methodologies included Wurtz coupling, electrochemical coupling, and catalytic dehydropolymerisation. The catalytic dehydropolymerisation of dialkyl and diaryl stannannes was also shown to be a unique way to prepare materials of this type.[14,20] Very recently it was reported that condensation routes to polystannanes involving dialkyltin diamides and dialkyl- or diaryl tin dihydrides could also be utilized.[14]

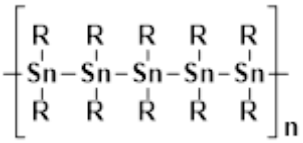

Figure 6. The chemical structure of polystannane (R = alkyl, aryl).

2.0.2 Challenges of Polystannanes

Photostability studies of polystannanes reveal that they readily degrade to smaller oligomers or cyclic species when exposed to daylight (350 – 500 nm).[14,21] Furthermore, upon exposure to moisture in air, polystannanes undergo hydrolysis and break down into smaller stannoxanes.[20]

Polystannanes are thermally stable up to 200 ºC in inert atmosphere as well as in dry air.[22] Polystannanes show sensitivity to the ambient, have greater stability in the solid state than in solution, and suffer a higher rate of degradation under light exposure compared to dark. [22,15] Furthermore, it was found that poly(dialkyl)stannanes degrade immediately upon exposure to light to five- and six-membered cyclic oligostannanes, whereas poly(diaryl)stannanes are stable in the dark in air for at least one week.[14,23] From work carried out by Caesri's group at ETH (Zurich), the degradation trends of poly(dialkyl)stannanes having alkyl side groups of varying lengths in the presence of different solvents and dyes was determined. It was demonstrated that the length of the alkyl side chain has no significant influence on the stability of these polymers.[14,23,24].

The same group later reported that the stability of polystannanes in light is dependent on the nature of the organic side groups.[25] They investigated the degradation behaviour of two polymers, poly[bis(4-butylphenyl)stannane] and poly(dibutyl)stannane under light. While the poly(diaryl)stannanes were found to be more stable towards light than the poly(dialkyl)stannanes in THF as well as in DCM.[25] The degradation mechanism proposed in this study is based on the random homolytic cleavage of Sn-Sn bonds in a polymer chain resulting in two smaller chains terminated with a radical (Figure 7).[25] The two aromatic groups

of the poly(diaryl)stannanes enhance the stability of the Sn-Sn backbone, and the Sn radical were able to "recombine" into a polymer chain more readily, unlike with dialkyl substituents. The recombination of the polystannanes may also be due to the radical delocalization throughout the aromatic ring, which decreases the probability of the radical reacting with polymer chains.[25]

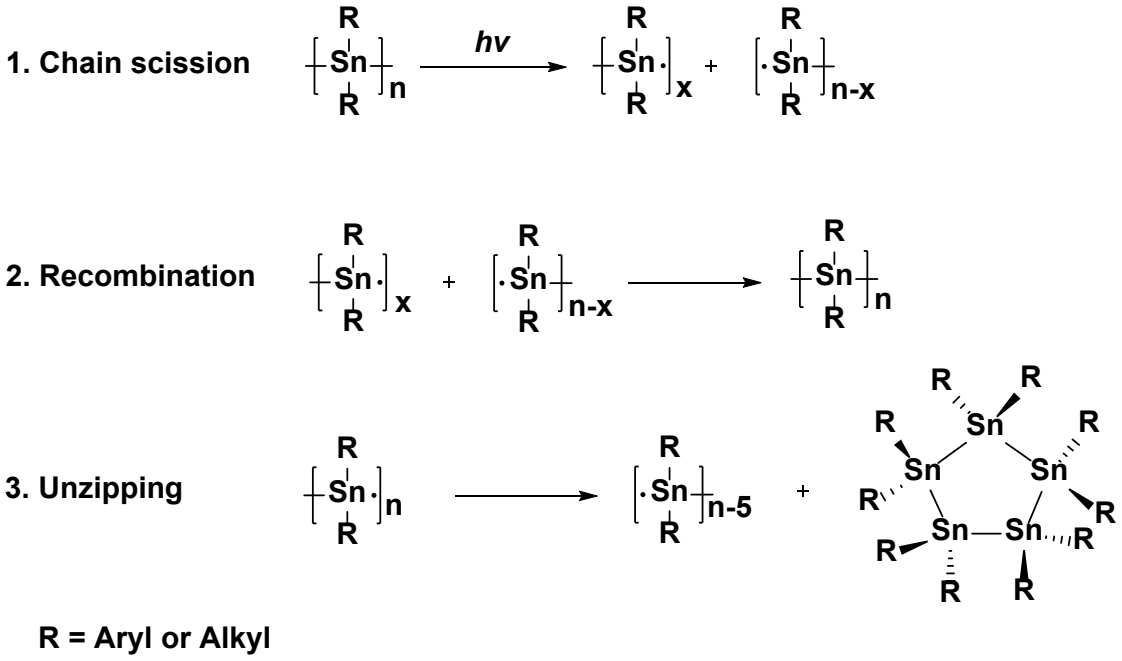

Figure 7. 1) Chain scission under laser flash photolysis 2) Recombination of polystannanes 3) Unzipping of polystannanes.[25]

2.0.3 Hypercoordinate Tin: A Pathway to Stable Polystannanes

In the early 2000s, research interest in Si, Ge and Sn compounds with hypervalent interactions increased extensively.[26] Interest in the coordination chemistry of these elements is caused by additional intra- or intermolecular coordination interactions.[26,27] In the early 1960's it was demonstrated that organotin compounds possess the ability to expand their coordination spheres based on earlier work by Pimental.[28] In 1969, the hypervalent structure was proposed by Musher to explain the structure of main group compounds that require octet expansion of the central atom (SiF_6).[29] The ions or molecules of the elements of Group 14-18 that possess more electrons than the octet within a valence shell are considered hypervalent, such as Ge, Sn, Pb. In the case of Sn, the donor lone pair of Group 14 elements is supplied by an (N, O, P, S)

ligand (Figure 8).[30] The first structurally characterized pentacoordinate organotin compound was a $PyMe_3SnCl$ in 1960s.[29] 5- and 6-coordinated Ge, Sn and Pb compounds have been extensively studied and have been shown to be more stable than their tetrahedral counter parts.[29-31]

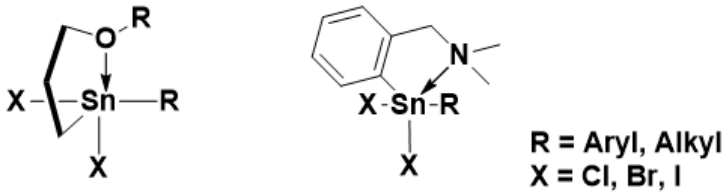

Figure 8. Examples of two different hypercoordinated Sn compounds.

2.0.4 3-center-4 Electron Concept

Prior to the 1950s, the hypervalent bonding was explained in terms of *d*-orbitals participation.[28] For Group 14, especially the lower table elements such as Ge or Sn, the *s* and *p* atomic orbitals are fully filled, therefore, the only "empty" orbital would be the 5*d*-orbitals ($5p^2$ for Sn). Two electronic configurations are envisioned to hold additional electrons that exceed the octet within the valence shell; dsp^3 or d^2sp^3.[28,32] Sn has five empty 5*d* which could participate in the formation of penta- and hexacoordinate structures. However, computational studies have shown that the *d* electron of Group 14 atoms (Ge, Sn and Pb) are too diffuse and too high in energy to participate in bonding.[32]

In 1951 Pimentel proposed the idea of a 3c-4e$^-$ bond using molecular orbital theory to describe hypervalent interactions. A simple description of the 3c-4e$^-$ bond model is the delocalization of one pair of bonding electrons to the two other substituents.[28] The 3c-4e$^-$ model suggests that ns^2 orbitals of metal atom could be used for bonding to equatorial ligands resulting in two-center bonds, while the np_z orbital could interact with an appropriate orbital of the axial ligands and a lone pair from the donor atom to form a hypervalent, 3c-4e$^-$ bond.[28]

In later years, progress in studies employing a 3c-4e$^-$ model has been confirmed by development in computational studies and quantum physics.[33] The hypervalent bonding of

molecules has also been investigated by von Schleyer *et. al*. who stated that the *d*-orbital concept is incorrect, and these orbitals are not important in the acceptance of electrons beyond the octet.[32] It has been determined that it is not possible for the *d* orbitals to hold extra electron density because of the high energy gap between n(*sp*) and n*d,* which makes the number of available metal orbitals deficient.[32]

From theoretical calculations, it has been established that for main group elements such as S and P, participation of *d* orbitals for hybridization with *s* and *p* orbitals of third period and heavier is negligible.[34,35,36] Therefore, a 3c-4e$^-$ bond is an electron-rich bond and the non-bonding molecular orbital becomes the highest occupied orbital.[36] In the 3c-4e$^-$ bond, the central atom has less than four pairs of electrons in the valence shell and does not exceed the Lewis octet due to the distribution of extra electron density on to ligands or substituents.[35]

Y.S. Cheung *et. al*.[35] and Sun and coworkers[36] stated that in contrast to a conventional valence-bond in which a bonding electron pair is shared by two atomic centers, a three-center bond results from bonding between three atomic centers, each of which contribute an orbital. A three-center bond may be formed from a *p*-orbital of the central atom and two ligand orbitals. For example, the two terminal ligands (X = F) and the central atom (A). The *p*-orbital of each F atom is directed along the bonding axis and is available for bonding with the *p*-orbital of the central atom along the same axis.[35,36]

From the viewpoint of molecular orbital theory, there will be three *p*-orbitals (bonding (σ) non-bonding (*n*) and antibonding (σ*)). A 3c-4e$^-$ bond occurs when four electrons fill the bonding (σ) and non-bonding (*n*) molecular orbitals (requires only three orbitals) (Figure 9). Compared to 3c-2e$^-$ bonds (e.g. B_2H_6), 3c-4e$^-$ bonding requires four orbitals (two from the central atom and one each from the two ligands) to bind the three centers and to accommodate the four electrons (two from the central atom and one from each ligand).[35]

The formation of a 3c-4e$^-$ bond saves an atomic orbital for this kind of 'orbital deficient' molecule, compared to 3c-2e$^-$ bond which is 'electron-deficient'. There are two important

features of 3c-4e$^-$ interactions: the first is that one σ-bonding electron pair is shared between two A-X bonds, and the second is that the A-X bonds are weaker (elongated). Another property is that, of the four available electrons, only two are shared by the central atom and the two ligands, with the remaining electrons located in the *n*-orbital.[35]

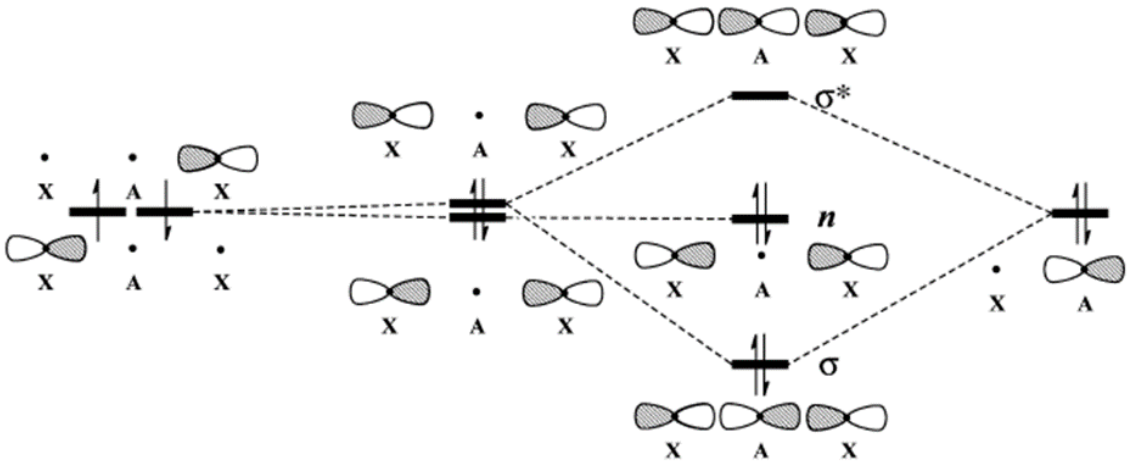

Figure 9. The M.O. diagram of 3c-4e$^-$ bond (bonding (σ), non-bonding (*n*) and anti-bonding (σ*). A *p*-orbital of the central atom A is used. The 3c-4e$^-$ bond consists of two electrons in the σ-orbital and two electrons in the n-orbital which categories the three centers. Adapted from reference 36.

3.0.1 Methods to Synthesize Polystannanes

Various reaction conditions can be applied to obtain tin polymers of specific structure and properties. Synthetic methodologies applied to polystannanes include Wurtz coupling, dehydropolymerisation[24] and more recently, condensation polymerisation.[20]

3.0.2 Catalytic Dehydrogenation

Polystannanes are readily synthesized by catalytic dehydrocoupling of alkyl or aryl tin dihydrides. Harrod *et al*.[37,38] had earlier reported the catalytic dehydrocoupling of silanes ($PhSiH_3$) and germanes ($PhGeH_3$) to oligosilanes and oligogermanes facilitated by Group IV metallocene (M = Ti, Zr) catalysts (Cp_2MR_2 (Cp = η^5-C_5H_5)). By contrast, transition metal complexes of Ti, Zr, Hf, Cr, Mo, W, Rh, Pt have been employed as catalysts for the dehydropolymerisation of primary and secondary stannanes.[37] Dehydropolymerisation has been demonstrated to be the most successful technique to achieve high molecular weight

polystannanes. Dehydrogenative coupling utilizes a suitable early or late transition metal catalyst to aid the removal of hydrogen from dihydrostannane monomers (Figure 10).

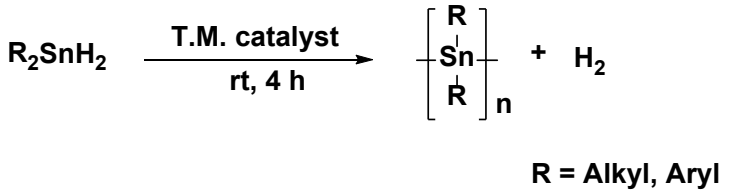

Figure 10. Synthesis of polystannanes *via* catalytic dehydrocoupling.

Dialkyl titanocene (Cp_2TiR_2, R = alkyl), zirconocene (Cp_2ZrR_2, R = alkyl), and Wilkinson's catalyst ($RhCl(PPh_3)_3$) are typical catalysts used for this reaction.[15] Wilkinson's catalyst is most suitable for the polymerisation of symmetrical dialkyl and asymmetrical aryl/alkyl dihydrides as it has been shown to give linear polystannanes with high molecular weights and in high yields.[39] An additional benefit observed with this catalyst is that there are no detectable amounts of cyclic by-products that must be isolated.[39]

3.0.3 Condensation Polymerisation

The Foucher group recently described the synthesis of alternating polystannanes using a condensation polymerisation route.[20,40] High purity tin dihydrides derivatives were stoichiometrically reacted with tin diamides (possibly with different or same R groups) in dry toluene or Et_2O at 0 °C for optimal polymerisation (Figure 11). This condensation method produces volatile diethyl amine, which can easily be removed under reduced pressure.[20,40]

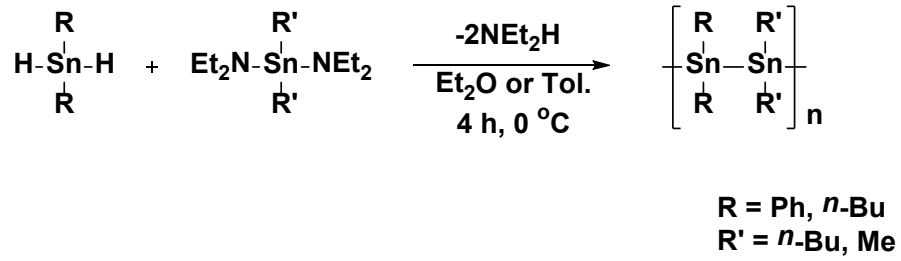

Figure 11. Preparation of alternating polystannanes.

3.0.4 Wurtz Coupling Polymerisation

Wurtz coupling was first used to form a C-C bond from the reaction of alkyl halides with Na metal. In later years, Kipping showed that Wurtz coupling can be used for preparation of materials having only organosilicon units in the backbone.[41] Wurtz coupling reactions involve dichlorodiorganosilane reacting with excess of a Na dispersion in a high-boiling-point solvent such as toluene or THF under reflux were first demonstrated by West and Miller in 1983.[42] In 1992, Zou *et. al*. reported the first synthesis of high molecular weight poly(di-*n*-butylstannane) (~10^4 Da) using a Wurtz-type coupling of (n-Bu)$_2$SnCl$_2$ in toluene/heptane in the presence of 15-crown-5.[20] In 1996, Molloy and coworkers identified the best reaction conditions using toluene as the reaction solvent (Figure 12) and achieved the $M_w > 1\times10^6$ Da.[43]

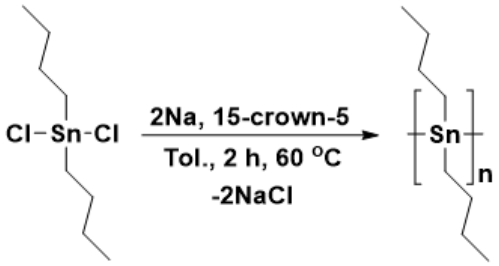

Figure 12. Wurtz coupling of (n-Bu)$_2$SnCl$_2$ done by Molloy and coworkers.[43]

In 2011, Caseri *et. al*. reported the polymerisation of dichlorodiorganostannanes with Na in 1:2 ratio in liquid NH$_3$.[44] These reaction conditions afforded the polymerisation of (n-Bu)$_2$SnCl$_2$ and (n-Oct)$_2$SnCl$_2$ to yield low molecular weight polystannanes having $M_w = 8.0 \times 10^3$ and $M_w = 6.0 \times 10^3$ Da, respectively. In general, there are several disadvantages of the Wurtz synthetic method; it has limited tolerance to functional groups, the yields are moderate, the reproducibility is poor, and it is dangerous due to the pyrophoric nature of Na metal and harsh reaction conditions.[45,46,47]

Objectives

The primary objective of this thesis was to develop film forming light and moisture stable polystannanes from select hypercoordinated monomers with and without the aid of a chromophore.

The following synthetic targets and objectives are as follows:

Chapter 1:

i) To develop new flexible hypercoordinated light and moisture stable polystannanes using azobenzene as chromophore. The hypothesis is that hypercoordinated polystannanes bearing chromophore are more stable than non-hypercoordinate polystannanes.

Chapter 2:

ii) Investigate smaller hypercoordinated flexible motifs as suitable monomers for polymers with improved stability. It is anticipated that more strongly datively bound ligands will further improve the stability of polystannanes.

Chapter 3:

iii) Explore the chemistry and stability of two different *C,O* and *C,N* rigid chelated light and moisture stable polystannanes and investigate their properties.

Special Notes

The following thesis will be broken into three research chapters. All experiments described in this thesis were performed by myself, apart from the crystallography analysis and DFT calculations, which were performed by Dr. Alan Lough from University of Toronto and Dr. Stephen Wylie from Ryerson University, respectively. Chapter 1 involves work where a chromophore (azobenzene) was used to photochemically and sterically stabilize the Sn-Sn polymer backbone. The polymerisation involved two different synthetic routes (dehydrogenation catalytic and condensation). This work was published in 2017. Pau, J.; Lough, A. J.; Wylie, R. S.; Gossage, R. A.; Foucher, D. A. Proof of Concept Studies Directed Towards Designed Molecular Wires: Property-Driven Synthesis of Air and Moisture-Stable Polystannanes. *Chem. Eur. J.* **2017**, *23*, 14367–14374.

Chapter 2 involved additional work on hypercoordinated polystannnanes where two interesting small tin dichloride precursors were synthesized and one was converted into a light and moisture stable polystannane. This work was supported by an undergraduate thesis student, Gloria D'Amaral, in the 2017-2018 academic year. One of the two polystannanes (R group = propyl hydroxide) showed a sharp T_m suggesting a semi-crystalline packing of the polymer chains. The sharp T_m polymer was also characterized by PXRD which showed evidence of crystalline order. This work was published in 2018, Pau, J.; D'Amaral, G. M.; Lough, A. J.; Wylie, R. S.; Foucher, D. A. Synthesis and Characterization of Readily Modified Poly(Aryl)(Alkoxy)Stannanes by Use of Hypercoordinated Sn Monomers. *Chem. Eur. J.* **2018**, *24*, 18762–18771.

This work continued into 2019 with other functional polystannanes (R = propyl OTs) which have been show to be substitutionally labile under simple S_N2 reaction conditions. Trials were carried out by myself and an undergraduate thesis student David Choi during the 2018-2019 academic year. Work is still on going in this area and is being drafted into an additional manuscript.

Chapter 3 focused on completing unfinished work on rigid *C,O* and *C,N* based chelated stannyl complexes. Work was shared with MSc graduate Julie Loungxay. My involvement was to prepare rigid tin monomers and carry out their polymerisations and subsequent characterizations. The work titled "Hypercoordinated Organotin (IV) Compounds Containing *C,O*- and *C,N*- Chelating Ligands: Synthesis, Characterizations, DFT Studies and Polymerization Behaviour" *J. Organomet. Chem.*, 900, 120910- is not in press

CHAPTER 1 - Proof of Concept Studies Directed Towards Designed Molecular Wires: Property-Driven Synthesis of Air and Moisture-Stable Polystannanes

Abstract

Polystannanes with azobenzene moieties designed to protect the Sn–Sn backbone from light and moisture-induced degradation are described. The azo-stannyl precursor **3** (70 %) is converted in good yields (88–91 %) to the mono- (**4**), and dichlorostannanes (**5**), by sequential chlorination, followed by further reduction of **5** to the dihydride (**6**) using $NaBH_4$ (78 %). All stannanes were characterised by NMR (^1H, ^{13}C, ^{119}Sn) spectroscopy and HRMS; in addition, **3**, **4** and **5** were structurally elucidated using X-ray diffraction analysis. Metal-free dehydrocoupling of **6** at RT leads exclusively to homopolymer (**7-i**) displaying an initial solution ^{119}Sn NMR signal (δ = -196 ppm) that migrates to δ = -235 ppm after 10 days (**7-f**). In contrast, metal-catalyzed dehydrocoupling of **6** in toluene at RT leads directly **7-f**. Random copolymers formed from **6** and $(n\text{-Bu})_2SnH_2$ at 4:1 (**8a**) and 1:1 (**8b**) ratios were compared to the alternating polystannane (**9**) prepared by the reaction of **6** with $(n\text{-Bu})_2Sn(NEt_2)_2$. DFT calculations of **3**–**6** indicate that hypercoordination at Sn is influenced by substituents and by solvation. Homopolymer **7** was found to have unprecedented moisture and light stability in the solid state for >6 months.

Introduction

1.0.1 Organic Chromophore Ligands

Recently, considerable research has been undertaken on different types of fluorescent or phosphorescent chromophore molecules owing to their utility for a number of applications including use of DSSCs, cosmetics and industrial dyes.[48] A chromophore is the functional part of a molecule responsible for its colour and is comprised of three components; donor, linker and acceptor.[49] When a molecule absorbs certain wavelengths of visible light (350 – 750 nm) and transmits or reflects others, colour results.[49] Chromophore properties arise where the energy difference between two different molecular orbitals falls within the range of the visible

spectrum. The visible light that hits the chromophore can then be absorbed by exciting an electron from its ground state into an excited state.[48] Our interest in this area involves the preparation of polystannanes bearing light absorbing azobenzene molecules. Polystannanes that incorporate this type of chromophore have the potential to be light stable and structurally resistant to nucleophilic attack and possess switchable properties.

1.0.2 Characteristics of Azobenzene

Azobenzene, first discovered in 1834,[50] is isolated as orange-red crystals with a low melting point (69 °C). It is a chromophore composed of two phenyl rings linked by an N=N double bond and are considered derivatives of diazene.[51] Diazenes absorb light strongly and are used as dyes in a variety of industries (Figure 13).[51]

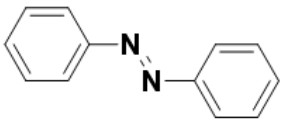

Figure 13. The chemical structure of azobenzene.

One of the most significant properties of azobenzene is the mechanism of the photo-isomerization involving *trans*- and *cis*-isomers.[50,52] The two isomers can be switched with exposure to particular wavelengths of light. With exposure to ultraviolet light (~ 320 nm), a *trans*- to *cis*- isomerization occurs. Absorption bands equivalent to the $S_0 \rightarrow S_2$ state are observed, corresponding to the energy gap of the π-π* symmetry-allowed transition. In a similar fashion, exposure to visible light (~ 440 nm), causes a *cis*- to *trans*- conversion and absorption bands equivalent to the $S_0 \rightarrow S_1$ state are observed, corresponding to the energy gap of the n-π* symmetry-forbidden transition (Figure 14).[50,51,52] Due to steric effects, the *cis*-isomer is considerably less stable than the *trans*; in addition, the *cis*-azobenzene can thermally relax back to the *trans*-isomer (Figure 15).

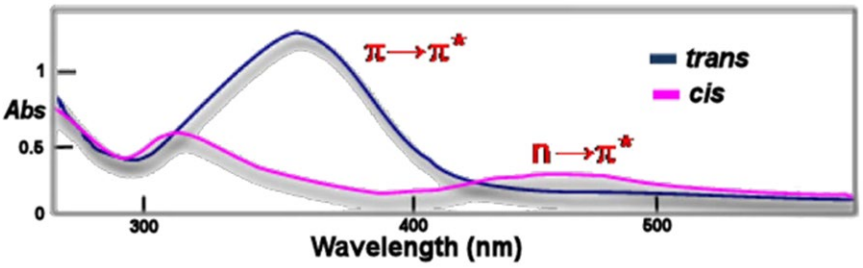

Figure 14. UV-Vis spectrum of an azobenzene.[50]

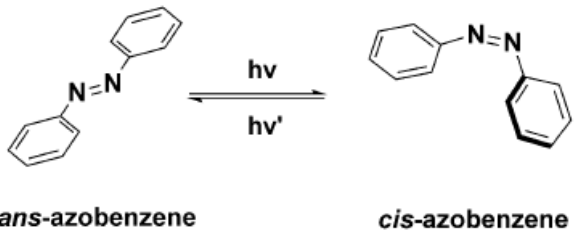

Figure 15. The light-induced *trans*-/*cis*- (*E*/*Z*) isomerisation of azobenzene.

Azobenzene can absorb the wavelength of the two lowest energies, n-π* and π-π* , which lie in the UV-Vis region (Figure 16).[50,53] As a rule, energetically favoured electron promotion will be from the highest occupied molecular orbital (HOMO) to the lowest unoccupied molecular orbital (LUMO), and the resulting species is in an excited state.[53]

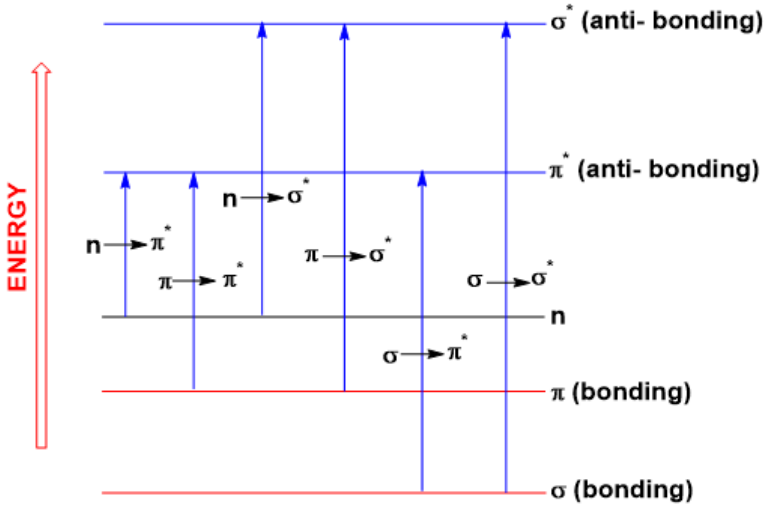

Figure 16. The different electronic transitions present in azobenzene.[50]

When azobenzene is exposed to light having an energy that matches a possible electronic transition within the molecule, some of the light energy will be absorbed by the azobenzene as the electron is promoted to a higher energy orbital.

Results & Discussion

1.1.1 Synthesis of Monomeric Tin Precursors and Dihydrides

Following procedures by Wardell *et. al*., stannyl compound **1** was synthesized using triphenyl tin hydride, allyl alcohol along with 0.2 mole % of AIBN (Scheme 2).[54] Reaction was achieve in a near quantitative yield (99 %).

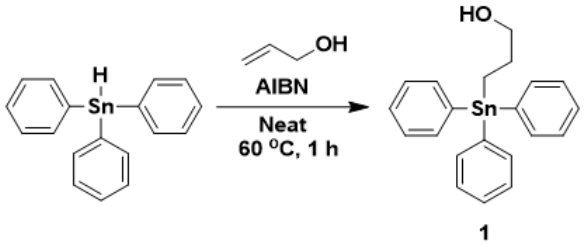

Scheme 2. Preparation of stannyl compound **1**.

Tosylation of **1** to **2** can be demonstrated (60 %) in a 2 h time frame using Yoshida's procedure (Scheme 3), in which a catalytic amount of the ammonium salt, $Me_3N{\cdot}HCl$, along with NEt_3, are added to the reaction mixture.[55] Traditional tosylation using pyridine does not work for this system. Typically, tosylation of alcohols is a well-recognized fundamental transformation. However, these tosylation reactions suffer some major problems, including an unwanted side reaction where the loss of tosylates into their chlorides occurs. The by-product will act as the poorer Cl^- nucleophile, resulting in low yield. Additionally, tosylation usually requires relatively long reaction times (~10 h) (Figure 17).[55] By adding the amine salt catalyst, the reaction time was greatly reduced. The purifying process outlined in Yoshida's paper is simple and involves an extraction with DCM/water to remove impurities to yield a pure product.[55]

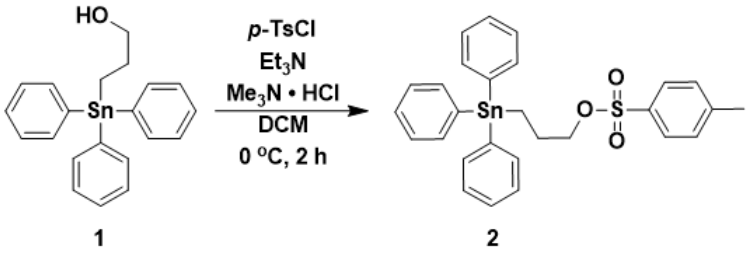

Scheme 3. The preparation of compound **2**.

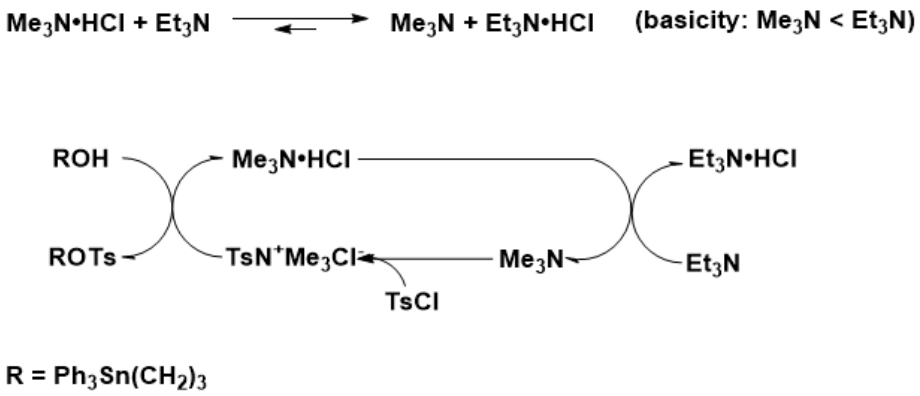

Figure 17. The proposed mechanistic cycle by Yoshida *et*. *al*. using $Me_3N{\cdot}HCl$.[55]

Initial attempts to prepare **3** substitution of 4-hydroxyazobenzene with allyl bromide, followed by hydrostannylation with Ph_3SnH, were not successful. However, the synthesis of **3** can be achieved by reacting 4-hydroxyazobenzene with **2** under S_N2 conditions (Scheme 4).[18] This process results in recovery, after column chromatography, of an air and moisture stable orange solid **3** (~70 %).

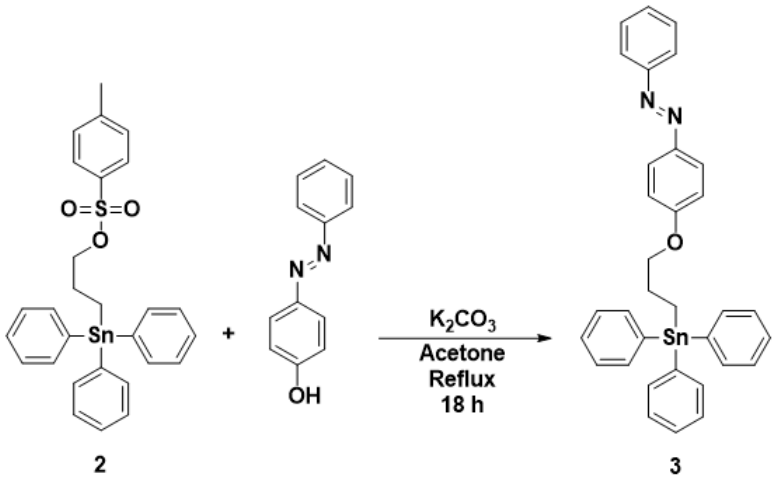

Scheme 4. S_N2 displacement reaction leading to **3**.

Compound **3** was then converted through stepwise chlorination (Scheme 4) to the mono- **4**, and dichlorostannanes **5** in good yields (88 % and 91 %, respectively) without the need for column chromatography.[56] Following conditions traditionally used to obtain tin dihydrides, **5** was reacted with $LiAlH_4$ (Et_2O: 0 °C; 3 h) unsuccessfully. When the more moderate hydrogenating agent $NaBH_4$ was used, **5** was cleanly converted to **6** (78 %) which was isolated as an orange–yellow coloured powder (Scheme 5).

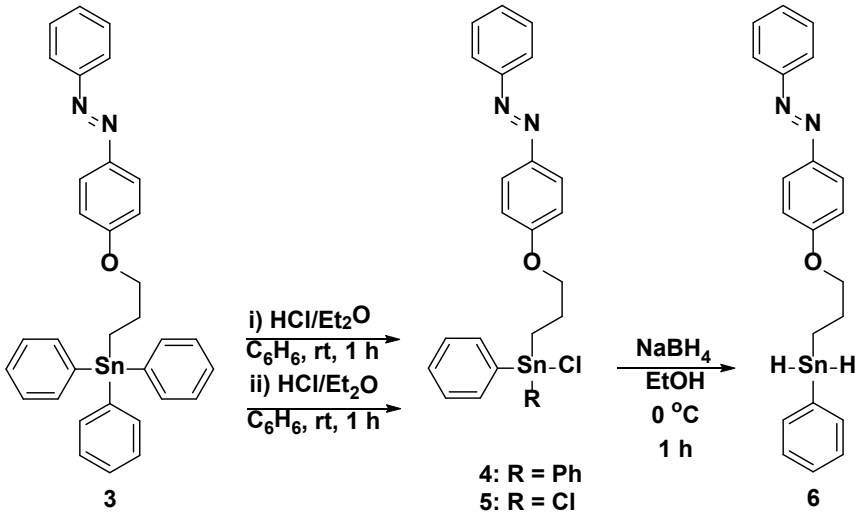

Scheme 5. Stepwise chlorination of **3** to **4** and **5**, and hydrogenation to **6**.

1.2.1 NMR Characterizations of Monomeric Tin Precursors and Dihydrides

The ^1H NMR ($CDCl_3$) spectra of **3**–**6** display three distinct sets of methylene resonances with large $^{119/117}Sn–H$ coupling constants (*J*) observed for the C*H*$_2$–Sn resonance (Table 1). The Sn–H resonance signal of **6** is observed at 5.51 ppm, with distinct $^{119/117}Sn$ satellites ($^1J_{119Sn–1H}$ = 918 Hz, $^1J_{117Sn–1H}$ = 878 Hz). The methylene protons in **6** are shifted upfield in comparison to **3** and the chloro-containing stannanes **4** and **5**. The ^{119}Sn NMR resonances for **4** and **5** are significantly deshielded (δ = -15.3 ppm and δ = -9.06 ppm, respectively). These downfield resonances are more consistent with a 5-coordinate geometry for both **4** and **5** in solution.[57] The ^{119}Sn NMR resonance for **3** is found at δ = -100 ppm, a value typical of tetrahedrally coordinated organotins.[18]

Table 1. Selected NMR data for stannyl compounds **3-6**.

Compounds	^{1}H NMR (ppm) (C*H*$_2$-O)	^{119}Sn NMR (ppm)
3*	4.03	-99.7
4*	4.14	-15.3
5*	4.22	-9.06
6**	3.46	-214.5
*$CDCl_3$, **C_6D_6		

1.3.1 Single Crystal X-ray Analysis of Monomeric Tin Precursors

The tin atoms of both conformers observed in the solid-state of **3** are pseudo-tetrahedral (τ_4 = 0.85, $\tau_{4'}$ = 0.87) with a Sn to O distance of ~4.9 Å, which lies well outside of the sum of the van der Waals radii (O···Sn = 2.3 Å) (Figure 18). On the other hand, **4** and **5** are formally 5-coordinate (**4**: τ_5 = 0.85, **5**: τ_5 = 0.46) and possess O···Sn distances of 2.775 Å and 2.729 Å respectively, in line with other 5-coordinate Sn species that have a dative oxygen interaction (Figures 19 and Figure 20).

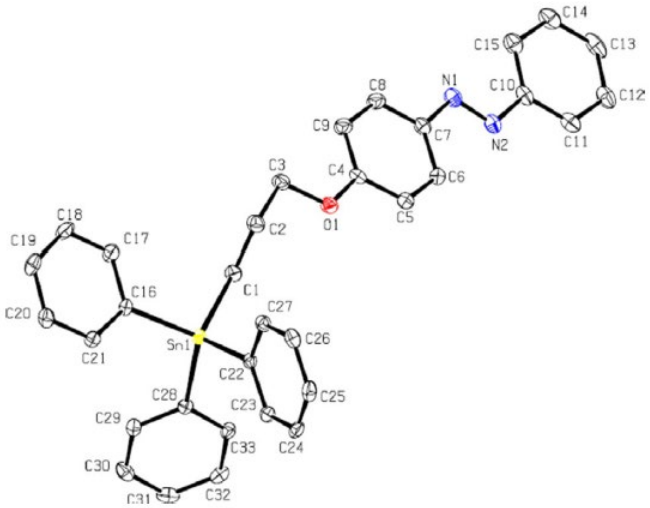

Figure 18. ORTEP representation of one of the conformers of **3** found in the unit cell. Thermal ellipsoids drawn at the 30% level. Selected interatomic distances [Å] and angles [°]: Sn(1)-C(16) 2.136(3), Sn(1)-C(22) 2.137(3), Sn(1)-C(28) 2.131(3), Sn(1)-C(1) 2.147(3), C(28)-Sn(1)-C(16) 112.06(11), C(28)-Sn(1)-C(22) 107.98(11), C(16)-Sn(1)-C(22) 106.58(12), C(28)-Sn(1)-C(1)109.26(12), C(16)-Sn(1)-C(1) 108.00(12), C(22)-Sn(1)-C(1) 113.01(12).

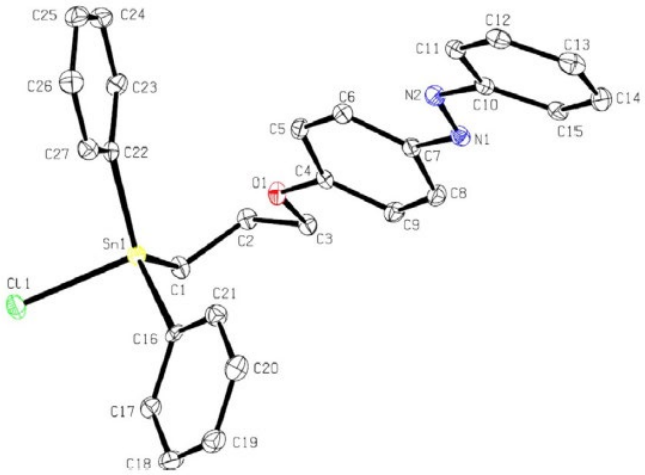

Figure 19. ORTEP representation of **4** found in the unit cell. Thermal ellipsoids drawn at the 30% level. Selected interatomic distances [Å] and angles [°]: Sn(1)-C(16) 2.155(3), Sn(1)-C(22) 2.126(3), Sn(1)-Cl(1) 2.4099(8), Sn(1)-C(1) 2.137(3), C(22)-Sn(1)-C(1) 124.05(14), C(22)-Sn(1)-C(16) 111.35(12), C(1)-Sn(1)-C(16) 116.35(13), C(22)-Sn(1)-Cl(1) 102.43(8), C(1)-Sn(1)-Cl(1) 97.67(9), C(16)-Sn(1)-Cl(1) 98.71(9).

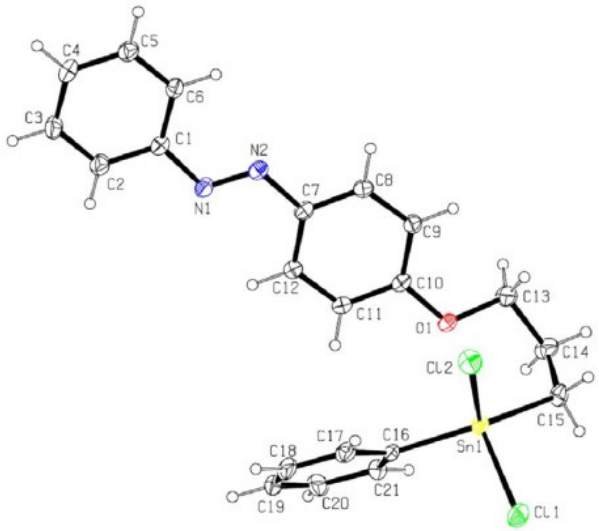

Figure 20. ORTEP representation of **5** found in the unit cell. Thermal ellipsoids drawn at the 30% level. Selected interatomic distances [Å] and angles [°]: Sn(1)-C(16) 2.109(3), Sn(1)-C(15) 2.120(3), Sn(1)-Cl(1) 2.3917(8), Sn(1)-Cl(2) 2.3469(7), C(15)-Sn(1)-Cl(1) 101.40(9), C(15)-Sn(1)-Cl(2) 106.93(9), C(16)-Sn(1)-Cl(2) 107.04(7), C(16)-Sn(1)-Cl(1) 101.48(7).

1.4.1 Polymerisations

Metal-free dehydrocoupling of **6** (Scheme 6) to polymer **7-i** was observed over a 10-day timeframe. A C_6D_6 solution of **6** in a Teflon sealed NMR tube protected from ambient light sources was monitored by NMR (^{1}H and ^{119}Sn) spectroscopy. Physical changes were observed, and these changes thus characterized (NMR). The transparent orange colour characteristic of **6**

in C_6D_6 was noticeably darkened, along with the precipitate from the solution, after 24 h. After 6 d, the colour of the observed semi-solid material changed from a dark yellow orange to a bright yellow colour (Figure 21).

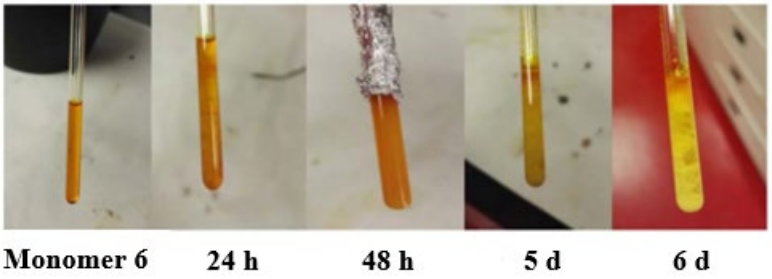

Figure 21. Physical changes of polymer **7-i** (metal-free polymerisation).

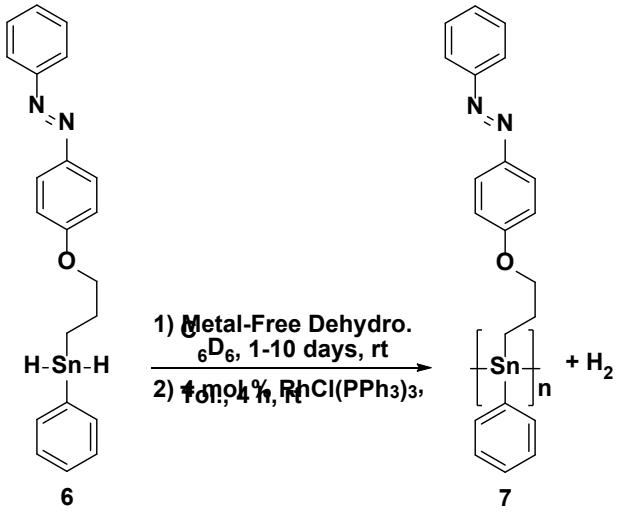

Scheme 6. Dehydropolymerisation of **6** to **7-i** and **7-f**.

The homopolymer **7-f** was also prepared by the slow addition of **6** (over 15 min) to a stirring toluene solution containing 4 mol % of catalyst [$RhCl(PPh_3)_3$] at RT for 4 h (Scheme 5). The sample volume was then reduced *in vacuo*. The crude polymer was then dissolved in 3 mL of THF and added dropwise into a 10-fold excess of cold hexanes, after which an orange–yellow semi-solid precipitated. Polymer **7-f** was recovered in 77 % yield by carefully decanting off the hexanes followed by drying (*in vacuo*). The polymer **7-f** is readily soluble in C_6D_6 and a ^{119}Sn NMR spectrum of this material revealed a chemical shift (-236 ppm), similar to the value observed in the final product **7-i** of the metal-free dehydrocoupling reaction.

Two random co-polymers **8a** and **8b** were also prepared (Scheme 7) by incorporating (n-Bu)$_2$SnH$_2$, at two different loadings (4:1 and 1:1) under catalytic dehydrocoupling. This was intended to produce a material with improved solubility profile. The polymerisations and polymer recovery were carried out under similar conditions used to prepare homopolymer **7**. These polymers are semi-solid in nature, were dried under reduced pressure and orange gels were thus isolated (Figure 22). The soluble polymers were characterized by ^{1}H, ^{13}C and ^{119}Sn NMR spectroscopy, elemental analysis, and GPC.

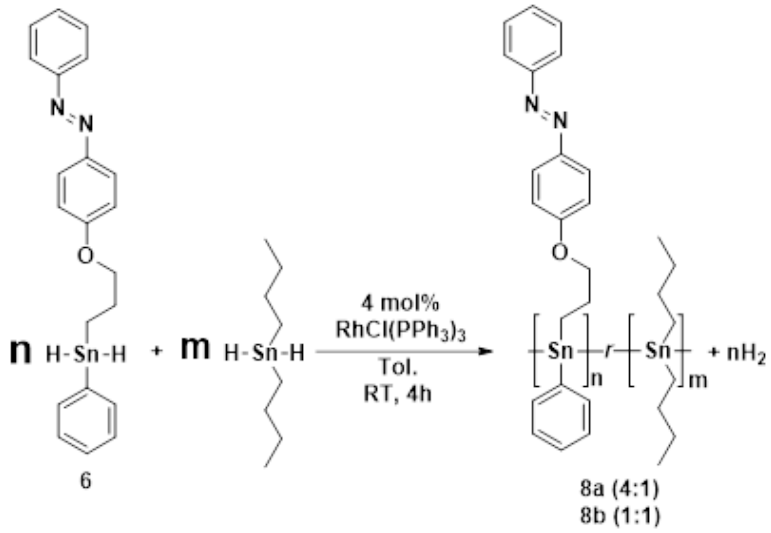

Scheme 7. Preparation of random copolymers **8a** and **8b**.

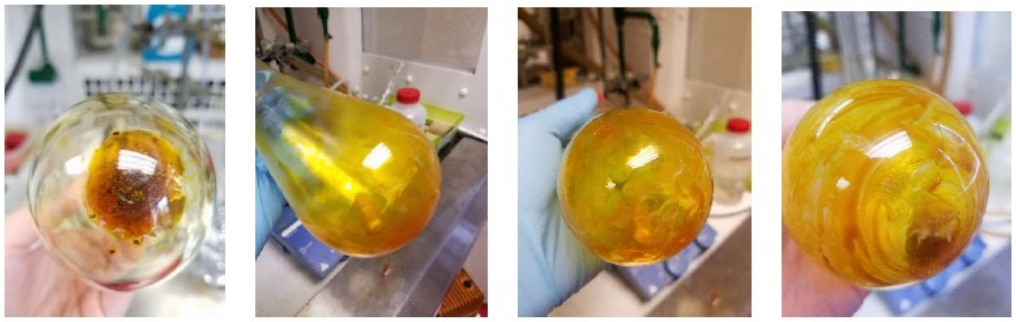

Figure 22. Polymers **7**, **8a**, **8b** and **9**, respectively.

The Foucher Group has previously demonstrated the condensation polymerisation of diaryl or dialkyl tin dihydrides with dialkyl tin diamides.[20] This led to the first examples of alternating polystannanes. The alternating polymer **9**, consisting of a 1:1 ratio of azo-stannyl and dibutyltin units, was constructed using this strategy. The polymerisation was carried out at

0 °C for 4 h in Et_2O solution, as shown in Scheme 8. The purification and recovery were similar to that used for polymers **7** and **8**. After washing with several portions of cold hexanes and drying *in vacuo*, an orange, low molecular weight semi-solid was recovered (53% yield).

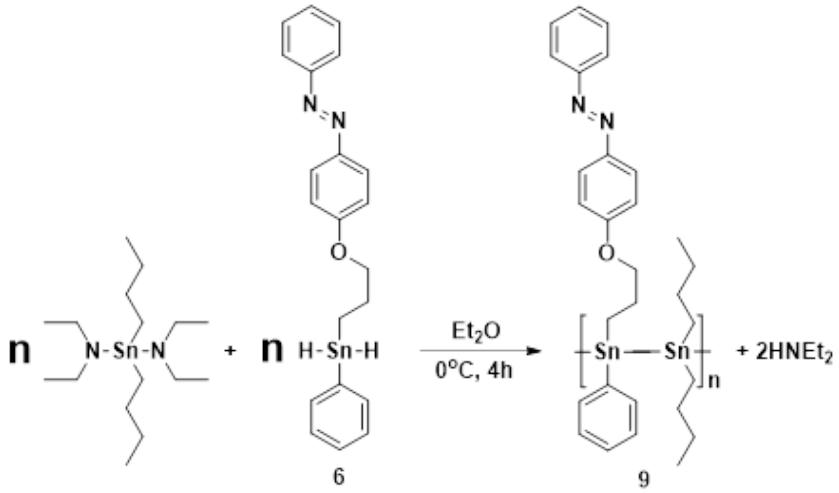

Scheme 8. Preparation of alternating polymer **9**.

1.5.1 Characterizations of AzoPolystannanes

The ^{119}Sn NMR spectra of **6** taken initially at t = 0, 6 and 24 h are shown in Figure 23.[15] There was an evident decrease in the relative integration of the ^{119}Sn NMR signal (i.e., the -215 ppm signal for **6** and a new resonance appeared at -198 ppm (for **7-i**). This value is typical of mixed aryl/alkyl polystannanes containing a propyloxy linkage.[58] After 5 d, the Sn resonance at -215 ppm had completely disappeared with only the resonance at -198 ppm remaining. Examination by ^{119}Sn NMR spectroscopy revealed that the -198 ppm polymer resonance was also decreasing in intensity and another new resonance at -236 ppm began to appear. ^{119}Sn NMR monitoring from the 7th to 10th d showed a further decrease in the intensity of the former resonance and a continued growth of the latter (Figure 23).

For polymer **7-f**, which was synthesized using Wilkinson's catalyst, the ^{119}Sn NMR spectrum of this material revealed one broad chemical shift at -236 ppm, like the value observed in the final product (10th day) of the metal-free dehydrocoupling reaction **7-i**.

Characteristic of the random copolymers **8a** and **8b** are two distinct ^{119}Sn resonances (-168 and -243 ppm) which are assigned to the -(*n*-Bu)$_2$Sn- and -(Ph)Sn-(CH$_2$)$_3$ O-(C$_6$H$_4$N=NC$_6$H$_5$)- segments, respectively.

For the alternating polymer **9**, the downfield signal at -167 ppm most likely represents the -(*n*-Bu)$_2$Sn- unit and the resonances at -243 ppm the azo-stannyl building block. For **9**, the alternating polymer presents three ^{119}Sn NMR resonances (Table 2) when the polymerisation was carried out by adding the diamide-tin to **6**, suggest that there may be both coordinated and free propyloxy units. This characteristic was also observed previously for other reported alternating polymers.[20,58] Polymers such as **10**, with similar flexible propyloxy ligands capable of datively bonding to Sn atoms, typically display ^{119}Sn resonances between -190 and -197 ppm.[18,58] A plausible explanation the observed spectroscopic behaviour is that there are datively bonded (O→Sn) and unbound propyloxy species along the polymer chain (Figure 24).

Table 2. ^{119}Sn NMR data for polymer **7-i**, **7-f**, **8a**, **8b**, **9** and **10**.

Compounds	^{119}Sn NMR (C$_6$D$_6$) (ppm)
7-i	-198, -235
7-f	-236
8a (4:1)	-168, -243
8b (1:1)	-167, -241
9	-167, -197, -240
10	-195

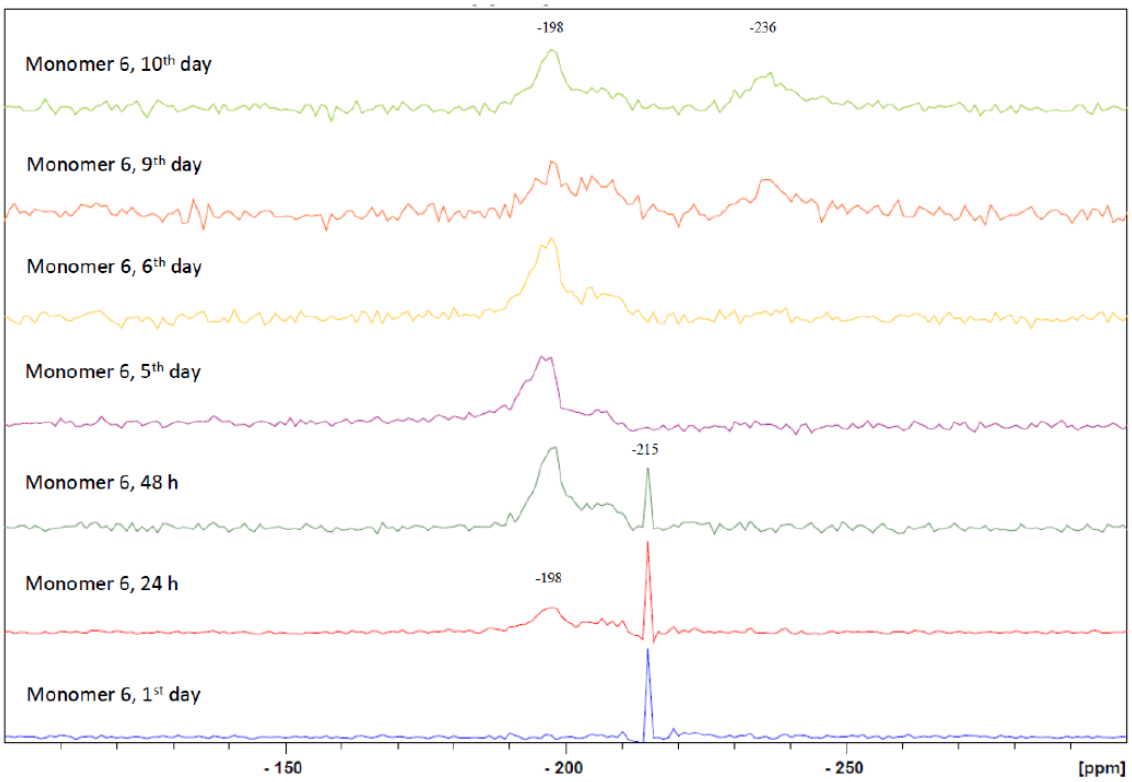

Figure 23. NMR assessment (day 1-10) of monomer **6** (metal-free polymerisation, **7-i**).

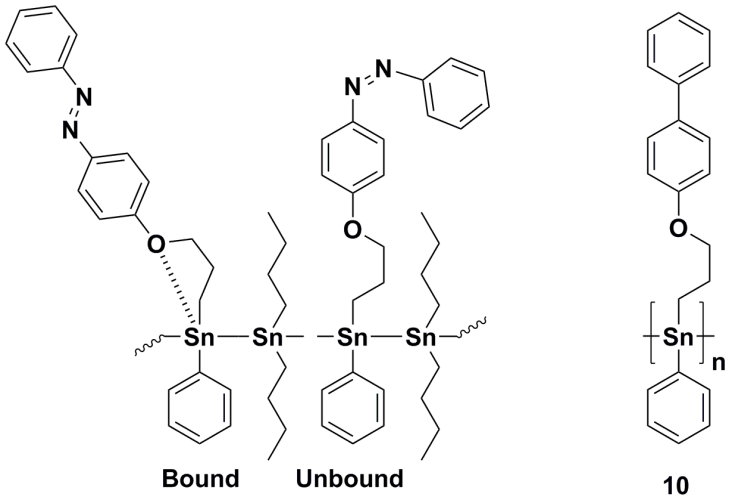

Figure 24. Bound and unbound polystannanes.

Only homopolymer **7-f** possessed a detectable T_g value at 22 °C, lower than that observed for polystannanes such as **10**. The absolute molecular weight and PDI of each polymer are listed in Table 3. The GPC chromatograms for all four new polymers in this study are shown in Figure 25. All polymers were bimodal and of moderate molecular weight. The corresponding values of the lower M_w fractions for **7-f** could not be determined.

Table 3. List of molecular weights and PDI of polymers **7-i** to **10**.

Compounds	M_w [Da] × 10^4	PDI [Đ]
7-f	2.85	1.1
8a (4:1)	3.53	2.4
8b (1:1)	1st 7.80	4.1
	2nd 2.84	2.0
9	1st 1.60	2.1
	2nd 1.22	2.0
10	2.45	1.8

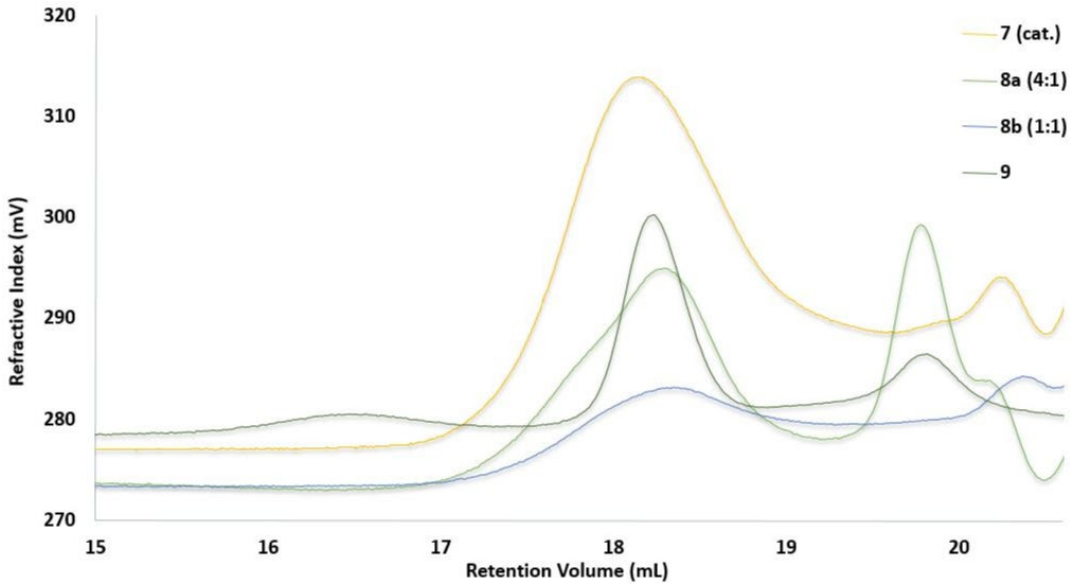

Figure 25. GPC chromatogram (R.I. only) of polymers **7-f**, **8a**, **8b**, and **9**.

UV-Vis spectroscopy of all the azo-containing tin compounds (**7-f** to **9**) were performed using benzene solutions of the materials. Unsurprisingly, all compounds showed nearly identical absorption characteristics assigned to azo-containing units presumably absorbing energy to initiate *E/Z* transformations in solution. In addition, five consecutive scans of all azo-containing tin polymers showed no evidence of degradation or photo scission when left in solution. UV-Vis characterization of solutions of polymers **8b** and **9** (C_6D_6) exposed to daylight, but sealed from moisture, displayed a decrease in signal intensity (57 % and 23 %, respectively)

over a 4 month period, whereas **7-f** was unchanged over the same time period (Figure 26). The decrease in absorption intensity for **8b** and **9** is likely due to the cleavage of Sn-Sn bonds (σ-σ* transitions masked by azo absorptions at 350–450 nm), whereas the azo *Z*- to *E*- absorption contributions are presumably consistent. Although the two copolymers are comprised of a similar number of stannylazo and dibutylstannyl units, the presumably more random polymeric structure appears to be more susceptible to chain cleavage. In comparison to **7-f** remains essentially stable under these conditions.

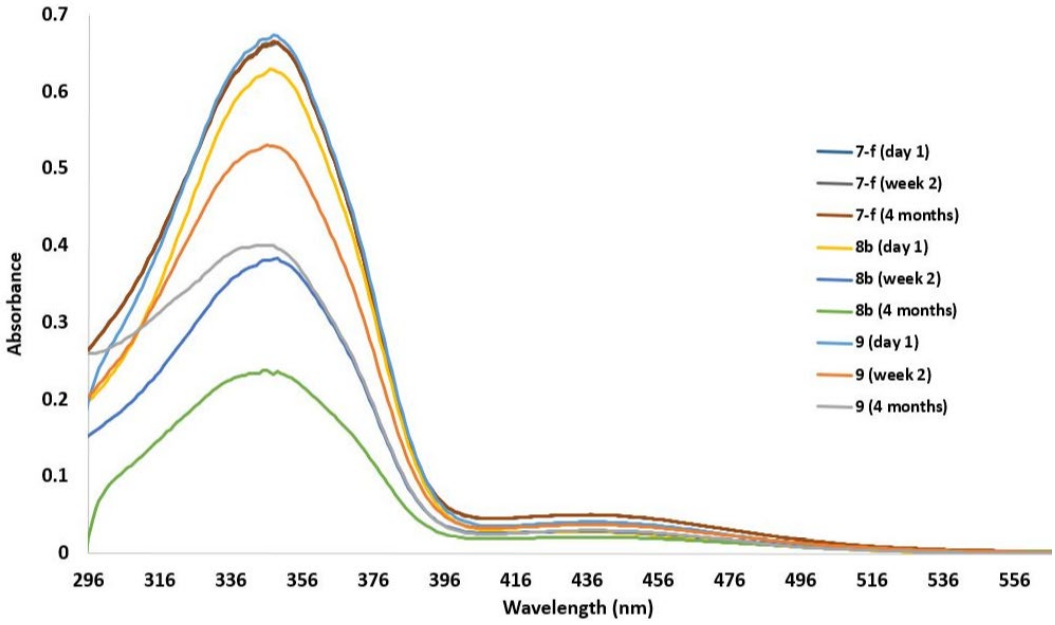

Figure 26. UV-Vis (C_6D_6) spectroscopy of polymers **7-f** to **9**.

1.6.1 Physical and NMR Stability Tests

Further evidence of the stability of the azo-containing polymers was observed for a ~100 mg sample of solid **7-f** which was left exposed to moist air and sunlight for extended intervals. After 6 months, the colour of the semi-solid darkened from light orange to a darker shade of orange. However, there was no observable change in the solubility properties of this material or in the NMR (^{119}Sn) resonances (-236 ppm only). This suggests long term stability with only the outer surface of this solid material being adversely affected. Compared to the gel-like orange coloured polymers **8a**, **8b** and **9** which were left inside open amber vials for slightly over one

month. These materials transformed to insoluble darker brown coloured semi-solids which could not be further characterized.

Conclusion

A five step synthesis was carried out to prepare a polymerizable azo-containing tin dihydride monomer **6**. The first azo-containing tin homopolymer **7-f**, copolymers **8a** and **8b** and alternating polymer **9** were prepared. Polymer **7-f** gave strong evidence of being stable to both moist air and visible light, whereas polymers **8a**, **8b** and **9** became insoluble and degraded. The azo-benzene functionality appears to provide unprecedented light stability to homopolystannanes and, in the case of **7-f**, provides the first evidence that a flexible, bulky, possibly coordinated unit can provide a level of moisture and oxidation resistance. This suggests that the future design of mixed polystannane polymers should incorporate monomers that are rich in protective functionalities, such as light absorbing groups and fragments with chelation potential.

CHAPTER 2 – Synthesis and Characterization of Readily Modified Poly(aryl)(alkoxy)stannanes by use of Hypercoordinated Sn Monomers

Abstract

Two aryl and alkoxy tin species from Chapter 1, compounds **1** and **2** were converted to thier dichlorido(aryl)(alkyl) tin derivatives, **11** and **13** respectively, and are key intermediates to tunable polystannane architectures. The materials were further investigated by single crystal XRD and a DFT analysis (not reported here) of their preferential "open and closed" geometries. Dichlorido compounds **11** and **13** were next converted to their respective dihydrides (**12**, **14**) and used as monomers for novel polystannane synthesis. The properties of two asymmetrical polystannanes prepared by dehydropolymerisation of dihydrido(aryl)alkylstannanes (**12** and **14**) were investigated. Polymer **19** (hydroxide analog) was a structurally simple, modest molecular weight, semi-crystalline light- and moisture-stable polystannane with NMR (^{119}Sn) evidence of a prominent O→Sn hypercoordination along the polymer backbone. Polymer **20** (tosylate analog) was of lower molecular weight, with no evidence of hypercoordination. Differential scanning calorimetry of polymer **19** revealed a reversible semi-crystalline nature, whereas an amorphous character was detected for polymer **20**. Polystannane **19** was also found to be exceptionally stable to both moisture and light (>6 months) and a promising candidate for the design of readily modified (i.e. tunable) film forming polystannane materials.

Polymer **20** on the other hand provided an opportunity to demonstrate that a library of hypercoordinate polystannanes could be accessed from single substitutionally labile polystannane post polymerisation. Currently, the synthesis of a functionalized polystannane from a substitutionally labile polystannane has yet to be explored. Preliminary work was undertaken on two novel model stannanes, a propylthioester **15** and propylmethoxy **16** species which were synthesized via S_N2 substitution reactions of the propyl tosylated **2**. The structures of the model stannanes were confirmed through ^{1}H, ^{13}C, ^{119}Sn, 2D-HSQC NMR and HRMS spectroscopy. Compound **17** (propylmethoxy) were further investigated by single crystal XRD.

Finally, the synthesis of the substitionally labile polymer was attempted, but not yet completed or fully characterized due to solubility issues.

Introduction

2.0.1 Hypercoordinated Tin Complexes

Several studies with both flexible and rigid hypercoordinate tin architectures have been reported in the literature (Figure 27).[13,40,58] They differ in the flexibility of the substituent at the tin center and the degree of dative bonding within the compound. In all instances, an increase of electron density at tin decreases its Lewis acidity and reduces its susceptibility to nucleophilic attack and improves its stability to moisture in the air. It has also been shown that the addition of aryl substituents[25] and the use of a chromophore[40] increases the stability to light due to the conjugation of the system.

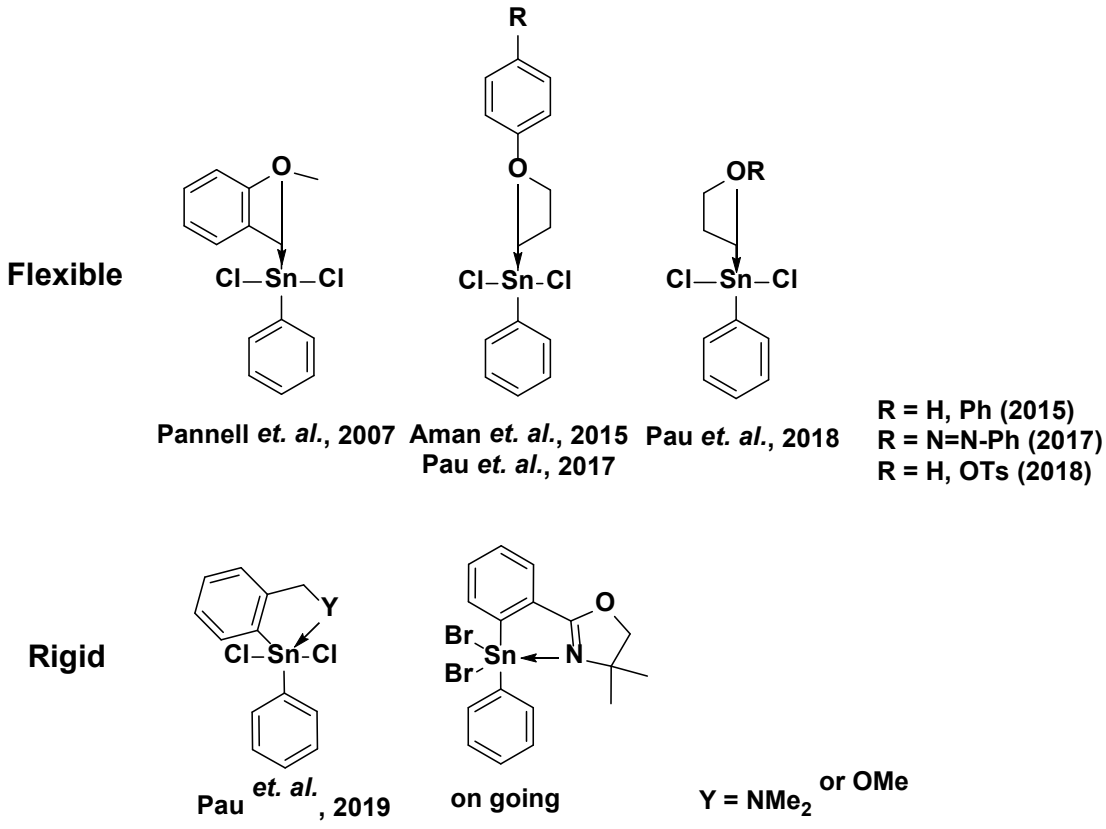

Figure 27. Flexible and rigid hypercoordinate tin architectures.

2.0.2 Polystannane Stability

The light and moisture stability of hypercoordinated polystannanes was investigated in Chapter 1. The use of hypercoordinated architectures at tin centers and a chromophore to provide both an electronic and steric solution to address these stability issues was demonstrated.[40] The use of light-absorbing azo-containing propyloxy substituents on the metal centers revealed strong hypercoordination in small molecule species, with evidence of two well-separated distinct tin signals in the ^{119}Sn NMR of polystannane **9**, assigned to both open and closed configurations of the polymer. This homopolymer proved to be stable to ambient conditions for > 1 year (Figure 28).[17,40,59]

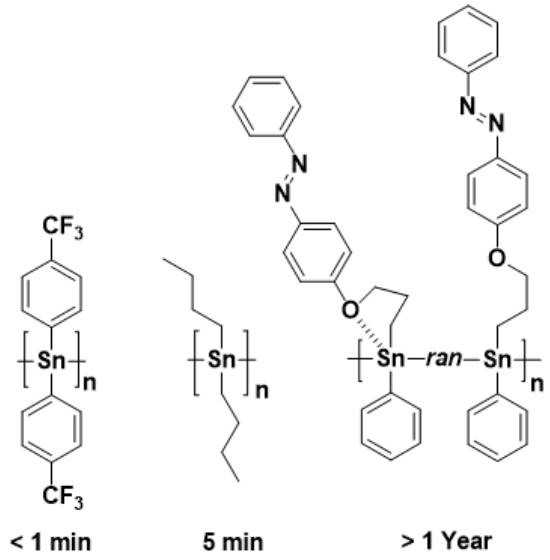

Figure 28. Relative solution stability of different polystannane backbones to visible light.

2.0.3 Design Rules for Stabilized Polystannanes

Construction of a wider variety stable polystannanes and the role of ligands in hypercoordination must be understood. Particularly those defined by three center–four electron (3c–4e$^-$) hypercoordination arrangements. These bonding motifs have been known for at least 50 years between later Group 14 elements (Si, Ge, Sn, Pb), electron-rich N, P, O, S donor atoms and axially coordinated electron-withdrawing substituents such as the halides.[26,57] The single X-ray structural data for several of these Sn species from the previous chapter and other research

reveal additional donor–ligand coordination to Group 14 elements along with an elongation of the ligand–metal bond at the *trans* position to the donating group. The hypercoordination to Sn center is theorized to be the result of a $2e^-$ donation from the formal *p*-orbital of the donating ligand into an empty non-bonding orbital of Sn, where it transfers the electron density continuously to an antibonding orbital of the electron-withdrawing substituent becoming 3c-$4e^-$.

The role of the Sn atom in hypercoordinated 3c–$4e^-$ interactions appears to function as an efficient electron shuttle; however, the mechanism is unknown. If the electron withdrawing substituents are replaced with one or two equally electron-deficient Sn atoms, the chances to deploy additional electron density to the Sn backbone could result in stronger Sn-Sn bonds. This would, in turn, possibly make the Sn-Sn bonds less susceptible to undergo cleavage in the presence of nucleophiles such as H_2O.[40,58,60]

Results & Discussion

2.1.1 Synthesis of Model Stannyl Precursors and Dihydrides

Compound **1** (Chapter 1**)** was prepared by the hydrostannylation reaction of allyl alcohol with Ph_3SnH in the presence of azobisisobutyronitrile (AIBN), and after washing the resulting solids with hexanes, isolated as a white powder.[54] Compound **1** was then brought through a series of stepwise chlorinations to convert to compound **11** using 1.0 M HCl/Et_2O in C_6H_6 for 1 h. The crude product was washed with hexane (3 × 20 mL) to give a pale-yellow solid in 72 % yield.[56] NMR spectroscopic analysis of **11** (^1H, ^{13}C; C_6D_6) was fully consistent with the expected structure. The ^{119}Sn NMR ($CDCl_3$) resonance for **11** was slightly downfield (δ = -80.4 ppm) in comparison to that of **1** (δ = -99.0 ppm). Compound **12** was synthesized through a standard hydrogenation with $LiAlH_4$ in Et_2O at 0 °C for 2 h, after which the reaction was quenched with degassed cold distilled water. The desired compound was isolated in 92 % yield as a pale-yellow translucent gel (Scheme 9). NMR (^1H, ^{13}C, C_6D_6) spectroscopic analysis of **12** was consistent with the expected structure, including the large $^{117/119}Sn$–H satellite coupling

resonances ($^{1}J_{119Sn\text{-}1H}$ = 1841 and $^{1}J_{117Sn\text{-}1H}$ = 1926 Hz, respectively) centered on the hydride signal (δ_H = 5.51 ppm). The ^{119}Sn NMR spectrum of **12** displayed a single resonance at δ = -214.9 ppm, typical for other known tin dihydrides. The hydride species is quite thermally sensitive compare to Ph_3SnH. It must be stored in the dark at -30 °C and could be kept in this way for 1-2 d without substantial decomposition.

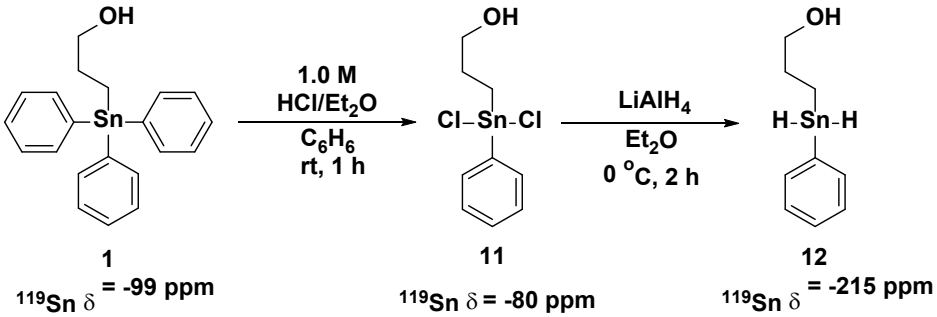

Scheme 9. Preparation of functional stannane monomers **11** and **12** *via* **1**.

Compound **2** was prepared following the conditions given by Yoshida *et. Al.*, as previously described.[55] Chlorination of **2** with HCl to give **13** proceeded in a single step and in a nearly quantitative yield. Conversion of the tosylated dichlorido tin compound **13** to the dihydride **14** was carried out with $NaBH_4$ in EtOH and isolated after workup (refer to experimental) in the form of a colourless liquid in 62 % yield. A milder hydride source $NaBH_4$ was selected due to the sensitivity at the O-S position, whereas a strong hydride source such as $LiAlH_4$ could easily cleave the O-S bond. The hydride resonance of **13** (δ_H = 5.31 ppm) was found slightly upfield in comparison to **11**, with the $^{117/119}$Sn–H coupling constants ($^{1}J_{119Sn\text{-}1H}$ = 1764 and $^{1}J_{117Sn\text{-}1H}$ = 1852 Hz, respectively), smaller by about 70–80 Hz (Scheme 10).

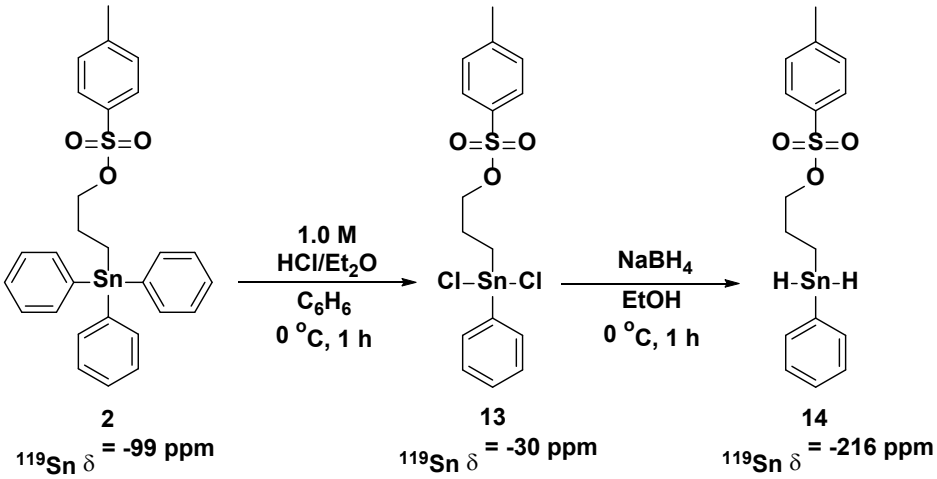

Scheme 10. Preparation of tosylate stannane monomers **12** and **13** *via* **2**.

A Williamson-Ether like synthesis was conducted by reacting **2** with K_2CO_3 as the base and thioacetic acid as the nucleophile in reflux for 2 h (Scheme 11). The reaction transformed from a clear solution to a viscous brown gel product **15** that was further purified by extraction using DCM in a 39 % yield. The ^{1}H, ^{13}C, ^{119}Sn, 2D-HSQC NMR ($CDCl_3$) and HRMS confirmed the expected compound structure. The ^{119}Sn NMR resonance of compound **15** is similar to other alkyl stannyl species such as compound **1** and **2** (δ = -99.2 and -99.7 ppm).

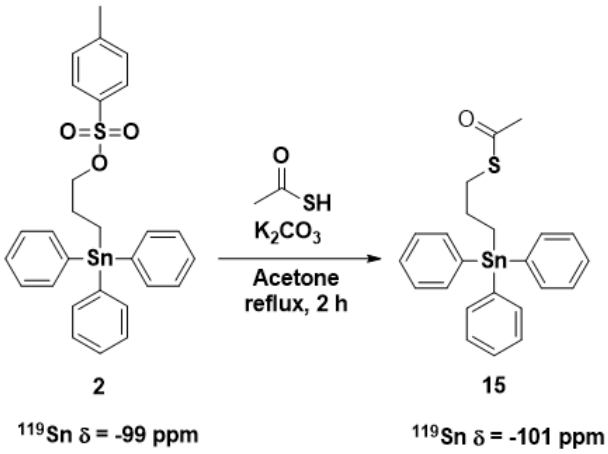

Scheme 11. Williamson-Ether like preparation of compound **15**.

Compound **16** was synthesized under a similar condition as **15** by reacting **1** with 25 % w/v solution of sodium methoxide in MeOH for 2 h in refluxing acetonitrile (Scheme 12). Initial reaction attempts with K_2CO_3 (base) and MeOH (reagent) were unsuccessful and likely a result of insufficient basicity to deprotonate MeOH. Other reaction attempts used NaOMe in a MeOH

solution but carried out in acetone which resulted only in the recovery of starting material. Since the NaOMe should be strong enough to deprotonate the MeOH, it is believed that acetone was being deprotonated before MeOH, leading to the formation of an aldol product (determined through NMR). Compound **16** was initially isolated in a 10 % yield after work up and was improved to 29 % yield by shortening the reaction time from 24 h to 2 h. The reaction was observed to fully convert after 1 h based an aliquot sample mid reaction. Due to time constraints, the reaction was not further optimized. The ^{1}H, ^{13}C, ^{119}Sn, 2D-HSQC NMR ($CDCl_3$) and HRMS revealed the compound structure. The ^{119}Sn of compound **16** is at δ = -100.0 ppm, similar to other propyl triphenyl stannanes **1** and **2**. The propylmethoxy triphenyl stannane **16**, the monochloro **17** and dichloro **18** species were analyzed by single X-ray crystal diffraction.

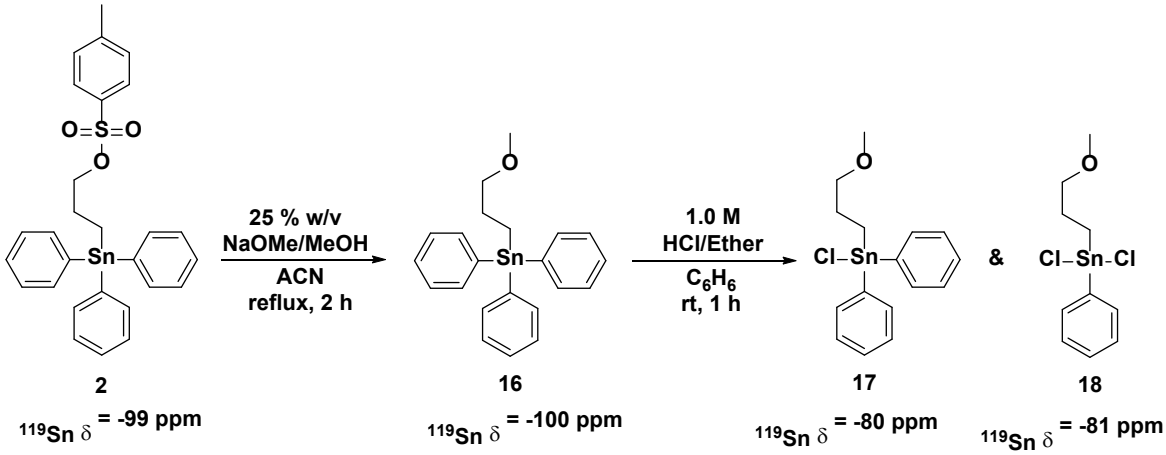

Scheme 12. Synthesis of **16** and chlorination of **17** and **18** *via* **2**.

2.2.1 NMR Characterizations of Monomeric Stannyl Precursors and Dihydrides

All the triphenylalkyl tin compounds (**1**, **2**, **15** and **16**) display a ^{119}Sn NMR ($CDCl_3$) resonance typically near δ = -100 ppm. The mono- and di-chloro species (**11**, **13**, **19** and **20**) are deshielded by the halide ligand(s). For example, using compound **11**, the ^{119}Sn shifted from δ = -99 ppm (compound **1**) to -80 ppm. From the solution NMR data, it reveals a small 3c-4e$^-$ hypercoordinate effect at the tin center where electron density is being drawn by one of the halide ligands.

NMR spectroscopic analysis of the dihydride **12** includes large $^{117/119}$Sn–H satellite coupling resonances ($^{1}J_{119Sn\text{-}1H}$ = 1841 and $^{1}J_{117Sn\text{-}1H}$ = 1926 Hz, respectively) centered on the hydride signal (δ_H = 5.51 ppm). The ^{119}Sn (C_6D_6) NMR spectrum of **12** displays a single upfield resonance at δ = -214.9 ppm, typical for tin dihydrides. In addition, in comparison to the dichloro species **11**, the ^{119}Sn resonance for **12** is upfield, and absent of a hypercoordination. Unfortunately, single crystal analysis of hydrides and dihydrides are rare thus prove difficult confirm the 4-coordinate geometry of these species. The hydride resonance of **14** (δ_H = 5.31 ppm) was found also upfield in comparison to **11**, with the $^{117/119}$Sn–H couplings ($^{1}J_{119Sn\text{-}1H}$ = 1764 and $^{1}J_{117Sn\text{-}1H}$ = 1852 Hz, respectively) (Figure 29).

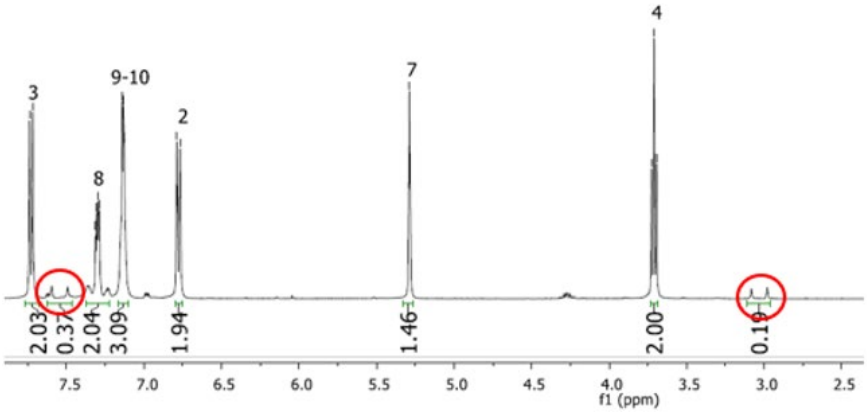

Figure 29. Dihydride resonances and the $^{117/119}$Sn–H satellites of compound **14** (circle in red).

2.3.1 Single Crystal X-ray Analysis of Tin Precursors

The geometry of compound **11** was revealed by single crystal X-ray diffraction (Figure 30). The 3c–4e$^-$ bonding motif between the tin, chlorine, and oxygen atoms can be discerned from the molecular configuration. The propyl oxygen atom was found in a position strongly suggesting dative bonding to the Sn center, with a notably shorter bond distance (2.40 Å). This is much shorter than other five-coordinate Sn species with a dative oxygen interaction (see Chapter 1). For instance the Sn-O bond length of 2.729 Å was found in the dichlorostannane compound **5** while Pannell *et. al.* observed a Sn-O bond length of 2.898 Å for the (*o*-MeO-C_6H_4)CH_2SnCl_2 species.[56] The Sn···O bond length of **11** was about 17 % larger than those

reported for tin complexes (2.05–2.14 Å) with truly covalent Sn-O bonds. In the hypercoordinated geometry of **10**, the axial Sn-Cl bond is notably elongated in comparison to the equatorial Sn-Cl bond (~0.09 Å).

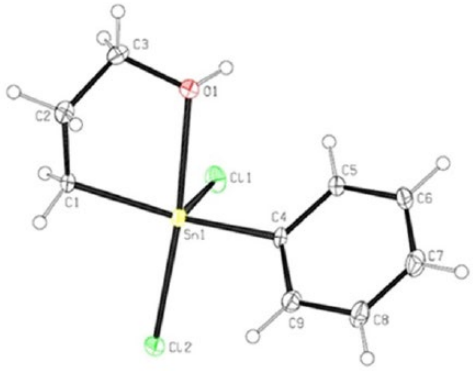

Figure 30. ORTEP representation of **11** found in the unit cell and selected bond lengths [Å] and angles [°]. Thermal ellipsoids drawn at the 30% level. Sn···O 2.400(3), Sn-Cl1 2.3766(14), Sn-Cl2 2.4509(12), Cl1-Sn-Cl2, 94.20(5), C1-Sn-C4 143.79(18), O···Sn-Cl2 173.88(9).

For compound **13**, a hypercoordinate interaction was clearly absent with the Sn···O distance of approximately 5.4 Å. The lack of an intramolecular dative interaction is likely related to the electron-withdrawing strength of the tosyl group. There was no evidence of intermolecular interactions of the propyl oxygen with neighboring tin centers in the unit cell, but one of the tosyl oxygen atoms (O3) was oriented towards the Sn center of another molecule of **13** with an Sn···O distance of 2.776 Å and a O3···Sn-Cl_2 angle of 176.3°. However, the geometry of the Sn center and near equivalence of the Sn-Cl bond lengths suggest a relatively weak intermolecular interaction without substantial hypercoordinate character (Figure 31).

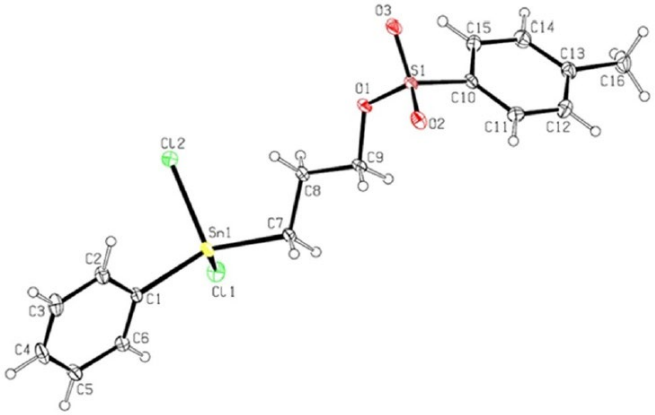

Figure 31. ORTEP representation of **13** found in the unit cell and selected bond lengths [Å] and angles [°]. Thermal ellipsoids drawn at the 30% level. Sn···O 5.418(3), Sn-Cl1 2.3660(6), Sn-Cl2 2.3776(6), Cl1-Sn-Cl2, 98.73(2), C1-Sn-C7 138.24(8), O1···S1-Cl0 105.88(9).

For compound **16**, the structure assumes a mildly distorted tetrahedral geometry where bond angles should be around 109.5°, rather than a hypercoordinated trigonal bipyramidal one. The Sn(1)-O(1) distance was calculated at 3.030(1) Å. This falls within the Van der Waals radii for Sn and O of 3.69 Å and exceeds the length of the typical Sn-O covalent bond length (2.05 Å) (Figure 32).

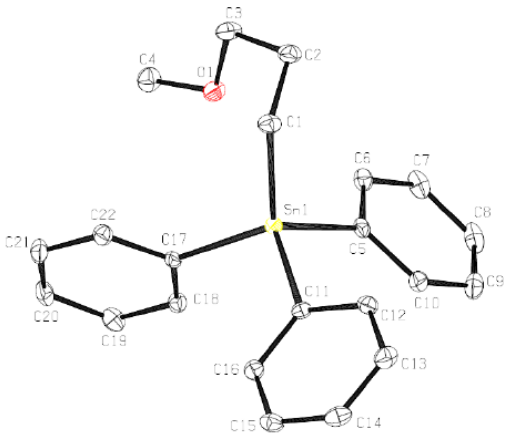

Figure 32. ORTEP representation of **16** found in the unit cell and selected bond lengths [Å] and angles [°]. Thermal ellipsoids drawn at the 30% level. Sn(1)-O(1) 3.030(1), Sn(1)-C(17) 2.145(2), Sn(1)-C(1) 2.148(2), Sn(1)-C(5) 2.148(2), Sn(1)-C(11) 2.160(2), C(17)-Sn(1)-C(1) 117.24(8), C(1)-Sn(1)-C(11) 104.78(8), C(1)-Sn(1)-C(5) 113.41(8), C(17)-Sn(1)-C(5) 107.30(8), C(1)-Sn(1)-C(11) 104.78(8), C(5)-Sn(1)-C(11) 105.71(8).

For crystal structure **17** (monochloride), it revealed a change in geometry from the tetrahedral triphenyl (compound **16**) to a distorted trigonal bipyramidal structure. A dative bonding interaction between Sn(1) and O(1) is responsible for the trigonal bipyramidal geometry. This is further supported by the bond angles changes which have shifted from being near 109.5° to being closer to 120° or 90°, as expected for trigonal bipyramidal.

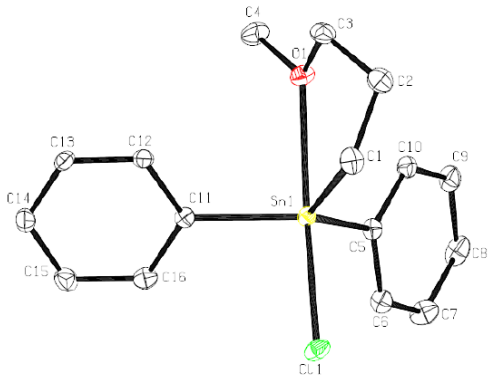

Figure 33. ORTEP representation of **17** found in the unit cell and selected bond lengths [Å] and angles [°]. Thermal ellipsoids drawn at the 30% level. Sn(1)-O(1) 2.518(3), Sn(1)-C(11) 2.140(3), Sn(1)-C(5) 2.144(3), Sn(1)-C(1) 2.144(3), Sn(1)-Cl(1) 2.453(4), C(11)-Sn(1)-C(5) 118.80(12), C(11)-Sn(1)-C(1) 114.90(13), C(5)-Sn(1)-C(1) 122.03(13), Cl(1)-Sn(1)-O(1) 172.57(8), C(11)-Sn(1)-O(1) 88.00(10), C(5)-Sn(1)-O(1) 87.93(13).

The crystal structure of **18** (dichloride) reveals the presence of five unique conformers within the crystal structure. Furthermore, extensive dative bonding was visible in the structure which adopts a trigonal bipyramidal geometry (Figure 34).

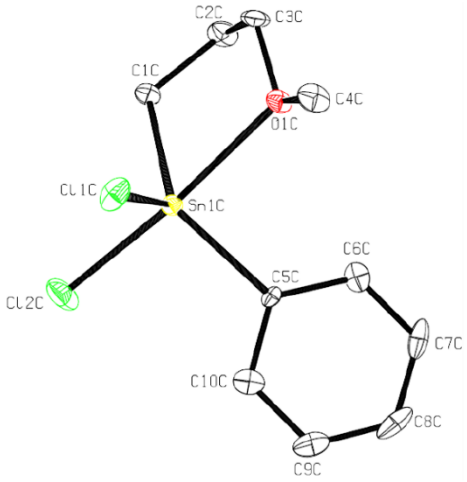

Figure 34. ORTEP representation of **18** found in the unit cell and selected bond lengths [Å] and angles [°]. Thermal ellipsoids drawn at the 30% level. Sn(1A)-O(1A) 2.441(5), Sn(1B)-

O(1B) 2.437(5), Sn(1C)-O(1C) 2.464(5), Sn(1D)-O(1D) 2.438(5), Sn(1E)-O(1E) 2.443(5), C(5)-Sn(1)-C(1) 141.6(5), Cl(1)-Sn(1)-Cl(2) 96.8(6), C(5)-Sn(1)-O(1) 86.5(4), C(1)-Sn(1)-O(1) 75.2(2), Cl(1)-Sn(1)-O(1) 87.08(53), Cl(2)-Sn(1)-O(1) 173.34(53).

2.4.1 Polymerisations and Substitution Trials

Homopolymers **19** and **20** were prepared by dehydropolymerisation reactions of **12** (hydroxide) and **14** (tosylate) involving the application of Wilkinson's catalyst in toluene at RT for 4 h (Scheme 13). Volatiles were thereafter removed *in vacuo* and the crude materials of **19** or **20** were then dissolved in a minimal volume of THF (~5 mL) and added slowly, dropwise, to 50 mL of a stirring cold hexanes. The resulting yellow coloured solids that formed were recovered by decanting, and after drying *in vacuo*, yellow powders of purified **19** or **20** were recovered in 78 % and 63 % yields, respectively.

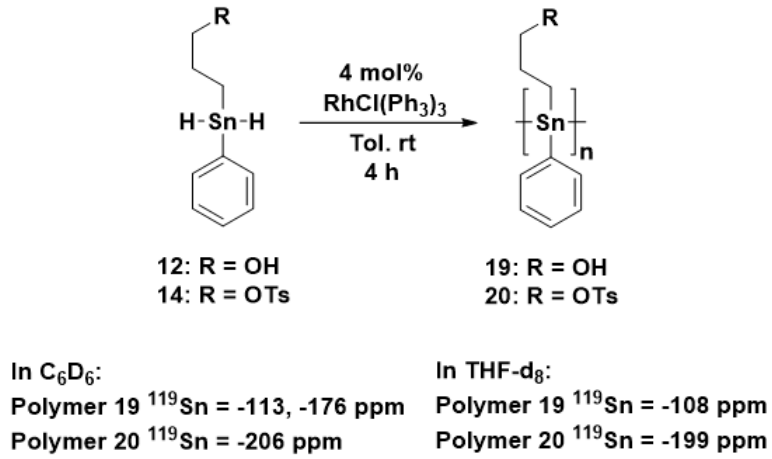

Scheme 13. Transition-metal-catalyzed dehydropolymerisation of tin dihydrides **12** and **14**.

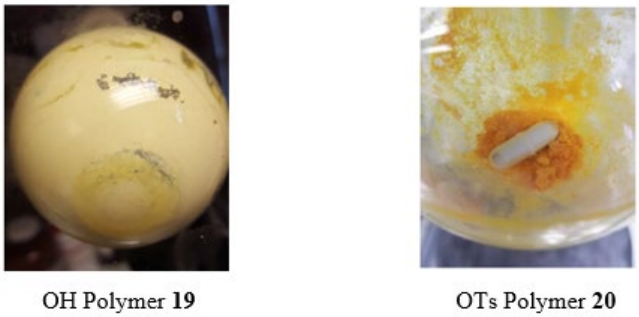

Figure 35. Physical appearance and colour of polymers **19** and **20**.

An attempt to substitute tosylate homopolymer **21** was carried out following similar S_N2 conditions used to synthesize compound **15** (Scheme 14). As mentioned earlier in the model stannanes, the solvent was switched to acetonitrile to improve solubility of the substituted polymer **20**. The reaction was carried out under N_2 and wrapped with tin foil to prevent any light degradation. The crude was then dried *in vacuo* and dissolved in THF (~5 mL) and precipitated in 10-fold excess of cold hexanes. A noticeable colour change was observed for the potential thioester homopolymer **21**. The tosyl homopolymer was orange (Figure 35), polymer **21** became dark yellow colour in comparison and the strong odour of the thioacetic acid was absent, suggesting the synthesis may have succeeded (Figure 36). Due to solubility issues and lack of access to solid-state NMR, further characterizations have not been completed at this time.

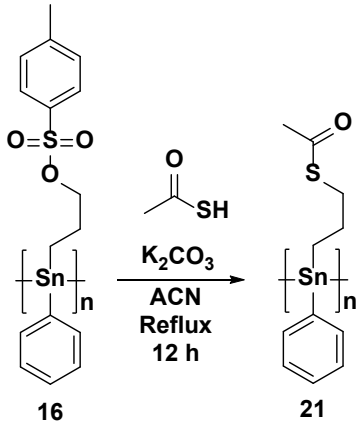

Scheme 14. Synthesis of polymer **21**.

Figure 36. Presumed crosslinked thioester homopolymer **21**.

2.5.1 Characterization of Flexible Tosylate and Hydroxide Polystannanes

The ^{1}H NMR spectroscopic (C_6D_6) analysis of **15** showed surprisingly well-resolved resonances for the aromatic and alkyl portions of the polymer; by contrast the ^{1}H NMR signals of purified **20** were notably broad. Interestingly, the ^{119}Sn NMR spectrum of **19** in C_6D_6 displayed two nearly equal intensity resonances (δ = -113.4 ppm and -176.0 ppm) (Figure 45b). This is attributed to the presence of both an open (lower field) configuration, and a closed (higher field) motif in which the OH group is datively bound to the tin, making it formally five-coordinate, similar to the azopolystannanes described in Chapter 1.

Interestingly, only a single sharp downfield resonance at -108 ppm was observed for polymer **19** when the NMR spectrum was recorded in THF-d_8 (Figure 37a). The ^{119}Sn NMR spectra of **20** (Figure 37c, d) in either THF-d_8 or C_6D_6 were similar and a broad resonance centered near -202 ppm, which is typical of chemical shifts of other polystannanes propyloxy linkages.[58] The differences between the ^{119}Sn NMR spectra in C_6D_6 and THF-d_8 are consistent with the relative coordinating ability of the related nondeuterated solvents as described by Alvarez *et. al*.[61] The THF-d_8 solvent likely overwhelms and displaces the intramolecular hypercoordinate bonding in the polymer, so that all propyloxy ligands lie in the open position of polymer **19**. However, for polymer **20** there is essentially no change beside in the NMR shift even using different deuterated solvents. One observation is that polymer **20** remain in the "open" conformation under any circumstances due to the presents of the strong withdrawing OTs group. The ^{119}Sn NMR chemical shifts for stannanes of this study are listed in Table 4.

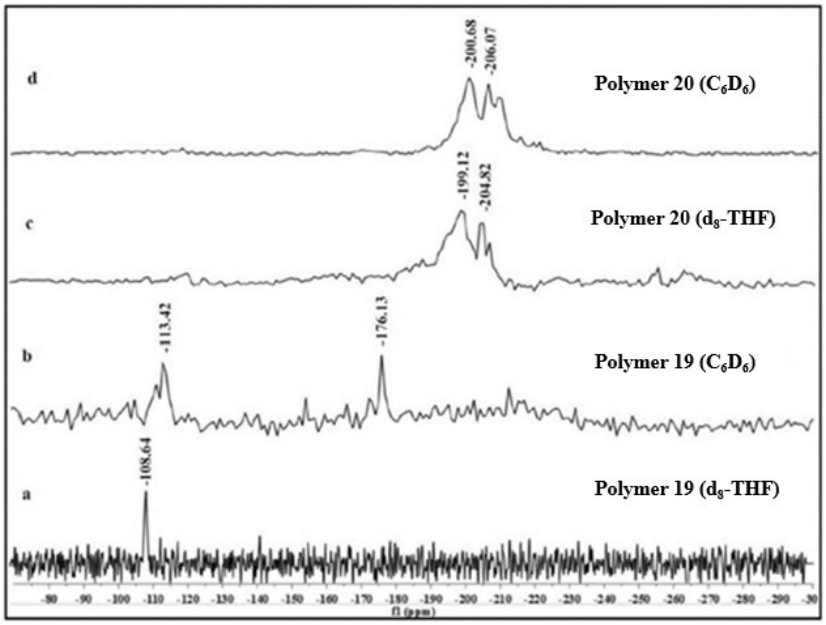

Figure 37. ^{119}Sn NMR spectra of **19** and **20**.

Table 4. ^{119}Sn NMR data for all compounds in Chapter 2.

Compounds	^{119}Sn ($CDCl_3$) (ppm)	^{119}Sn (C_6D_6) (ppm)	^{119}Sn (d_8-THF) (ppm)
1, 2, 17, 18	-99, -99, -101, -100	n/a	n/a
11, 13, 19, 20	-80, -30, -80, -81	n/a	n/a
12, 14	n/a	-215, -216	n/a
15	n/a	-113 & -176	-108
16	n/a	-206	-199

Figure 38 shows the absolute molecular weight (by GPC) for **19** revealing a narrowly dispersed, modest molecular weight polymer [42 kDa, polydispersity index (PDI) 1.16]. A lower molecular weight was found for the tosylate polymer **20** (31 kDa, PDI 1.20). In later attempts and optimizations of polymer **19**, there were a few trials the M_w reached >60 kDa.

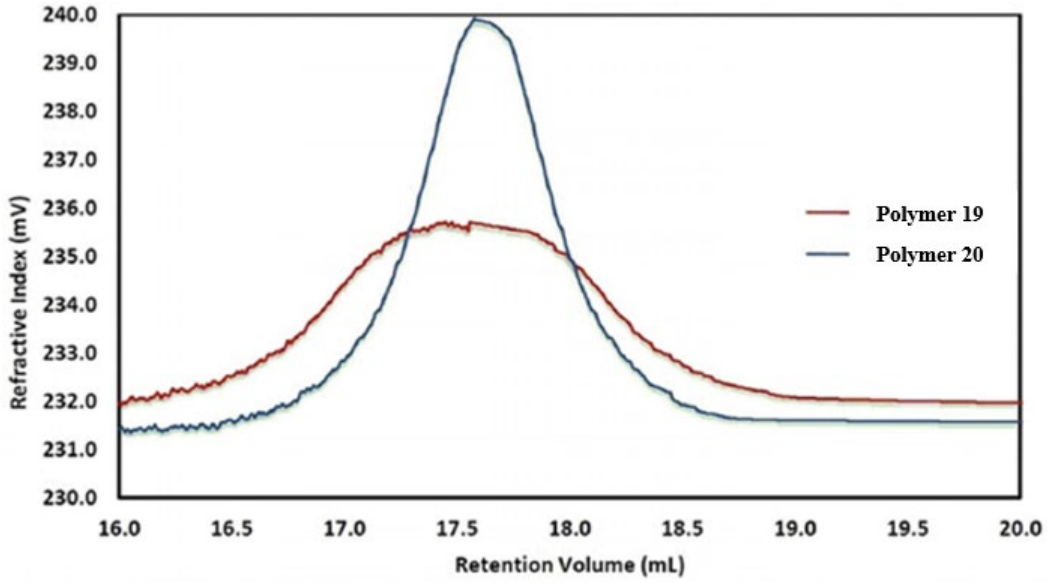

Figure 38. GPC chromatogram (refractive index, THF) of polystannanes **19** and **20**.

Thermal analysis of **19** and **20** was conducted by differential scanning calorimetry (DSC). Compound **19** was subjected to three consecutive heating/cooling cycles and showed no evidence of decomposition below 200 °C. A weak, reversible glass transition temperature (T_g) was detected at 49.3 °C and a strong reversible melting temperature (T_m) was observed at 110.1 °C (Figure 39). These results suggest a semi-crystalline nature for polymer **19**. In the case of **20**, only a weak T_g (65.9 °C) was detected and is more typical of amorphous polymers (refer to supplementary Figure S64.

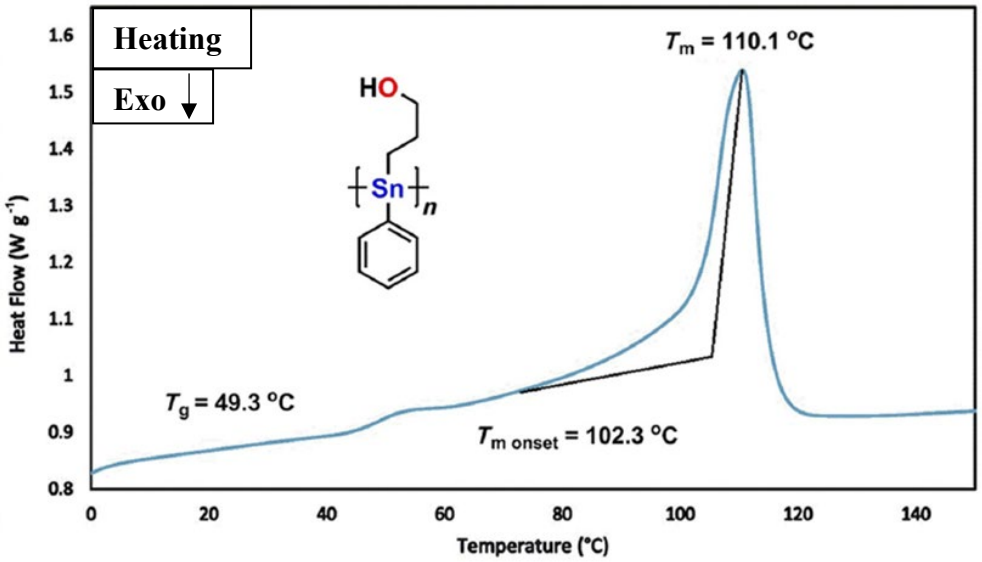

Figure 39. DSC thermogram for homopolymer **19**.

The morphology of polystannanes is of great interest due to the impact that hypercoordination in the solid state may have on the degree of crystallinity and conjugation in the backbone. The supposed semi-crystalline polymer **19** was found to be both air and moisture stable. Analysis of the polymer morphology of **19** by power X-ray diffraction (PXRD) without prior annealing, suggested some level of order, revealed by two broad peaks centered at scattering angle 2θ values of 7.1° and 19.7° (Figure 40). This corresponds to possible interchain *d*-spacings of 4.51 Å and 12.5 Å, respectively. The larger *d*-spacing is like that reported earlier by Caseri and co-workers (11.2–13.2 Å).[62] Further work to explore the nature of these *d*-spacings is ongoing.

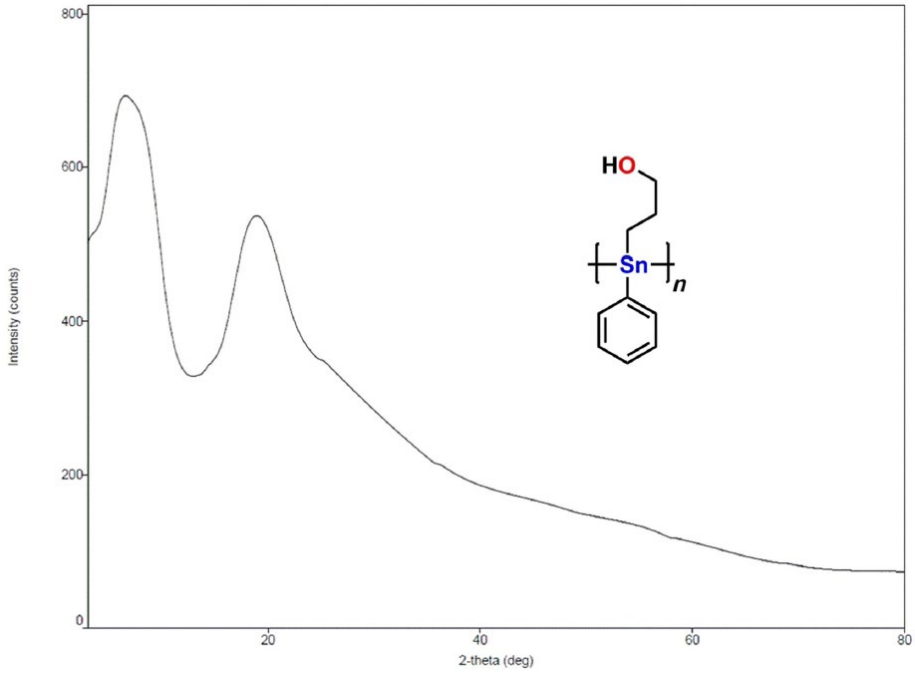

Figure 40. The PXRD diffractogram of polymer **19**.

2.6.1 Film Casting and Stability Tests

Polymer **19** has proven to be the most accessible and processable light and moisture stable polystannnes thus far. The tight intramolecular packing of the O–H bonds along with the partial hypercoordination present in **19** demonstrates the potential for this polymer to be conductive and thermally stable.

Two different approachs to film casting were attempted; spin coating and drop casting. For spin coating, the dissolved polymer (10 % w/v in THF) were spin coated onto a thin glass slide using a spin coater (Figure 41). However, the spin coating technique did not provide a homogeneous layer thickness. In addition, a considerable loss of materials during the spin operation occurred. Nonetheless, a thin transparent polymer layer was deposited on glass.

For drop casting, the result is more promising. A 40 kDa polymer was simply dissolved (10 % w/v in THF) and then slowly dropcast onto a Teflon plate and left to slowly air dry. However, the dried material was slightly brittle, but nearly film forming. A higher M_w polymer of **19** (>60 kDa) will likely give a better result. This process is still on going.

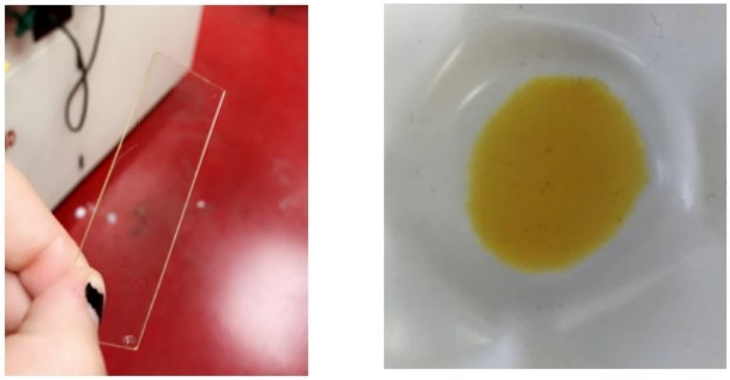

Figure 41. Physical results showing two different techniques that were used to film cast polymer **19** (10 % w/v in THF) a) Left: spin coating b) Right: drop casting.

Conclusion

The asymmetrical polystannane macromolecular intermediate **19** was prepared from the transition-metal-catalyzed dehydropolymerisation of dihydrido **12** in 78 % yield. Characterization of **19** by ^{119}Sn NMR spectroscopy in C_6D_6 revealed the presence of two equal intensity resonances at δ = -113 ppm and -176 ppm attributed to hypercoordinated and non-hypercoordinated Sn···O interactions along the polymer backbone. GPC analysis confirmed a narrowly dispersed high molecular weight polymer. Further analysis by DSC and PXRD revealed the semi-crystalline nature of **19**. Polymer **19** showed no evidence of decomposition after exposure to both ambient light and moist air for >6 months. Polymer **20** bearing a tosyl

substituent was also prepared by dehydropolymerisation and could become an important macromolecular intermediate to several stable, asymmetrical polystannanes. Investigation of the substitution chemistry of the tosyl macromolecular intermediate **2** was carried out in two phases. In the first phase, the substitution of triphenyl tosyl stannane was successfully established with two different nucleophiles, methoxide anion and thioacetate. In the second phase, conversion of polymer **20** to the corresponding thioacetate, **21**, yielded an insoluble, likely cross-linked polystannane.

CHAPTER 3 – Hypercoordinated Organotin (IV) Compounds and Polymers Containing *C,O*- & *C,N*- Chelating Ligands

Abstract

Two monoorganotin dichlorides [2-($MeOCH_2$)C_6H_4]$RSnCl_2$ (**24**: R = *n*-Bu; **25**: R = Me) were successfully prepared from the reaction of the organolithium, [2-($MeOCH_2$)C_6H_4]Li (**23**) with the appropriate trichloroalkyl stannane. Similarly, two dimethylamino stannanes including dichlorides [2-(Me_2NCH_2)C_6H_4]$RSnCl_2$ (**28**: R = *n*-Bu; **29**: R = Me) were prepared by reaction of the appropriate trichlorostannane and the organolithium [2-(Me_2NCH_2)C_6H_4]Li (**27**). Methoxylated and dimethylamino diorganotin dichlorides (**24**, **25**, **28**, **29**) were reduced with $LiAlH_4$ to produce new methoxylated [2-($MeOCH_2$)C_6H_4]$RSnH_2$ (**30**: R = *n*-Bu; **31**: R = Me) and dimethylamino [2-(Me_2NCH_2)C_6H_4]$RSnH_2$ (**32**: R = *n*-Bu; **33**: R = Me) dihydrides that are relatively stable below -20 ℃. Catalytic dehydrocoupling of *C,O*- (**30**) and *C,N*- (**32**) diorganotin dihydrides was explored using Wilkinson's catalyst at RT leading to the recovery of modest molecular weight polymers (**34**: $M_w = 3.03 \times 10^4$ Da, PDI = 1.4, **35**: $M_w = 3.10 \times 10^4$ Da, PDI = 1.86). The new rigid polymers were isolated in moderate (**34**: 65 %) and low yields (**35**: 18 %) and were found to be amorphous by DSC analysis.

Introduction

3.0.1 Rigid Organotin (IV) compounds

Organotin (IV) compounds possessing a flexible or rigid chelating organic ligand with O or N donor atoms capable of coordination interactions have been extensively investigated both in solution and in the solid state.[57] A common feature of these hypercoordinated species is the expansion in the coordination sphere of tin centers facilitated by additional intra- or intermolecular coordination interactions. In recent years, research interest in hypercoordinate derivatives of silicon,[57,63]germanium[30] and tin[64] with non-classical chemical bonds has increased largely due to their unusual structural properties and in the case of tin, their potential

suitability as polymerisable monomers. The resulting hypercoordinated metallopolymers are proposed to be stable towards light and moisture.[14]

Hypervalent halogenated organotin derivatives that possess the *C,N*-chelating ligand, [2-(Me_2NCH_2)C_6H_4]-, were first reported by van Koten and characterized by NMR (^1H, ^{13}C, ^{15}N, ^{119}Sn) spectroscopy and single-crystal X-ray diffraction studies.[65] The donor-acceptor interaction in hypercoordinated halogenated tin species of this type has shown and proven by other researchers. Consequently, as the Sn-N distance decreases in a hypervalent halogenated organotin derivative, the Sn-X (X = F, Cl, Br, I) bond typically elongates.[56]

The current study is focused on the syntheses and characterization of new and known rigid *C,O*- and *C,N*- tetraorganotins, tin dichlorides and dihydrides (Figure 42). Finally, a preliminary assessment of the polymerisation behaviour of hypercoordinated *C,O*- and *C,N*- tin dichlorides *via* hypercoordinated *C,O*- and *C,N*- tin dihydrides by metal-catalyzed dehydrocoupling is also described. All compounds were fully characterized under ^1H, ^{13}C and ^{119}Sn NMR.

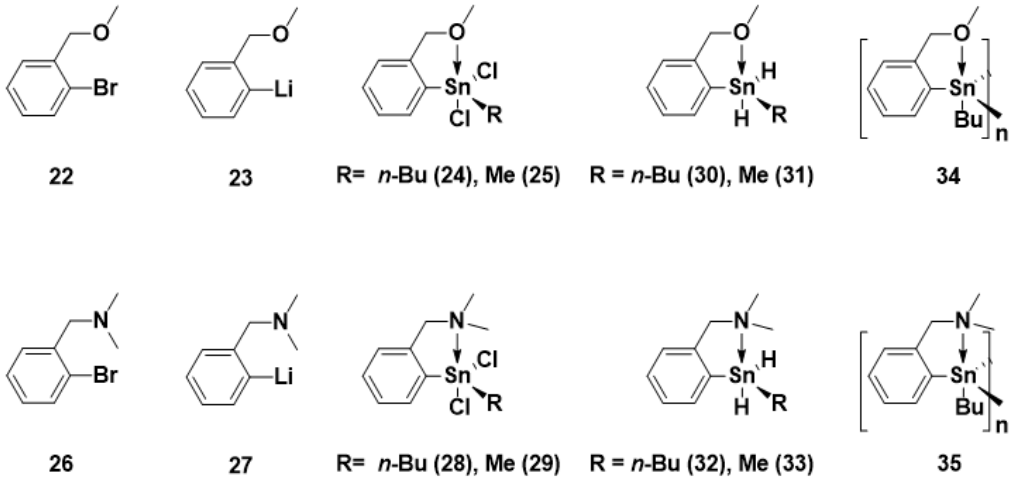

Figure 42. List of stannane compounds used in this study.

Results and Discussion

3.1.1 Synthesis of *C,O*- and *C,N*- Chelated Organotin Dichlorides and Dihydrides Precursors

Compound **22** was synthesized through a typical S_N2 reaction using sodium methoxide ($NaOCH_3$) in MeOH as a base and nucleophile. It was reacted with 2-bromobenzylbromide in a 1 to 1 ratio. The reaction was purified with extraction and a pure 84-90 % yield colourless oil was obtained. Similar to **22**, the *C,N*- analog **26** was prepared in high yield (88 %) and purity by heating 2-bromobenzylbromide with a large excess (7.5 eq.) of $HNMe_2$. The product was recovered by an initial extraction with 3 M HCl, followed by neutralization with 20 % NaOH and finally isolated from DCM. The pure product was obtained as yellow oil. This procedure was found to be superior with respect to a previously reported routes to these materials (Scheme 15).[66]

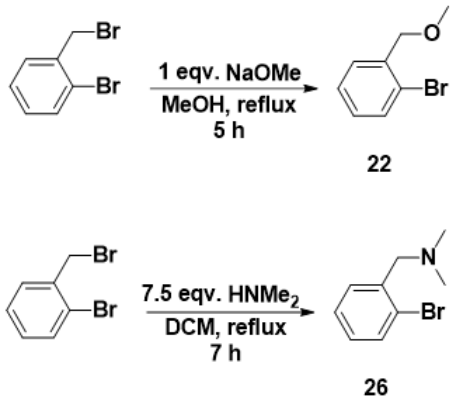

Scheme 15. The reaction conditions of the two different types of precursors ligand *C*,*O*- (Top) and *C*,*N*- (Bottom).

Compounds **22** and **26** undergo lithiation using 1.6 M *n*-BuLi in hexanes using a EtOAc/liquid N_2 -78 °C bath to afford a lithiated solution of **23** or **27**. Both compounds were used *in situ* and not isolated due to its pyrophoric nature. Both are shock sensitive and can ignite. Therefore, the solution of **23** or **27** was transferred *in situ* and reacted two different $RSnCl_3$ (R = *n*-Bu and Me) as a transmetalation reaction, isolating LiCl as a byproduct. All four transmetalations reactions were done at 0 °C and allowed to stir overnight. The reaction solution

was then pumped down *in vacuo* and dissolved in minimun amount of toluene to precipitate the byproduct LiCl. The salt was then filtered, and the remaining toluene solution was layered with hot hexanes, and decanted slowly until the top layer appeared to be clear. The methoxy dichlorides **24** and **25** were obtained as brown oils. Whereas the amino compounds **28** and **29** were obtained as white crystalline powders (Scheme 16).

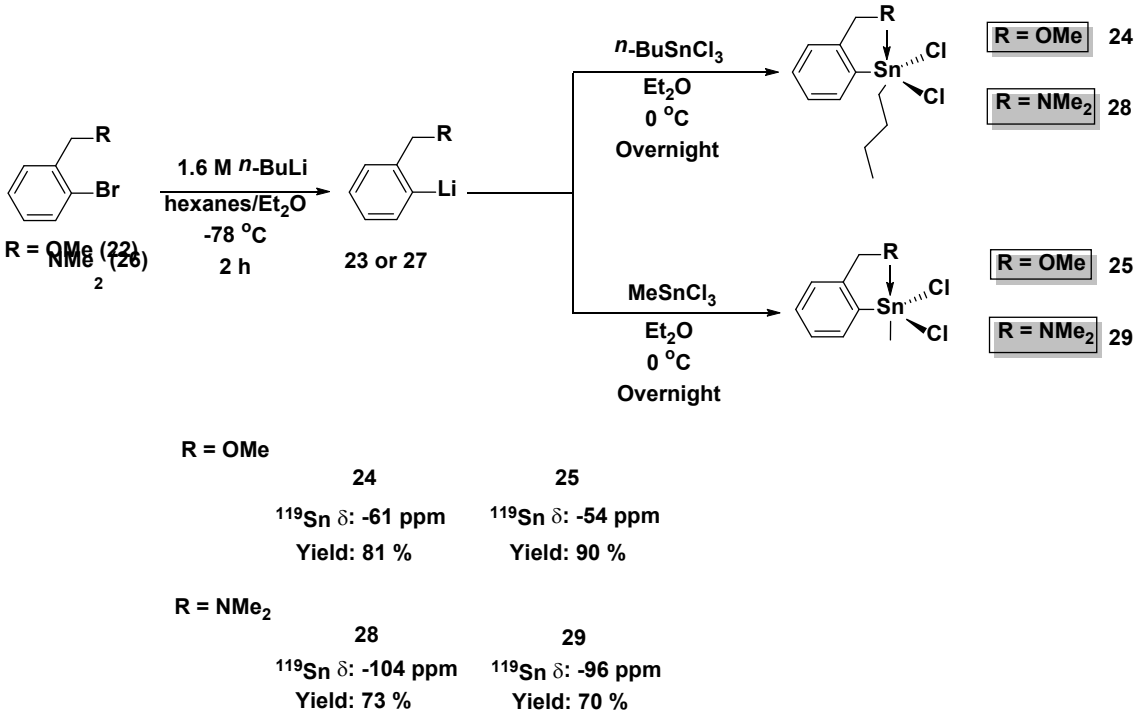

Scheme 16. Synthesis of **22**-**29**.

All four dichlorides (**24**, **25**, **28**, **29**) were hydrogenated by reaction with $LiAlH_4$ in Et_2O. The reactions were quenched with degassed distilled water, extracted and organic layer was kept and dried *in vacuo* (Scheme 17). All four dichlorides could likewise convert to dihydrides using $NaBH_4$ in EtOH as a source. The reaction time was shorter comparing to $LiAlH_4$ which was typically about 2 h. For the work up, degassed dry hexanes was first added into the reaction then followed by addition of degassed distilled water to quench the reaction. The organic layer retains will then hold the dihydride product, which was dried *in vacuo*. Comparing the reactivity of $LiAlH_4$ and $NaBH_4$, the latter is much mild. Although, the reaction took 1 to 1.5 h less time

than the $NaBH_4$, this method was not selected due to the percent yields differences. The $NaBH_4$ reactions are about 10 % yield lower comparing to $LiAlH_4$.

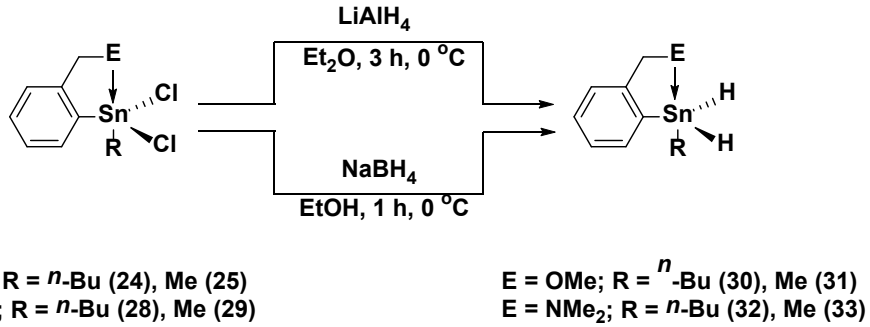

E = OMe; R = *n*-Bu (24), Me (25)
E = NMe_2; R = *n*-Bu (28), Me (29)

E = OMe; R = *n*-Bu (30), Me (31)
E = NMe_2; R = *n*-Bu (32), Me (33)

Scheme 17. Two different pathways to synthesize chelated dihydrides **30**-**33**.

3.2.1 NMR Characterization of *C,O*- and *C,N*- Chelated Organotin Dichlorides and Dihydrides Precursors

The ^{119}Sn NMR ($CDCl_3$) analysis showed a single resonance for **24** (δ = -61.0 ppm), **25** (δ = -54 ppm), **28** (δ = -104 ppm) and **29** (δ = -96 ppm). All four dichlorides follow the trend shifting downfield with halogen as ligands. Table 5 show that both *C,O*- analogue **24** and **25**, is a weaker donor to the Sn center compare to *C,N*- **28** and **29**. The stronger donor NMe_2 gave the tin resonances more upfield at around -100 ppm.

Table 5. The ^{119}Sn NMR ($CDCl_3$) shifts of dichlorides **24**, **25**, **28** and **29**.

Compounds (OMe)	^{119}Sn (δ) ppm	Compounds (NMe_2)	^{119}Sn (δ) ppm
24	-61	**28**	-104
25	-54	**29**	-96

The ^{1}H NMR spectrum of **30** (Figure 43) reveals distinctly large $^{119/117}Sn$-H coupling constants for the hydride signals. The ^{119}Sn NMR chemical shifts for **30** and **31** are shifted upfield compared to four coordinate tin dihydride analogues without chelating donor atoms. By comparing to **32** and **33**, the *C,N*- analogue also shows the same trend with the dichlorides shifting more upfield with stronger donor to *C,O*-.

C,N- containing tin dihydrides **32** and **33** possess a downfield ^{1}H NMR (C_6D_6) resonance (δ = 5.62 ppm and δ = 5.73 ppm) compared to tetracoordinated stannyl dihydrides ((*n*-Bu)$_2$SnH$_2$: δ = 4.78 ppm and Me$_2$SnH$_2$: δ = 4.46 ppm).[23,67] Another characteristic of the hypervalent amine diorganotin hydrides is that the $^{1}J_{119Sn\text{-}1H}$ coupling constants for **32** (1760 Hz) and **33** (1824 Hz) are slightly larger than those observed for tetrahedral coordinated diorganotin hydride analogues ((*n*-Bu)$_2$SnH$_2$ = 1675 Hz, Me$_2$SnH$_2$ = 1758 Hz). The ^{119}Sn chemical shifts of trigonal bipyramidal **32** and **33** stannanes are significantly more shielded compared to their structurally closest tetrahedrally coordinated analogs and are consistent with other reported chelating amino diorganotin dihydrides (Table 6).[68]

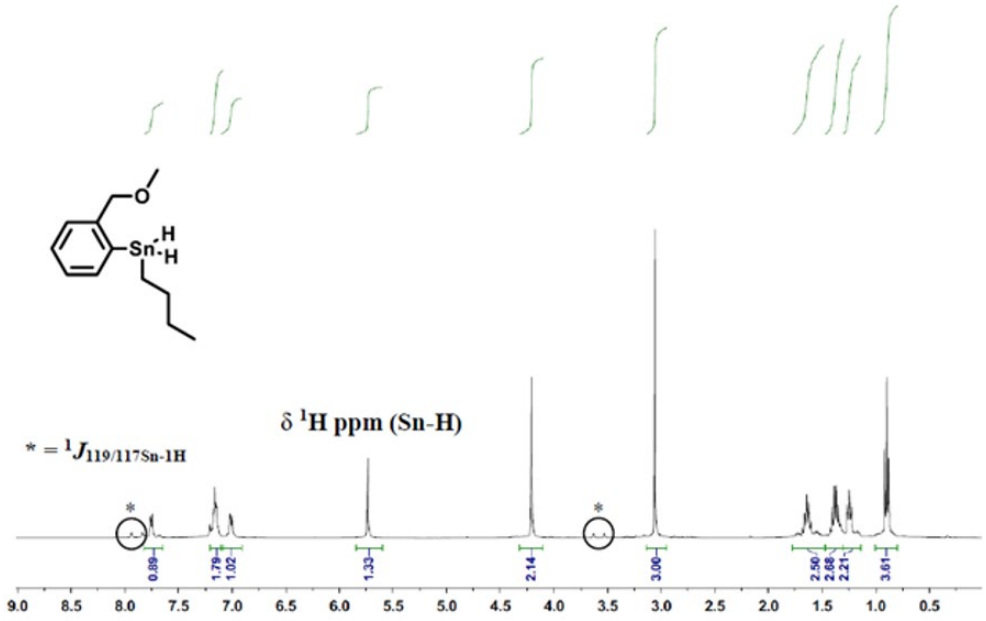

Figure 43. ^{1}H NMR (C_6D_6) spectrum of **30**.

Table 6. The ^{119}Sn NMR (C_6D_6) shifts of dihydrides **30**-**33**.

Compounds (OMe)	^{119}Sn (δ) ppm	Compounds (NMe_2)	^{119}Sn (δ) ppm
30	-210	**32**	-218
31	-223	**33**	-236

3.3.1 Single Crystal X-ray Analysis of *C,N*- Chelated Organotin Dichlorides

Compound **29** was crystallized by a previous PhD graduate, Aman A. Khan, from a CH_2Cl_2/hexanes (1:1) solution via slow evaporation and the molecular structure obtained by single crystal XRD (Figure 44). The geometry at the Sn center is distorted trigonal bipyramidal. A significant N→Sn intramolecular interaction is revealed by the short Sn-N distance (2.4082(13) Å). The N(1)-Sn(1)-Cl(2) bond angle is slightly distorted at 173.00 (3)º

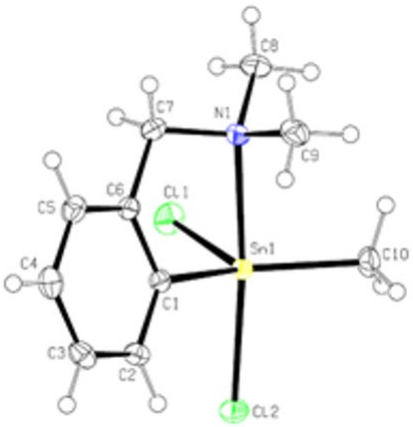

Figure 44. Molecular structure of **29**. Selected interatomic distances [Å]and angles [º]: Sn(1)-C(10) 2.1146(15), Sn(1)-C(1) 2.1156(15), Sn(1)-Cl(1) 2.3764(4), Sn(1)-N(1) 2.4082(13), Sn(1)-Cl(2) 2.4696(4), C(10)-Sn(1)-Cl(1) 111.39(5), C(1)-Sn(1)-Cl(1) 107.80(4), C(10)-Sn(1)-N(1) 92.46(6), C(1)-Sn(1)-N(1) 76.60(5), Cl(1)-Sn(1)-N(1) 88.33(3), C(10)-Sn(1)-Cl(2) 93.30(5), C(1)-Sn(1)-Cl(2) 96.42(4), Cl(1)-Sn(1)-Cl(2) 93.273(15), N(1)-Sn(1)-Cl(2) 173.00(3).

3.4.1 Polymerisation of *C,O*- and *C,N*- Chelated Organotin Dihydrides

Dehydrocoupling of the hypercoordinated compounds **30** and **32** was attempted using Wilkinson's catalyst. The *C,O*- and *C,N*- dihydride butyl monomers were selected to ensure good solubility and processability of any resulting polymer. Polymerisation conditions like those used previously for flexible stannanes in Chapters 1 and 2 were employed for the more rigid *C,O*- and *C,N*- stannanes. The polymerisations were carried out at RT in the absence of light in foil wrapped Schlenk flasks with 10 mL of degassed toluene containing 4 mol % of the Wilkinson's catalyst to which the monomer in the same solvent (6 mL) was slowly added and stirred for 4 h (Scheme 18).

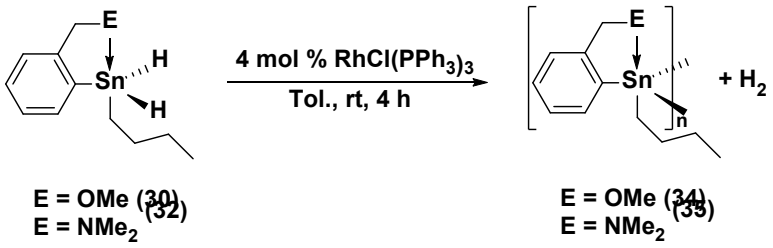

Scheme 18. Synthesis of rigid polystannanes **34** and **35**.

3.5.1 Characterizations of *C,O*- and *C,N*- Chelated Rigid Polystannanes

A yellow coloured polymer **34** was recovered from the dehydrocoupling of **30** in good yield (65 %), while a much darker yellow coloured polymer **35** was recovered from the polymerisation **32** in poor yield (18 %). After several attempts, only modest molecular weights were obtained for both rigid polymers (**34**: $M_w = 3.03 \times 10^4$ Da, PDI = 1.4, **35**: $M_w = 3.10 \times 10^4$ Da, PDI = 1.86). The degree of polymerisation is approximately 100 monomer units for **34** and 70 for **35** (Figure 45). However, trace oligomers of **35** were still observed within the polymer even after several purifications.

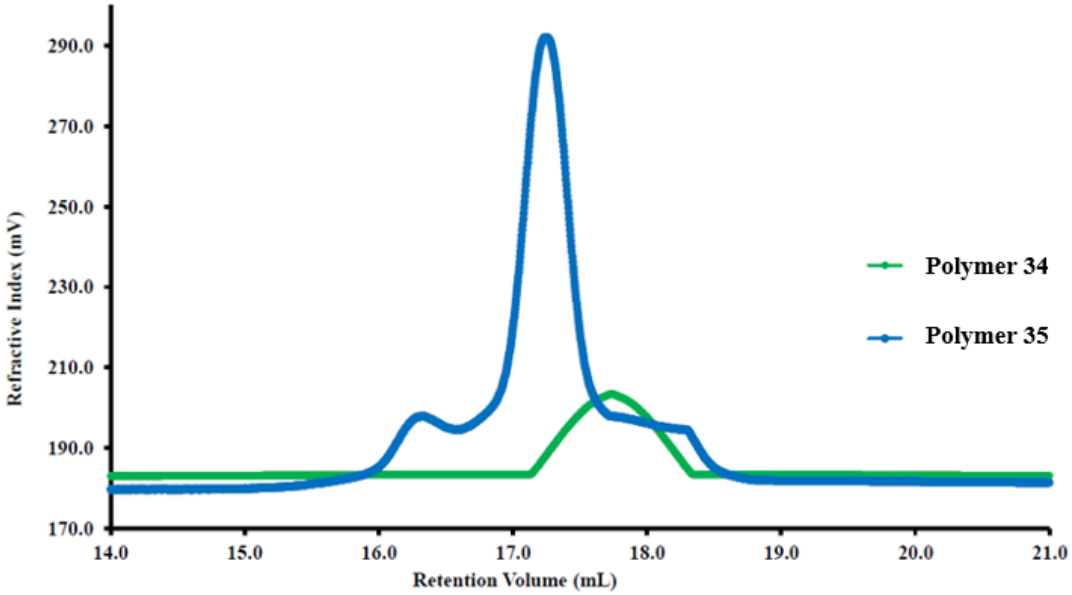

Figure 45. GPC of **34** and **35**. Refractive index (R.I.) trace shown for clarity.

Analysis by ^{1}H and ^{13}C NMR spectroscopy confirmed the expected polymer structures. The ^{119}Sn NMR spectroscopic evaluations of both compounds in two different deuterated

solvents (C_6D_6 and THF-d_8) reveals structural details (studies in Chapter 2).[69] Figure 46 (bottom) shows the presence of two resonances for **34**, with one substantially downfield (δ = -49 ppm) and the other shifted 150 ppm upfield. When **34** was run in THF-d_8 (Figure 46 middle), a known coordinating solvent, only a single resonance at δ = -44 ppm was observed. This would suggest that large excess of THF molecules were effectively displacing the Sn-O dative interaction of the chelating ligand, causing the complex to be effectively in an "open" position. When the THF-d_8 was removed from the solvent and redissolved in C_6D_6, (Figure 46 top) the sample did not return to its initial closed position, and no resonance at δ = -199.3 ppm was detected.

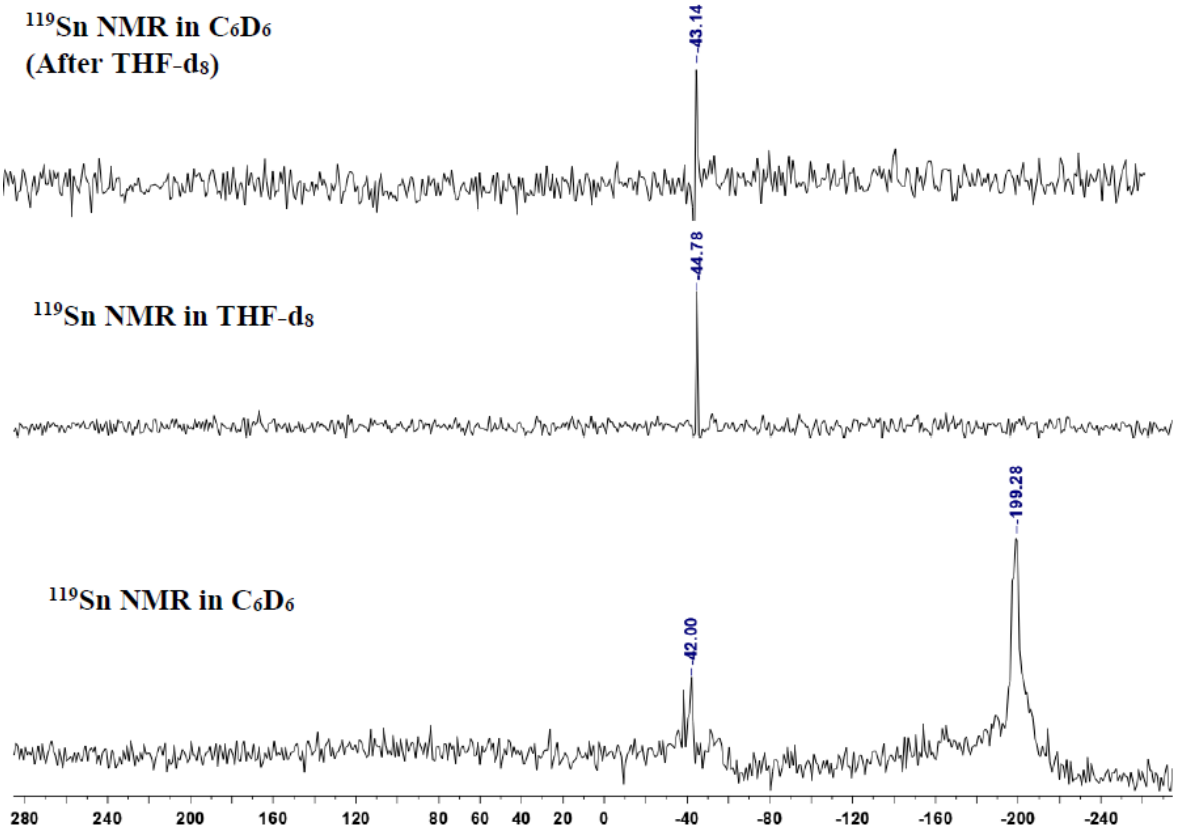

Figure 46. ^{119}Sn NMR of **34** in two different solvents: bottom C_6D_6, middle THF-d_8, and THF-d_8 sample dried and redispersed in C_6D_6.

When the same set of experiments were carried out for polymer **35**, only one upfield resonance at -149 ppm in C_6D_6 was observed (Figure 47 bottom), while the same sample in THF-d_8 (Figure 47 mid) showed two clear resonances similar to **34**, but with only a partial

redistribution from the upfield "closed" resonance to the "open" downfield resonance. When the THF-d_8 sample was resuspended in C_6D_6, and unlike polymer **34** (Figure 47 top) all of the "open" structural isomers returned to the "closed" state. This is good evidence that the NMe_2 functionality of **35** are more strongly donating and coordinating to Sn than the OMe functionality of **34**. This also suggests that the ability of these rigid dihydride monomers to undergo dehydrocoupling may be impacted by the strength of these dative interactions, which lead to low yields in the case of **32**.

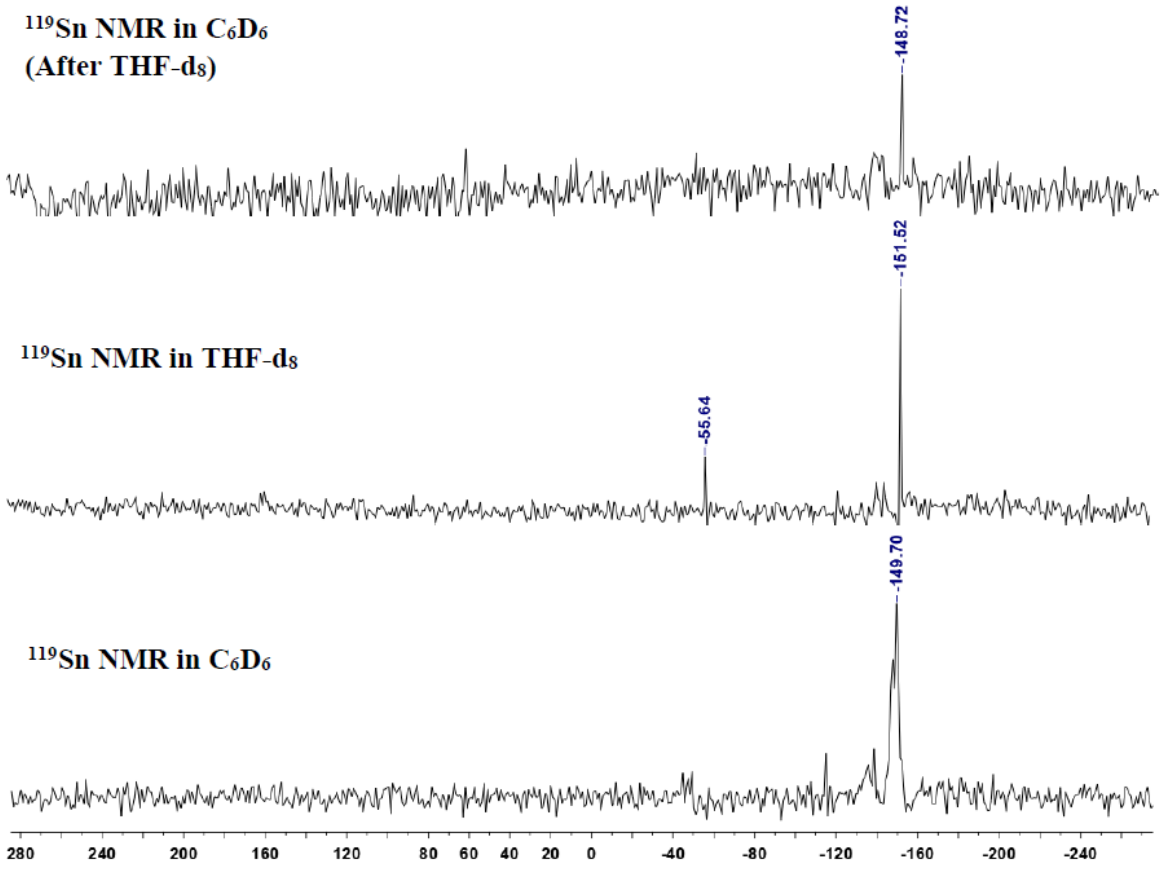

Figure 47. ^{119}Sn NMR of **35** in two different solvents: bottom C_6D_6, middle THF-d_8, and THF-d_8 sample dried and redispersed in C_6D_6.

A DSC study of **34** and **35** revealed the two polymers to have amorphous character absent of any crystalline behaviour. As shown in Figures S98 and S99, nearly identical T_g's near 11.5 ºC were recorded. The polymers showed no thermal behaviour changes when

annealed prior to running or after multiple scans. Unfortunately, at these low molecular weights, no polymer film could be prepared.

Conclusion

A series of known *C,O*- and *C,N*- rigid small molecule stannanes were prepared and characterized. Polymerisation of *C,O*- and *C,N*- dihydrides **30** and **32** using Wilkinson's catalyst has led to the first examples of modest molecular weight rigidly hypercoordinated polystannanes **34** and **35** respectively. Polymer characterization by DSC of **34** and **35** display relatively low T_gs, amorphous polymers. The polymers appear to be indefinitely stable to both air and moisture. If higher molecular weights are obtained through improved catalyst selection and polymerisation conditions, these rigid hypercoordinated polystannanes may be good candidates for polymeric wires.

EXPERIMENTAL

Material and Methods: Syntheses were carried out using standard Schlenk and glovebox protocols. ^{1}H NMR (400 MHz), ^{13}C{^{1}H} NMR (100.6 MHz), and ^{119}Sn{^{1}H} NMR (79.5 MHz) spectra for small molecules were recorded on a Bruker Avance 400 MHz NMR spectrometer with a 5 mm broad band fluorine observation (BBFO) direct probe. A ^{1}H pulse width of 308 was used, acquiring a spectral window of 8223 Hz (20 ppm) using relaxation delay of 1 s, acquisition time of 3.98 s, and acquiring 32000 points (16 scans). The ^{1}H 908 pulse width was 10.4 μs. A ^{13}C pulse width of ^{1}H 308 pulse width was used acquiring a spectral window of 24038 Hz (239 ppm) using relaxation delay of 2 s, acquisition time of 1.36 s, and acquiring 32000 points (4096 scans). The ^{13}C 908 pulse width was 8.7 μs. A ^{119}Sn 308 pulse width of was 8.75 μs, acquiring a spectral window of 100000 Hz (670 ppm), using a relaxation delay of 1 s, acquisition time of 0.33 s, and acquiring 32000 points (15360 scans) with inverse gated proton decoupling. ^{1}H and ^{13}C resonances were referenced internally to the deuterated solvent signals. All chemical shifts are given in δ (ppm) relative to the solvent and assigned to atoms. All *J* coupling values are reported as absolute values. Additional 1D ^{13}C and ^{119}Sn NMR data for polymers were acquired at the CSICOMP NMR facility at the University of Toronto. 1D ^{13}C NMR spectra were acquired using an Agilent DD2 spectrometer [n(^{13}C); 125.653 MHz, n(^{1}H); 499.663 MHz] equipped with either a 5 mm XSens ^{13}C-sensitive cold probe (Agilent Technologies, Inc., Santa Clara, USA). The 1D ^{13}C{^{1}H} NMR spectra were acquired with a standard CARBON pulse sequence at 25 °C, over a 30487.8 Hz spectral window with a 308 pulse width, 121952 points, a 0.2 s recycle delay, and 3200 transients. 1D ^{119}Sn spectra were acquired using an Agilent DD2 spectrometer [n(^{119}Sn); 186.378 MHz, n(^{1}H); 499.875 MHz] equipped with a OneNMR probe (Agilent Technologies, Inc., Santa Clara, USA). The 1D ^{119}Sn{^{1}H} NMR spectra were acquired with an s2pul pulse sequence at 25°C, over a 56818.2 Hz spectral window with a 458 pulse width, 113636 points, a 1.0 s recycle delay, and 5000 transients. Inverse gated proton decoupling was applied.

Elemental analysis was performed by Atlantic Microlab, Inc. of Norcross, GA, USA. Time-of-flight MS analyses were performed using a JMS-T1000LC mass spectrometer (JEOL Inc., Peabody, MA, USA) equipped with a direct analysis in real time (DART) ionization source (DART-SVP, Ionsense Inc., Saugus, MA, USA) at the University of Toronto. The DART source was operated with He gas, and the temperature was adjusted in the range 100–400 °C. Isotopic distributions for the observed ionic species were calculated using the Mass Center utility (JEOL) and were in good agreement with the measured mass spectra. All reagents and solvents were obtained from Sigma–Aldrich and used as received. Column chromatography was carried out on silica gel. Refractive index values were determined using TLC silica gel 60 aluminum-backed plates, eluting with the solvent system indicated below for each compound. Melting points were measured in open air using a Fischer Scientific melting point apparatus. Absolute molecular weights of polymers were determined by gel permeation chromatography (GPC) using a Viscotek Triple Model 302 Detector system equipped with a Refractive Index Detector (RI), a four-capillary differential viscometer (VISC) and a right angle (90°) laser light scattering detector. GPC columns were calibrated versus polystyrene standards (American Polymer Standards). A flow rate of 1.0 mL/min was used with ACS grade THF as eluent. GPC sample were prepared using 10–15 mg of polymers per mL THF and filtered using a 0.45 micron filter. UV/Vis absorption spectroscopy was carried out using a PerkinElmer Lambda 40 UV/Vis system. The University of Toronto X-ray Crystallography Lab was used to obtain X-ray structural information for compounds. Data was collected on a Bruker Kappa APEXDUO diffractometer using monochromatic Mo_{Ka} radiation (Bruker Triumph) and were measured using a combination of φ scans and ω scans. The data was processed using APEX2 and SAINT1 programs. Absorption corrections were carried out using SADABS software. The structures were solved using SHELXT2 and refined using SHELXL-20132 for full-matrix least-squares refinement that was based on F2.

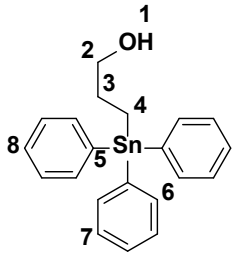

***Preparation of 3-(Triphenylstannyl) propan-1-ol* 1**

Prop-2-en-1-ol (0.80 mL, 13.70 mmol) was added to a clean, dry 50 mL Schlenk flask *via* syringe. Ph_3SnH (1.46 g, 4.15 mmol) and 2 mol % AIBN (45.00 mg, 0.27 mmol) were added to the allyl alcohol. The flask was evacuated, back filled with nitrogen and heated at 80-90 °C for 3 h. A white coloured solid formed when the solution cooled. The crude sample of **1** was washed with hexanes (3 × 10 mL) and the white coloured solid isolated by vacuum filtration. Yield 99.0 %; (1.45 g). mp 105 °C. ^{1}H NMR (400 MHz, $CDCl_3$, δ): 7.57-7.55 (m, 5H, H6), 7.38-7.37 (m, 10H, H7 & H8), 3.64 (t, $^3J_{H\text{-}H}$ = 6 Hz, 2H, H2), 2.01-1.94 (m, *2*H, H3), 1.53-1.29 (m, 2H, H4) ppm; $^{13}C\{^1H\}$ NMR (100 MHz, $CDCl_3$, δ): 139.1 (C5), 137.1 (C6), 128.9 (C8), 128.6 (C7), 65.7 (C2), 29.4 (C3), 6.7 (C4) ppm; ^{119}Sn NMR (79.5 MHz, $CDCl_3$, δ): -99.2 ppm. These data agree well with previous reports.[54]

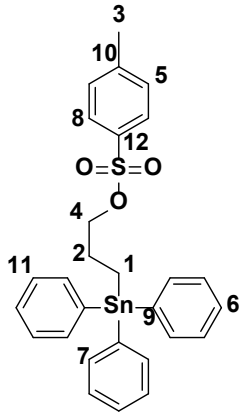

***Preparation of 3-(Triphenylstannyl) propyl 4-methylbenzenesulfonate* 2**

Compound **1** (0.65 g, 1.59 mmol), *p*-toluenesulfonyl chloride (*p*-TsCl) (0.45 g, 2.38 mmol), triethylamine (Et_3N) (0.32 mL, 3.18 mmol) and trimethylamine hydrochloride (Me_3N•HCl) (0.15 g, 1.59 mmol) were added to a dry, clean 50 mL round bottom flask containing DCM (≈ 20 mL) and stirred for 2 h. The solution was then extracted with water (3 × 20 mL). The organic

extracts were dried over $MgSO_4$ and further dried *in vacuo* to obtain a transparent highly viscous semisolid of **2**. Yield 60 % (0.39 g). ^{1}H NMR (400 MHz, $CDCl_3$, δ): 7.77-7.75 (m, 2H, H8), 7.53-7.51 (m, 6H, H7), 7.41-7.39 (m, 9H, H6 & H11), 7.33- 7.31 (m, *2*H, H5), 4.04 (t, $^3J_{H-H}$ = 8 Hz, 2H, H4), 2.45 (s, 3H, H3), 2.07-1.99 (m, 2H, H2), 1.44-1.40 (m, 2H, H1) ppm; $^{13}C\{^1H\}$ NMR (100 MHz, $CDCl_3$, δ): 144.6 (C12), 137.9 (C9), 136.9 (C7), 133.1 (C10), 129.8 (C8), 129.1 (C6), 128.6 (C11), 127.8 (C5), 73.0 (C4), 26.0 (C2), 21.6 (C3), 5.8 (C1) ppm; ^{119}Sn NMR (79.5 MHz, $CDCl_3$, δ): -99.7 ppm.

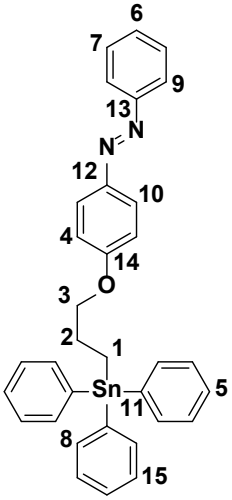

***Preparation of (E)/(Z)-1-phenyl-2-(4-(3-triphenylstannyl-propoxy)phenyl)diazene* 3**

Compound **2** (0.70 g, 1.24 mmol) and 4-hydroxyazobenzene (0.25 g, 1.24 mmol) along with K_2CO_3 (0.34 g, 2.49 mmol) were added in a 100 mL Schlenk flask containing acetone (≈ 50 mL) respectively. The solution was then heated to reflux temperature (90 °C) for 18 h in a sealed flask and then allowed to cool. After the removal of solvent under reduced pressure, the residue was extracted with Et_2O (3 × 10 mL). The organic extracts were first dried over $MgSO_4$, and finally the solvent removed *in vacuo* to obtain an orange coloured solid. Compound **3** was further purified by preparative column chromatography on silica gel eluted with 4:1 ratio of hexanes/ethyl acetate. Yield 70 % (0.51 g); mp 104 °C. ^{1}H NMR (400 MHz, $CDCl_3$, δ): 7.90-7.86 (m, 4H, H9 & H10), 7.59-7.57 (m, 5H, H8), 7.56-7.53 (m, 3H, H7), 7.51-7.49 (m, 1H, H6), 7.46-7.37 (m, 10H, H15 & H5), 6.90-6.87 (m, 2H, H4), 4.04 (t, $^3J_{H-H}$ = 6 Hz, 2H, H3), 2.29-2.22 (m, *2*H, H2), 1.68-1.64 (m, 2H, H1) ppm; $^{13}C\{^1H\}$ NMR (100 MHz, $CDCl_3$, δ): 161.4

(C12), 152.8 (C13), 146.9 (C14), 138.5 (C11), 137.0 (C8), 129.0 (C6), 129.0 (C5), 128.6 (C15), 124.7 (C4), 122.5 (C9), 114.7 (C10), 70.8 (C3), 26.2 (C2), 6.8 (C1) ppm; ^{119}Sn NMR (79.5 MHz, $CDCl_3$, δ): -99.6 ppm. HRMS-DART (m/z) = 591.14584 (M + H) calculated for $^{12}C_{33}{}^{1}H_{31}{}^{14}N_2{}^{16}O_1{}^{120}Sn_1$; found 591.14685. UV-Vis (C_6H_6) (*trans*-/*cis*-) λ_{max} (ε, L mol^{-1} cm^{-1}); (*trans*-) 348 nm (14791), (*cis*-) 443 nm (1413), (*cis*-) 443 nm (2512).

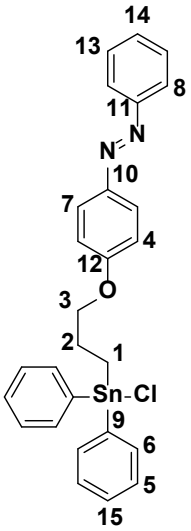

***Preparation of (E)-1-(4-(3-(chlorodiphenylstannyl)-propoxy)phenyl)-2-phenyldiazene* 4**

In a sealed 100 mL Schlenk flask containing a solution of compound **3** (0.20 g, 0.34 mmol) in C_6H_6 (≈ 20 mL) was added 1.0 M HCl/Et_2O (0.34 mL, 0.34 mmol) by syringe and stirred at room temperature for 1 h. The pure product was precipitated in hexane (3 × 10 mL). After removal of solvent (decanting), the residual solvent was removed *in vacuo* to obtain a bright yellow solid. A pure sample of compound **4** was obtained. Yield 88 % (0.18 g); mp 129-130 °C. ^{1}H NMR (400 MHz, $CDCl_3$, δ): 7.86-7.84 (d, $^3J_{H\text{-}H}$ = 7.6 Hz, 2H, H8), 7.72-7.70 (d, $^3J_{H\text{-}H}$ = 8.9 Hz, 2H, H7), 7.66-7.64 (m, 4H, H6), 7.51-7.47 (m, 3H, H13 & H14), 7.45-7.37 (m, 10H, H5, H6 & H15), 6.67-6.65 (m, 2H, H4), 4.14 (t, $^3J_{H\text{-}H}$ = 5.5 Hz, 2H, H3), 2.46- 2.40 (m, *2*H, H2), 2.04-1.86 (tt, $^2J_{1H\text{-}1H}$ = 7 Hz, $^2J_{119Sn\text{-}1H}$ = 33 Hz, 2H, H1) ppm; ^{13}C{^{1}H} NMR (100 MHz, $CDCl_3$, δ): 160.2 (C10), 152.6 (C11), 147.3 (C12), 139.2 (C9), 135.9 (C6), 130.0 (C14), 129.0 (C15), 128.8 (C5), 124.3 (C4), 122.5 (C8), 115.1 (C7), 70.3 (C3), 25.6 (C2), 14.1 (C1) ppm; ^{119}Sn NMR (79.5 MHz, $CDCl_3$, δ): -15.2 ppm. HRMS-DART (m/z) = 549.07556 (M + H)

calculated for $^{12}C_{27}{}^{1}H_{26}{}^{35}Cl_{1}{}^{14}N_{2}{}^{16}O_{1}{}^{120}Sn_{1}$; found 549.07585. UV-Vis (C_6H_6) (*trans*-/*cis*-) λ_{max} (ε, L mol^{-1} cm^{-1}); (*trans*-) 345 nm (21878), (*cis*-) 440 nm (166), (*cis*-) 440 nm (2188).

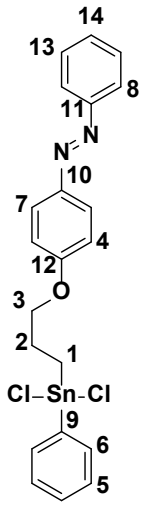

***Preparation of (E)-1-(4-(3-(dichloro(phenyl)stannyl-propoxy)phenyl)-2-phenyldiazene* 5**

In a sealed 100 mL Schlenk flask a C_6H_6 (≈ 20 mL), solution of **4** (0.20 g, 0.39 mmol) was first prepared and 1.0 M HCl/Et_2O (0.40 mL, 0.39 mmol) was next added by syringe and stirred at room temperature for 1 h and sampled by ^{1}H NMR to test for completion. Additional aliquots of the 1.0M HCl/Et_2O solution was added until the reaction was brought to completion. The solution was then precipitated into dry hexanes (≈ 20 mL) and the recovered solids dried *in vacuo* to obtain a dark red coloured solid of **5**. Yield 91 % (0.18 g); mp 106-107 °C. ^{1}H NMR (400 MHz, $CDCl_3$, δ): 7.86-7.85 (d, $^3J_{H\text{-}H}$ = 7.4 Hz, 2H, H8), 7.76-7.74 (d, $^3J_{H\text{-}H}$ = 8.8 Hz, 2H, H7), 7.64-7.62 (m, 2H, H6), 7.50-7.48 (m, 3H, H5), 7.40-7.36 (m, 3H, H13 & H14), 6.80-6.78 (m, 2H, H4 & H12), 4.20 (t, $^1J_{H\text{-}H}$ = 5.3 Hz, 2H, H3), 2.54-2.48 (m, *2*H, H2), 2.19-2.16 (tt, $^2J_{1H\text{-}1H}$ = 6.8 Hz, $^2J_{119Sn\text{-}1H}$ = 37.3 Hz, 2H, H1) ppm; $^{13}C\{^1H\}$ NMR (100 MHz, $CDCl_3$, δ): 159.6 (C12), 152.6 (C11), 147.7 (C10), 139.9 (C9), 134.8 (C6), 130.6 (C14), 129.0 (C15), 128.3 (C5), 124.3 (C7), 122.6 (C12), 115.8 (C4), 69.8 (C3), 25.0 (C2), 22.1 (C1) ppm; ^{119}Sn NMR (79.5 MHz, $CDCl_3$, δ): -9.0 ppm. HRMS-DART (m/z) = 507.00529 (M + H) calculated for $^{12}C_{21}{}^{1}H_{21}{}^{35}Cl_{2}{}^{14}N_{2}{}^{16}O_{1}{}^{120}Sn_{1}$: 507.00556. UV-Vis ($C_6H_6$) (*trans*-/*cis*-) λ_{max} (ε, L mol^{-1} cm^{-1}); (*trans*-) 345 nm (2291), (*cis*-) 444 nm (1023), (*cis*-) 444 nm (3020).

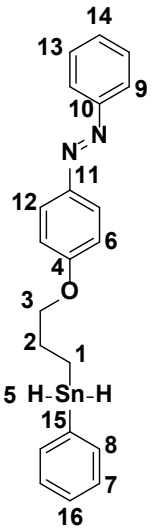

***Preparation of (E)-1-phenyl-2-(4-(3-(phenylstannyl)-propoxy)phenyl)diazene* 6**

An etheral solution (30 mL) containing **5** (0.18 g, 0.36 mmol) and a solution of $NaBH_4$ in EtOH (0.13, 3.56 mmol) were added to 100 mL Schlenk flask, and stirred at 0 °C for 10 min. The reaction was allowed to warm to room temperature and stirred for an additional 15 min. 50 mL of 5 °C degassed distilled water was added to the solution containing **6** over 30 min and stirred. The solution was then extracted with hexanes (3 × 20 mL) and dried over $MgSO_4$. The solvent was removed under reduced pressure to obtain a transparent orange – yellow coloured powder. Yield 78 % (0.14 g). ^{1}H NMR (400 MHz, C_6D_6, δ): 8.09-8.07 (m, 4H, H9 & H12), 7.45-7.43 (m, 2H, H8), 7.24-7.20 (m, 3H, H13 & H14), 7.14-7.09 (m, 3H, H7 & H8), 6.80-6.77 (m, 2H, H6), 5.51 (s, 2H, H5), 3.46 (t, $^{3}J_{H\text{-}H}$ = 6.1 Hz, 2H, H3), 1.89-1.69 (tq, $^{2}J_{1H\text{-}1H}$ = 13.8 Hz, $^{2}J_{119Sn\text{-}1H}$ = 34.3 Hz, 2H, H2), 1.04-1.00 (m, 2H, H1) ppm; ^{13}C{^{1}H} NMR (100 MHz, C_6D_6, δ): 161.4 (C11), 153.1 (C10), 147.3 (C4), 137.3 (C15), 136.0 (C8), 130.1 (C14), 128.9 (C16), 128.6 (C7), 124.9 (C6), 122.7 (C9), 114.7 (C12), 70.0 (C3), 26.8 (C2), 4.4 (C1) ppm; ^{119}Sn NMR (79.5 MHz, C_6D_6, δ): -214.5 ppm. HRMS-DART (m/z) = 439.01754 (M + H) calculated for $^{12}C_{21}{}^{1}H_{23}{}^{14}N_2{}^{16}O_1{}^{120}Sn_1$: 438.0745. UV-VIS ($C_6H_6$) (*trans*-/*cis*-) λ_{max} (ε, L mol^{-1} cm^{-1}); (*trans*-) 349 nm (350), (*cis*-) 445 nm (14), (*cis*-) 445 nm (45).

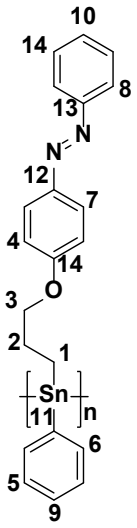

Preparation of homopolymer 7-f

A toluene solution (9 mL) containing $RhCl(PPh_3)_3$ (0.02 g, 0.02 mmol) was added to a foil wrapped 50 mL Schlenk flask, and stirred at room temperature (20 min) for activation. Thereafter, **6** in 9 mL of toluene (0.25 g, 0.57 mmol) was added dropwise over 20 min to the catalyst solution. The reaction was stirred at RT for 4 h. The mixture was then reduced in volume (*vacuo*) to roughly 5 mL and using a double tipped cannula, transferred to a 100 mL foil wrapped Schlenk flask contained a stirring solution of cold hexanes. An orange-yellow precipitate formed immediately, and the solution was stirred for additional 5 min and then allowed to settle. The top layer of the solution was then extracted using a double tipped cannula needle. The residues were dried *in vacuo* to obtain a transparent orange coloured semi-solid. Yield 77 % (0.19 g). ^{1}H NMR (400 MHz, C_6D_6, δ): 8.07 (bm, 4H, H7 & H8), 7.59 (bm, 2H, H6), 7.21 (bm, 4H, H14 & H5), 7.10-6.76 (bm, 4H, H4, H10& H9), 3.67-3.34 (bm, 2H, H3), 1.85-1.23 (bm, 4H, H2 & H1) ppm; $^{13}C\{^{1}H\}$ NMR (100 MHz, C_6D_6, δ): 161.4 (C12), 153.1 (C13), 147.3 (C14), 137.3 (C11), 136.0 (C6), 130.1 (C10), 128.9 (C9), 128.6 (C5), 124.9 (C4), 122.7 (C8), 114.7 (C7), 70.0 (C3), 26.8 (C2), 4.4 (C1) ppm; ^{119}Sn NMR (79.5 MHz, C_6D_6, δ): -236.0 ppm. E.A.: Anal. Calcd. C, 57.97; H, 4.63. Found: C, 54.81, H: 4.63. UV-Vis (C_6H_6) (*trans*-/*cis*-) λ_{max} (ε, L mol^{-1} cm^{-1}); (*trans*-) 348 nm (2270), (*cis*-) 441 nm (96), (*cis*-) 441 nm (180).

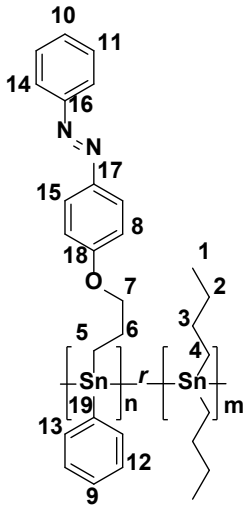

***Preparation of random co-polymer* 8a (4:1)**

A toluene solution (9 mL) containing $RhCl(PPh_3)_3$ (0.03 g, 0.02 mmol) were added to a foil wrapped 50 mL Schlenk flask, and stirred at RT (20 min) for activation. Thereafter, **6** (0.30 g, 0.68 mmol) and $(n\text{-}Bu)_2SnH_2$ (0.65 g, 2.75 mmol) in 9 mL of toluene were added dropwise over 20 min into the catalyst solution. The reaction stirred at RT for 4 h. The mixture was then reduced in volume (*in vacuo*) to roughly 5 mL and using a double tipped cannula, transferred to a 100 mL foil wrapped Schlenk flask contained a solution of cold hexanes. With stirring, an orange yellow precipitate formed immediately, and the solution was allowed to stir for extra 5 min then settled into two layers. The top layer was then isolated by double tipped. The remaining residues were dried under reduced pressure to obtain a transparent orange coloured gel. Yield 46 % (0.21 g). ^1H NMR (400 MHz, C_6D_6, δ): 8.07 (bm, 4H, H14 & H15), 7.72 (bm, 2H, H13), 7.21 (bm, 4H, H11 & H12), 7.02-6.81 (bm, 4H, H8, H10 & H9), 3.60-3.56 (bm, 2H, H7), 1.89-1.04 (bm, 22H, H1-H6) ppm; $^{13}C\{^1H\}$ NMR (100 MHz, C_6D_6, δ): 161.6 (C17), 152.8 (C16), 147.1 (C18), 134.6 (C19), 132.0 (C13), 131.9 (C10), 131.1 (C9), 128.9 (C12), 125.0 (C8), 122.7 (C14), 114.3 (C15), 71.2 (C7), 28.1 (C5), 27.9 (C4), 24.4 (C6), 24.0 (C3), 22.6 (C2), 13.8 (C1) ppm; ^{119}Sn NMR (79.5 MHz, C_6D_6, δ): -167.9 ppm, -242.6 ppm. E.A.: Anal. Calcd. C, 46.57; H, 6.78. Found: C, 47.68, H: 5.40. UV-Vis (C_6H_6) (*trans*-/*cis*-) λ_{max} (ε, L mol^{-1} cm^{-1}); (*trans*-) 349 nm (7147), (*cis*-) 445 nm (796), (*cis*-) 446 nm (862).

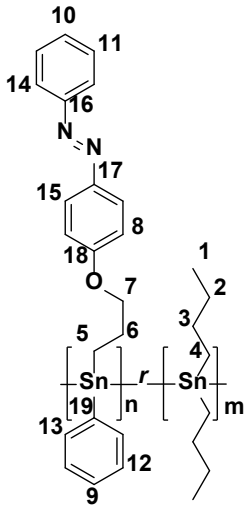

***Preparation of random co-polymer* 8b (1:1)**

A toluene solution (9 mL) containing $RhCl(PPh_3)_3$ (0.02 g, 0.02 mmol) was added to a foil-wrapped 50 mL Schlenk flask, and stirred at RT (20 min) for activation. After 20 m, **6** (0.24 g, 0.55 mmol) and $(n\text{-}Bu)_2SnH_2$ (0.13 g, 0.55 mmol) in 9 mL of toluene were added dropwise over 20 min into the catalyst solution. The reaction was stirred at RT for 4 h. The mixture was then reduced in volume (*in vacuo*) to roughly 5 mL and using a double tipped cannula, transferred to a 100 mL foil wrapped Schlenk flask contained a solution of cold hexanes. With stirring, an orange yellow coloured precipitate formed immediately, and the solution was stirred for additional 5 min, and allowed to settle into two layers. The top layer was then extracted out using a double-tipped cannula, and the remaining residues dried (*in vacuo*) to obtain a transparent orange coloured gel. Yield 58 % (0.21 g). ^1H NMR (400 MHz, C_6D_6, δ): 8.09 (bm, 4H, H14 & H15), 7.67 (bm, 2H, H13), 7.21 (bm, 4H, H11 & H12), 7.00-6.77 (bm, 4H, H8, H10 & H9), 3.59-3.55 (bm, 2H, H7), 1.85-1.09 (bm, 22H, H1-H6) ppm; $^{13}C\{^1H\}$ NMR (100 MHz, C_6D_6, δ): 161.6 (C18), 153.0 (C17), 147.1 (C16), 134.8 (C19), 132.0 (C13), 131.3 (C10), 130.1 (C9), 128.9 (C12), 125.0 (C8), 122.7 (C14), 114.6 (C15), 70.7 (C7), 28.1 (C5), 27.6 (C4), 25.4 (C6), 24.5 (C3), 22.6 (C2), 13.8 (C1) ppm; ^{119}Sn NMR (79.5 MHz, C_6D_6, δ): -161.6 ppm, -240.7 ppm. E.A.: Anal. Calcd. C, 52.14; H, 5.73. Found: C, 50.92, H: 5.17. UV-Vis (C_6H_6) (*trans*-/*cis*-) λ_{max} (ε, L mol^{-1} cm^{-1}); (*trans*-) 348 nm (83843), (*cis*-) 445 nm (3517), (*cis*-) 445 nm (5223).

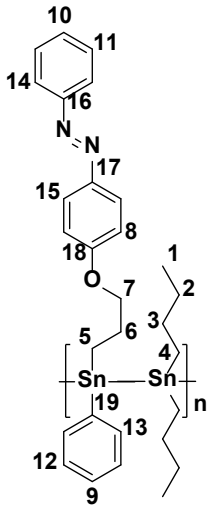

***Preparation of alternating polymer* 9**

An etheral solution (9.00 mL) containing **6** (0.25 g, 0.57 mmol) was cooled to -20 °C in a foil-wrapped 50 mL Schlenk flask. Another 50 mL Schlenk flask contained a solution of 1,1-dibutyl-*N,N,N′,N′*-tetraethylstannanediamine, (*n*-Bu)$_2$Sn(NEt$_2$)$_2$ (0.22 g, 0.57 mmol) in 9.00 mL EtOH was also cooled to 0 °C. The alcoholic solution containing the amide was added dropwise (20 min) to the cold (-20 °C) etheral solution containing **6** with stirring. The reaction was then allowed to warm to RT and stirred for 4 h. The mixture was then reduced in volume (*vacuo*) to roughly 5 mL and using a double tipped cannula, transferred to a 100 mL foil wrapped Schlenk flask contained a solution of cold hexanes. With stirring, a dark orange coloured precipitate formed immediately, and the solution was stirred for additional 5 min and allowed to settle into two layers. The top layer was then extracted out using a double-tipped cannula. The remaining residues were dried (*in vacuo*) to obtain a thick transparent dark orange coloured gel. Yield 53 % (0.20 g). ^{1}H NMR (400 MHz, C$_6$D$_6$, δ): 8.06 (bm, 4H, H14 & H15), 7.64 (bm, 2H, H13), 7.20 (bm, 4H, H11 & H12), 7.11-6.85 (bm, 4H, H8, H10 & H9), 3.66-3.59 (bm, 2H, H7), 1.85-1.02 (bm, 22H, H1-H6) ppm; ^{13}C{^{1}H} NMR (100 MHz, C$_6$D$_6$, δ): 161.7 (C18), 153.0 (C16), 147.1 (C17), 136.7 (C19), 129.6 (C13), 128.7 (C10), 125.9 (C9), 124.2 (C12), 123.5 (C8), 122.0 (C14), 113.8 (C15), 71.0 (C7), 27.7 (C5), 27.6 (C4), 25.4 (C6), 23.7 (C3), 21.0 (C2), 13.0 (C1) ppm; ^{119}Sn NMR (79.5 MHz, C$_6$D$_6$, δ): -166.8 ppm, -208.1 ppm, -240.4 ppm. E.A.: Anal. Calcd.

C, 52.14; H, 5.73. Found: C, 50.38, H: 5.79. UV-Vis (C_6H_6) (*trans*-/*cis*-) λ_{max} (ε, L mol^{-1} cm^{-1}); (*trans*-) 349 nm (69758), (*cis*-) 445 nm (2953), (*cis*-) 445 nm (5519).

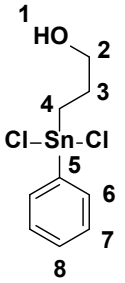

***Preparation of 3-(dichloro(phenyl)stannyl)propan-1-ol* 11**

In a 100 mL dry Schlenk flask, 1.0 M solution of HCl in Et_2O (2.45 mL) was added to a solution of **1** in C_6H_6 (25 mL). This was repeated for a second time for full conversion. The mixture was stirred at RT for 1 h and the solvent removed *in vacuo* to obtain **11** as a pale-yellow powder. The crude product was washed with hexanes (3 × 20 mL) and brought to dryness. Yield 72 % (0.92 g); mp 96.5 °C; ^{1}H NMR (400 MHz, $CDCl_3$): δ = 7.89–7.70 (m, 2H, H6), 7.55–7.36 (m, 3H, H7, H8), 3.85 (s, 2H, H2), 2.86 (s, 1H, H1), 2.17–2.14 (m, H3, 2H), 1.87 (t, $^3J_{H\text{-}H}$ = 6.9 Hz, 2H, H4,) ppm; $^{13}C\{^1H\}$ NMR (100 MHz, $CDCl_3$): δ = 141.2 (C5), 135.2 (C6), 130.7 (C7), 129.1 (C8), 129.1 (C8), 62.5 (C2) ppm; ^{119}Sn NMR (149 MHz, $CDCl_3$): δ = -80.5 ppm. HRMS-DART: m/z calcd for $^{12}C_9{}^1H_{12}{}^{35}Cl^{16}O_1{}^{120}Sn_1$: 290.95996 [M-Cl] +; found: 290.95880.

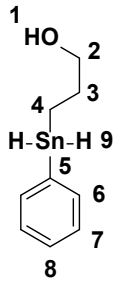

***Preparation of 3-(phenylstannyl)propan-1-ol* 12**

A solution of **11** (0.73 g, 2.24 mmol) in Et_2O (5 mL) was added to a 1m solution of $LiAlH_4$ in Et_2O (2.24 mL) in Et_2O (10 mL) in 100 mL Schlenk flask at 0 °C. After 4 h, the reaction was warmed to room temperature and distilled degassed water (12 mL) was added to the solution to quench the reaction. The organic layer was removed, and the solvent was removed under reduced pressure to obtain **12** as a pale-yellow coloured, translucent gel. Yield 92 % (0.53 g);

^{1}H NMR (400 MHz, C_6D_6): δ = 7.47–7.39 (m, 2H, H6), 7.17–7.11 (m, 3H, H7, H8), 5.51 (s, 2H, H9, $^{1}J_{117Sn\text{-}H}$ = 1841 Hz, $^{1}J_{119Sn\text{-}H}$ =1926 Hz), 3.35 (t, $^{3}J_{H\text{-}H}$ = 6.27 Hz, 2H, H2), 2.60 (s, 1H, H1), 1.71–1.64 (m, 2H, H3), 1.08–1.00 (m, 2H, H4) ppm; ^{13}C{^{1}H} NMR (100 MHz, C_6D_6): δ = 137.4 (C6), 128.5 (C7 & C8), 64.7 (C2), 30.1 (C3), 4.4 (C4, $^{1}J_{117/119Sn\text{-}C}$ = 401.3 Hz) ppm; ^{119}Sn NMR (149 MHz, C_6D_6): δ = -214.9 ppm. HRMS-DART: m/z: calcd for $^{12}C_9{}^{1}H_{14}{}^{16}O_1{}^{120}Sn_1$ + H+: 256.99884 [M+H] + calculated for; found: 256.99912.

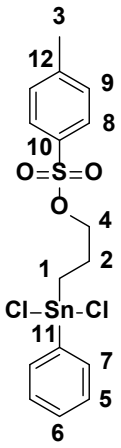

Preparation of 4-(dichloro(phenyl)stannyl)butyl 4-methylbenzenesulfonate **13**

3-(Triphenylstannyl)propyl 4-methylbenzenesulfonate, **2**, (0.10 g, 0.18 mmol) in C_6H_6 (20 mL) was added 1.0 M HCl/Et_2O (0.18 mL, 0.18 mmol) by syringe and stirred at 0°C for 1 h. The pure product was then precipitated into a large volume of hexane (100 mL) with stirring. After decanting, the residual solvent was removed *in vacuo* to obtain a white coloured solid of **13** in near quantitative yield. Yield 99 % (0.20 g); mp 102 °C; ^{1}H NMR (400 MHz, $CDCl_3$): δ = 7.80–7.74 (m, 2H, H8), 7.74–7.73 (m, 2H, H7), 7.72–7.52 (m, 3H, H6, H5), 7.34–7.32 (m, 2H, H9), 4.15–4.13 (t, $^{3}J_{H\text{-}H}$ = 5.5 Hz, 2H, H4), 2.44 (s, 3H, H3), 2.26–2.23 (t, $^{3}J_{H\text{-}H}$ = 12.5 Hz, 2H, H2), 1.97–1.94 (t, $^{3}J_{H\text{-}H}$ = 7.6 Hz, 2H, H1) ppm; ^{13}C{^{1}H} NMR (100 MHz, $CDCl_3$): δ = 145.1 (C10), 138.7 (C12), 134.8 (C11), 132.5 (C7), 131.6 (C9), 130.0–129.5 (C5 & C6), 128.0 (C8), 71.1 (C4), 24.5 (C3), 21.7 (C2), 21.0 (C1) ppm; ^{119}Sn NMR (79.5 MHz, $CDCl_3$): δ = 30.1 ppm; elemental analysis calc'd (%): C 40.04, H 3.78; found: C 41.40, H 3.87.

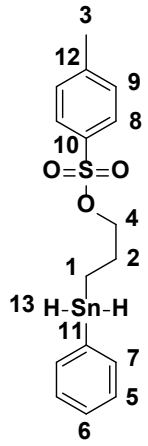

***Preparation of 3-(phenylstannyl)propyl 4-methylbenzenesulfonate* 14**

An EtOH solution (10 mL) containing **13** (0.21 g, 0.44 mmol) was added to a solution of $NaBH_4$ (0.15 g, 4.40 mmol) in EtOH (8 mL) in a 100 mL Schlenk flask, and stirred at 0 °C for 1 h. 20 mL of ice cold degassed distilled water was added to the solution containing crude **14**. The solution was then extracted with hexane (3 × 20 mL) and dried over $MgSO_4$. The mixture containing **14** was filtered, and solvent removed under reduced pressure to obtain a transparent colourless liquid. Yield 62 % (0.11 g); ^{1}H NMR (400 MHz, C_6D_6): δ = 7.75–7.73 (m, 2H, H8), 7.40–7.31 (m, 2H, H7), 7.14–7.13 (m, 3H, H6, H5), 6.73–6.71 (m, 2H, H9), 5.31 (s, $^1J_{117Sn-H}$ = 1764 Hz, $^1J_{119Sn-H}$ = 1851.6 Hz, 2H, H13), 3.74–3.71 (t, $^3J_{H-H}$ = 6.3 Hz, 2H, H4), 1.85 (s, 3H, H3), 1.54–1.47 (q, $^2J_{H-H}$ = 13.9 Hz, $^1J_{H-H}$ = 7.2 Hz, 2H, H2), 0.74–0.70 (t, $^3J_{H-H}$ = 8.2 Hz, 2H, H1) ppm; $^{13}C\{^1H\}$ NMR (100 MHz, C_6D_6): δ = 143.8 (C10), 137.3 (C12), 135.3 (C11), 134.2 (C7), 129.4 (C9), 128.6–128.4 (C5 & C6), 127.8 (C8), 71.8 (C4), 26.8 (C3), 20.7 (C2), 3.1 (C1) ppm; ^{119}Sn NMR (79.5 MHz, C_6D_6): δ = -216.2 ppm. HRMS-DART m/z: calcd for $^{12}C_{16}{}^1H_{20}{}^{16}O_3{}^{32}S_1{}^{120}Sn_1$ +H+: 411.00769 [M+H] +; found: 411.00809.

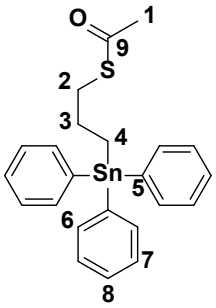

Preparation of (3-(methylsulfinyl) propyl)triphenylstannane **15**

In a 50 mL round bottom flask, **2** (0.50 g, 0.89 mmol), K_2CO_3 (0.16 g, 1.11 mmol) and thioacetic acid (0.15 g, 0.89 mmol) were placed in acetone (25 mL). The reaction was heated under reflux and stirred for 24 h. A colour change was observed, and the crude product was an orange brown liquid. The crude products was then extracted with DCM (20 mL) and washed thrice with distilled H_2O (3 × 20 mL). The organic phase was dried with $MgSO_4$ and dried *in vacuo*. The final product was a viscous brown liquid. Yield: 0.16 g, 39 %. ^{1}H NMR (400 MHz, $CDCl_3$): δ = 7.56 (m, 6H, H6), 7.40 (m, 9H, H7 & H8), 2.95 (t, $^{3}J_{H\text{-}H}$ = 8 Hz, 2H, H2), 2.33 (s, 3H, H1), 1.98 (m, 2H, H3), 1.56 (m, 2H, H4). $^{13}C\{^{1}H\}$ NMR (400 MHz, $CDCl_3$): δ = 195.8 (C9), 138.4 (C5), 137.0 (C6), 129.6-128.6 (C7& C8), 33.5 (C1), 30.7 (C2), 26.9 (C3), 22.7 (C4) ppm. ^{119}Sn NMR (79.5 MHz, $CDCl_3$): δ = -101.4 ppm. HRMS-DART m/z: calc'd for $^{12}C_{16}{}^{1}H_{20}{}^{16}O_3{}^{32}S_1{}^{120}Sn_1$ (M+Na): 485.01520 [M+H] +; found: 485.04527.

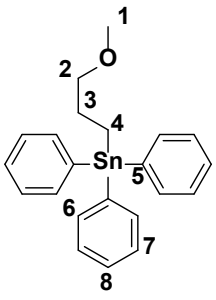

Preparation of (3-methoxypropyl)triphenylstannane **16**

In a 50 mL round bottom flask, **2** (0.50 g, 0.89 mmol) and a 25 % w/v solution of sodium methoxide in methanol (2.74 mL, 1.78 mmol) placed in acetonitrile (25 mL). The reaction was heated under reflux and stirred for 2 h. A yellow solution was observed and extracted with DCM (20 mL) and thrice washed with distilled H_2O (3 × 20 mL). The organic phase was dried

with $MgSO_4$ and evaporated. The crude product was washed thrice with MeOH and afforded a purified white powder. Yield: 0.10 g (26 %). ^{1}H NMR (400 MHz, $CDCl_3$): δ = 7.60 (m, 6H, H6), 7.19 (m, 9H, H7 & H8), 3.10 (t, $^3J_{H\text{-}H}$ = 4 Hz, 2H, H2), 2.86 (s, 3H, H1), 1.91 (m, 2H, H3), 1.43 (m, 2H, H4) ppm. $^{13}C\{^1H\}$ NMR (400 MHz, $CDCl_3$): δ = 139.7 (C5), 137.1 (C6), 128.6-127.5 (C7 & C8), 74.6 (C2), 57.7 (C1), 26.5 (C3), 7.59 (C4) ppm. ^{119}Sn NMR (79.5 MHz, $CDCl_3$): δ = -100.0 ppm. HRMS-DART: 443.0729 m/z (M+Na) +.

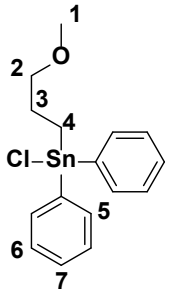

***Preparation of chloro(3-methoxypropyl)diphenylstannane* 17**

In a dry 50 mL Schlenk flask, **16** (100 mg, 0.49 mmol) in benzene (10 mL) was added. Then 1.0 M HCl/Et_2O (0.30 mL, 0.49 mmol) was added by syringe and stirred for 1 h at room temperature. The residual solvent was removed *in vacuo* to obtain a white coloured solid of **17** in near quantitative yield. Yield: 85.00 mg (91 %). ^{1}H NMR (400 MHz, $CDCl_3$): δ = 7.71 (m, 4H, H5), 7.44 (m, 6H, H6 & H7), 3.52 (t, $^3J_{H\text{-}H}$ = 4 Hz, 2H, H2), 2.95 (s, 3H, H1), 2.17 (m, 2H, H3), 1.80 (m, 2H, H4) ppm. ^{119}Sn NMR (79.5 MHz, $CDCl_3$): δ = -82.1 ppm. Insufficient sample for ^{13}C NMR spectroscopy and HRMS. However, a single crystal X-ray structure determination was obtained.

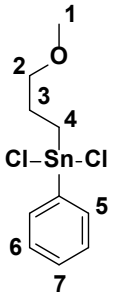

***Preparation of dichloro(3-methoxypropyl)(phenyl)stannane* 18**

In a dry 50 mL Schlenk flask compound **17** (0.09 g, 0.26 mmol) in C_6H_6 (10 mL) was added. Then 1.0 M HCl/Et_2O (0.20 mL, 0.26 mmol) was added by syringe and stirred for 1 h at room

temperature. The residual solvent was removed *in vacuo* to obtain a white coloured solid of **18** in near quantitative yield. Yield: 0.07 g (90 %). ^{1}H NMR (400 MHz, $CDCl_3$): δ = 7.71 (m, 2H, H5), 7.46 (m, 3H, H6 & H7), 3.60 (t, $^{3}J_{H\text{-}H}$ = 4 Hz, 2H, H2), 3.30 (s, 3H, H1), 2.21 (m, 2H, H3), 1.97 (m, 2H, H4) ppm. ^{119}Sn NMR (79.5 MHz, $CDCl_3$): δ = -81.0 ppm. Insufficient sample for ^{13}C NMR spectroscopy and HRMS. However, a single crystal X-ray structure determination was obtained.

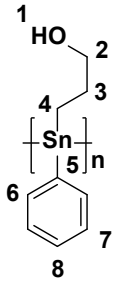

***Preparation of hydroxy homopolymer* 19**

A solution of $RhCl(PPh_3)_3$ (0.08 g, 0.08 mmol) in toluene (10 mL) was added to a foil-wrapped 100 mL Schlenk flask. The solution mixture was stirred at RT for 10 min to activate the catalyst. A solution of **12** (0.53 g, 2.06 mmol) in toluene (5 mL) was added to the catalyst solution, and the reaction was stirred at RT for 4 h. The solvent was removed *in vacuo* and the crude product was dissolved in a minimal amount of THF (<1 mL) and transferred dropwise to a 100 mL flask containing a stirring solution of cold hexane (50 mL). A yellow precipitate formed immediately, and the solution was stirred for an additional 5 min and then allowed to settle. The hexane layer was removed with a Pasteur pipette. The solid was dried *in vacuo* to obtain **19** as a dry yellow coloured powder. Yield = 78 %; M_w = 42,000 Da, PDI = 1.16; ^{1}H NMR (400 MHz, C_6D_6): δ = 7.59–6.95 (m, 5H, H6–H8), 3.57–3.54 (m, 2H, H2), 1.28–1.22 (m, 2H, H3), 0.89–0.82 (m, 2H, H4) ppm; ^{13}C{^{1}H} NMR (100 MHz, C_6D_6): δ = 139.0 (C7), 133.2 (C8), 132.9 (C5), 130.0 (C6), 69.9 (C2), 31.6 (C3), 27.3 (C4) ppm; ^{119}Sn NMR (149 MHz, C_6D_6): δ = -113.4 & -176.1 ppm; elemental analysis calcd (%): C 42.41, H 4.75; found: C 39.52, H 4.54.

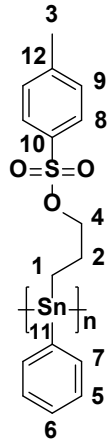

***Preparation of tosyl-polymer* 20**

A solution containing $RhCl(PPh_3)_3$ (0.03 g, 0.04 mmol) in toluene (9.00 mL) was added to a foil-wrapped 50 mL Schlenk flask and stirred at 0 °C (20 min) for activation. Thereafter, **14** in 9.00 mL of toluene (0.36 g, 0.88 mmol) was added dropwise over 20 min to the catalyst solution. The reaction was stirred at 0 °C for 4 h. The mixture was then reduced in volume (*in vacuo*) to roughly 5 mL and, using a double tipped cannula, transferred to a 100 mL foil wrapped Schlenk flask containing a stirring solution of cold hexane (50 mL). An orange yellow precipitate formed immediately, and the mixture was stirred for additional 5 min and then allowed to settle. The top layer of the solution was then extracted using a double tipped cannula needle. The residues were dried *in vacuo* to obtain an orange yellow solid. Yield 63 % (0.23 g); M_w = 31,000 Da, PDI= 1.20; ^{1}H NMR (400 MHz, C_6D_6): δ = 7.91 (bm, 2H, H8), 7.76–7.37 (bm, 5H, H5-H7), 6.88–6.83 (bm, 2H, H9), 3.73 (bm, 2H, H4), 1.88– 1.54 (bm, 5H, H2 & H3), 1.23 (bm, 2H, H1) ppm; $^{13}C\{^1H\}$ NMR (100 MHz, C_6D_6): δ = 144.1 (C10), 138.1 (C12), 137.1 (C6), 133.8 (C11), 133.8 (C7), 131.9 (C9), 126.3 (C8), 72.9 (C4), 29.5 (C2), 21.1 (C1), 14.0 (C3) ppm; ^{119}Sn NMR (79.5 MHz, C_6D_6): δ = -206.0 ppm; E.A. calcd (%): C 46.98, H 4.44; found: C 45.45, H 4.30.

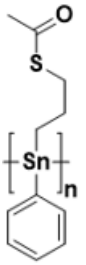

***Attempted Preparation of Situational Labile thioester homopolymer* 21**

In a dry, foil wrapped 100 mL Schlenk flask, high purity of **20** (0.20 g, 0.49 mmol) and K_2CO_3 (0.13 g, 0.99 mmol) was added inside glovebox. Afterwards, ACN (25 mL), thioacetic acid (0.07 mL, 0.88 mmol) were added *via* syringe. Reaction was stirred at reflux for 24 h under N_2 atmosphere. The reaction was dried *in vacuo*, dissolved in minimum amount of THF (~5 mL) and slowly precipitated dropwise into a 150 mL Schlenk flask containing cold hexanes (~60 mL) with stirring. The solution was decanted and the residual precipitate recovered as a dark yellow coloured powder (Yield 0.14 g). Unfortunately, due to solubility issues, further characterization could not be completed.

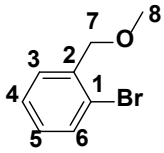

***Preparation of 2-Bromobenzyl methyl ether, $BrC_6H_4CH_2OCH_3$* 22**

$NaOCH_3$ (3.39 g, 62.6 mmol) was dissolved in 40 mL of CH_3OH and added to 2-bromobenzyl bromide (15.6 g, 62.4 mmol) in a two neck round bottom flask equipped with a condenser and heated to reflux for 5 h. The reaction mixture was cooled to room temperature and the solvent removed under reduced pressure. A mixture of 100 mL of hexane and Et_2O (1:1) was added to flask. The organic layer was washed with (2 × 50 mL) water and (2 × 50 mL) of brine, and finally dried over $MgSO_4$. The solvent was removed under reduced pressure to obtain a colourless oil of 1-bromo-2-(methoxymethyl)benzene. NMR spectral data (^1H, ^{13}C) was comparable to that reported in the literature.[70] Yield: 10 g (84 %). ^1H NMR (400 MHz, $CDCl_3$, δ): 7.57 (dd, $^4J_{H\text{-}H}$ = 0.9 Hz, $^3J_{H\text{-}H}$ = 7.9 Hz, 1H, H6) 7.55 (dd, $^4J_{H\text{-}H}$ = 0.7 Hz, $^3J_{H\text{-}H}$ = 7.6 Hz,

1H, H3), 7.33 (dt, $^{4}J_{H\text{-}H}$ = 0.8 Hz, $^{3}J_{H\text{-}H}$ = 7.4 Hz, 1H, H4), 7.15 (dt, $^{4}J_{H\text{-}H}$ = 1.6 Hz, $^{3}J_{H\text{-}H}$ = 7.9 Hz, 1H, H5), 4.55 (s, 2H, H7), 3.49 (s, $^{1}J_{13C\text{-}1H}$ = 141.2 Hz, 3H, H8) ppm; ^{13}C NMR (100 MHz, $CDCl_3$, δ): 137.6 (C2), 132.5 (C3), 129.0 (C6), 128.9 (C4), 127.4 (C5), 122.7 (C1), 73.9 (C7), 58.6 (C8) ppm.

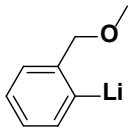

***Preparation of [2-(MeOCH$_2$)C$_6$H$_4$]Li* 23**

1.6 M solution of *n*-BuLi (26.00 mL, 41.60 mmol) in hexane was added dropwise to a solution of 2-bromobenzyl methyl ether (8.37 g, 41.60 mmol) in 40 mL of hexane at -78 ºC over 30 min. The solution became yellow and hazy with the addition of *n*-BuLi. A yellow tinged white coloured solid began to precipitate from solution after 1 h. The reaction mixture was stirred for another hour then transferred to the next reaction *in situ*. The material was not characterized.

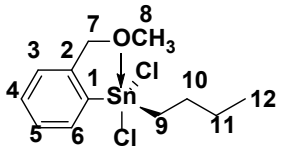

***Preparation of [2-(MeOCH$_2$)C$_6$H$_4$]n-BuSnCl$_2$* 24**

[2-(CH_3OCH_2)C_6H_4]Br (2.00 g, 9.95 mmol) in 30 mL of hexane was added to a 100 mL dry Schlenk flask equipped with a magnetic stirrer and septum. The solution was cooled to -78 ºC and 1.6 M *n*-BuLi in hexane (6.20 mL, 9.92 mmol) was then added. The cooling bath was removed after 30 min and the lithiated reagent allowed to react with a solution of *n*-$BuSnCl_3$ (2.75 g, 9.75 mmol) in 15 mL hexane/Et_2O (1:1) at 0 ºC that was slowly added to the reaction mixture and stirred for 3 h. The solvent was removed under reduced pressure and the residue taken up in toluene (25 mL) and decanted. The solvent was removed under reduced pressure to give a clear, orange-brown coloured oil. The product **24** was further purified by extraction with hot hexanes. Yield: 2.92 g (81 %). ^{1}H NMR (400 MHz, $CDCl_3$, δ): 8.11 (m, 1H, H6), 7.41-7.47 (m, 2H, H4, H5), 7.22 (m, 1H, H3), 4.75 (s, 2H, H7), 3.65 (s, 3H, H8), 1.85 (m, 4H, H10 &

H9), 1.43 (q, $^{3}J_{H\text{-}H}$ = 7.2 Hz, 2H, H11), 0.95 (t, $^{3}J_{H\text{-}H}$ = 7.3 Hz, 3H, H12) ppm; $^{13}C\{^{1}H\}$ NMR (100 MHz, $CDCl_3$, δ): 141.8 (C2, $^{2}J_{119/117Sn\text{-}13C}$ = 48 Hz), 136.0 (C5, $^{3}J_{119/117Sn\text{-}13C}$ = 55 Hz), 134.9 (C3), 130.8 (C4), 128.3 (C1, $^{1}J_{119Sn\text{-}13C}$ = 81 Hz, $^{1}J_{117Sn\text{-}13C}$ = 78 Hz), 125.2 (C6, $^{2}J_{119Sn\text{-}13C}$ = 74 Hz, $^{2}J_{117Sn\text{-}13C}$ = 70 Hz), 73.8 (C7, $^{3}J_{119/117Sn\text{-}13C}$ = 18 Hz), 59.0 (C8), 27.9 (C9, $^{1}J_{119Sn\text{-}13C}$ = 652 Hz, $^{1}J_{117Sn\text{-}13C}$ = 624 Hz), 27.1 (C11, $^{3}J_{119/117Sn\text{-}13C}$ = 40 Hz), 26.0 (C10, $^{2}J_{119Sn\text{-}13C}$ = 106 Hz, $^{2}J_{117Sn\text{-}13C}$ = 102 Hz) 13.6 (C12) ppm; $^{119}Sn\{^{1}H\}$ NMR (149 MHz, $CDCl_3$, δ): -61.0 ppm. HRMS-DART (m/z): $[M^{+}]$ + H_2O, Calcd. for $C_{12}H_{22}Cl_2O_2Sn$ 386.00907; found 386.00918. Found: C, 39.36, H, 4.93. Calc. for $C_{27}H_{26}OSn$: C, 39.18, H, 4.93.

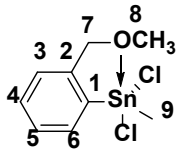

***Preparation of [2-(MeOCH$_2$)C$_6$H$_4$]MeSnCl$_2$* 25**

[2-(CH_3OCH_2)C_6H_4]Br (0.50 g, 2.48 mmol) in 20 mL of hexane was added to a 100 mL dry Schlenk flask equipped with a magnetic stirrer and septum. 1.6 M *n*-BuLi in hexane (1.55 mL, 2.48 mmol) was slowly added at -78 ºC. The cooling bath was removed for 30 min, and the lithiated reagent allowed to react with a solution of $MeSnCl_3$ (0.58 g, 2.08 mmol) in 10 mL of hexane/Et_2O (1:1) at -78 ºC added slowly to the reaction mixture. The reaction mixture was warmed to room temperature, stirred for 3 h and solvent removed under reduced pressure. The residue was taken up in toluene (20 mL), decanted and the solvent removed under reduced pressure to give clear, brown oil. Yield: 0.67 g (98 %). ^{1}H NMR (400 MHz, $CDCl_3$, δ): 8.12 (m, 1H, H6), 7.46 (m, 2H, H4, H5), 7.21 (m, 1H, H3), 4.77 (s, 2H, H7, $^{3}J_{119/117Sn\text{-}1H}$ = 9.0 Hz), 3.42 (s, 3H, H8), 1.26 (s, 3H, H9, $^{1}J_{119Sn\text{-}1H}$ = 83 Hz, $^{1}J_{117Sn\text{-}1H}$ = 79 Hz) ppm; $^{13}C\{^{1}H\}$ NMR (100 MHz, $CDCl_3$, δ): 141.7 (C2), 136.3 (C4), 134.6 (C1), 131.1 (C3), 128.6 (C5), 125.2 (C6), 73.9 (C7), 58.8 (C8), 8.4 (C9) ppm; $^{119}Sn\{^{1}H\}$ NMR (149 MHz, $CDCl_3$, δ): -54.2 ppm. HRMS-DART (m/z): $[M^{+}]$ + H_2O, Calc. for $C_9H_{12}Cl_2OSn$ 343.96309; found 343.96336.

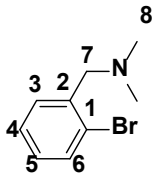

***Preparation of 2-Bromo-N,N-dimethylbenzylamine, $BrC_6H_4CH_2N(CH_3)_2$* 26**

16.00 mL of a 33 % $HNMe_2$ solution (120.0 mmol) was added dropwise to 4.00 g (16.00 mmol) of 2-bromo-benzylbromide, $BrC_6H_4CH_2Br$, dissolved in 30 mL of DCM in 100 mL Schlenk flask. The reaction mixture was heated at 42 ºC under N_2 in a closed system for 7 h. The product was extracted with 3 M HCl (3 × 30 mL) and the extract neutralized with an alkaline solution containing 20 % NaOH. The product, $BrC_6H_4CH_2N(CH_3)_2$ was isolated by extraction with DCM. Yield: 3.02 g (87 %). NMR data (^1H, ^{13}C) agreed with reported values.[66] ^1H NMR (400 MHz, $CDCl_3$, δ): 7.53 (dd, $^4J_{H\text{-}H}$ = 0.9 Hz, $^3J_{H\text{-}H}$ = 7.9 Hz, 1H, H6), 7.42 (dd, $^4J_{H\text{-}H}$ = 1.3 Hz, $^3J_{H\text{-}H}$ = 7.6 Hz, 1H, H3), 7.27 (dt, $^4J_{H\text{-}H}$ = 0.9 Hz, $^3J_{H\text{-}H}$ = 7.5 Hz, 1H, H4), 7.11 (dt, $^4J_{H\text{-}H}$ = 1.6 Hz, $^4JH\text{-}H$ = 7.8 Hz, 1H, H5), 3.52 (s, 2H, H7), 2.30 (s, $^1J_{13C\text{-}1H}$ = 133.0 Hz, 6H, H8) ppm; $^{13}C\{^1H\}$ NMR (100 MHz, $CDCl_3$, δ): 138.1 (C1), 132.7 (C6), 130.9 (C3), 128.4 (C4), 127.2 (C5), 124.7 (C2), 63.2 (H7), 45.5 (H8) ppm.

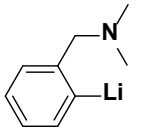

***Preparation of [2-(Me_2NCH_2)C_6H_4]Li* 27**

63.00 mL (100.0 mmol) of 1.6 M solution of *n*-BuLi in hexane was added dropwise to a solution of 13.52 g (100.0 mmol) of *N,N*-dimethylbenzylamine in 150 mL Et_2O at -78 ºC. The solution became yellow and hazy during the addition of *n*-BuLi. A white coloured solid began to precipitate out of solution after 1 h. The reaction mixture was stirred for another hour and transferred *in situ* to the next reaction. The lithated starting material was not further characterized.

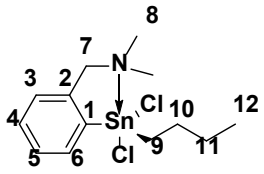

***Preparation of [2-(Me$_2$NCH$_2$)C$_6$H$_4$]n-BuSnCl$_2$* 28**

A suspension of 2.00 g (14.20 mmol) of [2-(Me$_2$NCH$_2$)C$_6$H$_4$]Li in 30 mL Et$_2$O was added dropwise (over 30 min) to a 4.00 g (14.20 mmol) *n*-BuSnCl$_3$ dissolved in 20 mL Et$_2$O at 0 °C. The reaction mixture was kept at this temperature for 1 h, and the aloud to warm to RT and stirred overnight. The crude product was separated by decantation in the glove box. The solvent was removed under reduced pressure, and the product extracted with hot hexane, and a white product recovered after cooling. Yield: 3.94 g (73 %).^{1}H NMR (400 MHz, CDCl$_3$, δ): 8.18 (m, 1H, H6), 7.41 (m, 2H, H5), 7.20 (m, 1H, H3), 3.74 (s, 2H, H7), 2.43 (s, 6H, H8), 1.92-1.80 (m, 4H, H10 & H9), 1.45 (q, $^{3}J_{\text{H-H}}$ = 7.2 Hz, 2H, H11), 0.95 (t, $^{3}J_{\text{H-H}}$ = 7.3 Hz, 3H, H12) ppm; ^{13}C{^{1}H} NMR (100 MHz, CDCl$_3$, δ): 141.1 (C1, $^{1}J_{119/117\text{Sn-13C}}$ = 48 Hz), 139.6 (C2), 137.0 (C6, $^{2}J_{119\text{Sn-13C}}$ = 65 Hz, $^{2}J_{117\text{Sn-13C}}$ = 63 Hz), 130.9 (C4, $^{4}J_{119/117\text{Sn-13C}}$ = 15 Hz), 128.6 (C5, $^{3}J_{119\text{Sn-13C}}$ = 89 Hz, $^{3}J_{117\text{Sn-13C}}$ = 85 Hz), 127.4 (C3, $^{3}J_{119\text{Sn-13C}}$ = 74 Hz, $^{3}J_{117\text{Sn-13C}}$ = 72 Hz,), 63.4 (C7, $^{3}J_{119/117\text{Sn-13C}}$ = 34 Hz), 45.1 (C8), 27.4 (C11, $^{3}J_{119\text{Sn-13C}}$ = 44 Hz, $^{3}J_{117\text{Sn-13C}}$ = 42 Hz), 27.2 (C9, $^{1}J_{119\text{Sn-13C}}$ = 694 Hz, $^{1}J_{117\text{Sn-13C}}$ = 664 Hz), 26.3 (C10, $^{2}J_{119\text{Sn-13C}}$ = 120 Hz, $^{2}J_{117\text{Sn-13C}}$ = 115 Hz), 13.7 (C12) ppm; ^{119}Sn{^{1}H} NMR (149 MHz, CDCl$_3$, δ): -104.0 ppm.

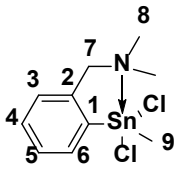

***Preparation of [2-(Me$_2$NCH$_2$)C$_6$H$_4$]MeSnCl$_2$* 29**

A suspension of 0.29 g (2.08 mmol) of [2-(Me$_2$NCH$_2$)C$_6$H$_4$]Li in 30 mL Et$_2$O (30 min) was added dropwise to 0.50 g (2.08 mmol) MeSnCl$_3$ dissolved in 20 mL Et$_2$O at -78 °C. The reaction mixture was stirred for 3 h at RT. The crude product was separated by decantation in the glove box. The solvent was removed under reduced pressure. The product obtained was purified by

extraction with toluene and solvent was removed under reduced pressure. The product was white solid. ^{1}H NMR (400 MHz, $CDCl_3$, δ): 8.18 (m, 1H, H6, $^{2}J_{119Sn\text{-}1H}$ = 100 Hz, $^{2}J_{117Sn\text{-}1H}$ = 96 Hz), 7.44 (m, 2H, H4&H5), 7.20 (m, 1H, H3), 3.76 (s, 2H, H7), 2.44 (s, 6H, H8), 1.26 (s, 3H, H9, $^{2}J_{119Sn\text{-}1H}$ = 84.0 Hz, $^{2}J_{117Sn\text{-}1H}$ = 76.0 Hz) ppm; ^{13}C{^{1}H} NMR (100 MHz, $CDCl_3$, δ): 141.9 (C2, $^{2}J_{119/117Sn\text{-}13C}$ = 50 Hz), 138.5 (C1), 137.0 (C3, $^{2}J_{119Sn\text{-}13C}$ = 67 Hz, $^{2}J_{117Sn\text{-}13C}$ = 65 Hz), 131.2 (C4), 128.7 (C6, $^{2}J_{119Sn\text{-}13C}$ = 93 Hz), 127.4 (C5, $^{3}J_{119Sn\text{-}13C}$ = 79 Hz, $^{3}J_{119Sn\text{-}13C}$ = 76 Hz), 63.2 (C7, $^{3}J_{119/117Sn\text{-}13C}$ = 40 Hz), 44.9 (C8), 8.0 (C9, $^{1}J_{119Sn\text{-}13C}$ = 696 Hz, $^{1}J_{117Sn\text{-}13C}$ = 669 Hz) ppm; ^{119}Sn{^{1}H} NMR (149 MHz, $CDCl_3$, δ): -96.4 ppm.

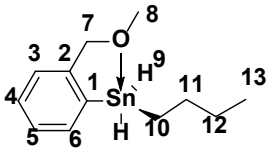

***Preparation of [2-(MeOCH$_2$)C$_6$H$_4$]n-BuSnH$_2$* 30**

A solution of **24** (0.50 g, 1.35 mmol in 15 mL of Et_2O) was added dropwise to a suspension of $LiAlH_4$ (0.11 g, 7.00 mmol in 15 mL of Et_2O), and stirred at 0 ºC for 3 h. The reaction was quenched with 5 mL of degassed and chilled water. The organic layer was separated, and the aqueous layer extracted with Et_2O (3 × 10 mL). The combined organic layers were dried over anhydrous $MgSO_4$. The solvent was removed under reduced pressure to yield **30** as a yellow coloured oil. Yield: 0.28 g (70 %). ^{1}H NMR (400 MHz, $CDCl_3$, δ): 7.80 (m, 1H, H6), 7.21 (m, 2H, H4&H5), 7.06 (m, 1H, H3), 5.78 (s, $^{1}J_{119Sn\text{-}1H}$ = 1727 Hz, $^{1}J_{117Sn\text{-}1H}$ = 1677 Hz, 2H, H9), 4.27 (s, 2H, H7), 3.12 (s, 3H, H8), 1.70 (dt, $^{3}J_{H\text{-}H}$ = 2.0, 7.9 Hz, 2H, H11), 1.42 (sext, $^{3}J_{H\text{-}H}$ = 7.5, 2H, H12), 1.30 (tt, $^{3}J_{H\text{-}H}$ = 1.7, 8.1 Hz, 2H, H10), 0.96 (t, $^{3}J_{H\text{-}H}$ = 7.3 Hz, 3H, H13) ppm; ^{13}C{^{1}H} NMR (100 MHz, $CDCl_3$, δ): 145.0 (C2, $^{2}J_{119/117Sn\text{-}13C}$ = 26 Hz), 139.3 (C6, $^{2}J_{119/117Sn\text{-}13C}$ = 39 Hz), 137.2 (C1, $^{1}J_{119Sn\text{-}13C}$ = 522 Hz, $^{1}J_{117Sn\text{-}13C}$ = 498 Hz), 128.7 (C5, $^{3}J_{119/117Sn\text{-}13C}$ = 12 Hz), 127.7 (C4), 127.4 (C3), 76.1 (C7, $^{3}J_{119/117Sn\text{-}13C}$ = 19 Hz), 57.1 (C8), 30.6 (C11, $^{2}J_{119/117Sn\text{-}13C}$ = 22 Hz), 27.1 (C10, $^{1}J_{119/117Sn\text{-}13C}$ = 67 Hz), 13.9 (C12), 10.2 (C13) ppm;

$^{119}Sn\{^{1}H\}$ NMR (149 MHz, C_6D_6, δ): -210.0 ppm. HRMS-DART (m/z): [M^+], Calc. for $^{12}C_{12}{}^{1}H_{19}{}^{16}O^{116}Sn$ 295.04534; found 295.04595.

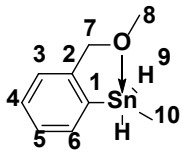

***Preparation of [2-(MeOCH$_2$)C$_6$H$_4$]MeSnH$_2$* 31**

A solution of **25** (0.52 g, 1.60 mmol in 15 mL of Et_2O) was added dropwise to a suspension of $LiAlH_4$ (0.34 g, 3.00 mmol in 15 mL of Et_2O), and stirred at 0 ºC for 3 h. The reaction was quenched with 10 mL of degassed and chilled water. The organic layer was separated and the aqueous layer extracted with Et_2O (3 × 10 mL). The combined organic layers were dried over anhydrous $MgSO_4$. The solvent was removed under reduced pressure to yield **31** as a yellow coloured oil. Yield: 0.35 g (85 %). The product began to decompose as soon as the temperature started rise after the removal of solvent. ^{1}H NMR (400 MHz, C_6D_6, δ): 7.65-7.64 (m, 1H, H5'), 7.46-7.44 (m, 1H, H5), 7.34-7.32 (m, 1H, H7'), 7.12-7.08 (m, 2H, H4' & H6'), 6.98-6.95 (m, 2H, H4 & H6), 6.93-6.88 (m, 1H, H7), 5.54 (s, 2H, H9 & H9'), 4.36 (s, 2H, H2'), 4.14 (s, 2H, H2), 3.10 (s, 3H, H1'), 2.98 (s, 3H, H1), 0.35-0.34 (s, 3H, H8 & H8') ppm; $^{13}C\{1H\}$ NMR (100 MHz, C_6D_6 , δ): 144.6 (C10'), 138.5 (C10), 138.1 (C3'), 136.5 (C3), 128.5-128.3 (C4'-C7'), 127.3-126.9 (C4-C7), 75.5 (C2'), 73.5 (C2), 57.8 (C1'), 56.5 (C1), -12.1 (C8'), -12.3 (C8) ppm; $^{119}Sn\{^{1}H\}$ NMR (149 MHz, C_6D_6, δ): -222.8 ppm. HRMS-DART (m/z): [M^+ - H], Calc. for $C_9H_{13}OSn$ 256.99967; found 256.99884.

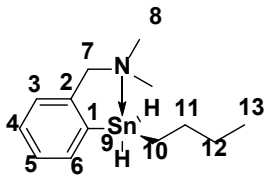

***Preparation of [2-(Me$_2$NCH$_2$)C$_6$H$_4$]n-BuSnH$_2$* 32**

A solution of 1.59 g (4.16 mmol) of **28** in 30 mL Et_2O was added dropwise in 5.00 mL (5.00 mmol) of $LiAlH_4$ (1.0 M in Et_2O) in 50 mL Et_2O at 0 °C. The reaction mixture was stirred for

3 h at 0 °C. The reaction was quenched with 15.00 mL of chilled deoxygenated water. The organic layer was separated and dried over anhydrous $MgSO_4$, and the solvent removed under reduced pressure. A yellow oily product was obtained. The product is relatively stable at -20 °C. Yield: 1.05 g (81 %).^{1}H NMR (400 MHz, $CDCl_3$, δ): 7.78 (m, 1H, H6), 7.13 (m, 2H, H4 & H5), 6.94 (m, 1H, H3), 5.72 (s, $^1J_{119Sn-H}$ = 1760 Hz, $^1J_{117Sn-H}$ = 1680 Hz, 2H, H9), 3.12 (s, 2H, H7), 1.88 (s, 6H, H8), 1.70 (m, 2H, H11), 1.62 (m, 2H, H10), 1.14 (m, 2H, H12), 0.90 (t, 3H, H13) ppm; ^{13}C{^{1}H} NMR (100 MHz, $CDCl_3$, δ): 145.4 (C2, $^2J_{119/117Sn-13C}$ = 25 Hz), 139.5 (C1), 139.2 (C6, $^2J_{119Sn-13C}$ = 44 Hz), 128.9 (C3, $^4J_{119/117Sn-13C}$ = 12 Hz), 128.1 (C5, $^3J_{119/117Sn-13C}$ = 69 Hz), 127.5 (C4), 65.4 (C7, $^2J_{119/117Sn-13C}$ = 23 Hz), 44.0 (C8), 30.9 (C12, $^2J_{119/117Sn-13C}$ = 21 Hz), 27.3 (C11, $^1J_{119/117Sn-13C}$ = 65 Hz), 14.0 (C13), 10.4 (C10, $^1J_{119Sn-13C}$ = 434 Hz, $^1J_{117Sn-13C}$ = 415 Hz) ppm; ^{119}Sn{^{1}H} NMR (149 MHz, $CDCl_3$, δ): -217.5 ppm. HRMS-DART (m/z): [M+H] Calcd. for $C_{13}H_{23}NSn$ = 313.08524, found 314.09337.

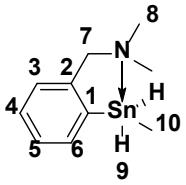

***Preparation of [2-(Me$_2$NCH$_2$)C$_6$H$_4$]MeSnH$_2$* 33**

A suspension of 0.24 g (0.71 mmol) of **29** in 20 mL Et_2O was added dropwise to 1.50 mL (1.50 mmol) of $LiAlH_4$ (1.0 M in Et_2O) in 30 mL Et_2O at 0 °C. The reaction mixture was stirred for 3 h at 0 °C. The reaction was quenched with 10 mL of chilled deoxygenated water. The organic layer was separated and dried over anhydrous $MgSO_4$, and the solvent removed under reduced pressure. A yellow oily product of **33** was obtained, the dihydride is relatively stable over a one-week period at -20 °C. ^{1}H NMR (400 MHz, $CDCl_3$, δ): 7.78 (m, 1H, H6), 7.15 (m, 2H, H4 & H5), 6.95 (m, 1H, H3), 5.63 (q, $^1J_{119Sn-1H}$ = 1824 Hz, $^1J_{117Sn-1H}$ = 1756 Hz, 2H, H9), 3.13 (s, 2H, H7), 1.87 (s, 6H, H8), 0.35 (t, $^1J_{119/117Sn-1H}$ = 60 Hz, 3H, H10) ppm; ^{13}C{^{1}H} NMR (100 MHz, $CDCl_3$, δ): 145.0 (C2, $^2J_{119/117Sn-13C}$ = 27.0 Hz), 138.9 (C1), 138.5 (C6, $^2J_{119/117Sn-13C}$ = 47.0 Hz), 128.6 (C5, $^3J_{119/117Sn-13C}$ = 12.0 Hz), 127.8 (C4), 127.2 (C3), 64.9 (C7, $^3J_{119/117Sn-13C}$ =

24.0 Hz), 43.6 (C8), 11.3 (C9, $^{1}J_{119Sn\text{-}13C}$ = 392 Hz, $^{1}J_{117Sn\text{-}13C}$ = 382 Hz) ppm; $^{119}Sn\{^{1}H\}$ NMR (149 MHz, $CDCl_3$, δ): -235.8 ppm. HRMS-DART (m/z): [M^+ - H] Calcd. for $C_{10}H_{16}NSn$ = 270.03047, found = 270.03257.

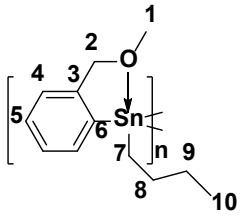

***Preparation of ([2-(MeOCH$_2$)C$_6$H$_4$]n-BuSn)$_n$ Polymer* 34**

A solution containing $RhCl(PPh_3)_3$ (0.16 g, 0.18 mmol) in toluene (10 mL) was added to a foil-wrapped 50 mL Schlenk flask and stirred at RT for 20 min. Thereafter, **30** in 10 mL of toluene (1.31 g, 4.38 mmol) was added dropwise over 20 min to the catalyst solution. The reaction was allowed to stir at RT for 4 h. The toluene mixture was brought to dryness *in vacuo*. The crude solid was re-dissolved in 5 mL of THF and then added dropwise to a 100 mL foil wrapped Schlenk flask containing a stirring solution of cold hexane (60 mL) for precipitation. A bright yellow precipitate formed immediately, and the mixture was stirred for additional 5 min and then allowed to settle. The top layer of the solution was then decanted. The residues were dried *in vacuo* to obtain a bright yellow solid. Yield 65 % (0.84 g); M_w = 30,300 Da, PDI = 1.42. ^{1}H NMR (400 MHz, C_6D_6, δ): 7.73-7.69 (bm, 2H, H4), 7.03–7.00 (bm, 2H, H5), 4.78–4.28 (bm, 2H, H2), 3.32-2.95 (bm, 3H, H1), 2.10–1.45 (bm, 9H, H7-H10) ppm; $^{13}C\{1H\}$ NMR (100 MHz, C_6D_6, δ): 132.2 (C6), 131.3 (C3), 128.3-125.0 (C4 & C5), 76.7 (C2), 57.6 (C1), 29.2-26.7 (C7-C9), 13.7 (C10) ppm; $^{119}Sn\{^{1}H\}$ NMR (149 MHz, C_6D_6, δ): -42.0, -199.3 ppm; Elemental analysis calcd (%): C 48.53, H 6.11; found: C 43.70, H 5.82.

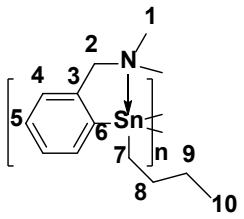

***Preparation of ([2-(Me$_2$NCH$_2$)C$_6$H$_4$]n-BuSn)$_n$ Polymer* 35**

A solution containing $RhCl(PPh_3)_3$ (60.0 mg, 0.06 mmol) in toluene (8 mL) was added to a foil-wrapped 50 mL Schlenk flask and stirred at RT for 20 min. Thereafter, **32** in 8 mL of toluene (0.50 g, 1.62 mmol) was added dropwise over 20 min to the catalyst solution. The reaction was allowed to stir at RT for 4 h. The mixture was then brought to dryness *in vacuo*. The crude product was re-dissolved in 5 mL of THF and added dropwise to a 100 mL foil wrapped Schlenk flask containing a stirring solution of cold hexane (50 mL) for precipitation. A bright yellow precipitate formed immediately, and the mixture was stirred for additional 5 min and then allowed to settle. The top layer of the solution was then decanted. The residues were dried in vacuo to obtain a bright yellow solid. Yield 17 % (0.09 g); M_w = 21,800 Da, PDI = 1.86. ^{1}H NMR (400 MHz, C_6D_6, δ): 7.76-7.71 (bm, 2H, H4), 7.06–7.01 (bm, 2H, H5), 3.55–3.48 (bs, 2H, H2), 2.21 (bs, 6H, H1), 1.87–1.47 (bm, 6H, H7-H9), 1.24 (bs, 3H, H10) ppm; ^{13}C{1H} NMR (100 MHz, C_6D_6, δ): 144.1 (C6), 137.4 (C3), 132.0 (C4), 131.2 (C5), 64.3 (C2), 44.9 (C1), 28.2-26.9 (C7-C9), 13.7 (C10) ppm; ^{119}Sn{^{1}H} NMR (149 MHz, C_6D_6, δ): -149.7 ppm; THF-d_8: -55.6, -151.6 ppm. Elemental analysis calcd (%):C 50.36, H 6.83; found: C 48.46, H 6.41.

APPENDIX

List of Appendices Figures

CHAPTER 1 NMR Spectra

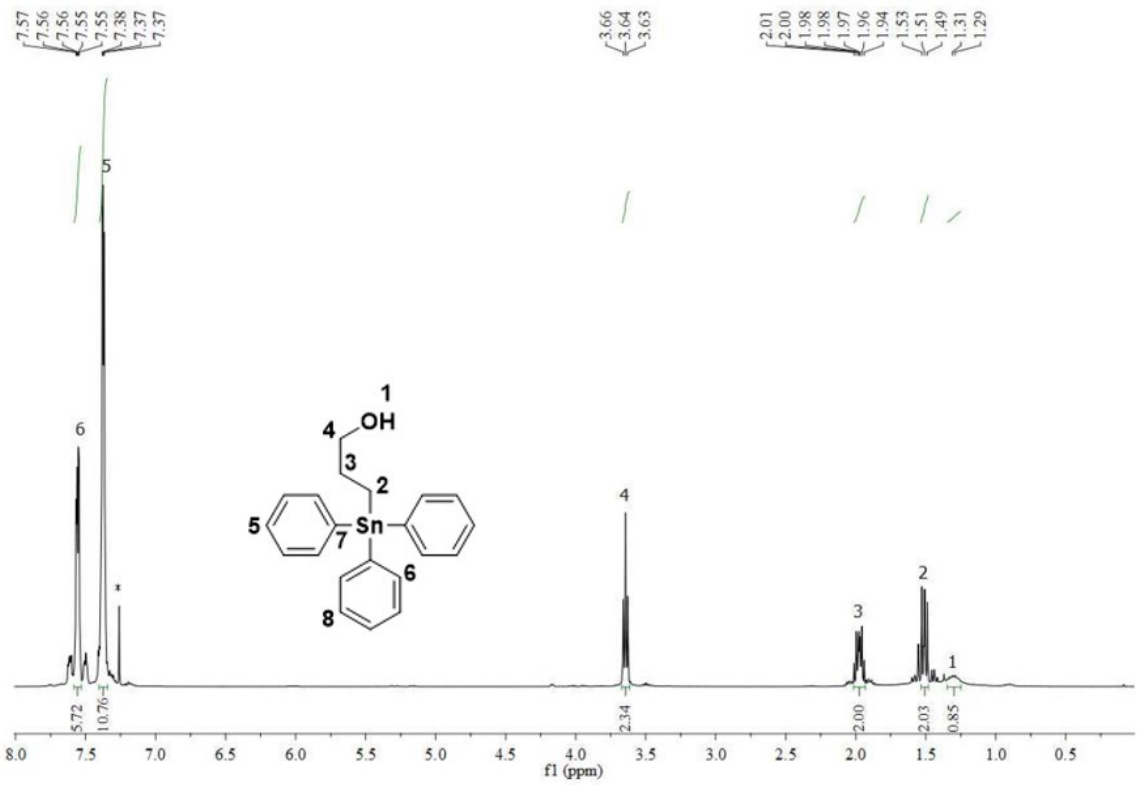

Figure S1. ^{1}H NMR spectrum of **1** in $CDCl_3$

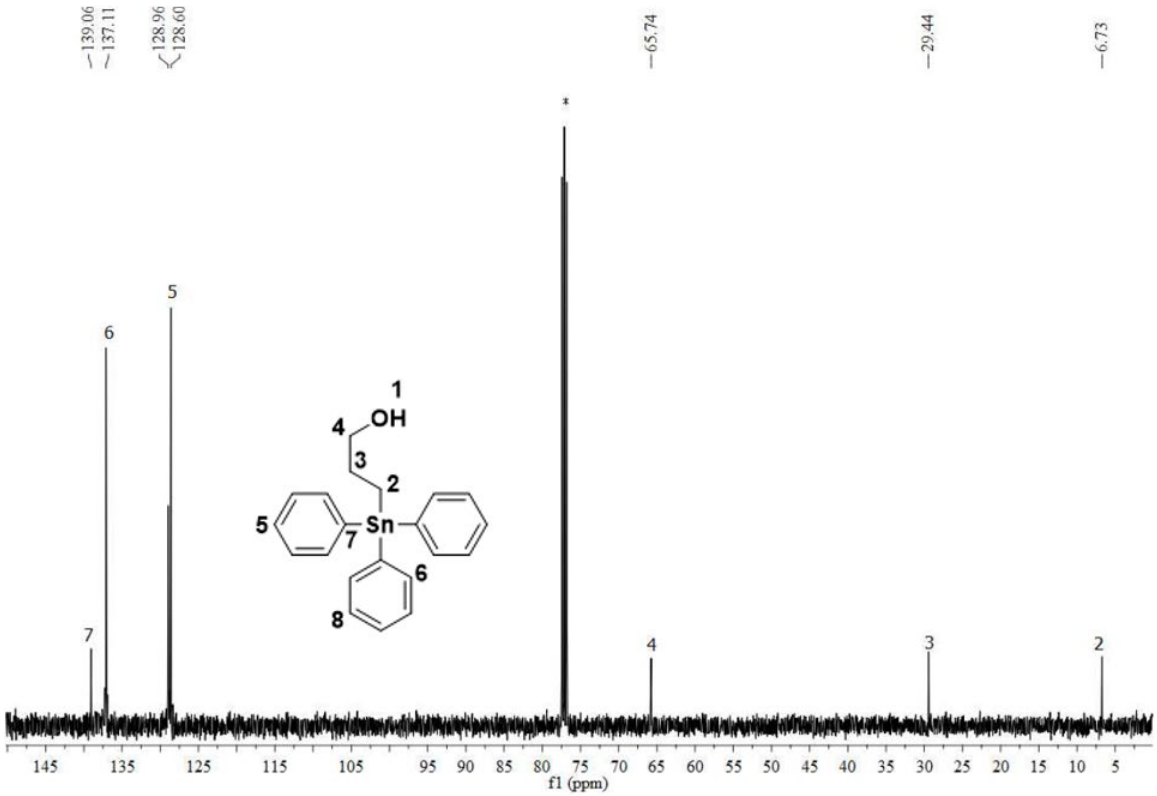

Figure S2. $^{13}C\{^{1}H\}$ NMR spectrum of **1** in $CDCl_3$

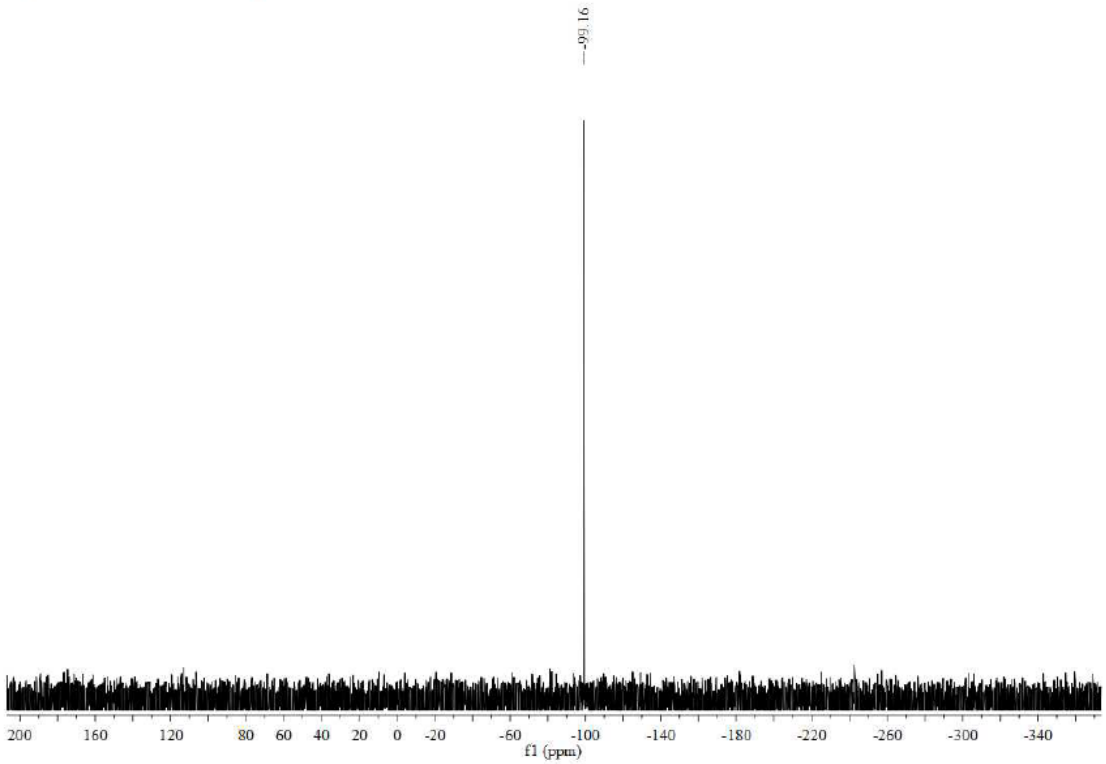

Figure S3. $^{119}Sn\{^{1}H\}$ NMR spectrum of **1** in $CDCl_3$

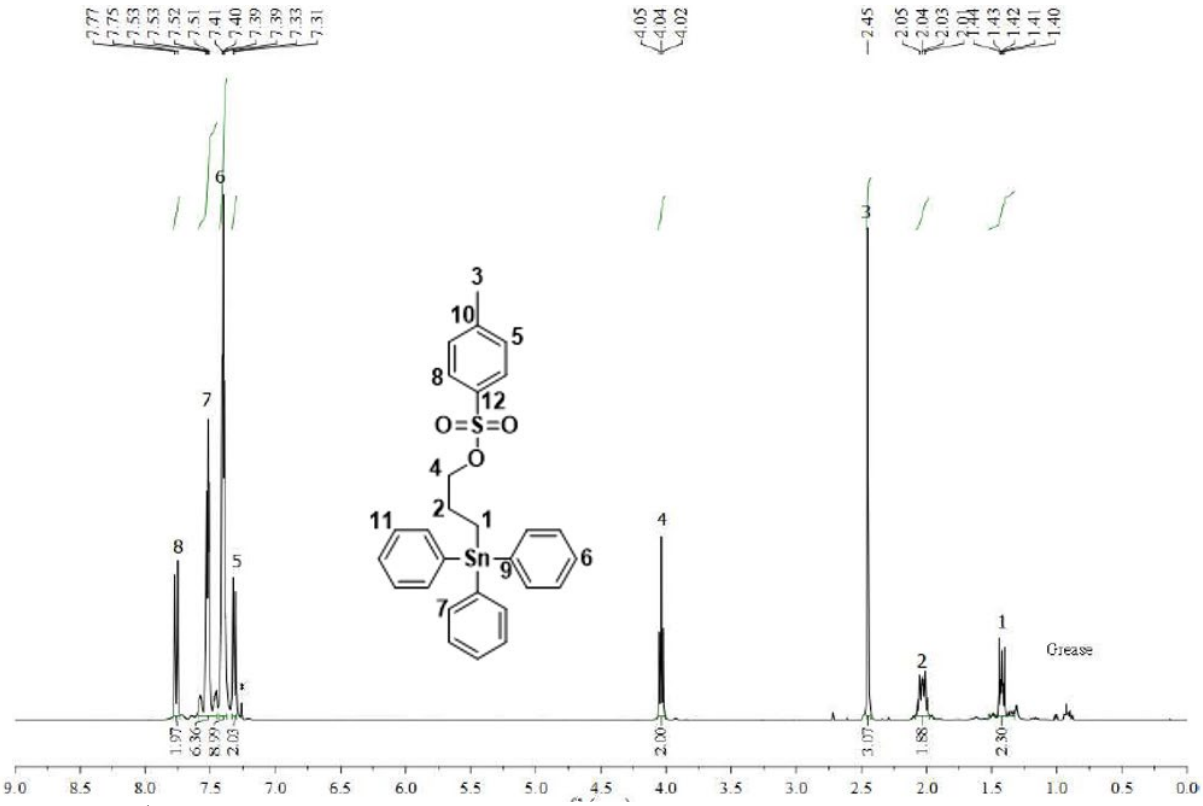

Figure S4. ^{1}H NMR spectrum of **2** in $CDCl_3$

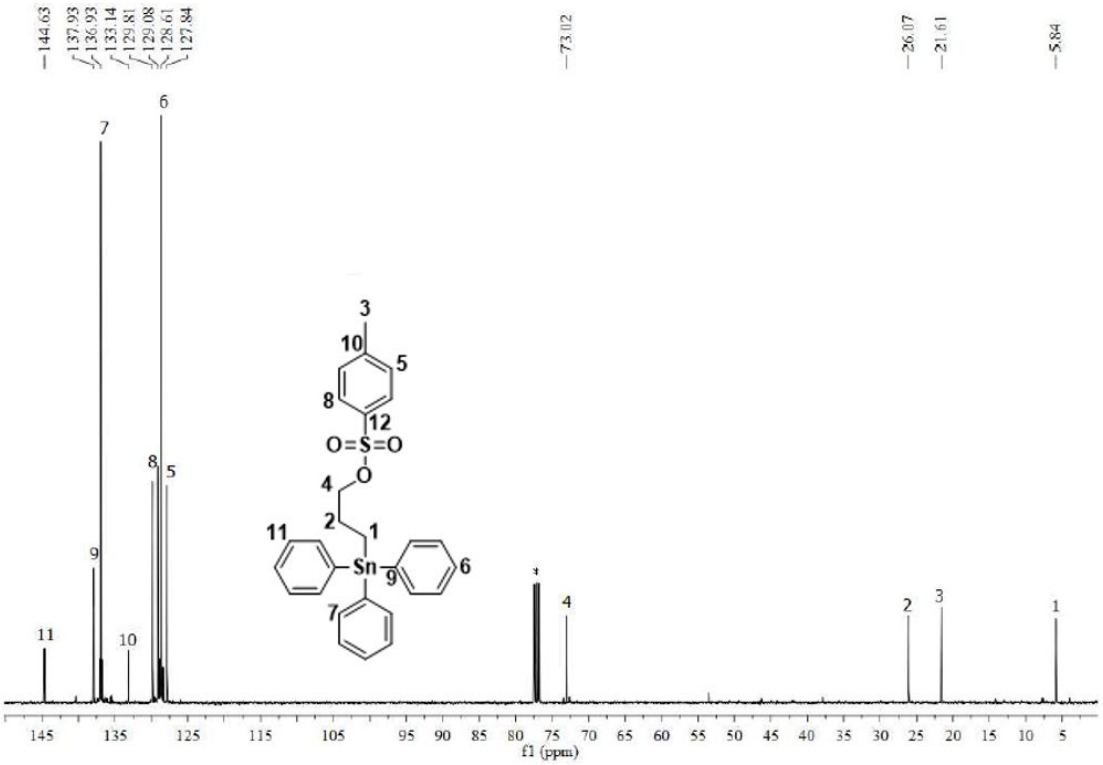

Figure S5. $^{13}C\{^{1}H\}$ NMR spectrum of **2** in $CDCl_3$

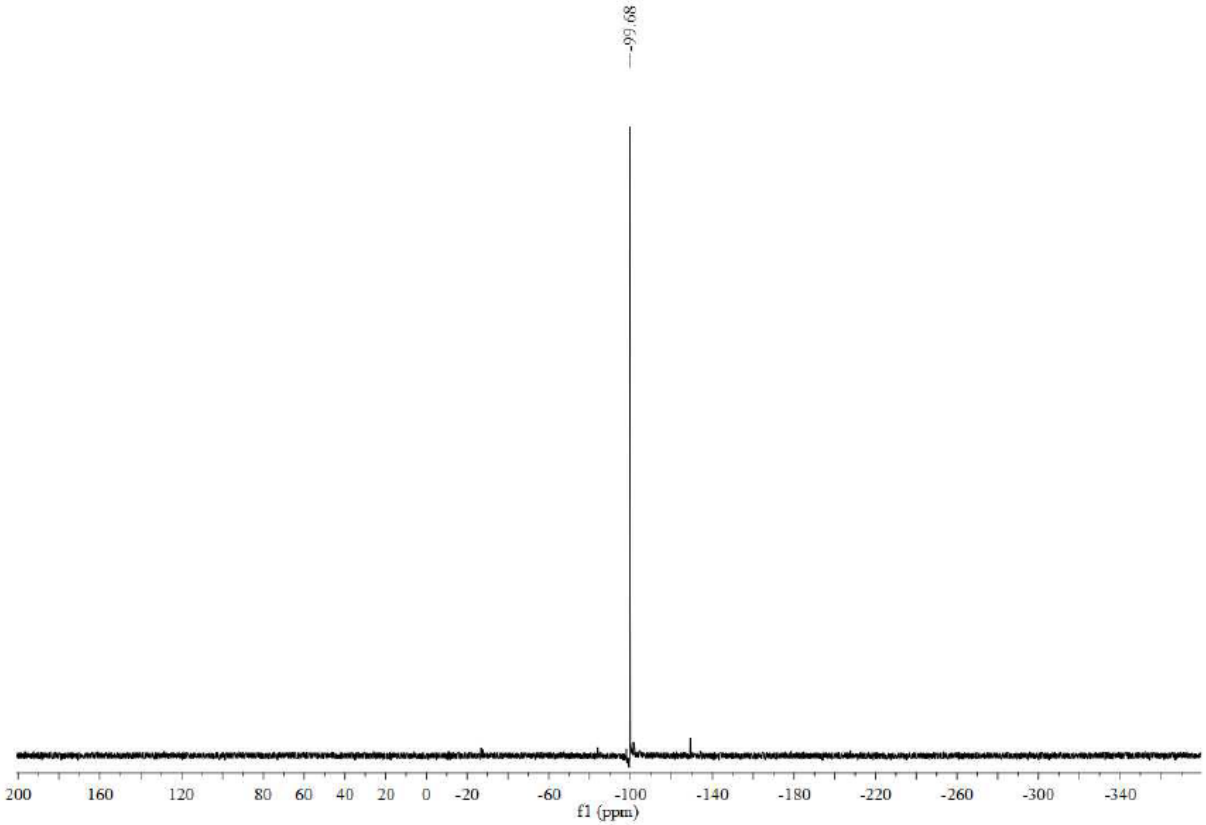

Figure S6. $^{119}Sn\{^{1}H\}$ NMR spectrum of **2** in $CDCl_3$

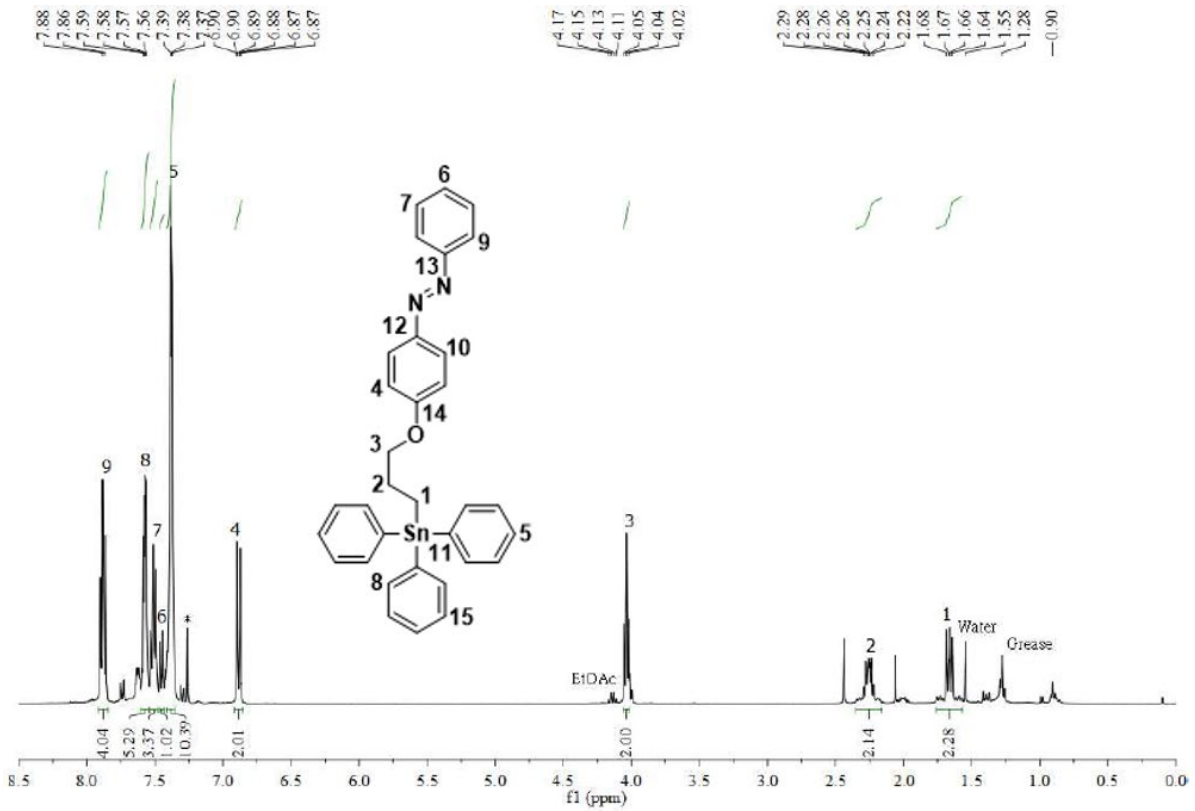

Figure S7. ^{1}H NMR spectrum of **3** in $CDCl_3$

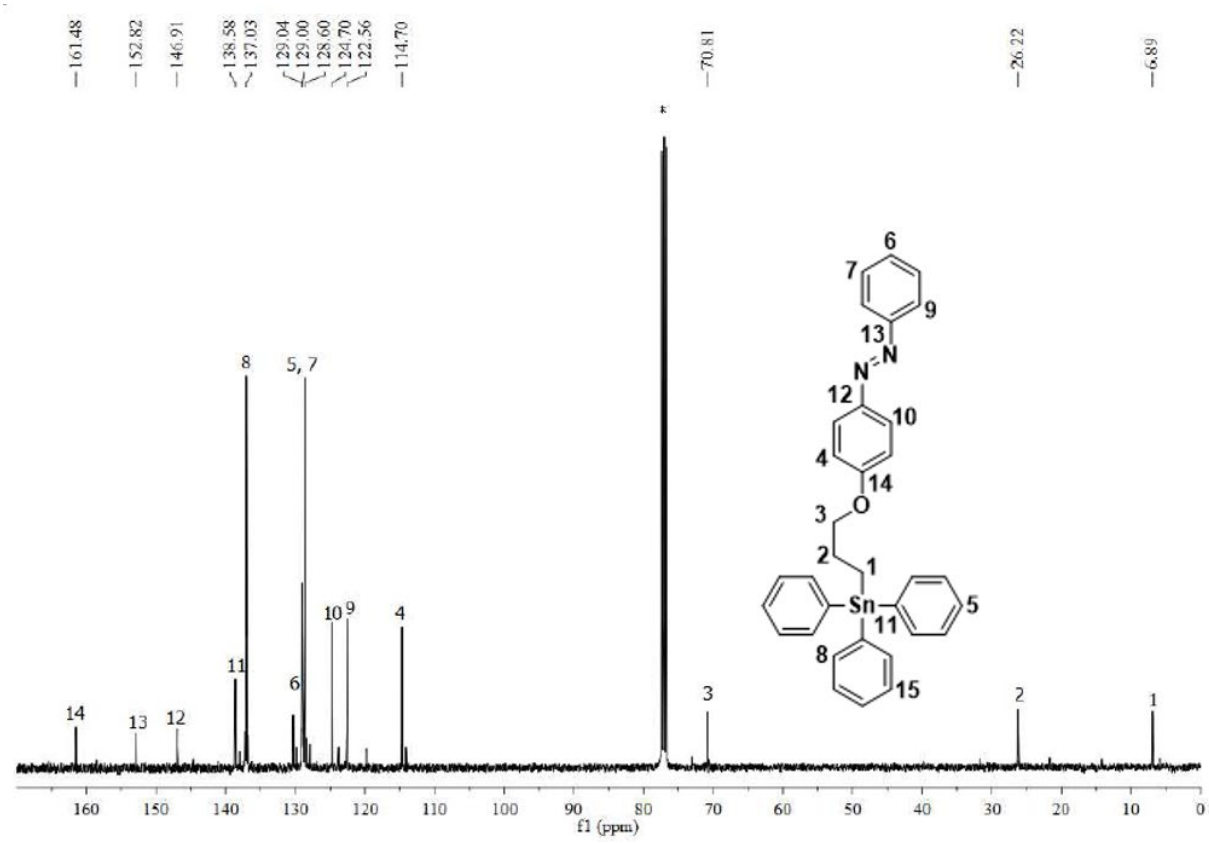

Figure S8. $^{13}C\{^{1}H\}$ NMR spectrum of **3** in $CDCl_3$

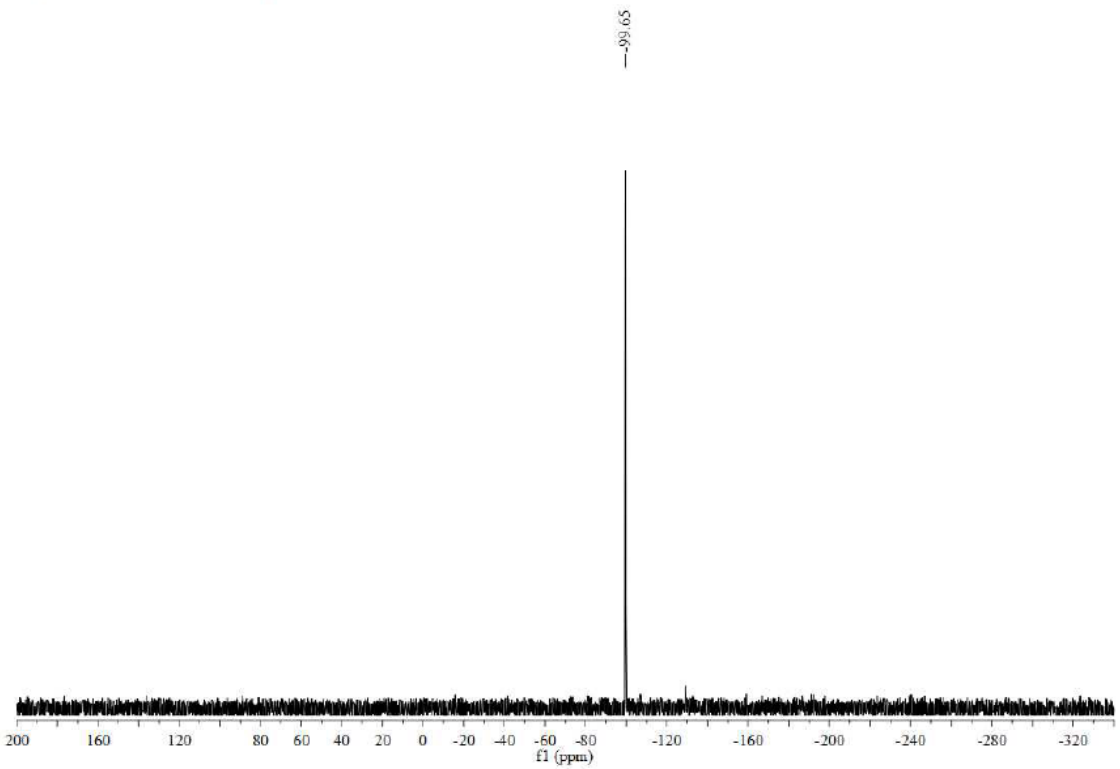

Figure S9. $^{119}Sn\{^{1}H\}$ NMR spectrum of **3** in $CDCl_3$

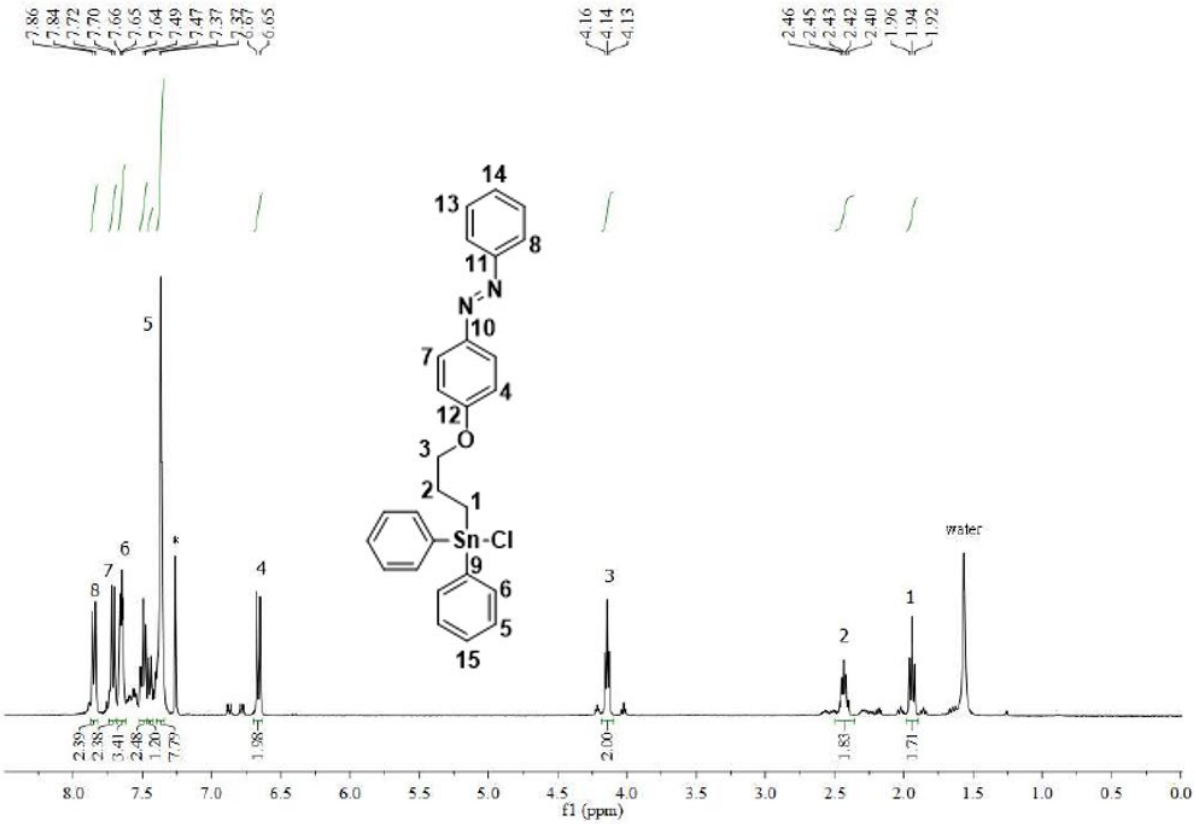

Figure S10. ^{1}H NMR spectrum of **4** in $CDCl_3$

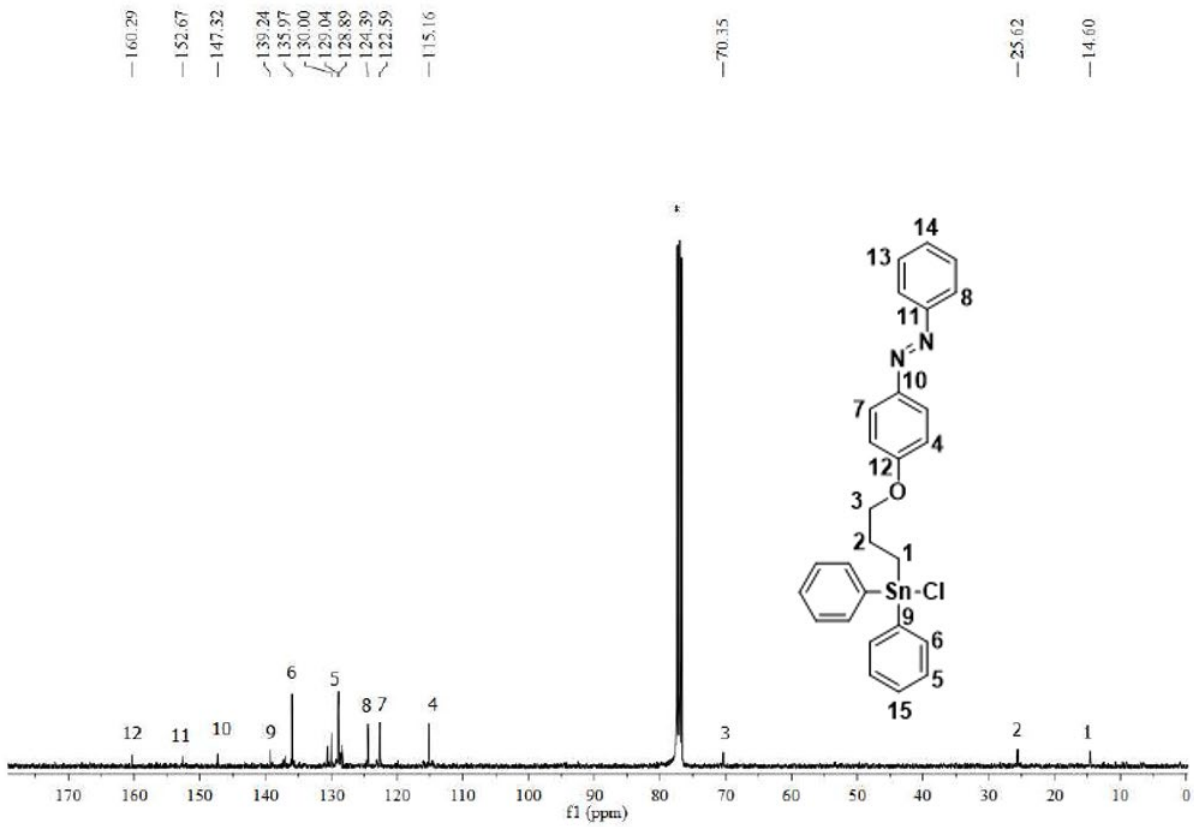

Figure S11. $^{13}C\{^{1}H\}$ NMR spectrum of **4** in $CDCl_3$

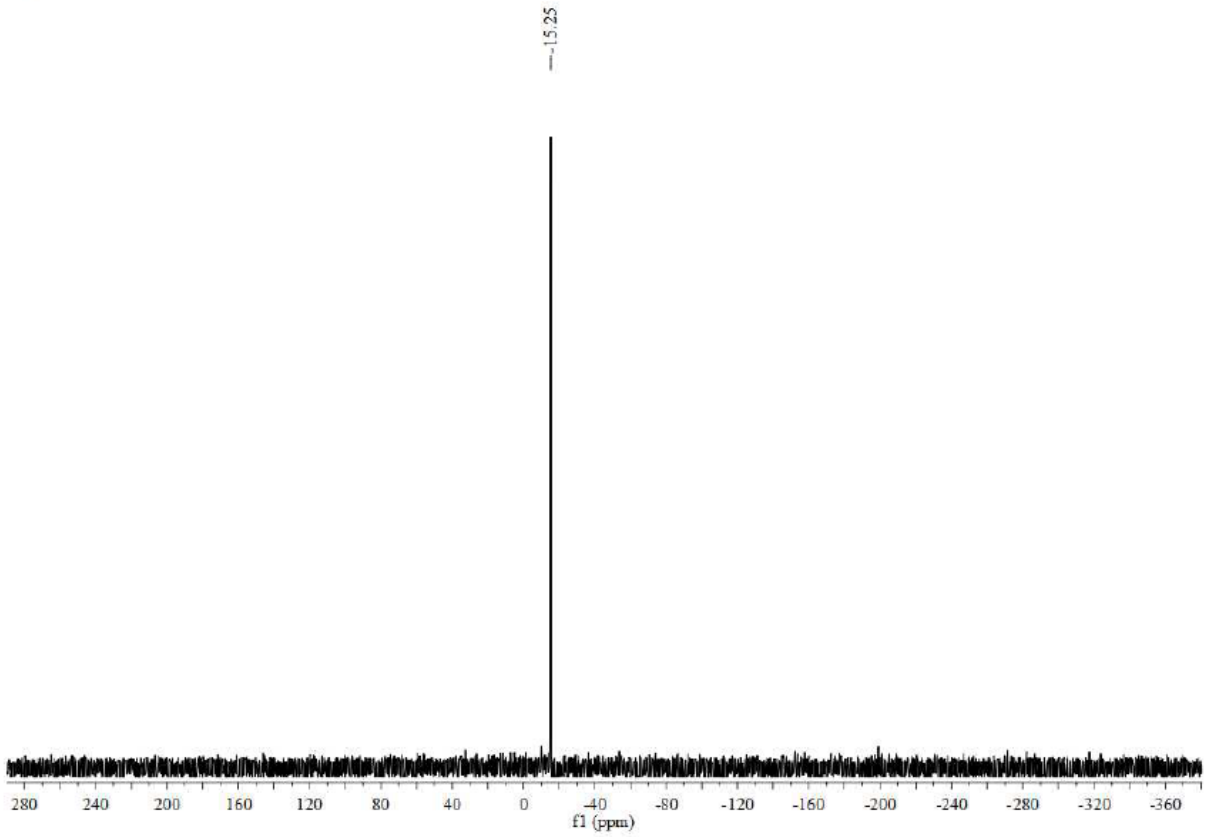

Figure S12. $^{119}Sn\{^{1}H\}$ NMR spectrum of **4** in $CDCl_3$

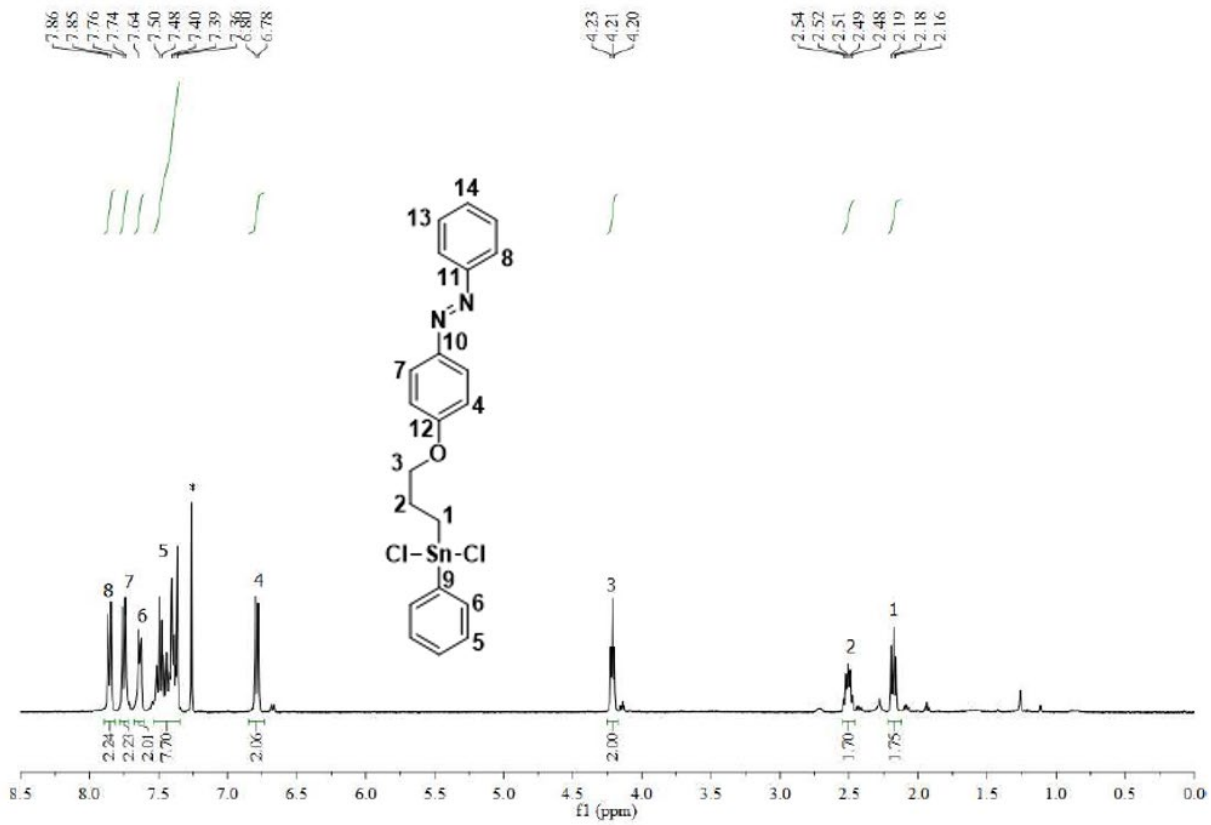

Figure S13. ^{1}H NMR spectrum of **5** in $CDCl_3$

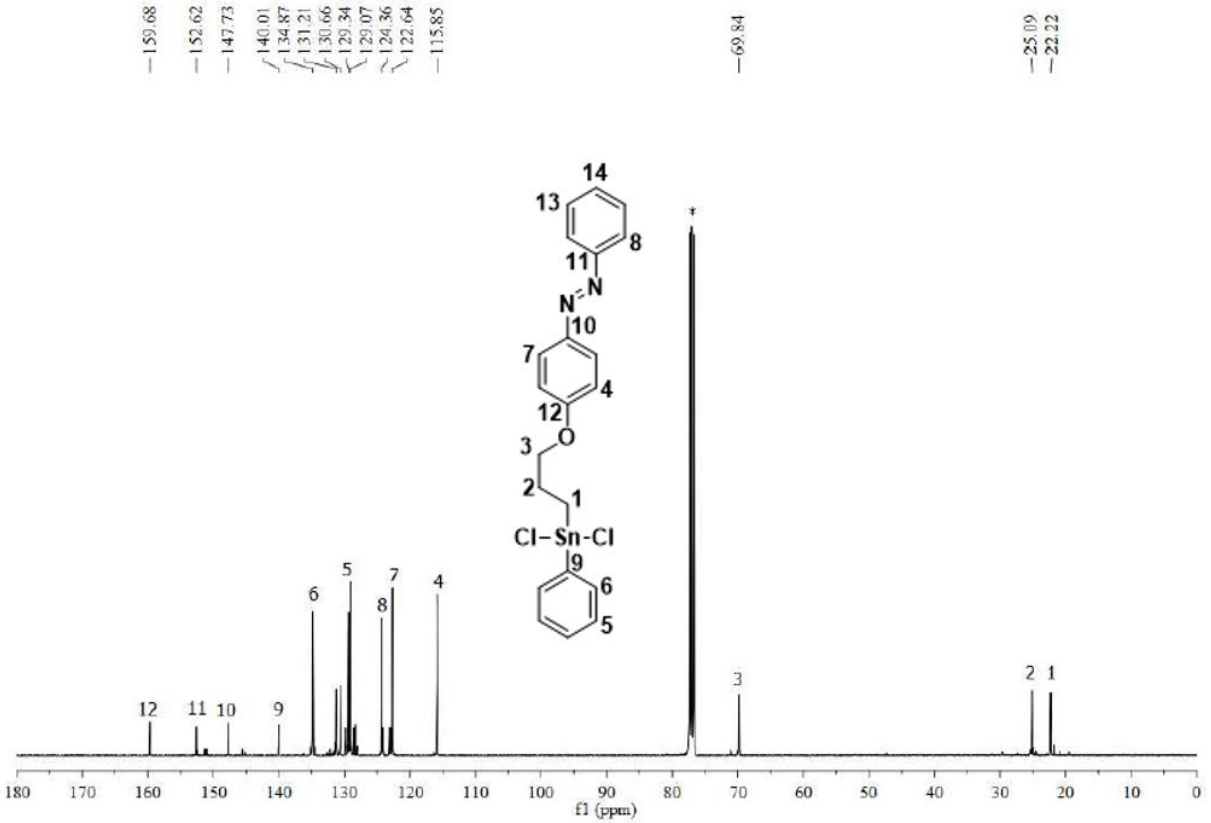

Figure S14. $^{13}C\{^{1}H\}$ NMR spectrum of **5** in $CDCl_3$

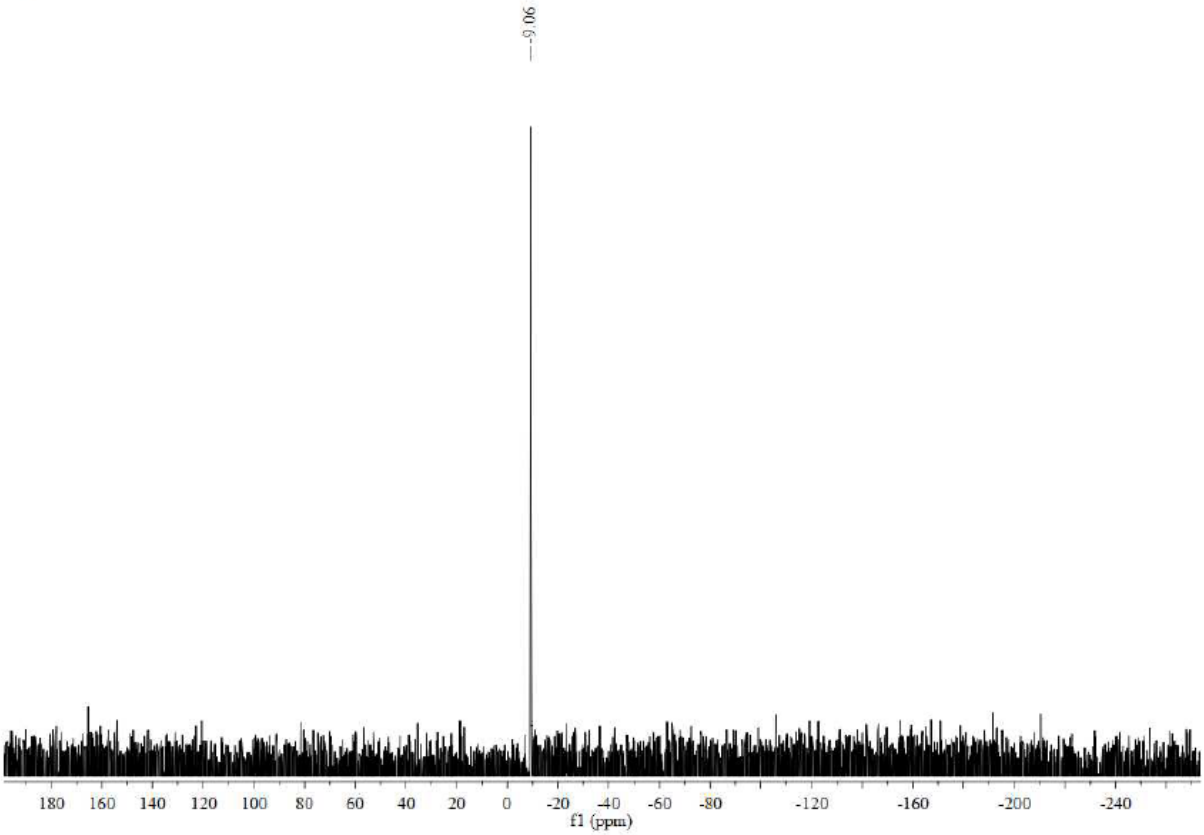

Figure S15. $^{119}Sn\{^{1}H\}$ NMR spectrum of **5** in $CDCl_3$

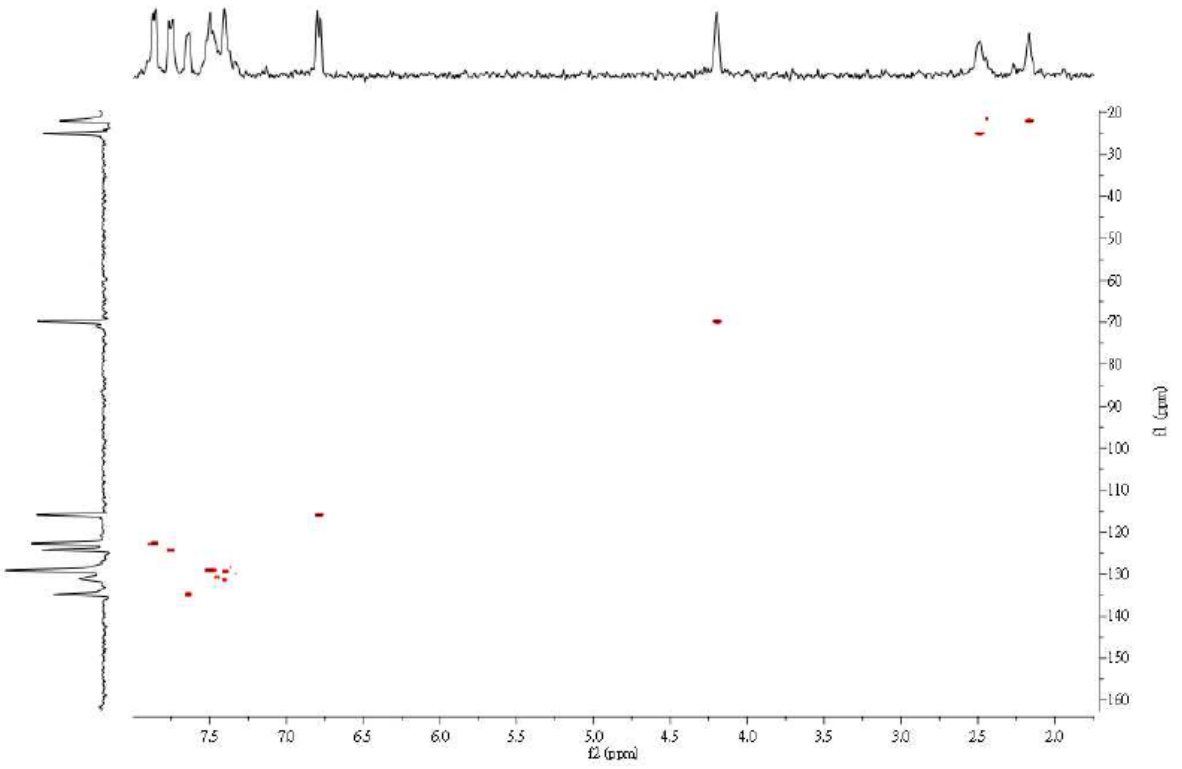

Figure S16. HSQC 2D-NMR spectrum of **5** in $CDCl_3$

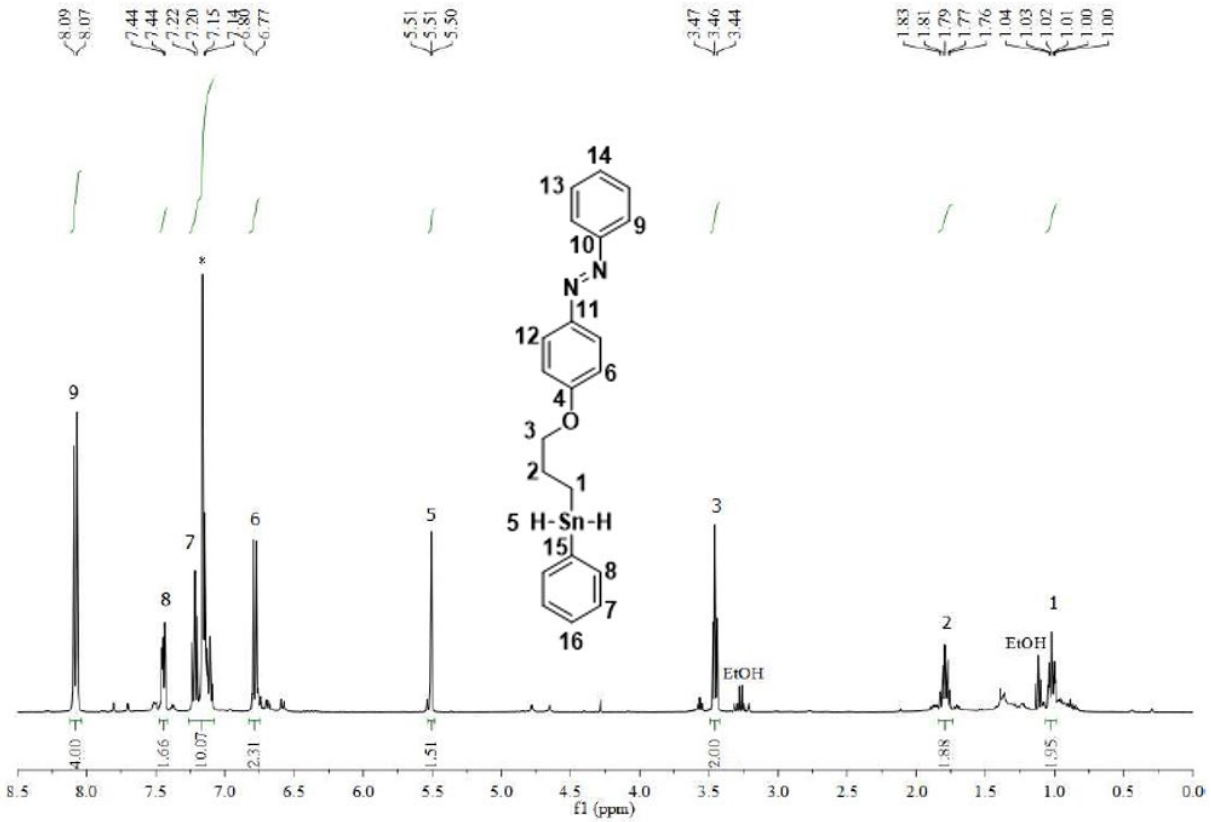

Figure S17. ^{1}H NMR spectrum of **6** in C_6D_6

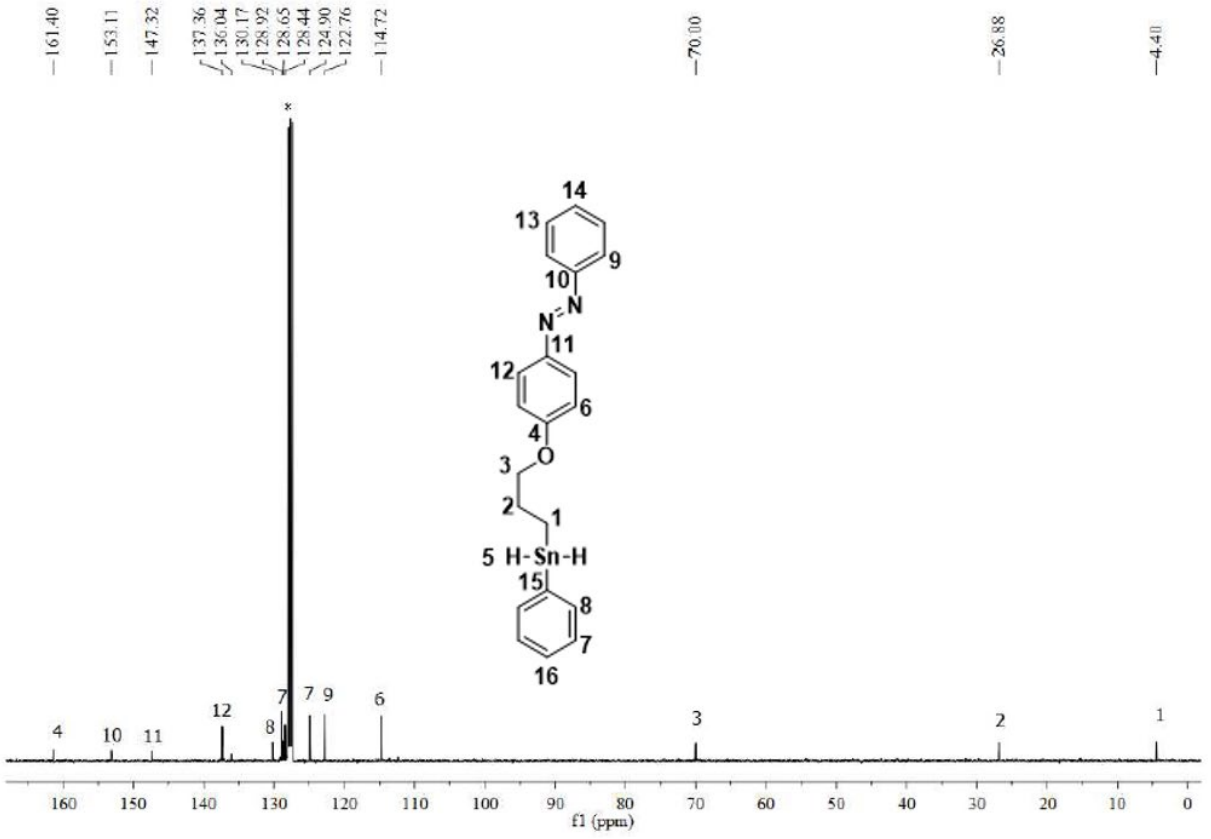

Figure S18. $^{13}C\{^{1}H\}$ NMR spectrum of **6** in C_6D_6

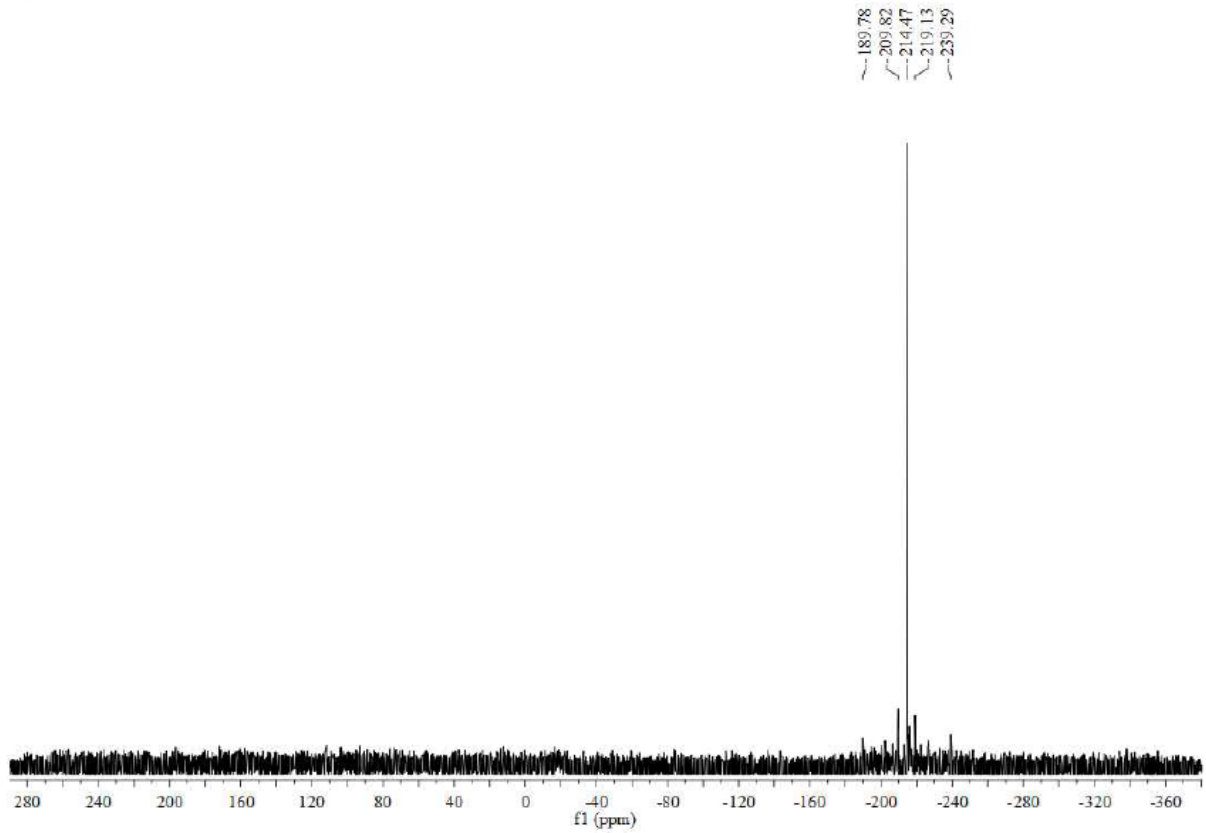

Figure S19. $^{119}Sn\{^{1}H\}$ NMR spectrum of **6** in C_6D_6

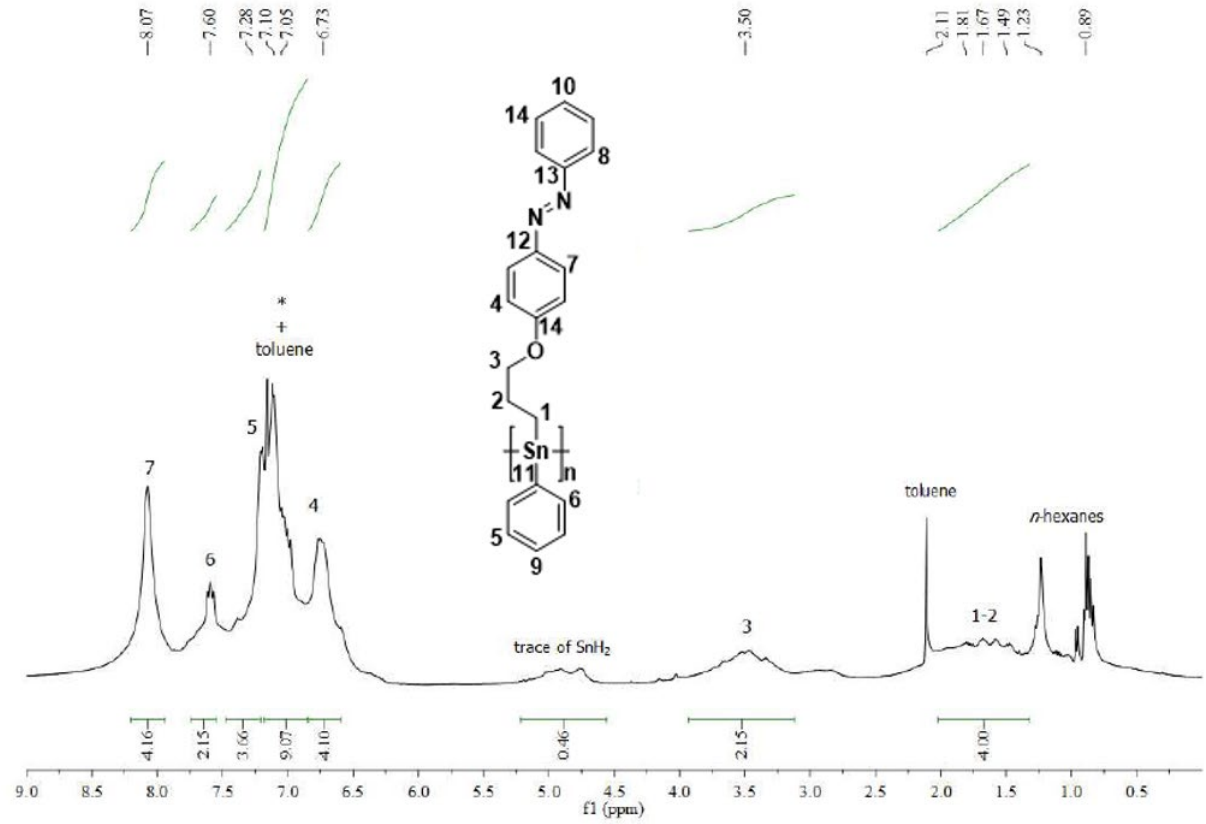

Figure S20. ^{1}H NMR spectrum of **7-f** in C_6D_6

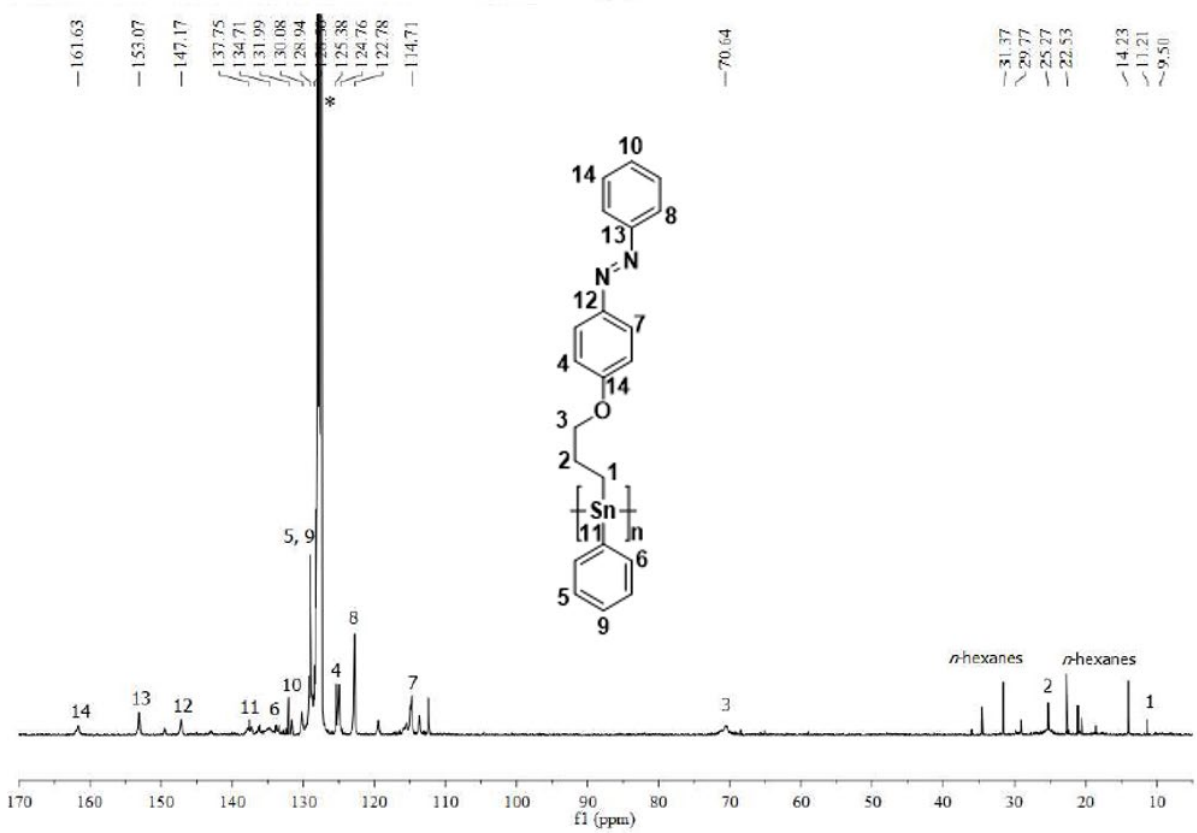

Figure S21. $^{13}C\{^{1}H\}$ NMR spectrum of **7-f** in C_6D_6

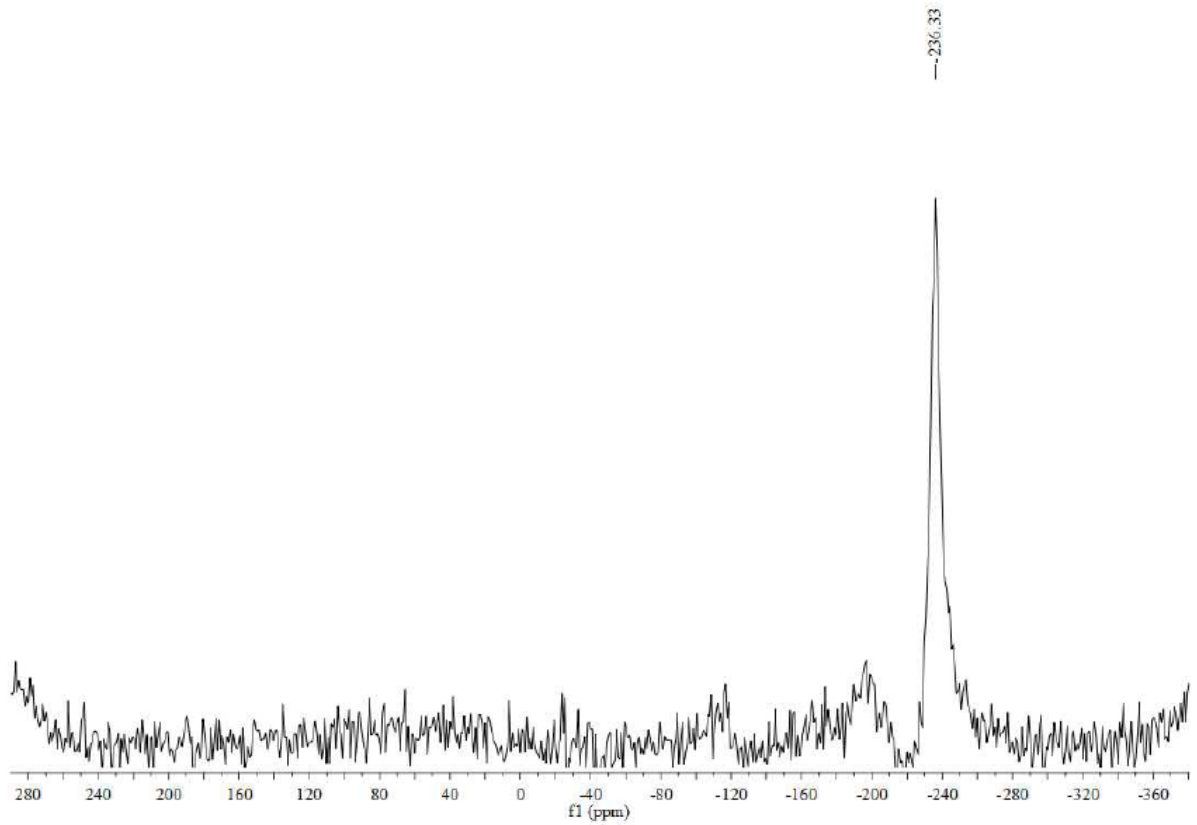

Figure S22. $^{119}Sn\{^{1}H\}$ NMR spectrum of **7-f** in C_6D_6

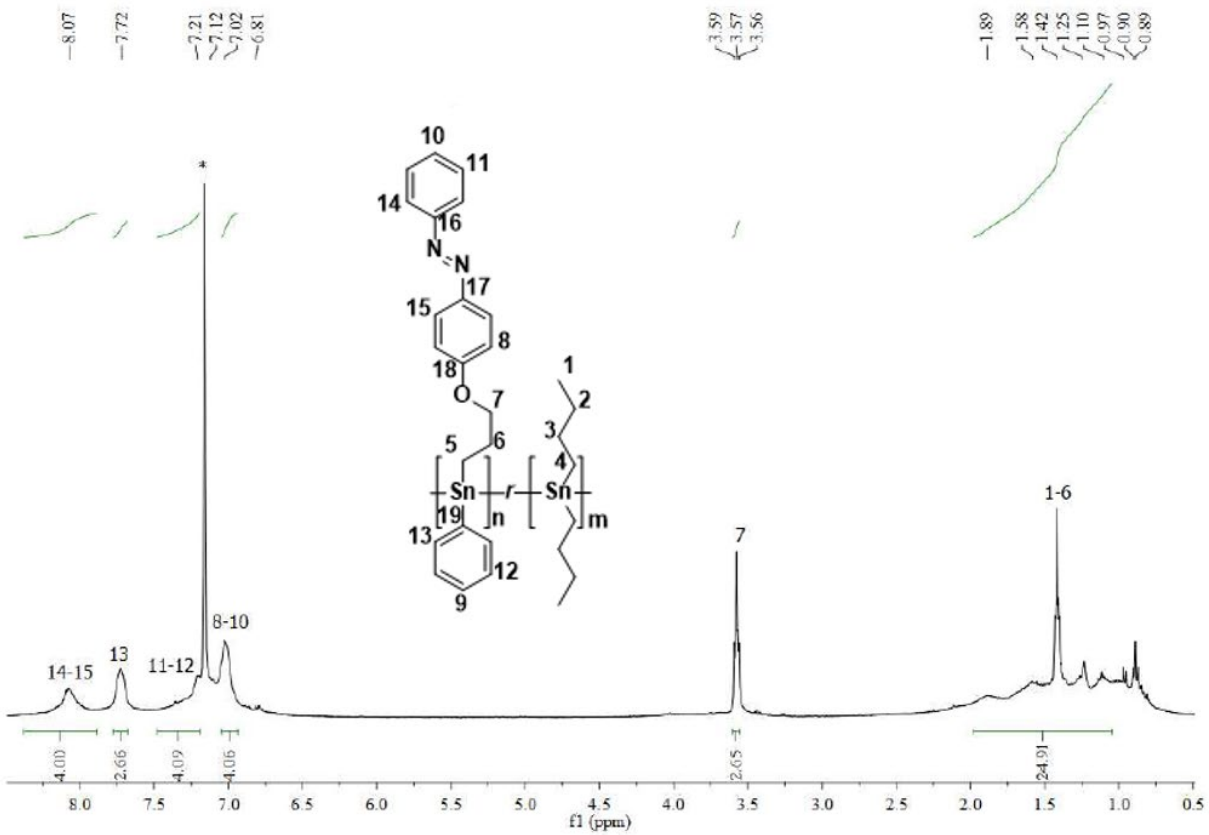

Figure S23. ^{1}H NMR spectrum of **8a (4:1)** in C_6D_6

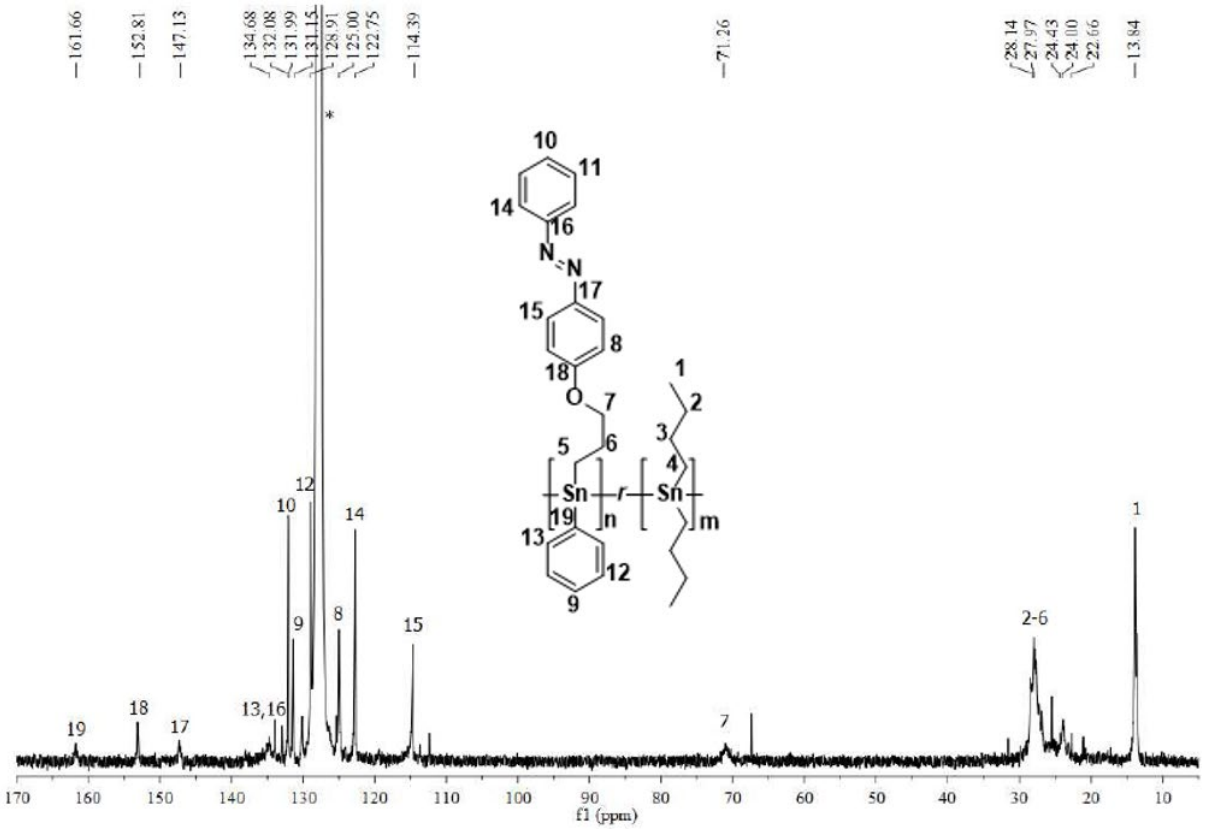

Figure S24. ^{13}C{^{1}H} NMR spectrum of **8a (4:1)** in C_6D_6

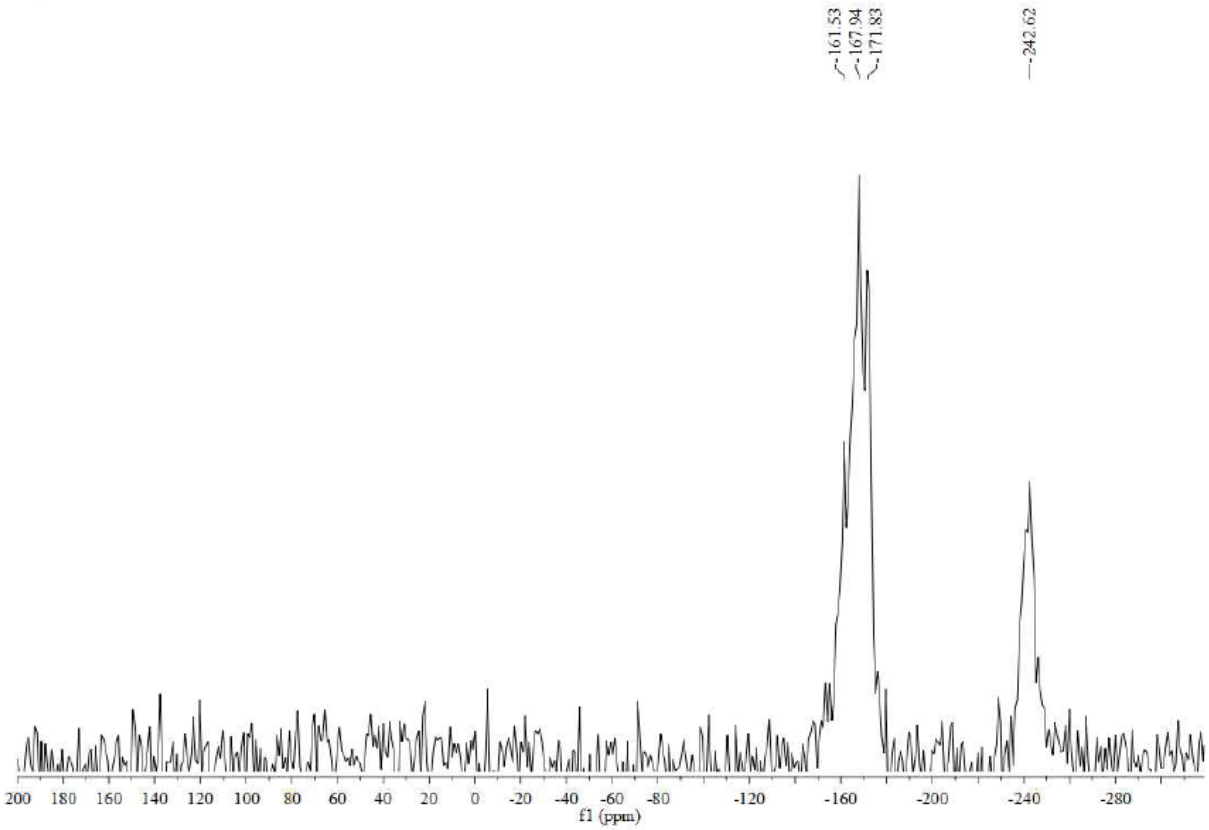

Figure S25. $^{119}Sn\{^{1}H\}$ NMR spectrum of **8a (4:1)** in C_6D_6

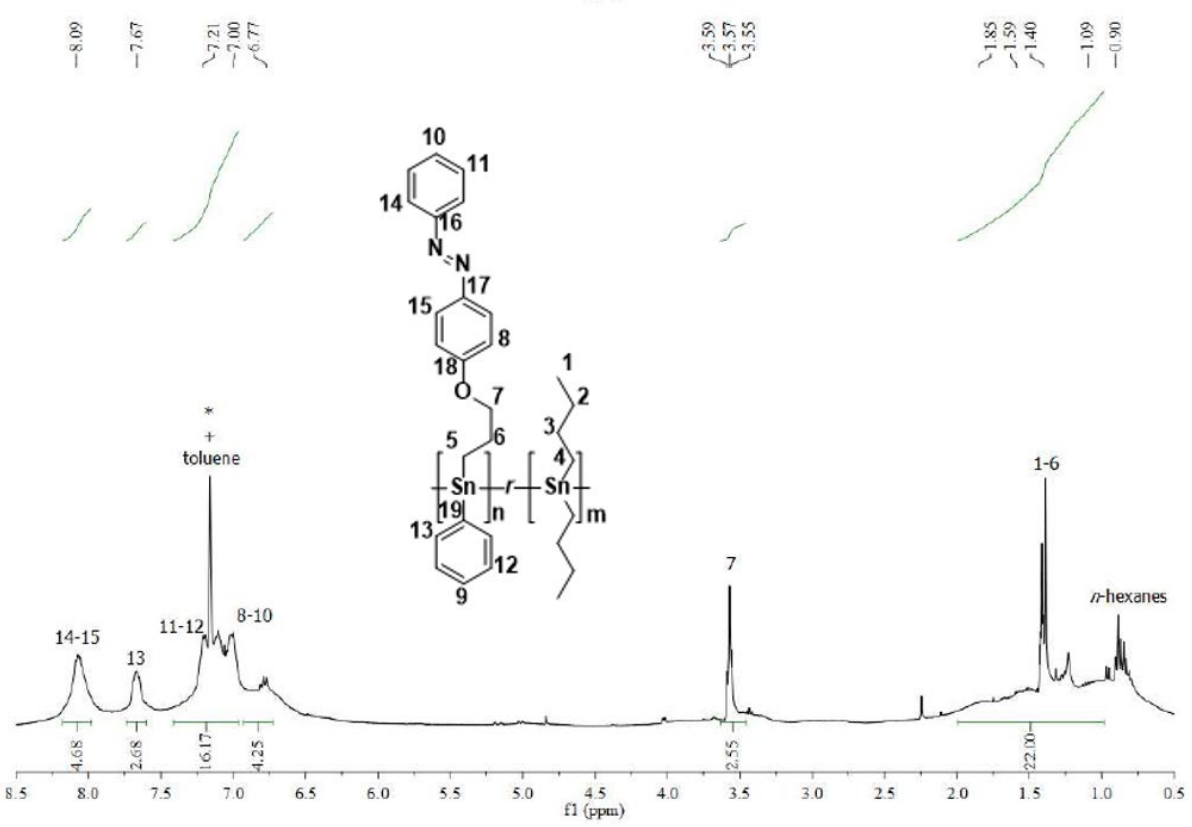

Figure S26. ^{1}H NMR spectrum of **8b (1:1)** in C_6D_6

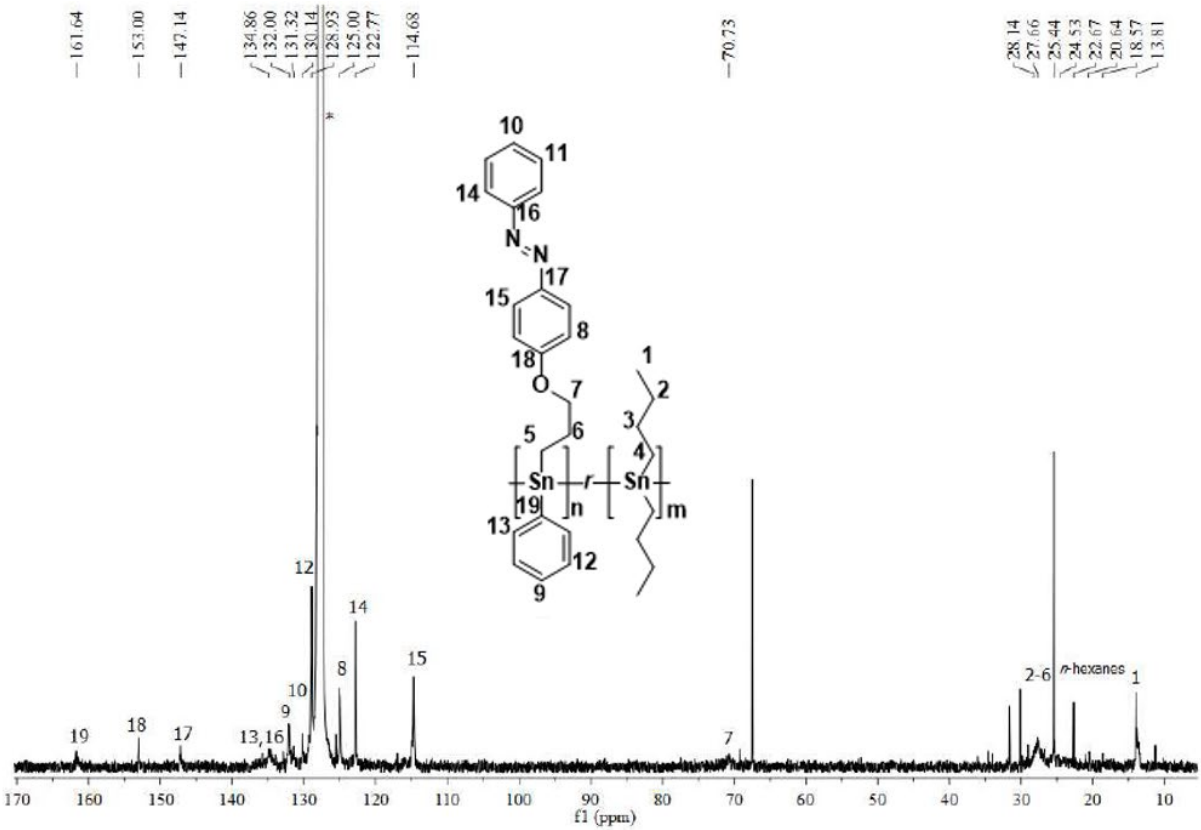

Figure S27. $^{13}C\{^{1}H\}$ NMR spectrum of **8b (1:1)** in C_6D_6

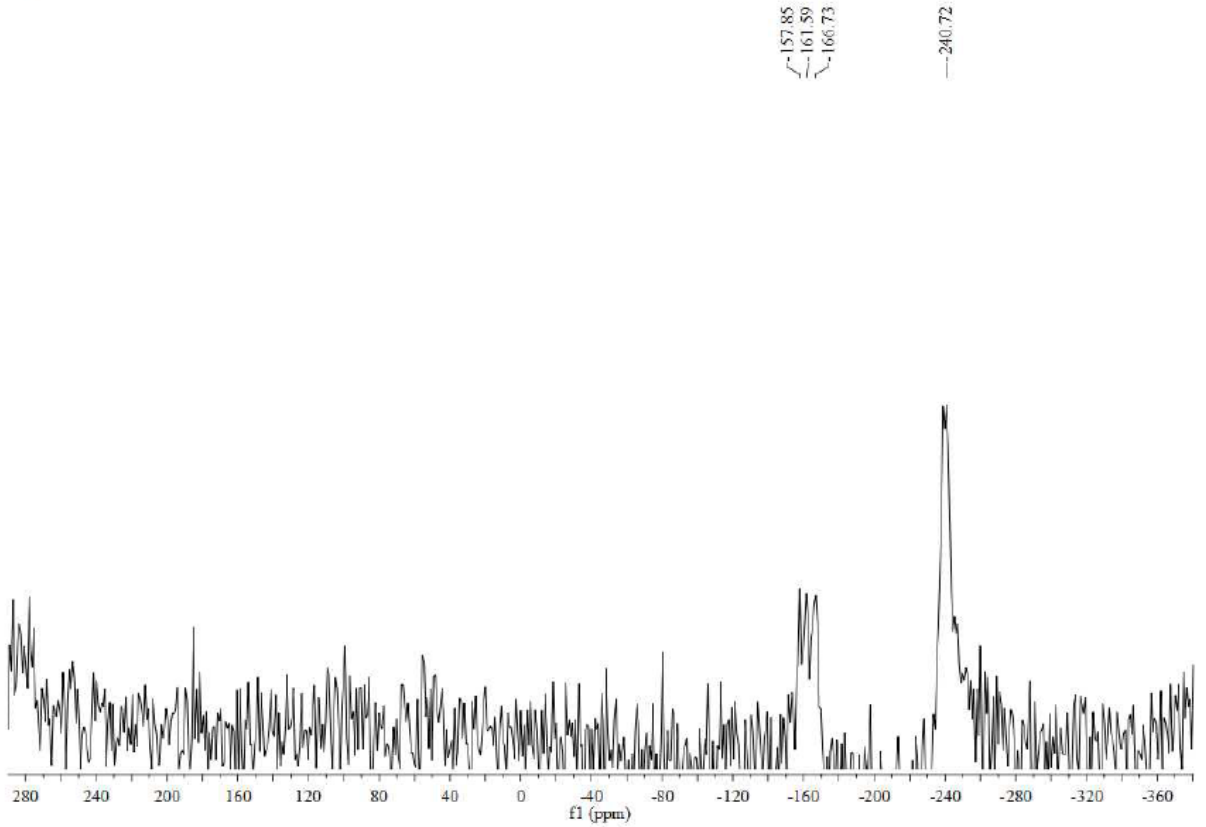

Figure S28. $^{119}Sn\{^{1}H\}$ NMR spectrum of **8b (1:1)** in C_6D_6

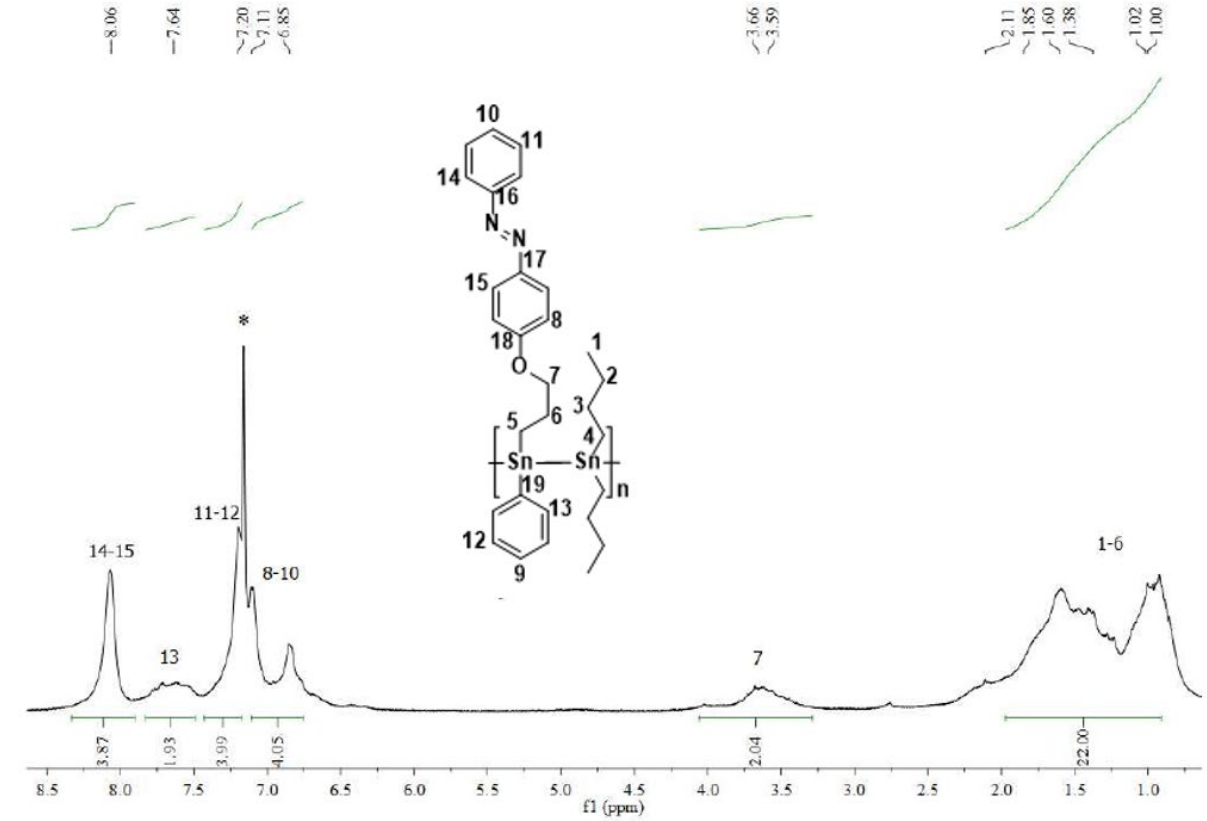

Figure S29. ^{1}H NMR spectrum of **9** in C_6D_6

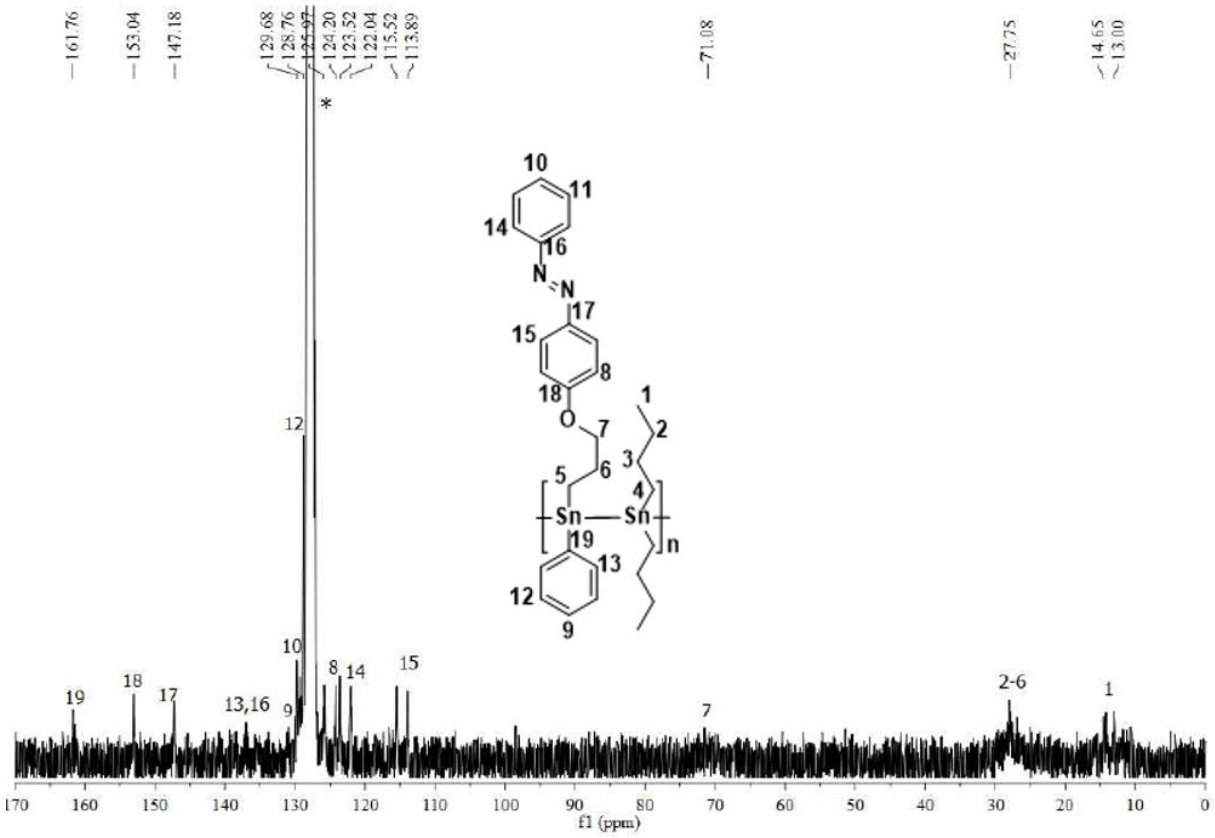

Figure S30. $^{13}C\{^{1}H\}$ NMR spectrum of **9** in C_6D_6

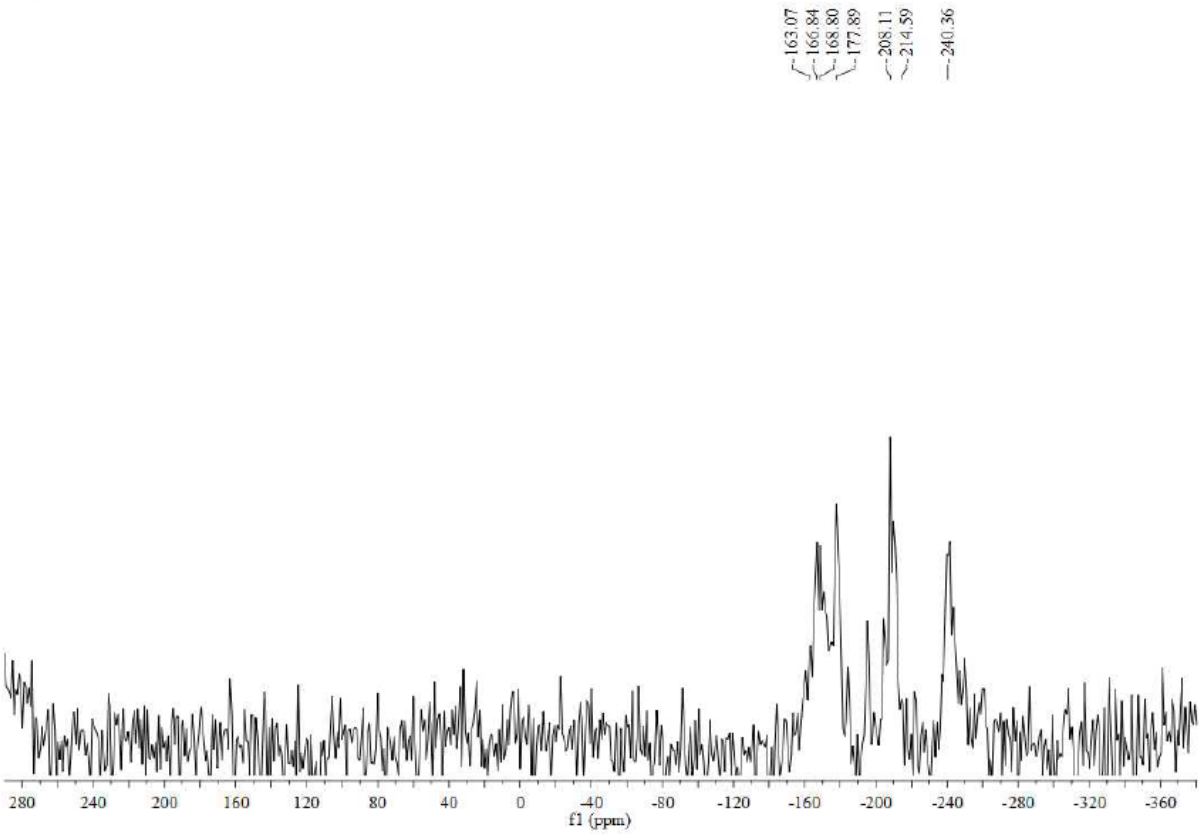

Figure S31. $^{119}Sn\{^{1}H\}$ NMR spectrum of **9** in C_6D_6

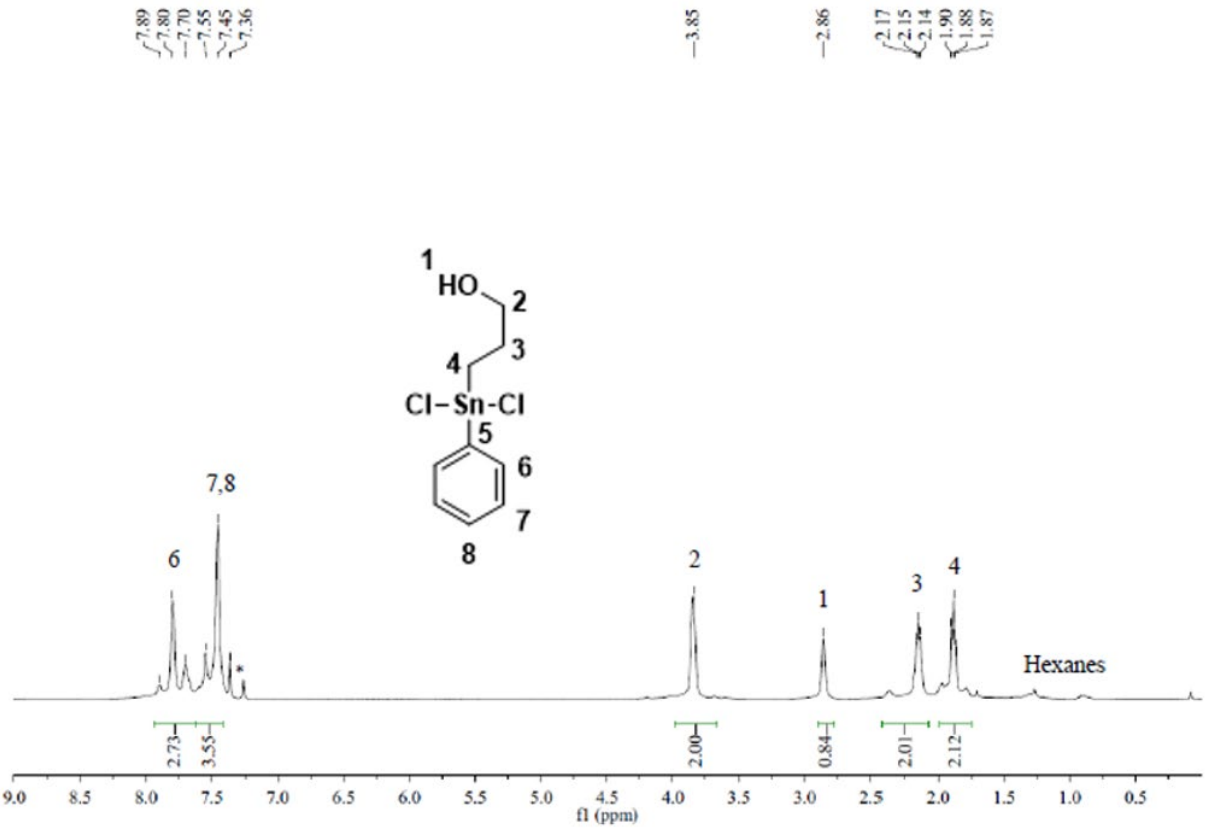

Figure S32. ^{1}H NMR spectrum of **11** in $CDCl_3$

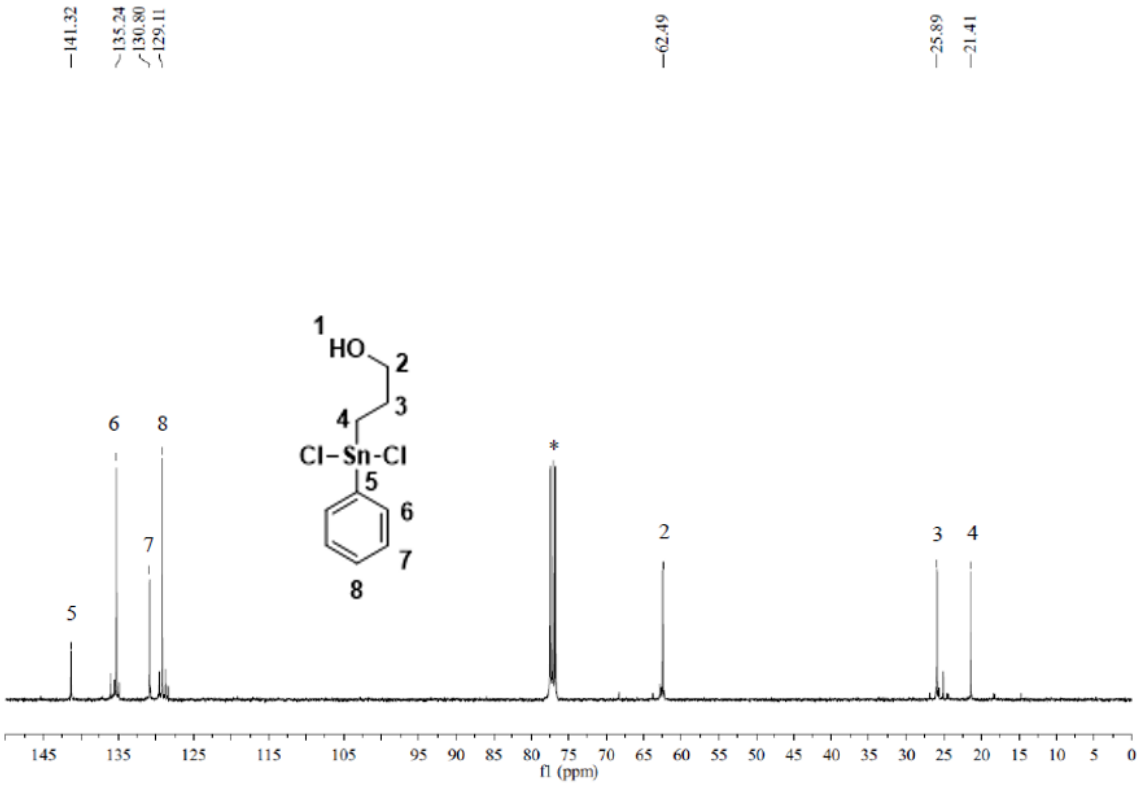

Figure S33. $^{13}C\{^{1}H\}$ NMR spectrum of **11** in $CDCl_3$

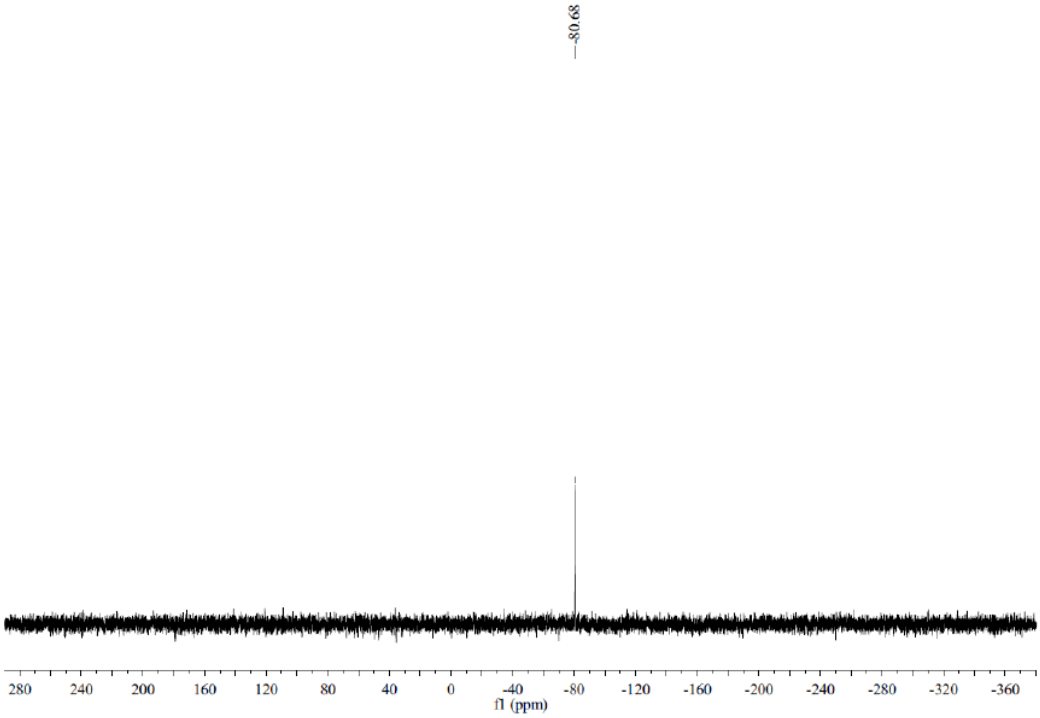

Figure S34. $^{119}Sn\{^{1}H\}$ NMR spectrum of **11** in $CDCl_3$

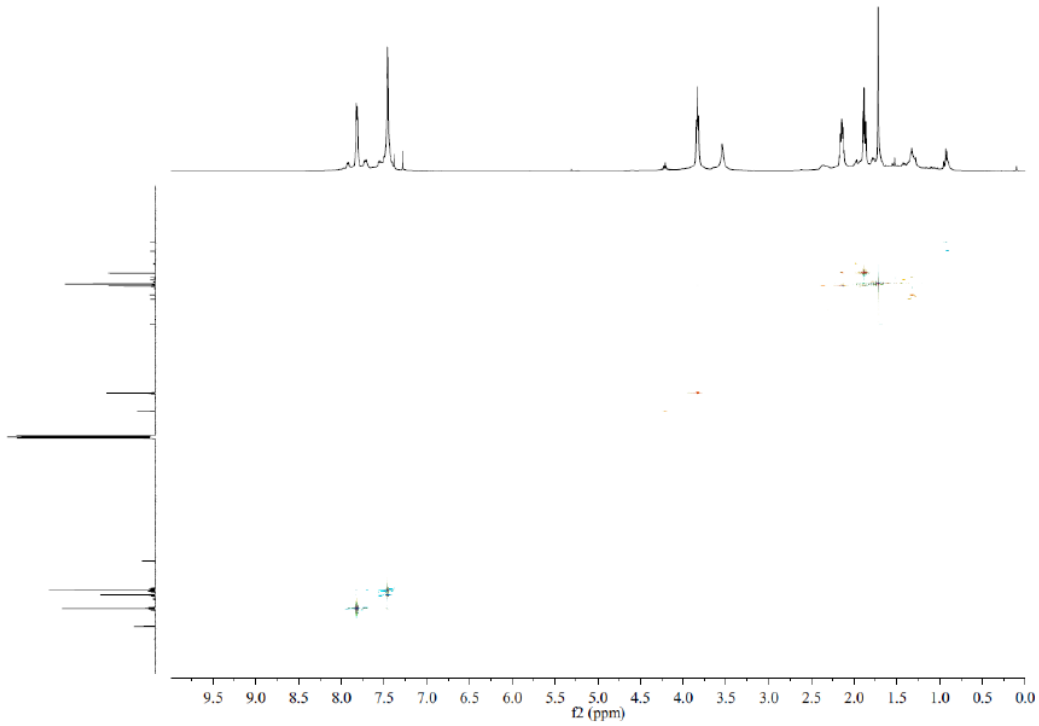

Figure S35. HSQC 2D-NMR spectrum of **11** in $CDCl_3$

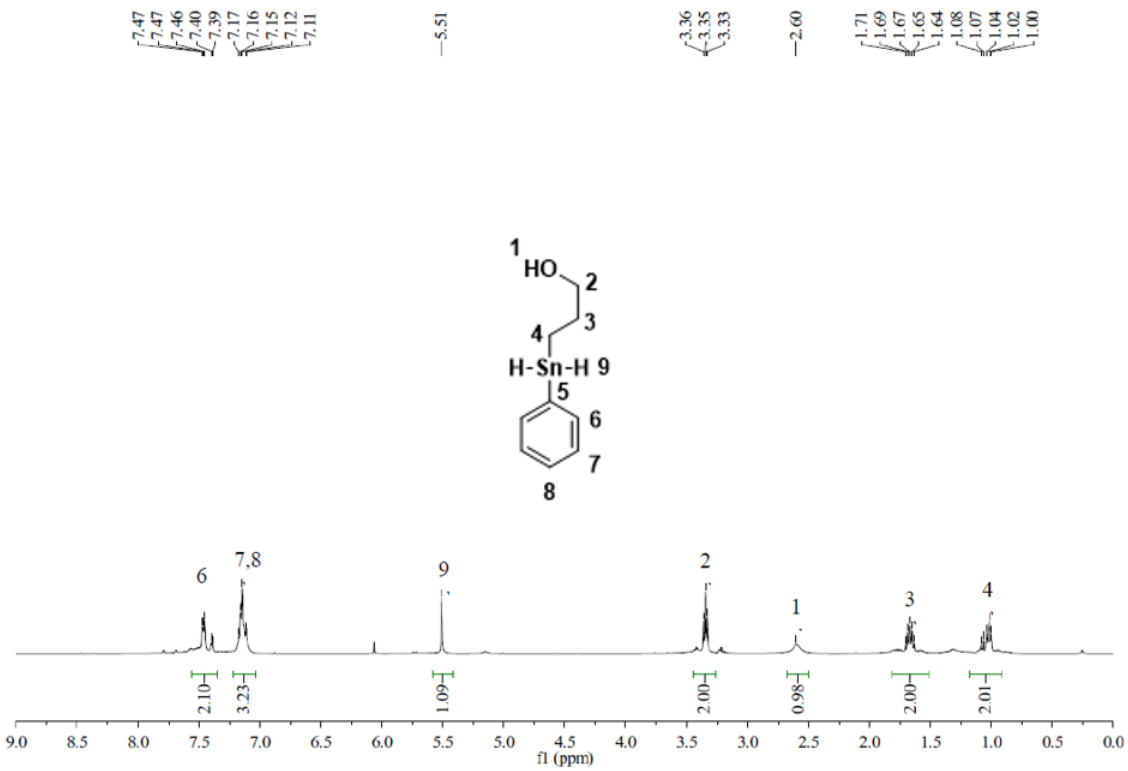

Figure S36. ^{1}H NMR spectrum of **12** in C_6D_6

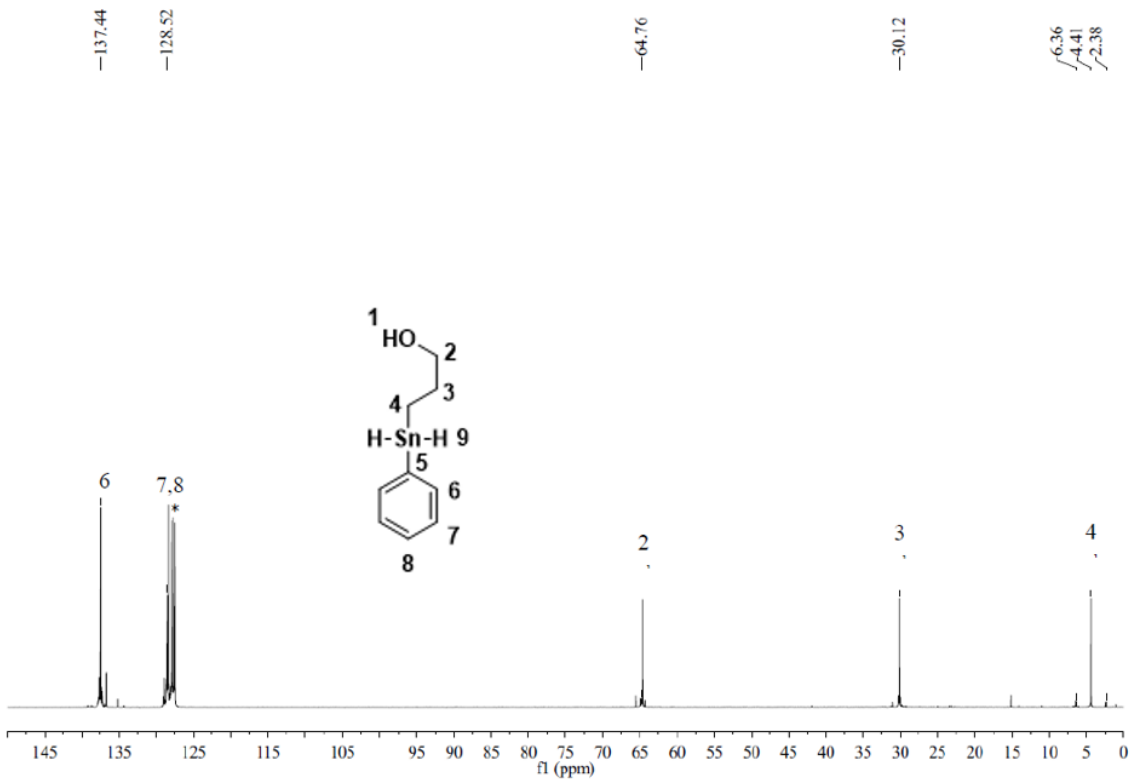

Figure S37. $^{13}C\{^{1}H\}$ NMR spectrum of **12** in C_6D_6

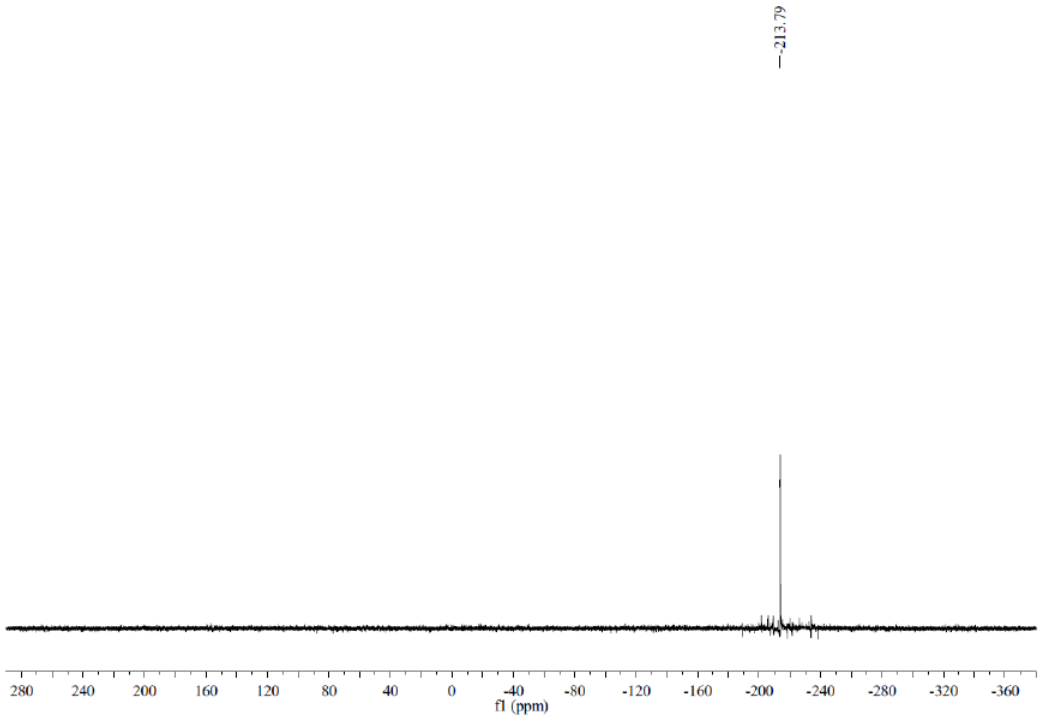

Figure S38. $^{119}Sn\{^{1}H\}$ NMR spectrum of **12** in C_6D_6

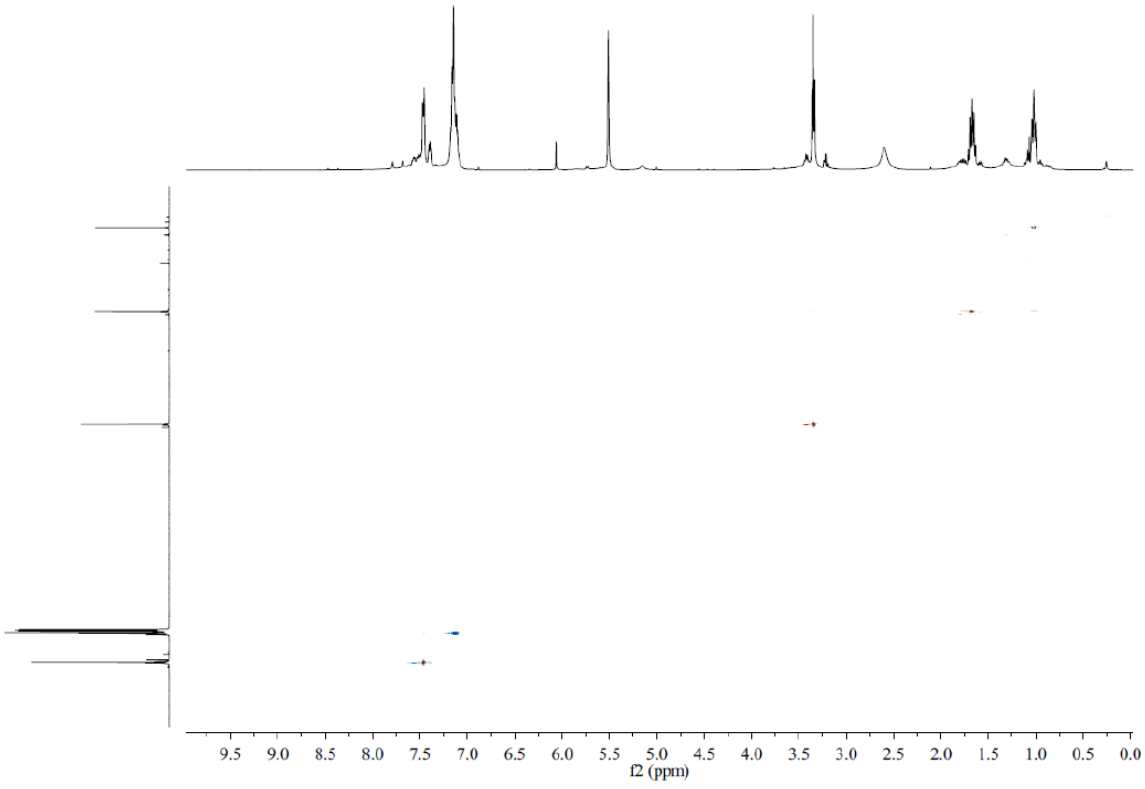

Figure S39. HSQC 2D-NMR spectrum of **12** in C_6D_6

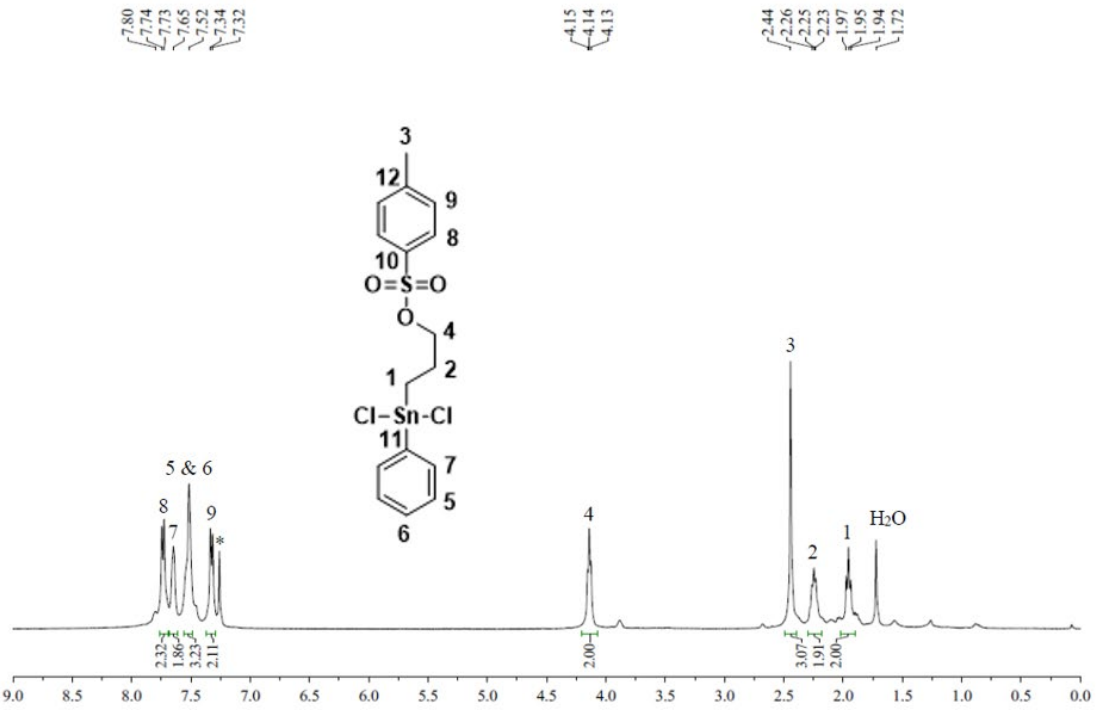

Figure S40. ^{1}H NMR spectrum of **13** in $CDCl_3$

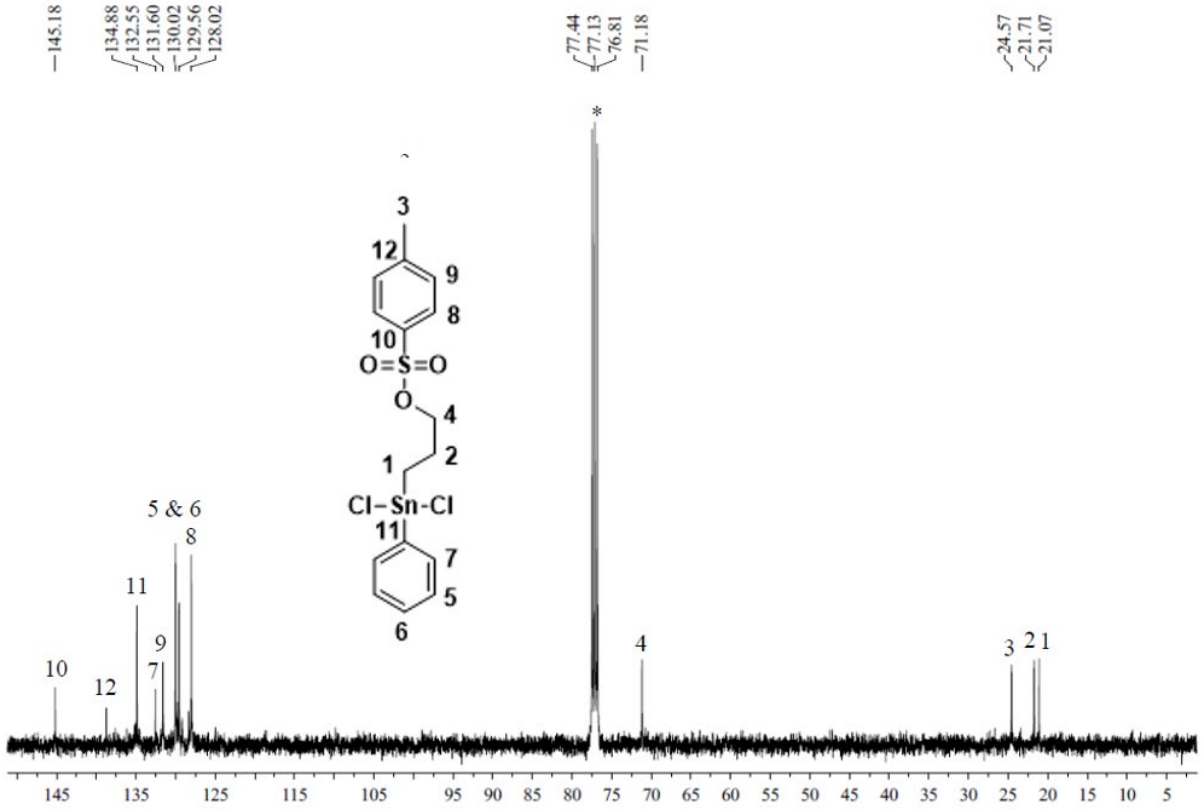

Figure S41. $^{13}C\{^{1}H\}$ NMR spectrum of **13** in $CDCl_3$

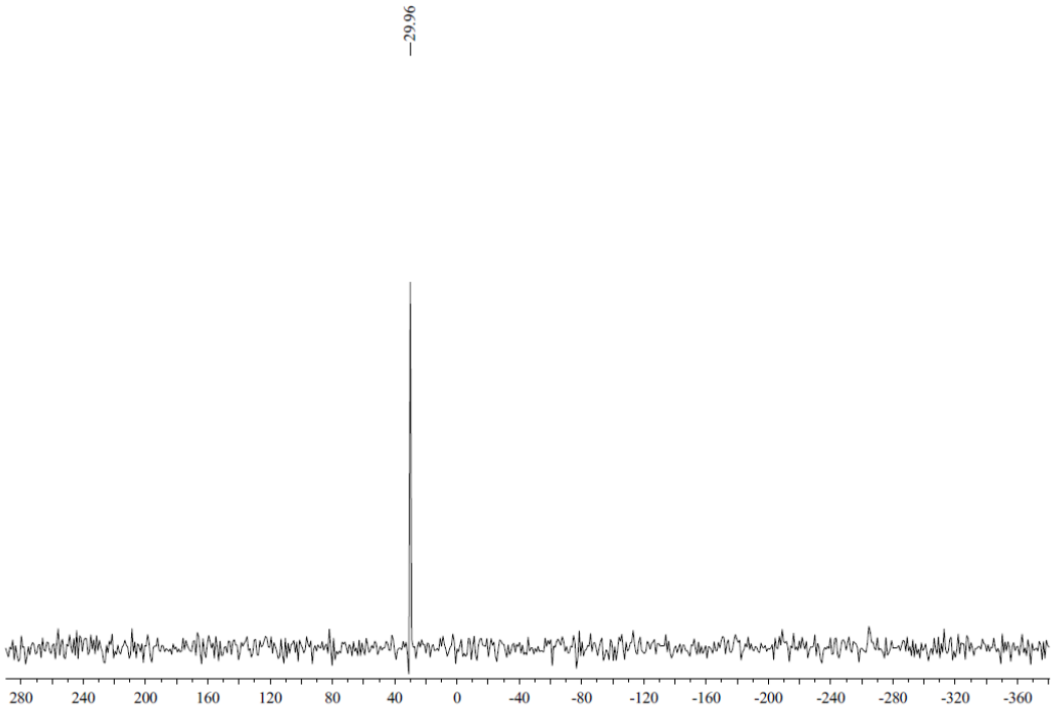

Figure S42. $^{119}Sn\{^{1}H\}$ NMR spectrum of **13** in $CDCl_3$

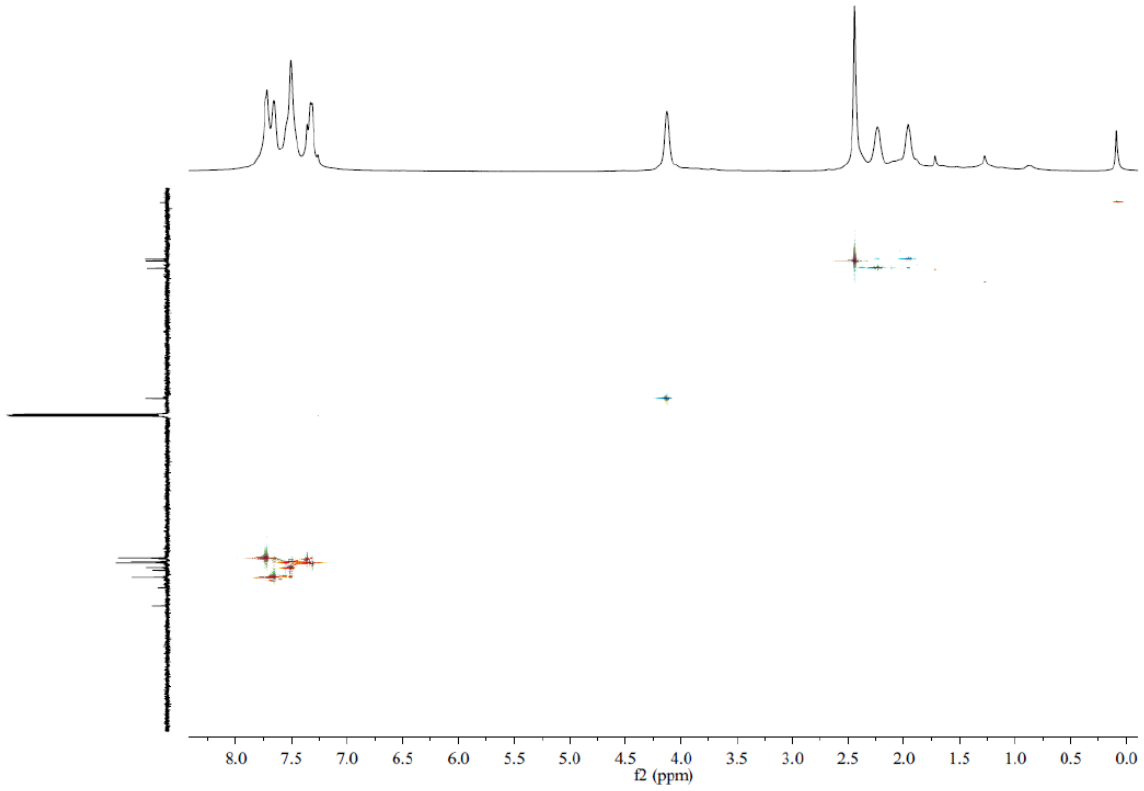

Figure S43. HSQC 2D-NMR spectrum of **13** in $CDCl_3$

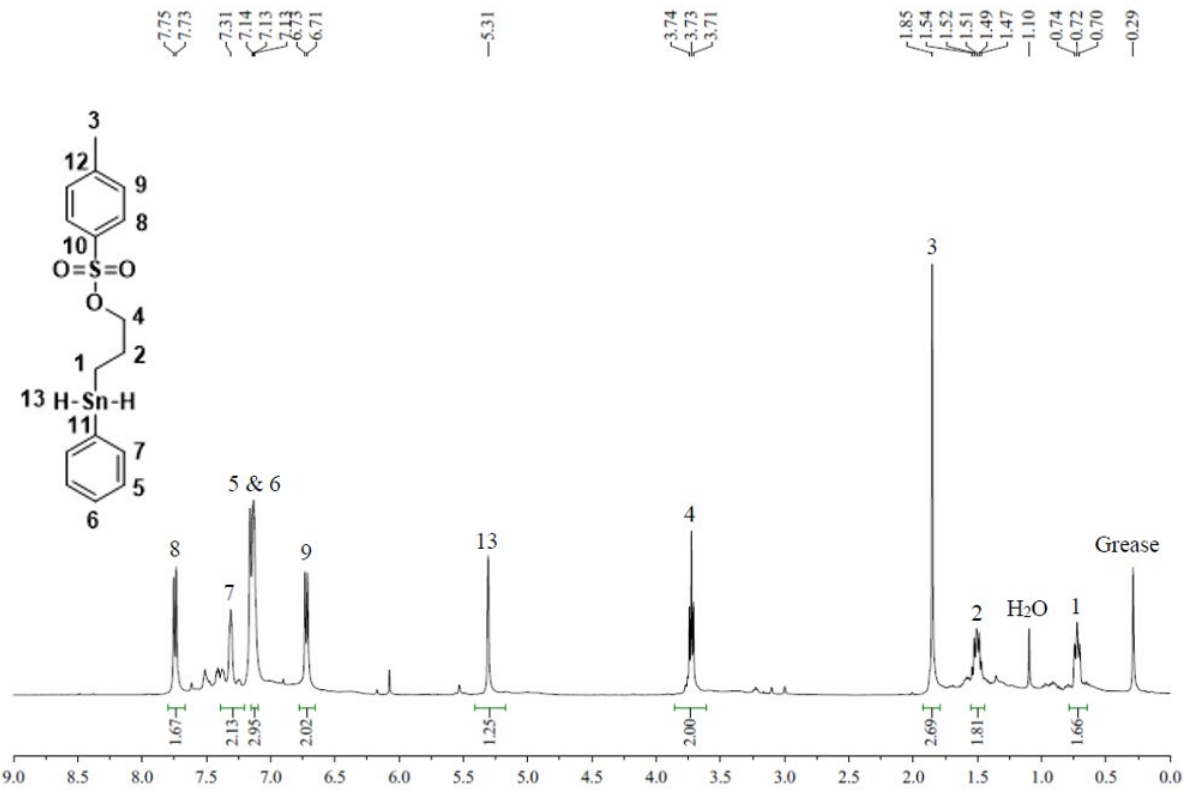

Figure S44. ^{1}H NMR spectrum of **14** in C_6D_6

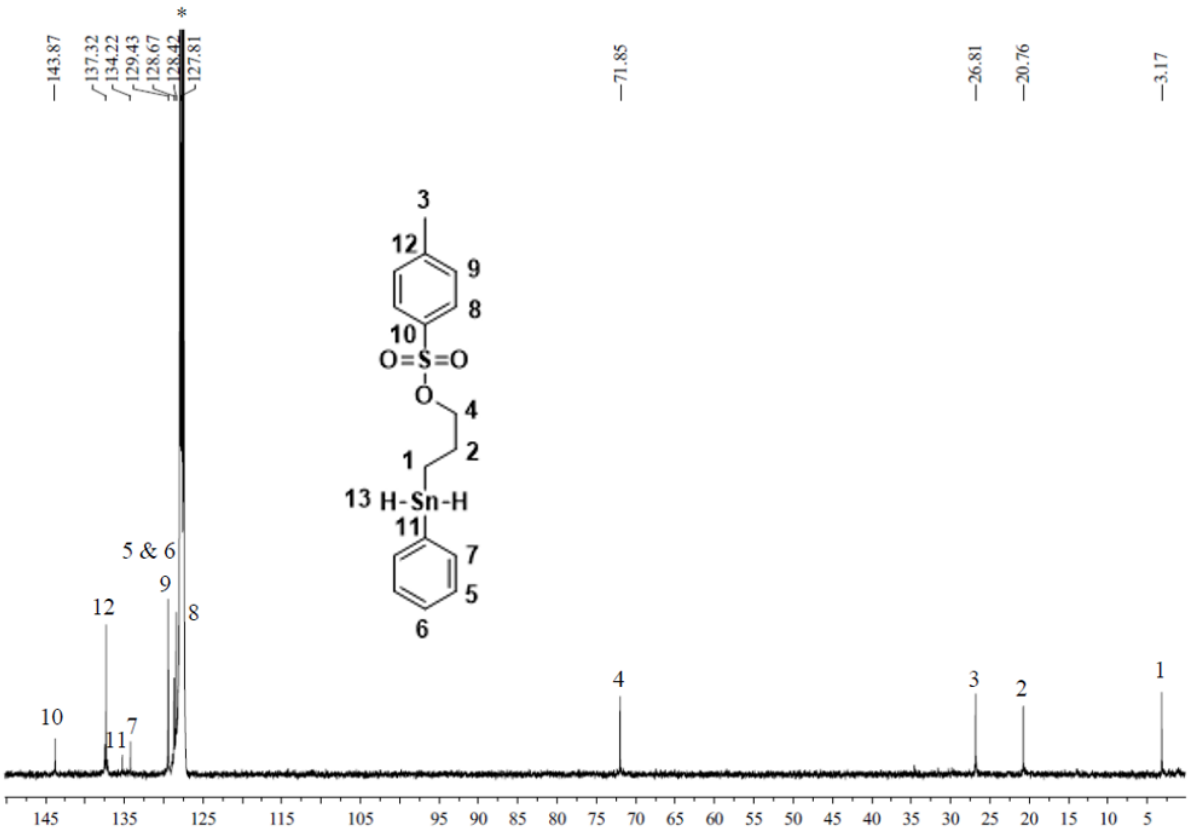

Figure S45. $^{13}C\{^{1}H\}$ NMR spectrum of **14** in C_6D_6

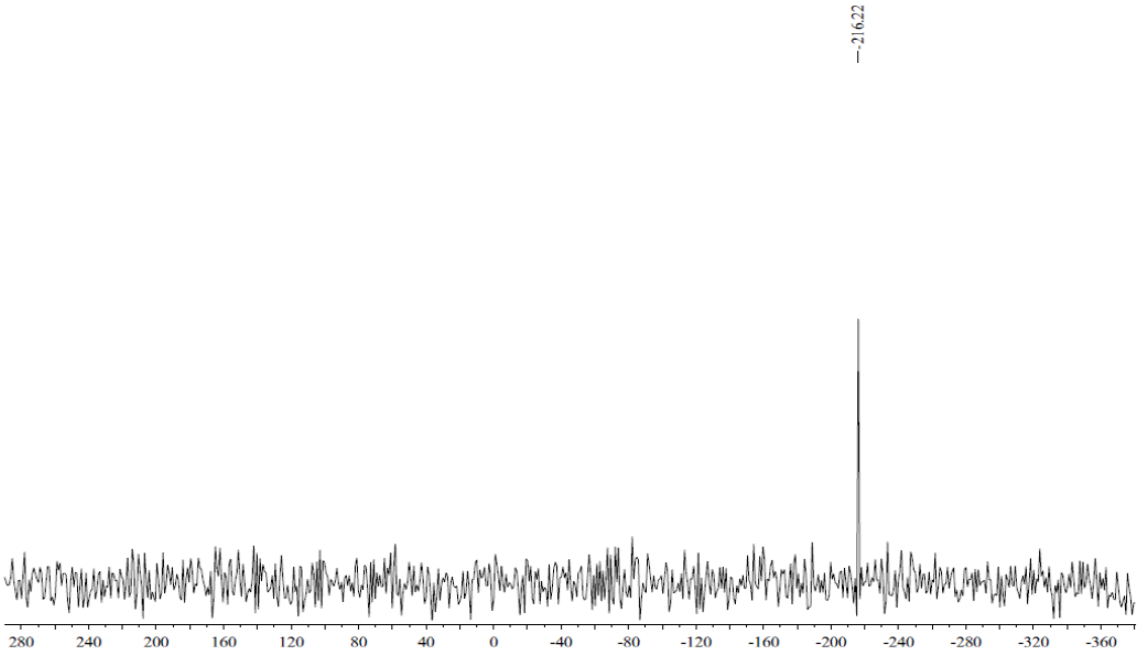

Figure S46. $^{119}Sn\{^{1}H\}$ NMR spectrum of **14** in C_6D_6

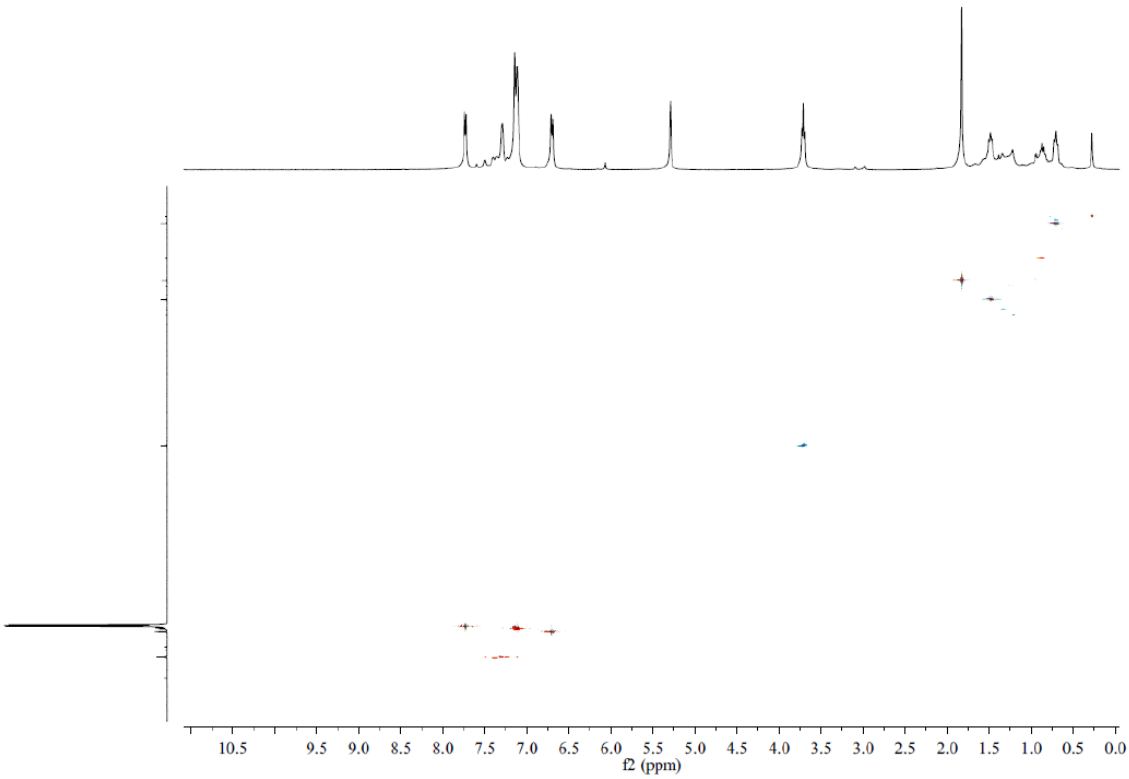

Figure S47. HSQC 2D-NMR spectrum of **14** in C_6D_6

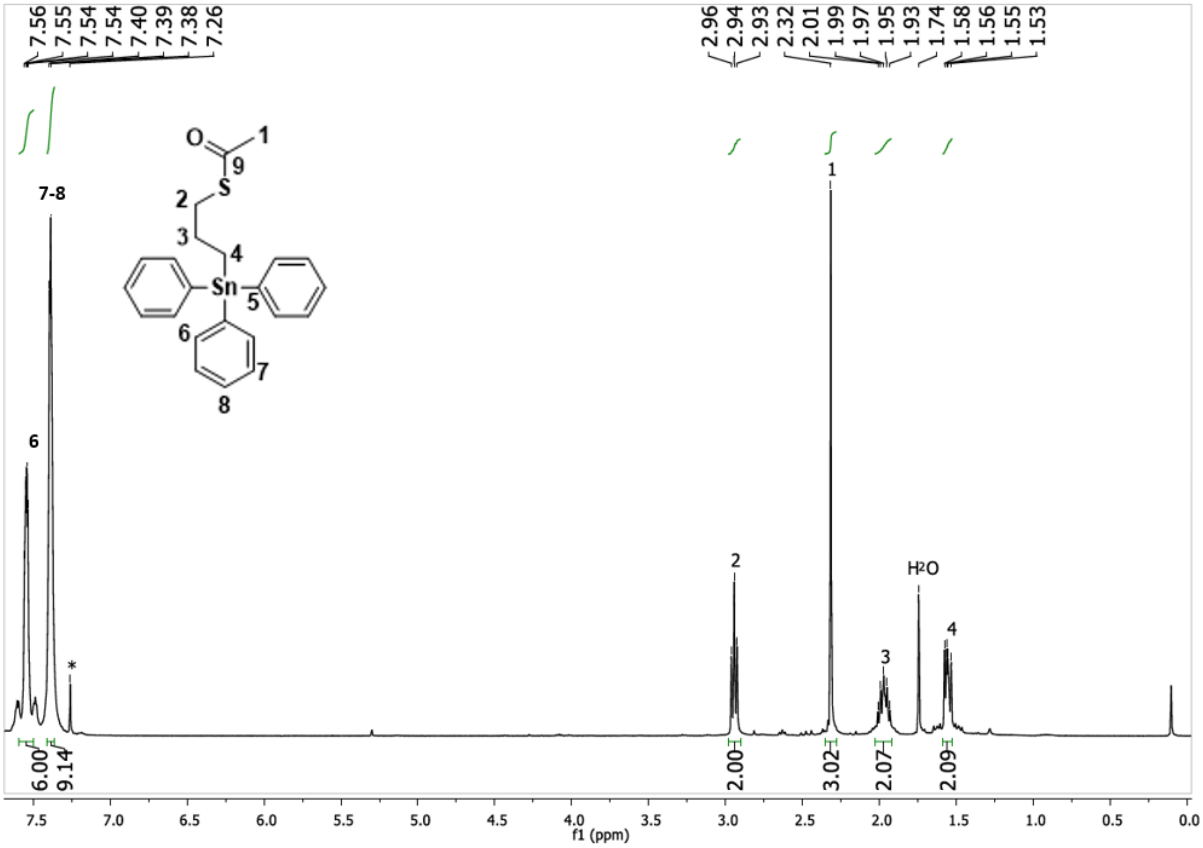

Figure S48. ^{1}H NMR spectrum of **15** in $CDCl_3$

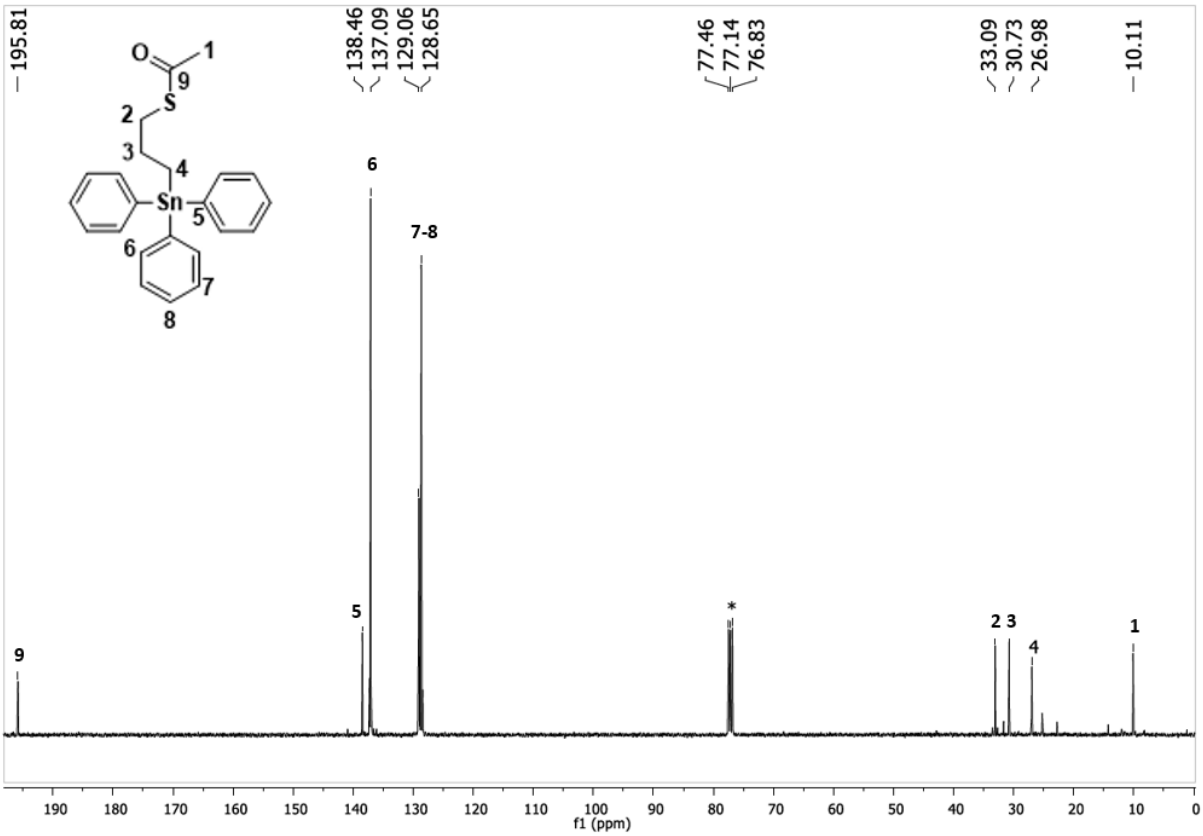

Figure S49. $^{13}C\{^{1}H\}$ NMR spectrum of **15** in $CDCl_3$

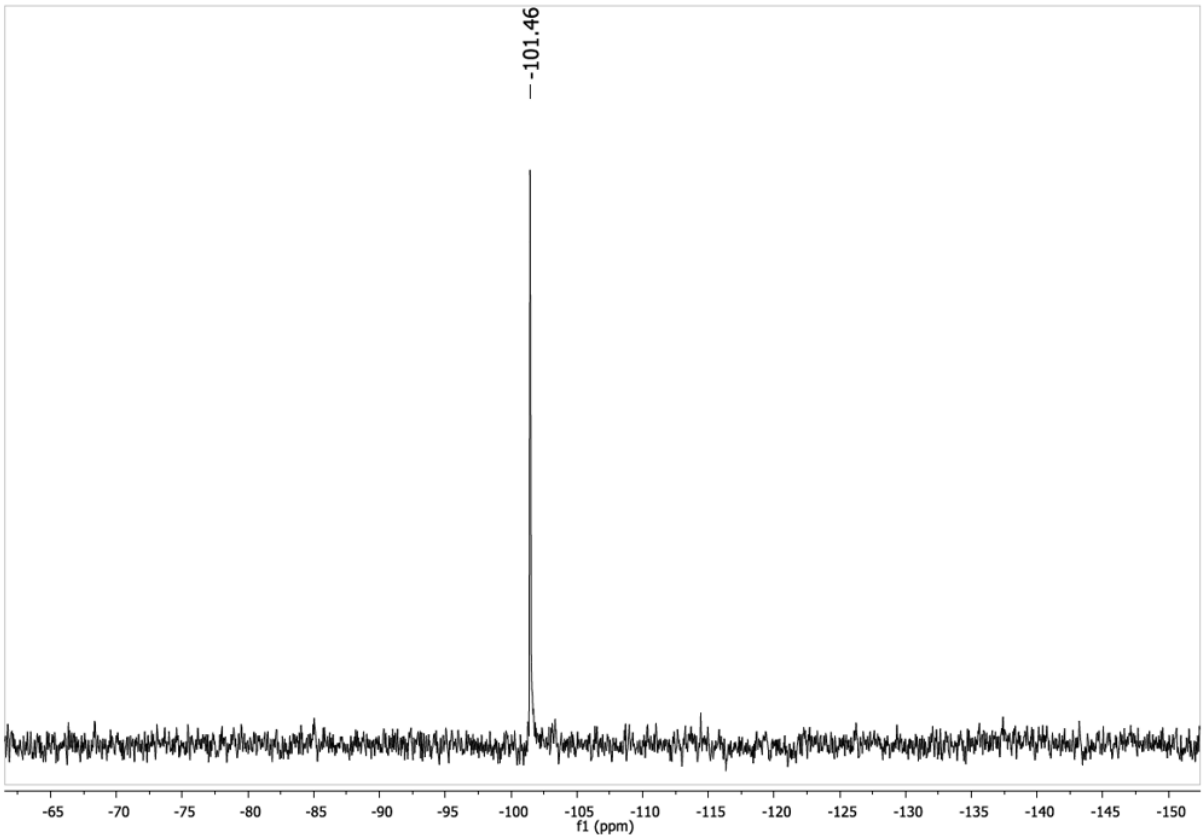

Figure S50. $^{119}Sn\{^{1}H\}$ NMR spectrum of **15** in $CDCl_3$

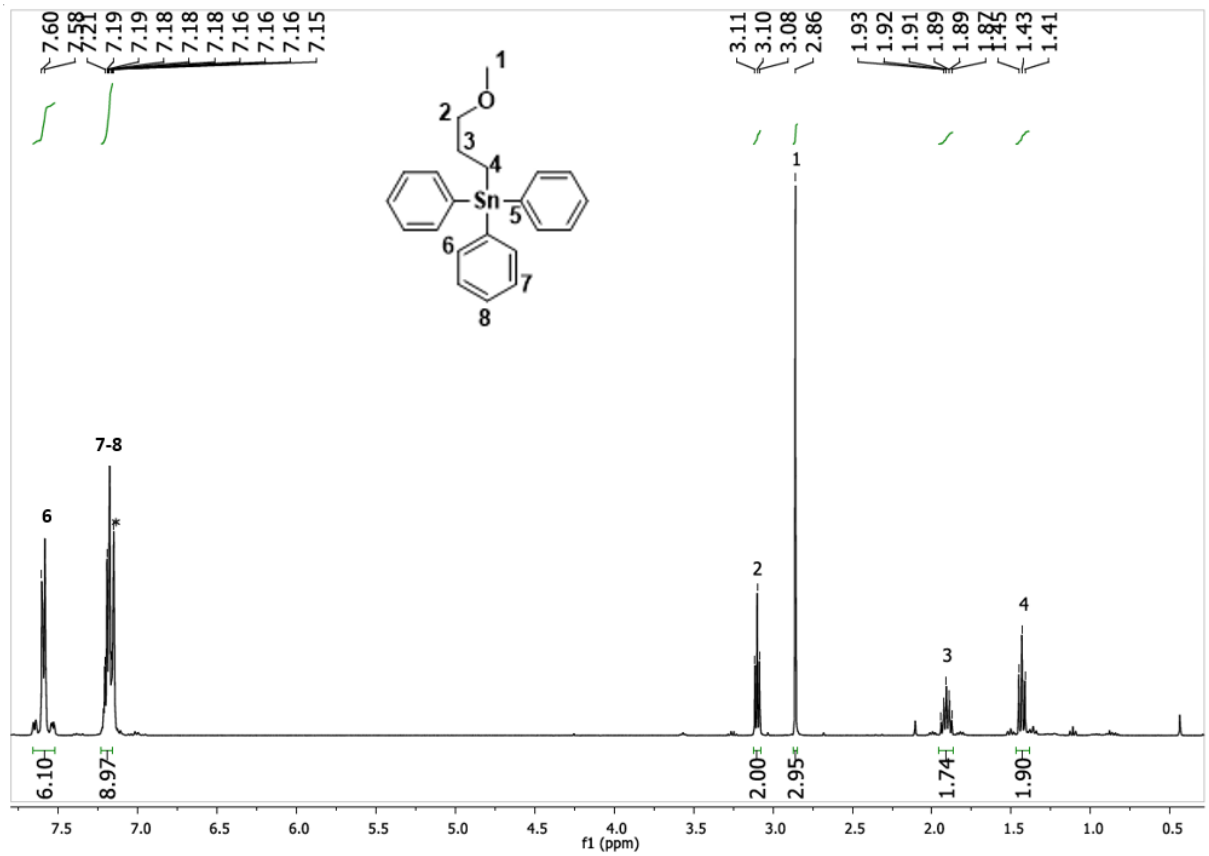

Figure S51. ^{1}H NMR spectrum of **16** in C_6D_6

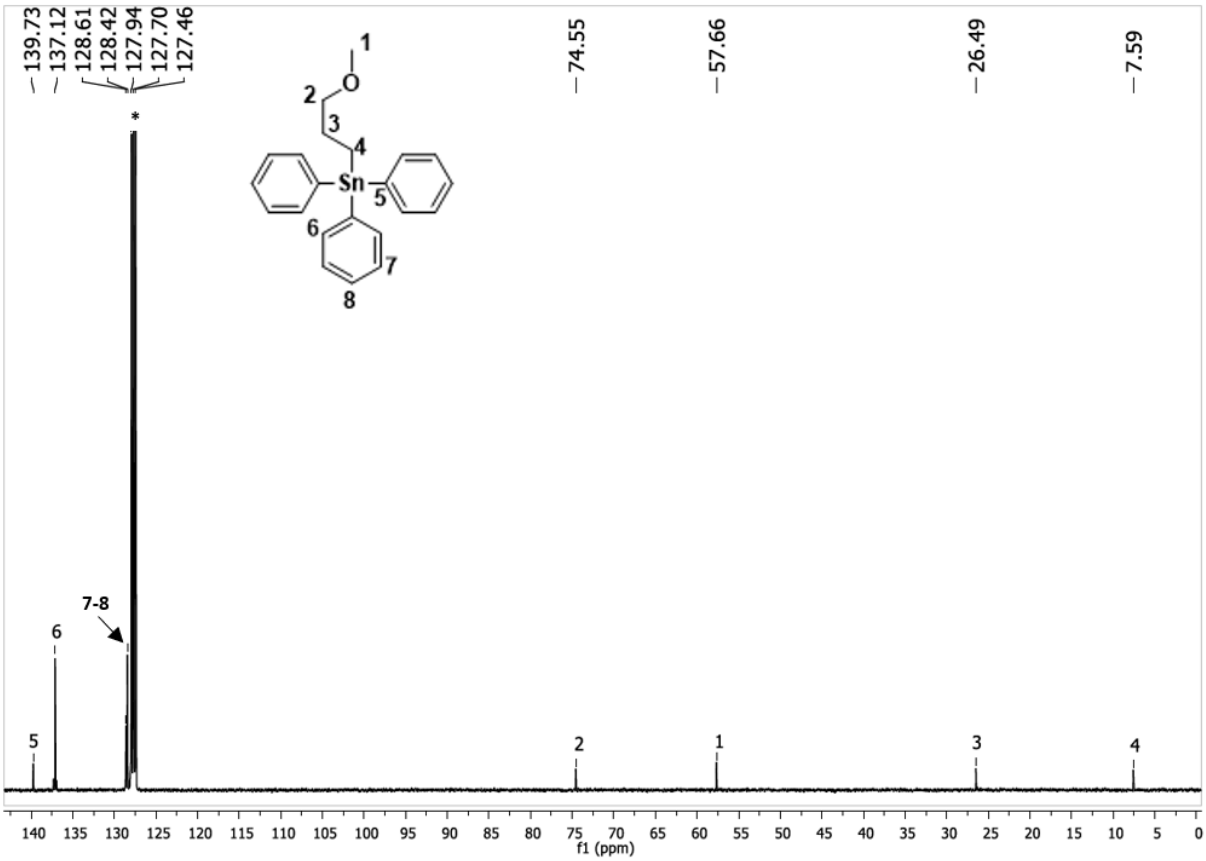

Figure S52. $^{13}C\{^{1}H\}$ NMR spectrum of **16** in C_6D_6

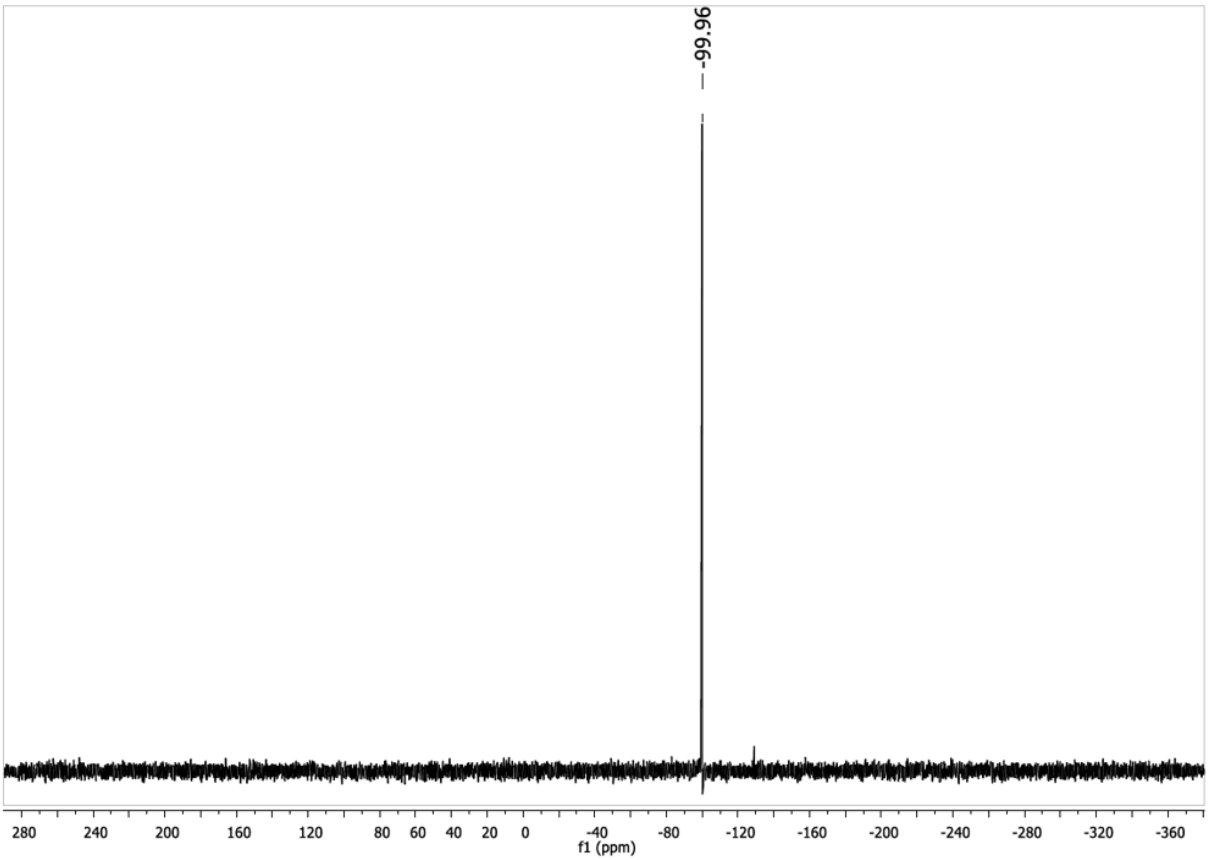

Figure S53. $^{119}Sn\{^{1}H\}$ NMR spectrum of **16** in C_6D_6

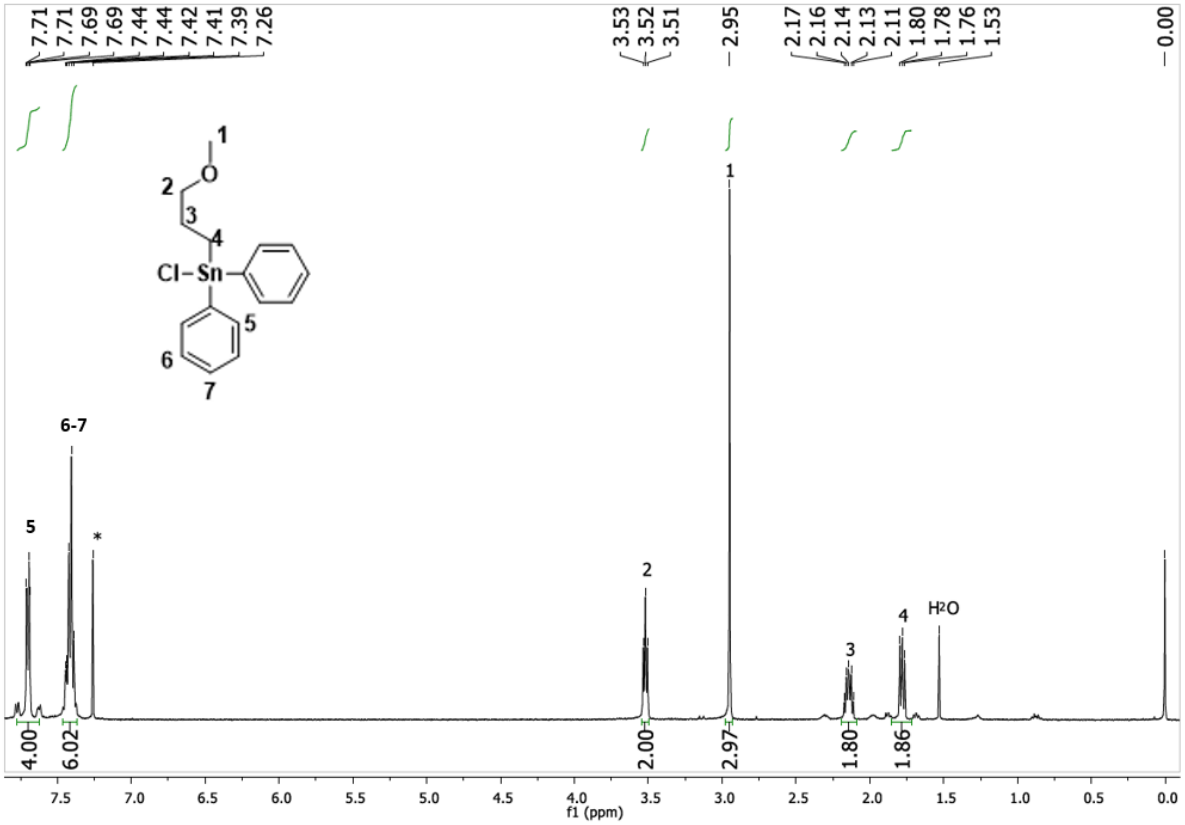

Figure S54. ^{1}H NMR spectrum of **17** in $CDCl_3$

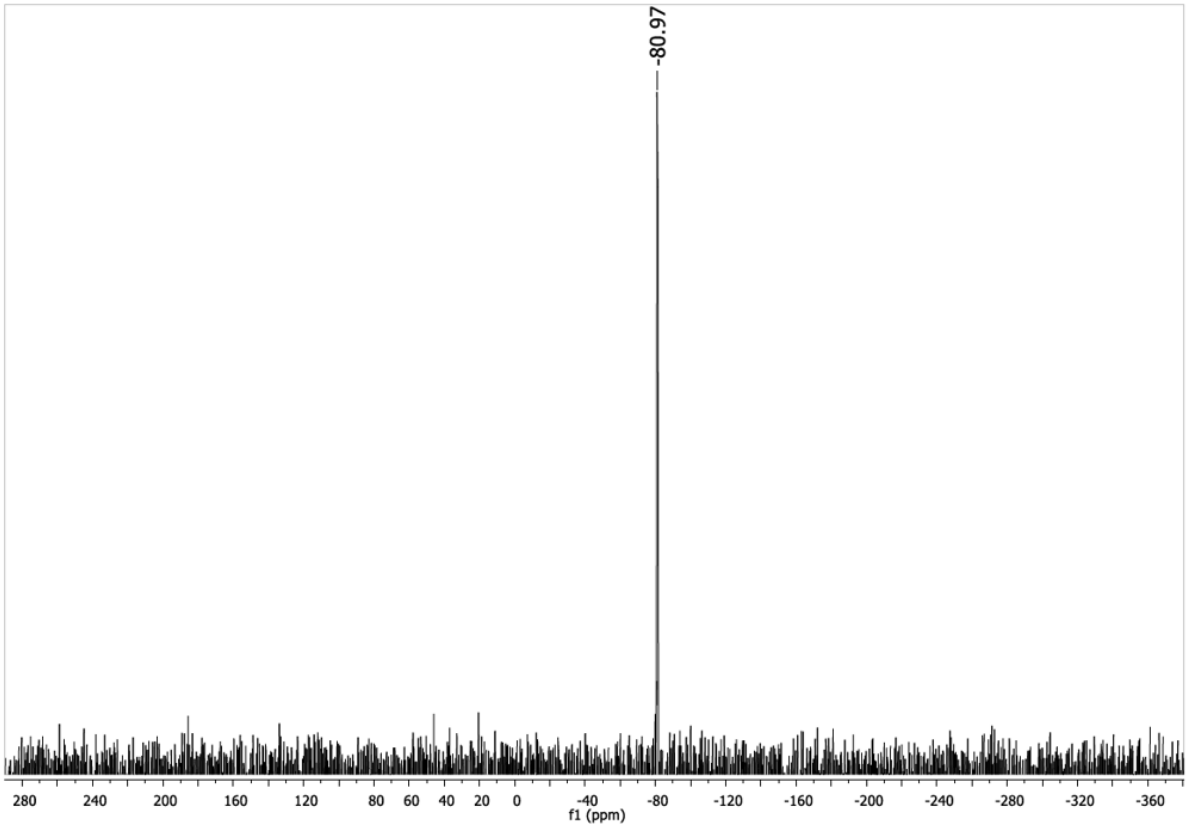

Figure S55. $^{119}Sn\{^{1}H\}$ NMR spectrum of **17** in $CDCl_3$

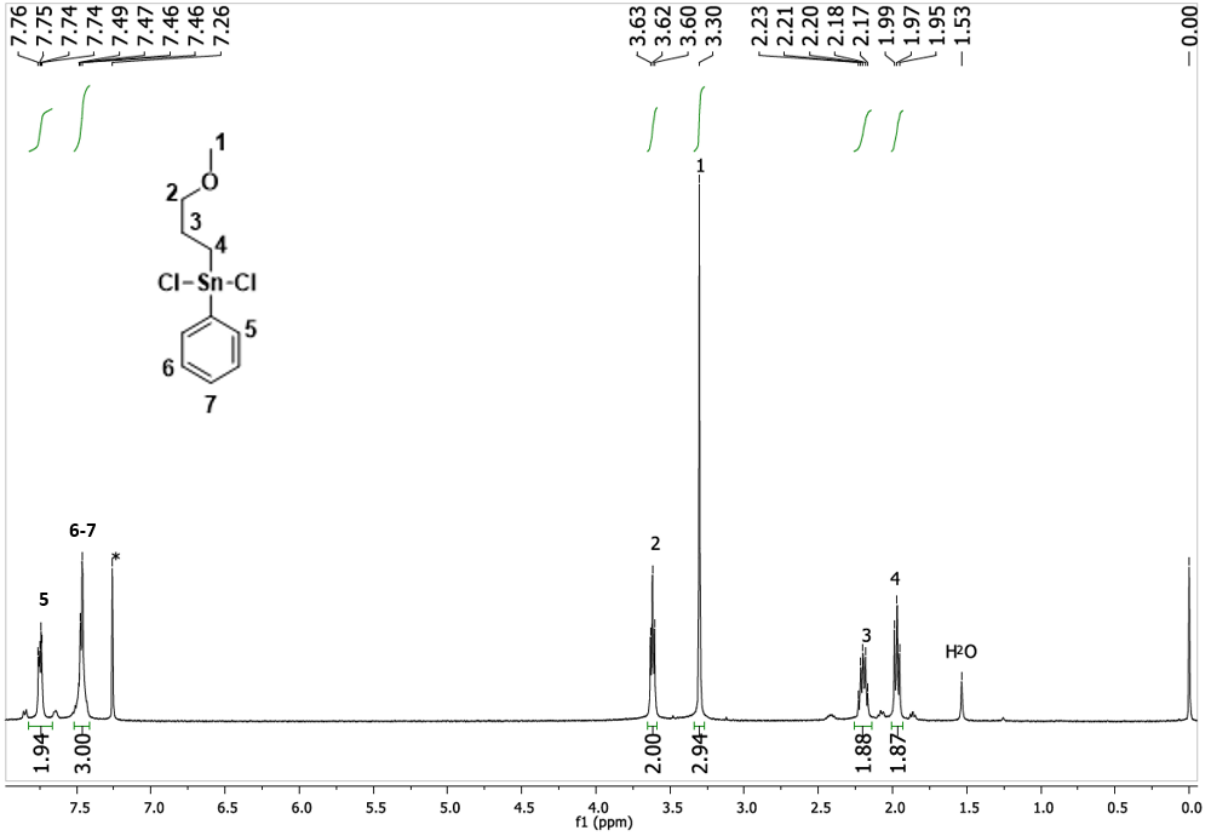

Figure S56. ^{1}H NMR spectrum of **18** in $CDCl_3$

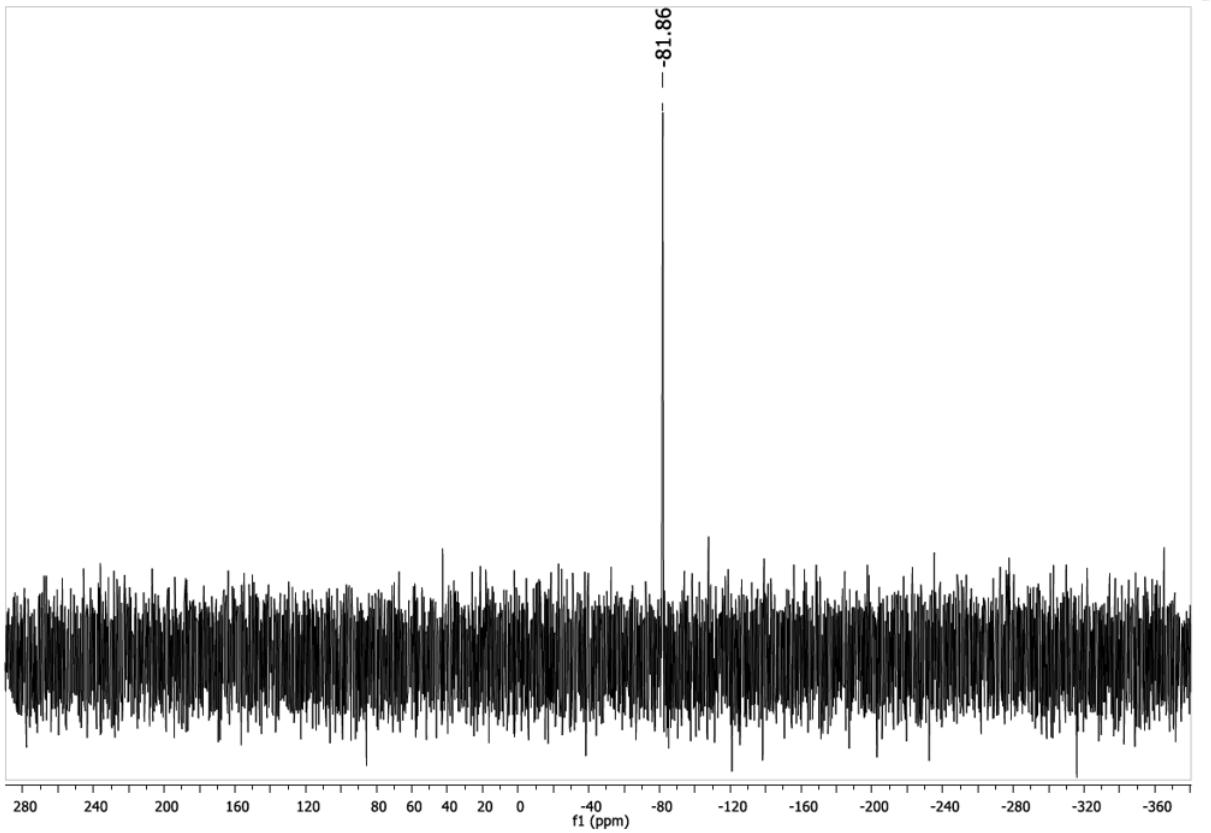

Figure S57. $^{119}Sn\{^{1}H\}$ NMR spectrum of **18** in $CDCl_3$

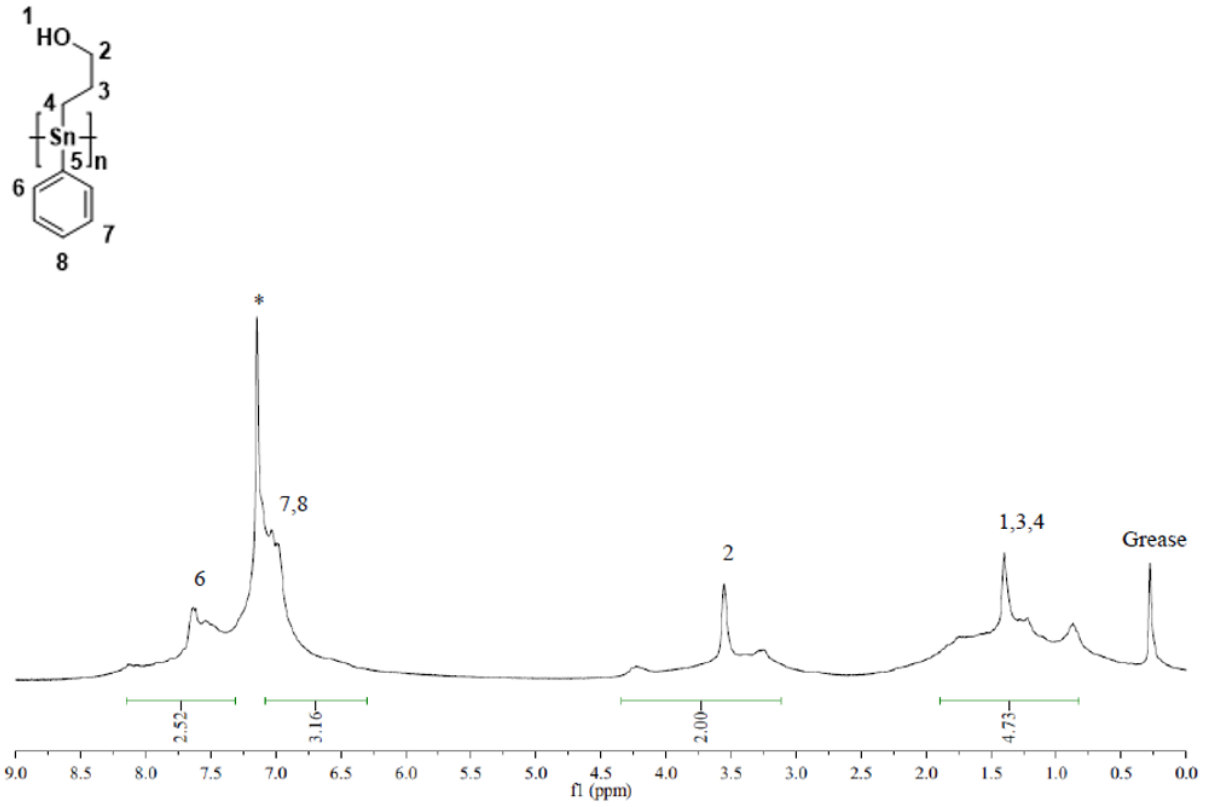

Figure S58. ^{1}H NMR spectrum of **19** in C_6D_6

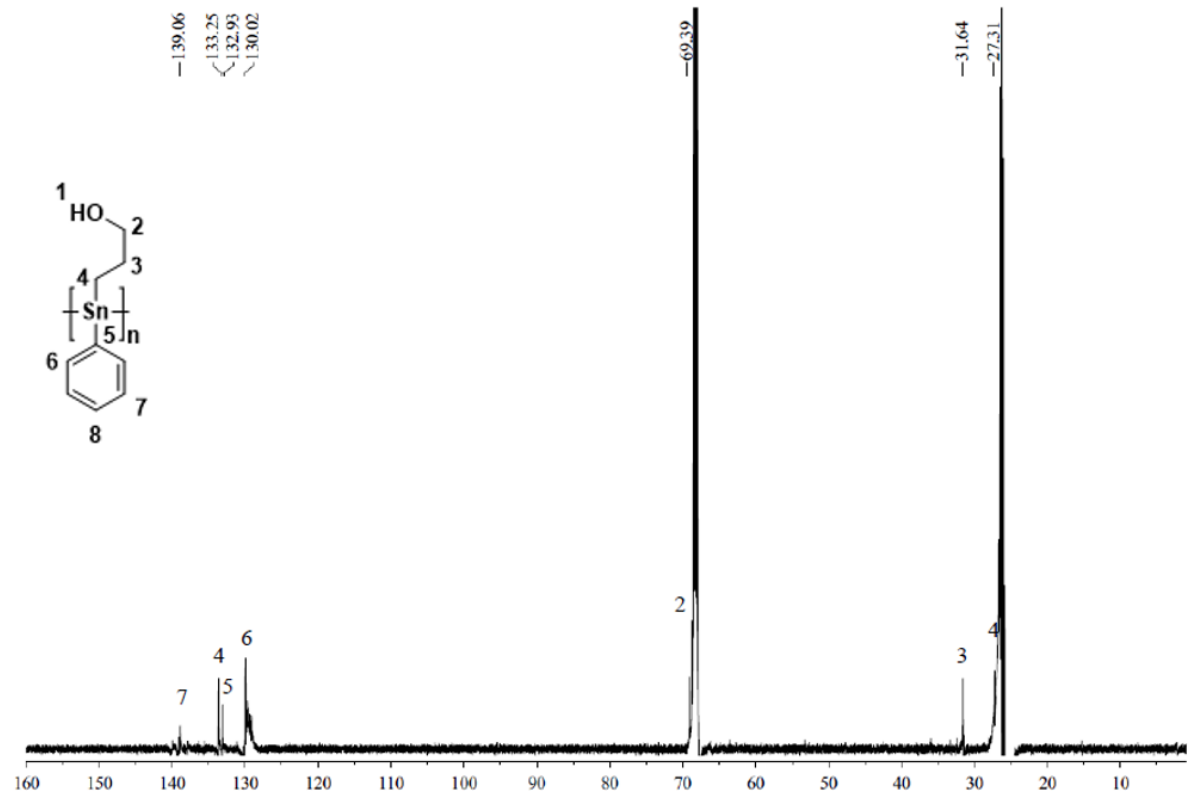

Figure S59. $^{13}C\{^{1}H\}$ NMR spectrum of **19** in C_6D_6

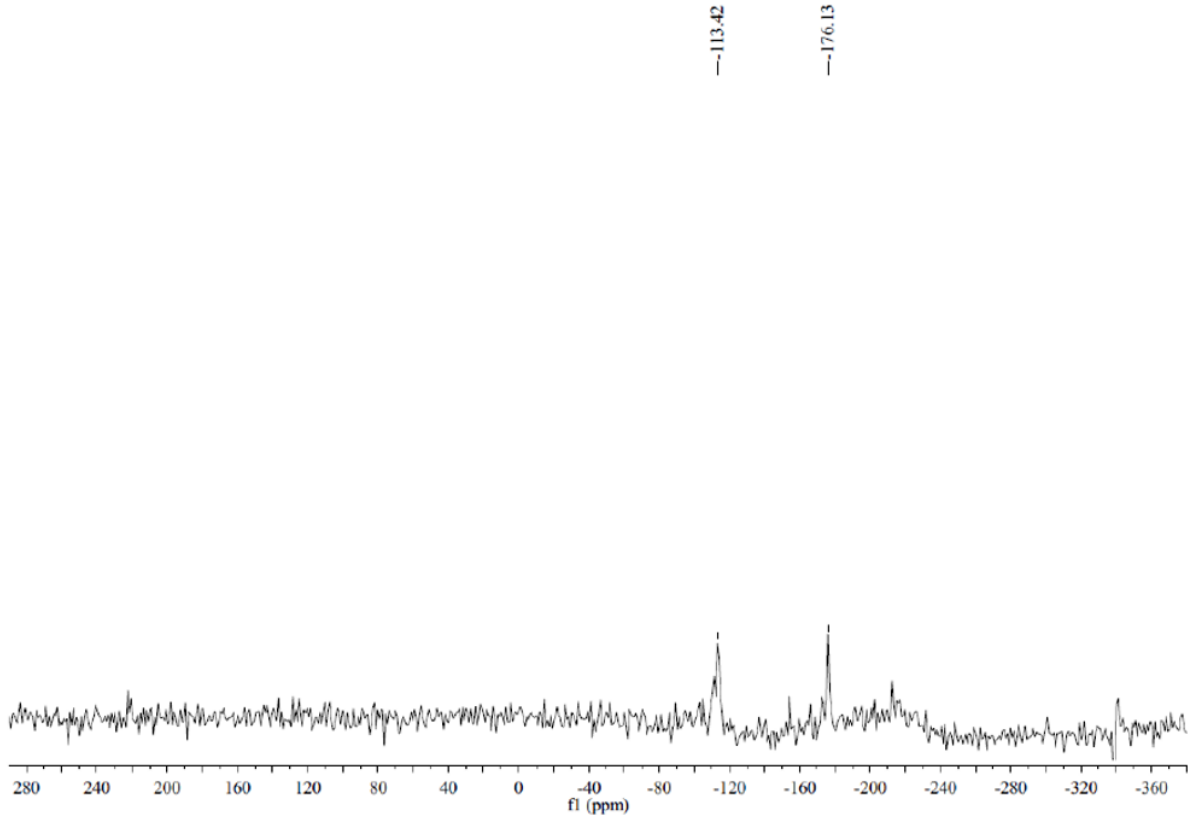

Figure S60. $^{119}Sn\{^{1}H\}$ NMR spectrum of **19** in C_6D_6

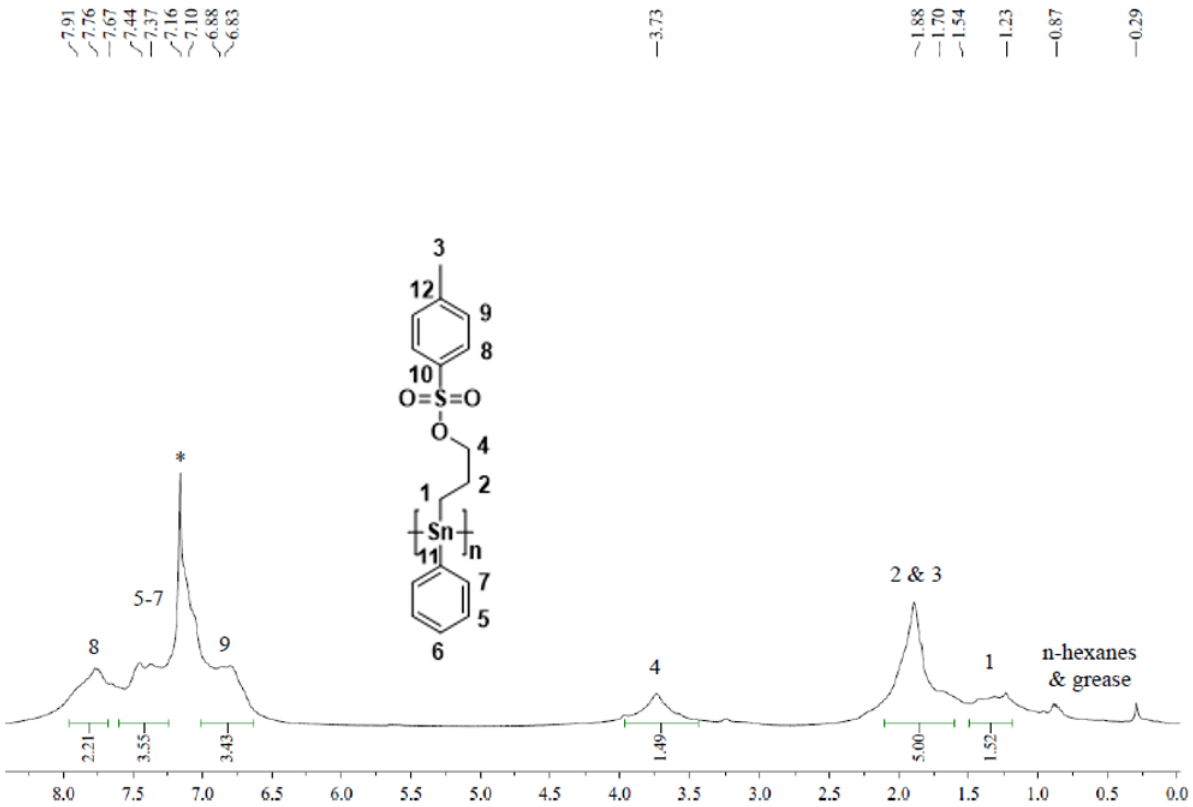

Figure S61. ^{1}H NMR spectrum of **20** in C_6D_6

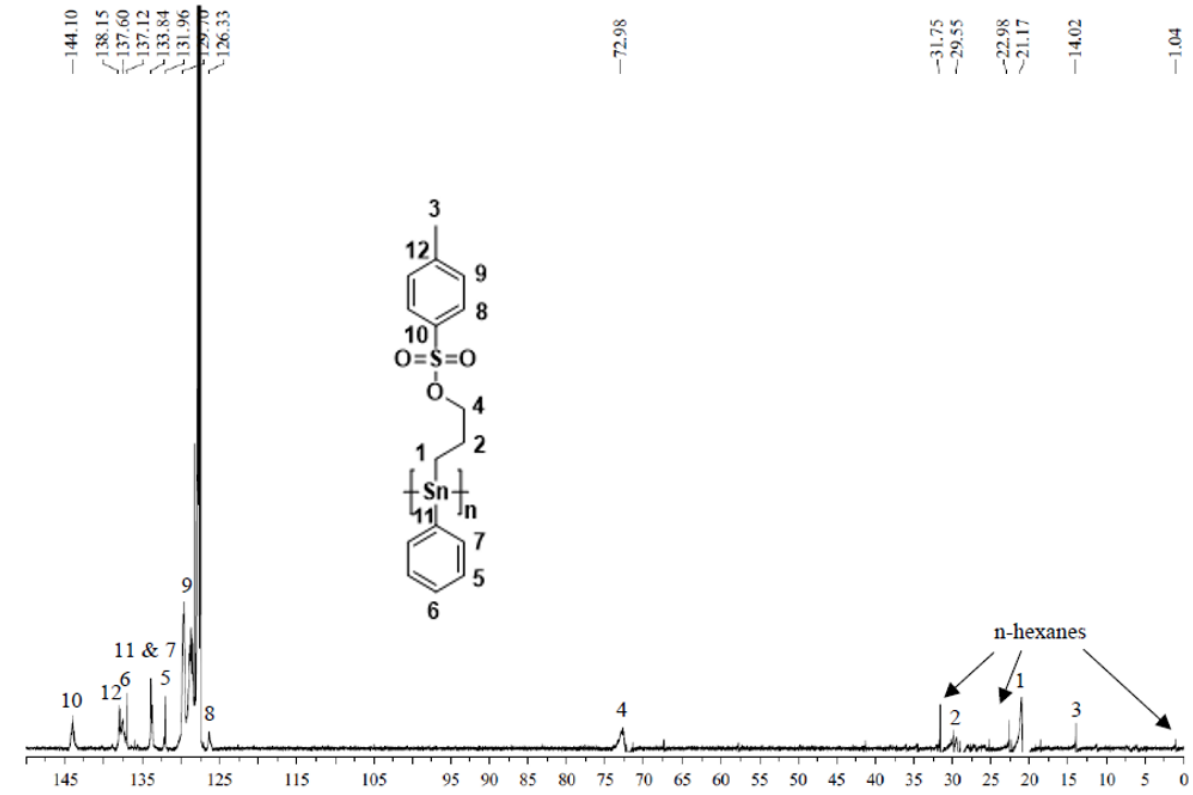

Figure S62. $^{13}C\{^{1}H\}$ NMR spectrum of **20** in C_6D_6

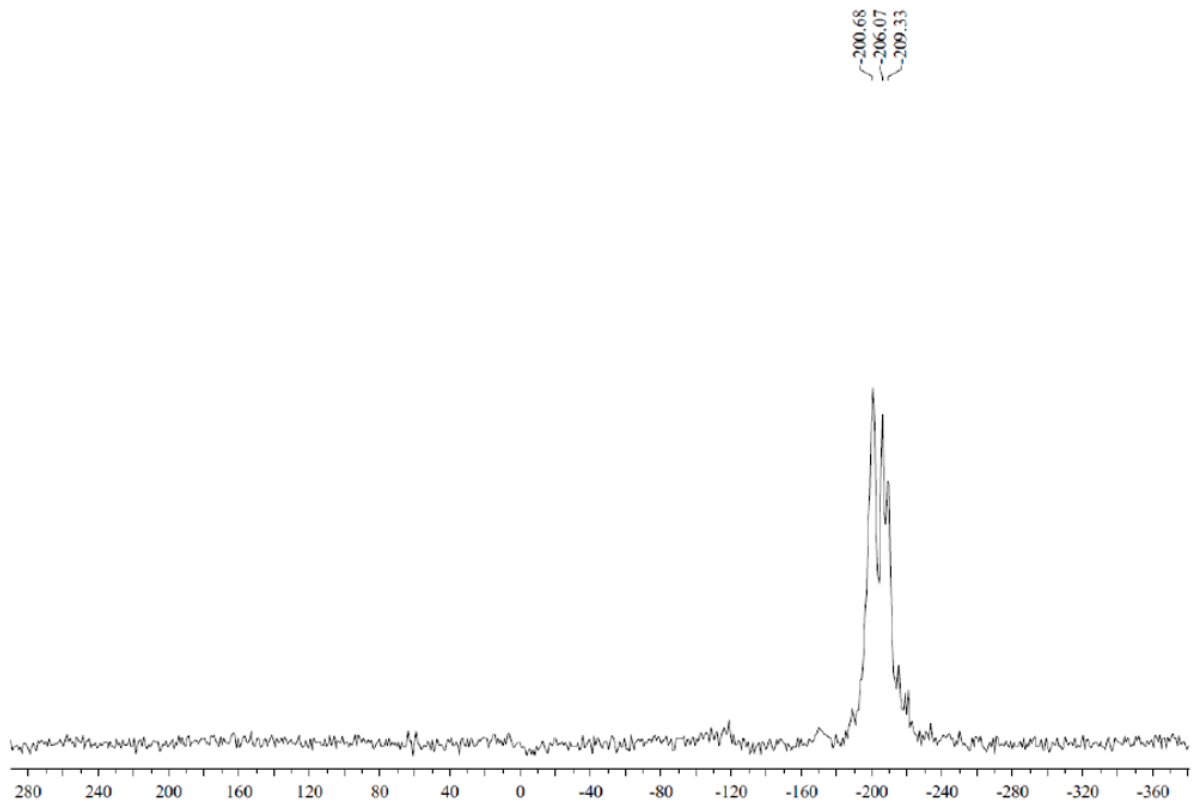

Figure S63. $^{119}Sn\{^{1}H\}$ NMR spectrum of **20** in C_6D_6

CHAPTER 2: DSC Traces

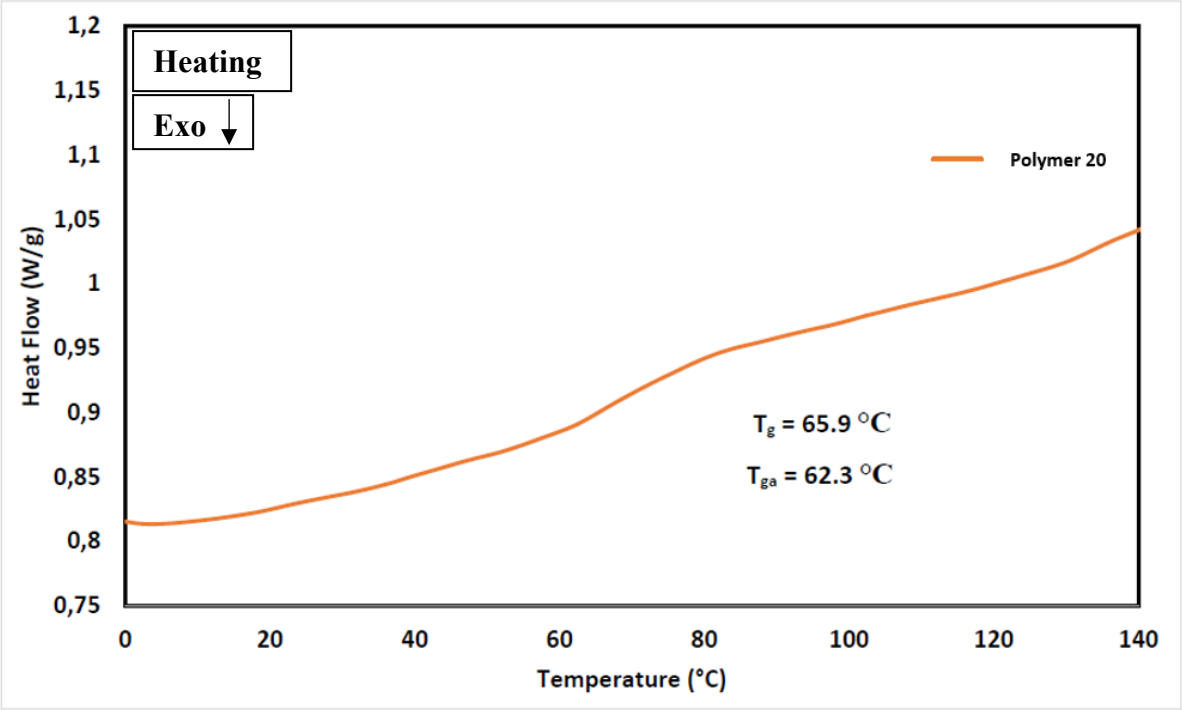

Figure S64. DSC spectra for polymer **20**

CHAPTER 3: NMR Spectra

*****Majority of the NMR data were provided by previous thesis student*****

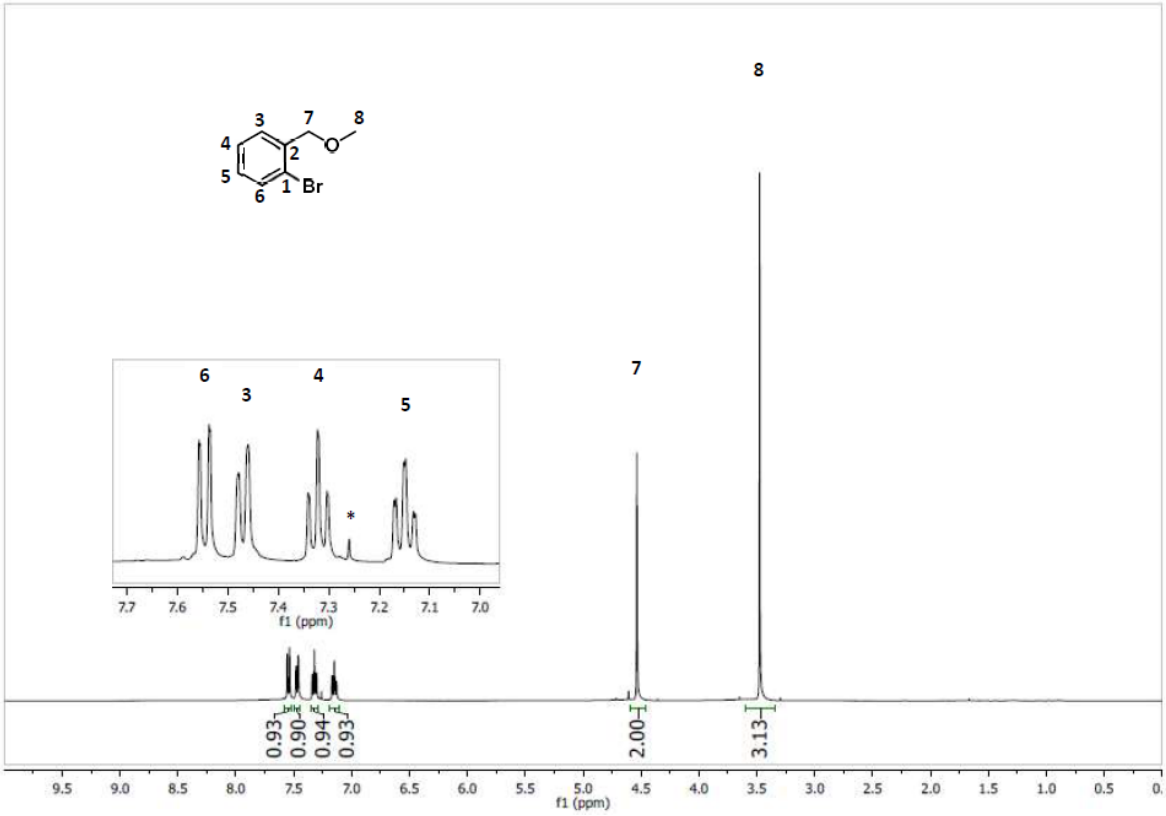

Figure S65. ^{1}H NMR spectrum of **22** in $CDCl_3$

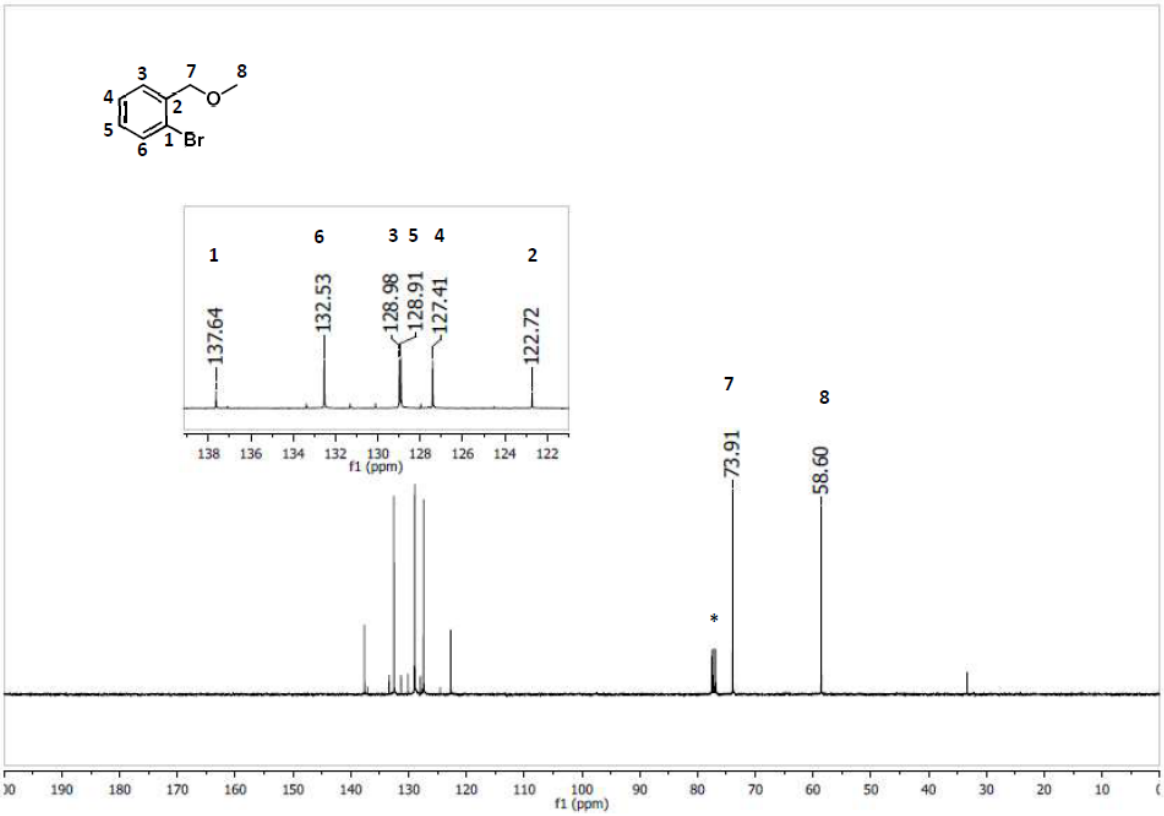

Figure S66. $^{13}C\{^{1}H\}$ NMR spectrum of **22** in $CDCl_3$

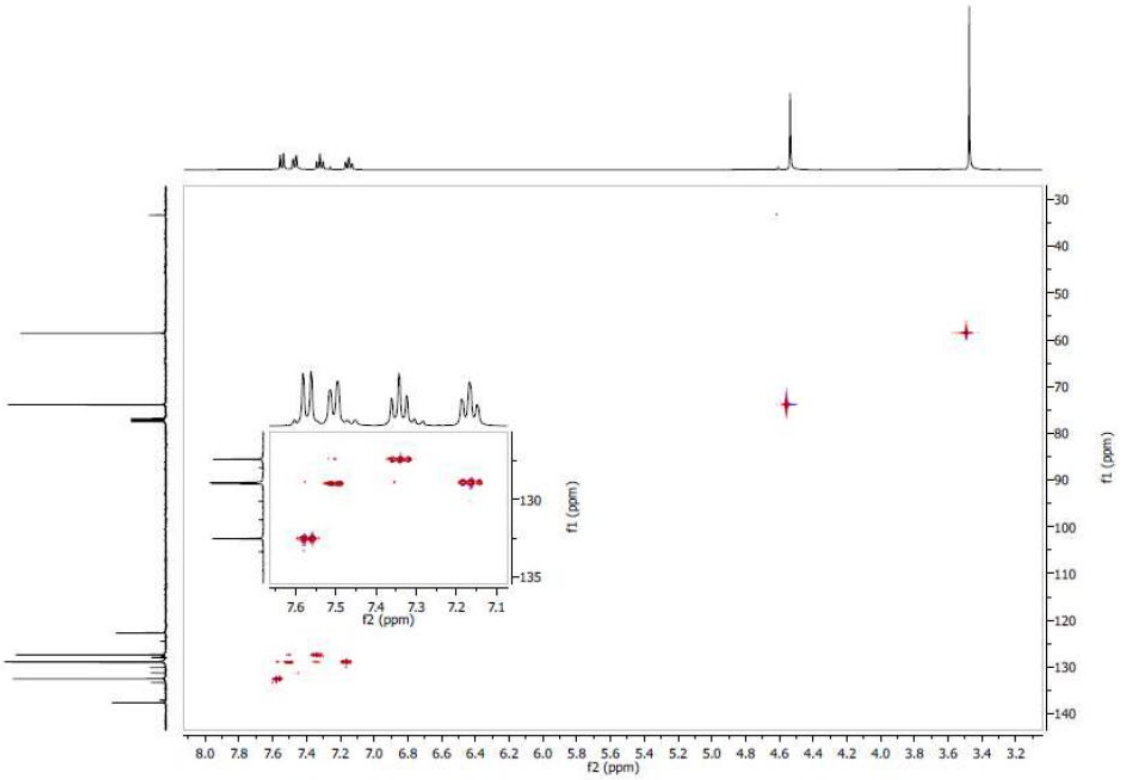

Figure S67. HSQC 2D-NMR spectrum of **22** in $CDCl_3$

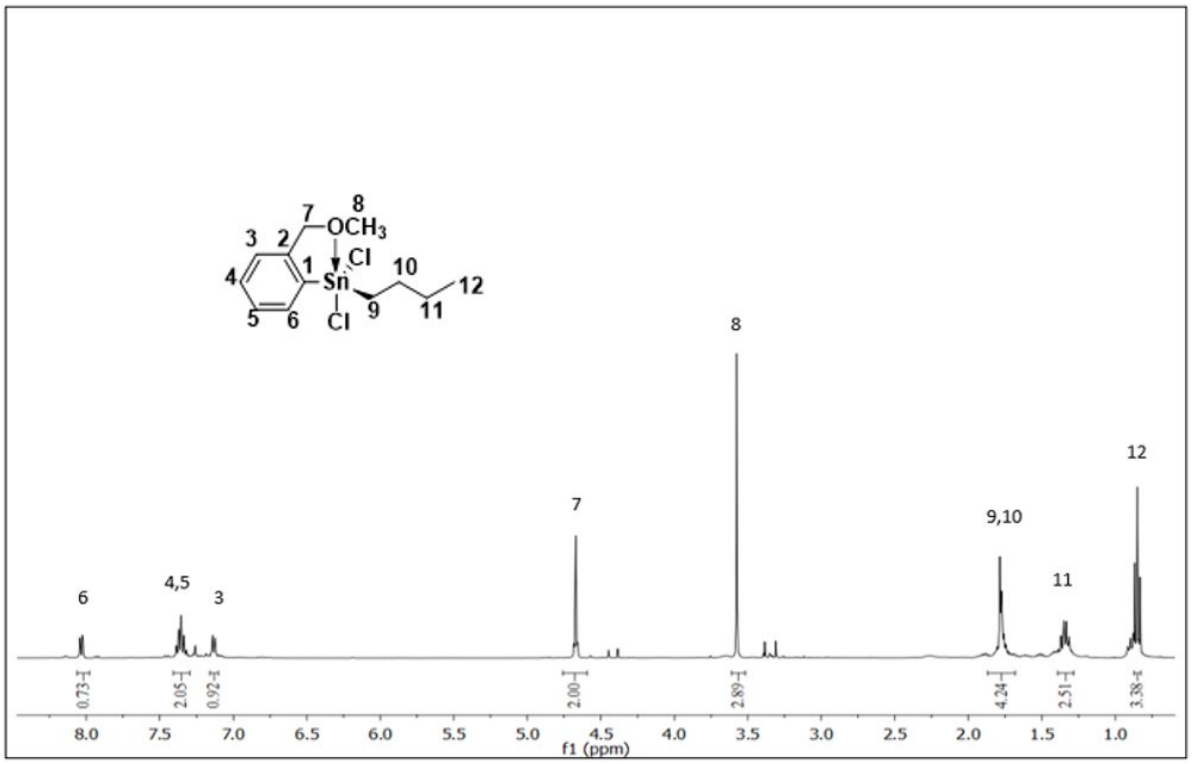

Figure S68. ^1H NMR spectrum of **24** in $CDCl_3$

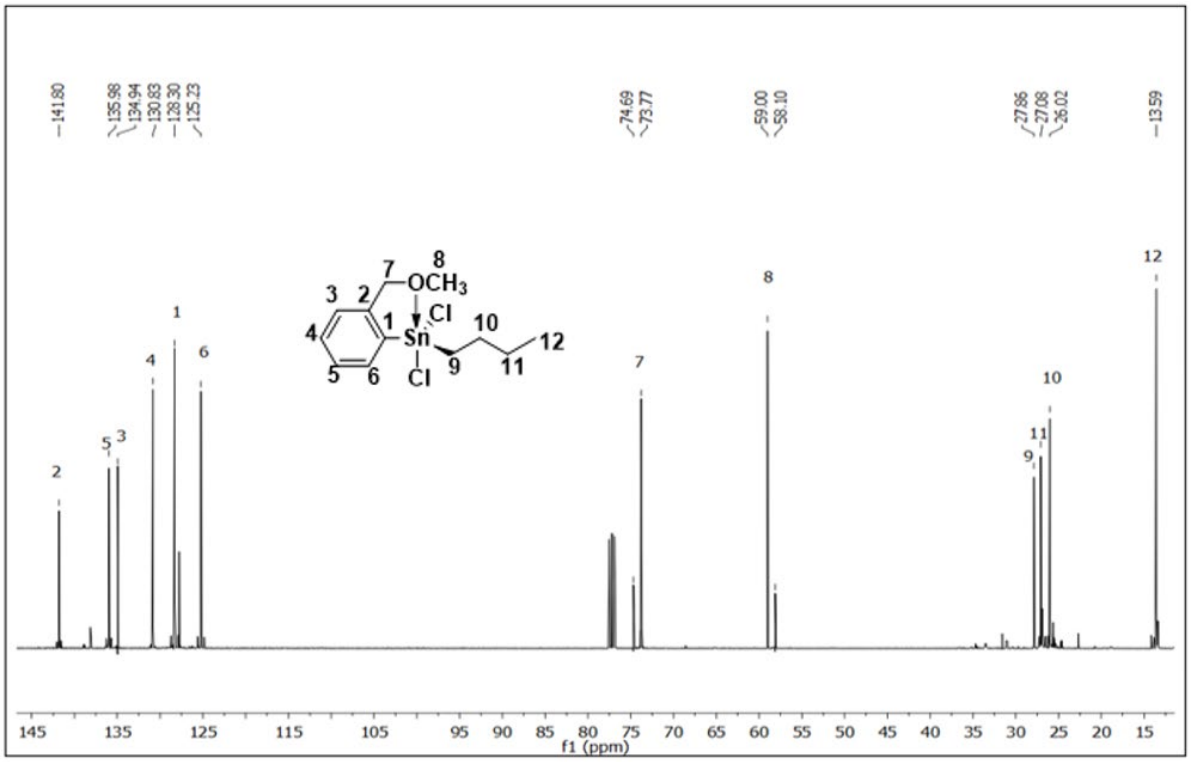

Figure S69. $^{13}C\{^{1}H\}$ NMR spectrum of **24** in $CDCl_3$

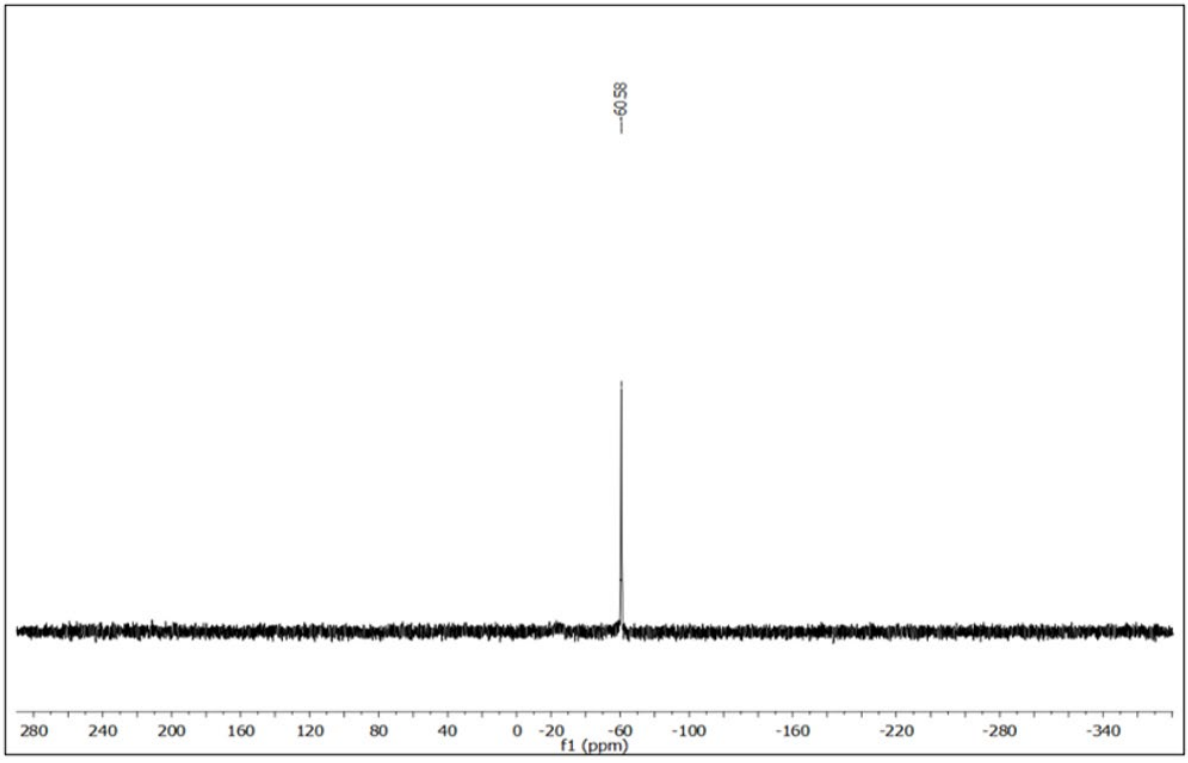

Figure S70. $^{119}Sn\{^{1}H\}$ NMR spectrum of **24** in $CDCl_3$

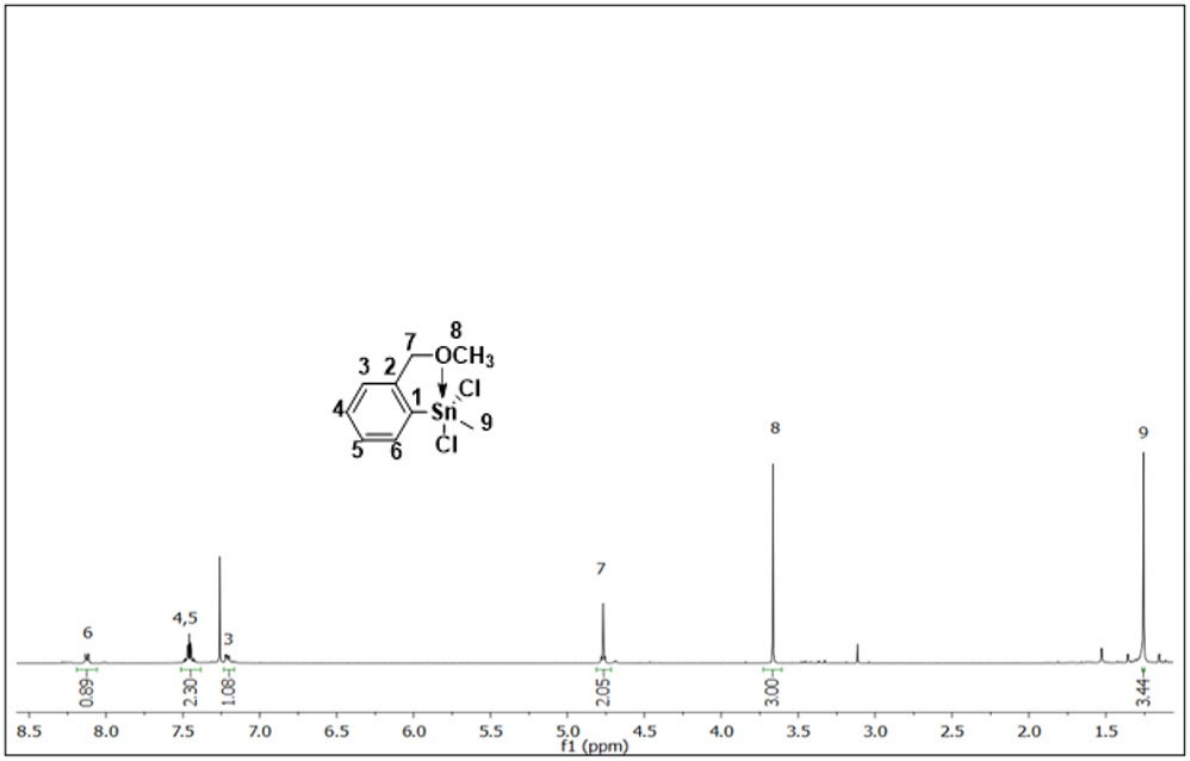

Figure S71. ^{1}H NMR spectrum of **25** in $CDCl_3$

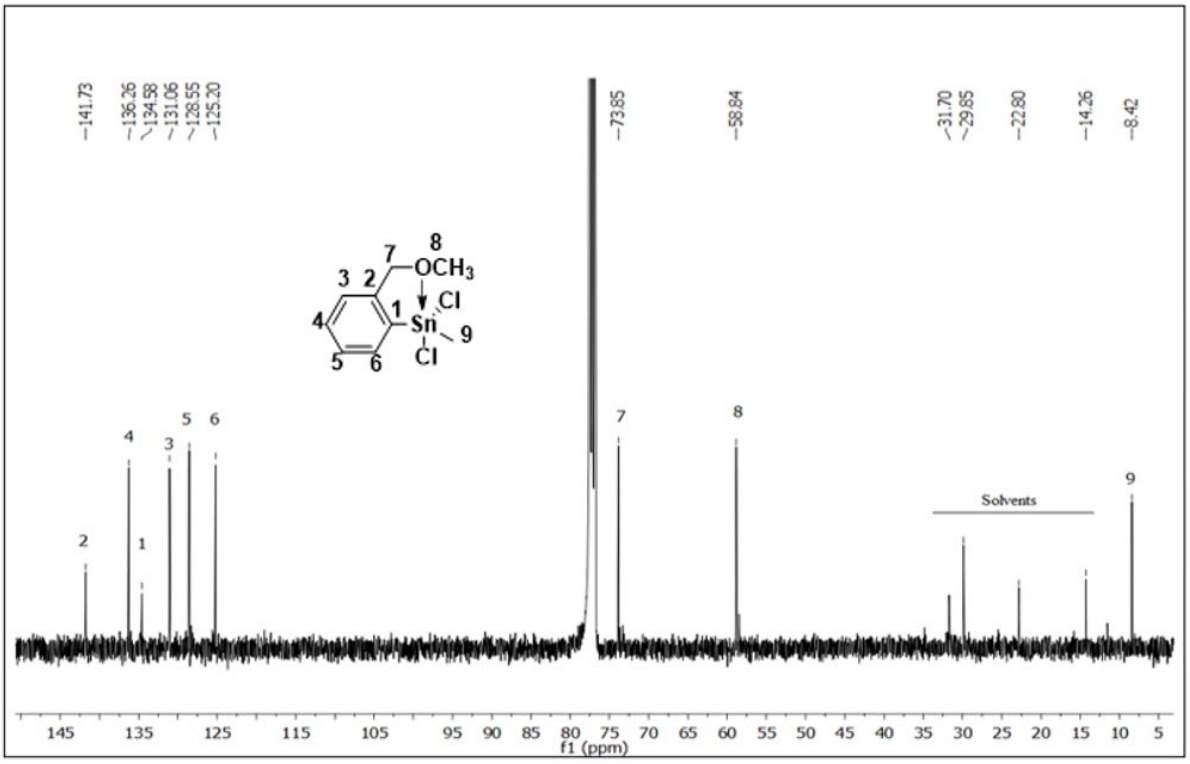

Figure S72. $^{13}C\{^{1}H\}$ NMR spectrum of **25** in $CDCl_3$

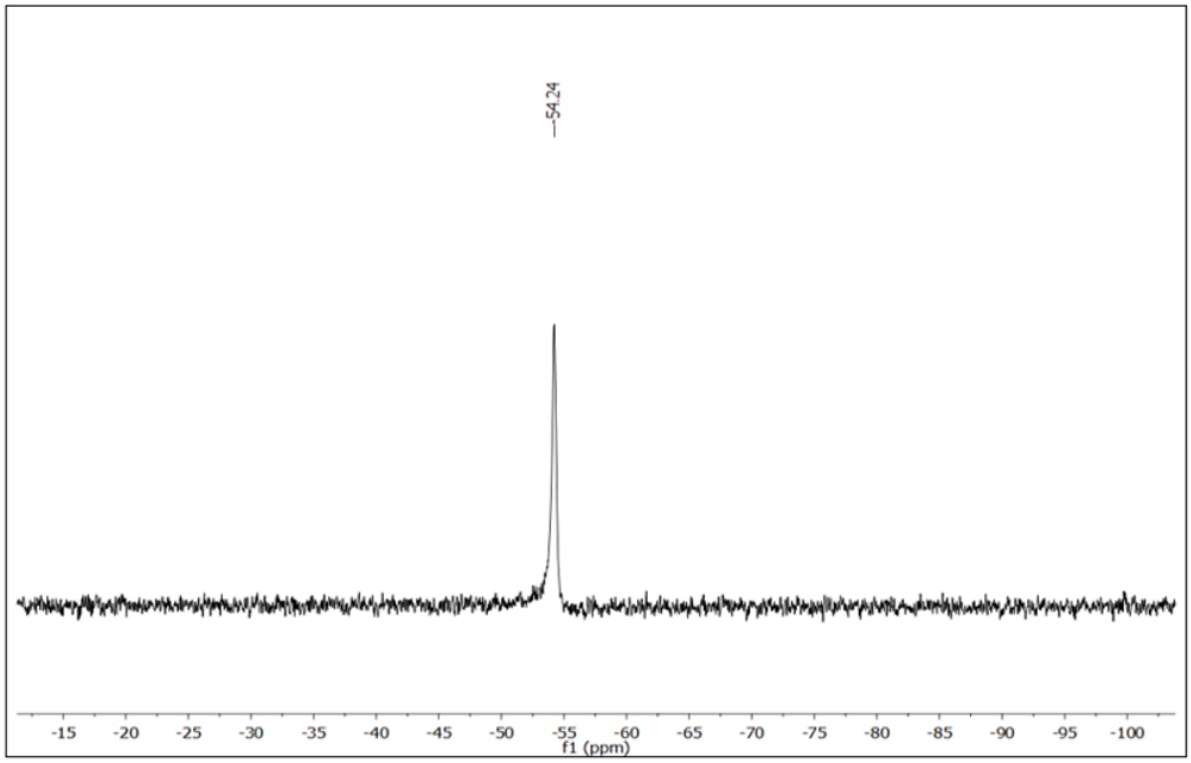

Figure S73. $^{119}Sn\{^{1}H\}$ NMR spectrum of **25** in $CDCl_3$

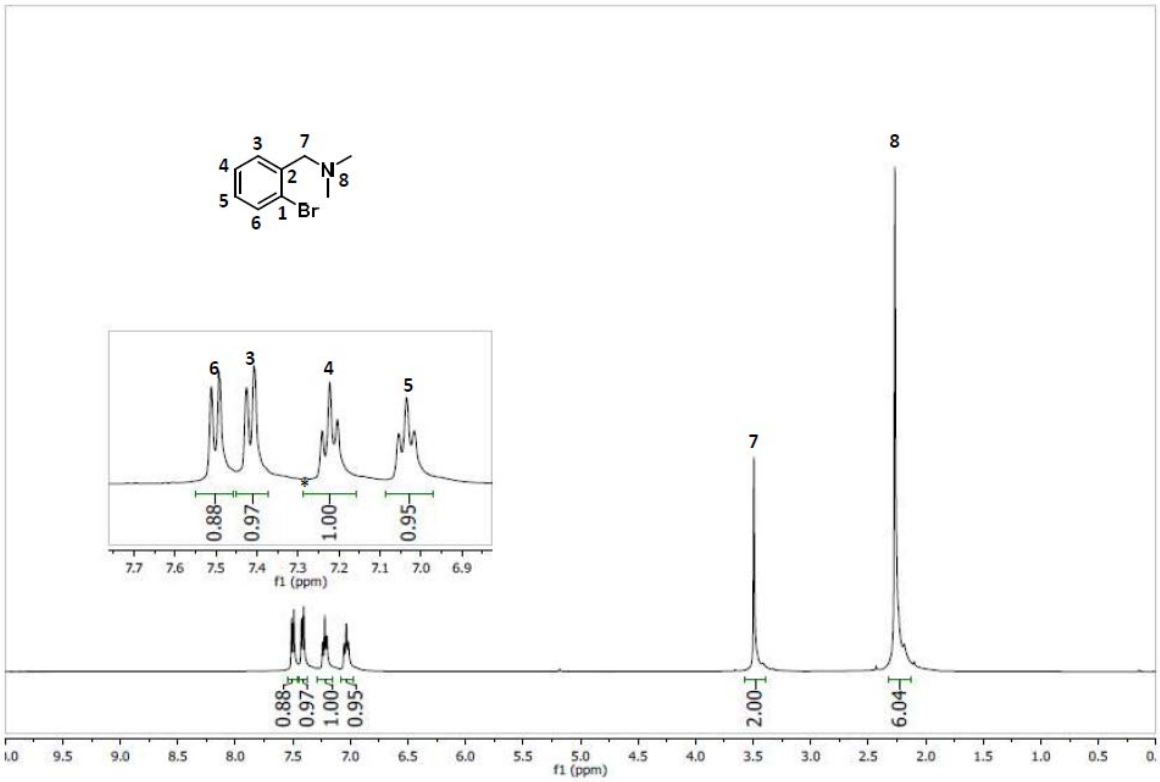

Figure S74. ^{1}H NMR spectrum of **26** in $CDCl_3$

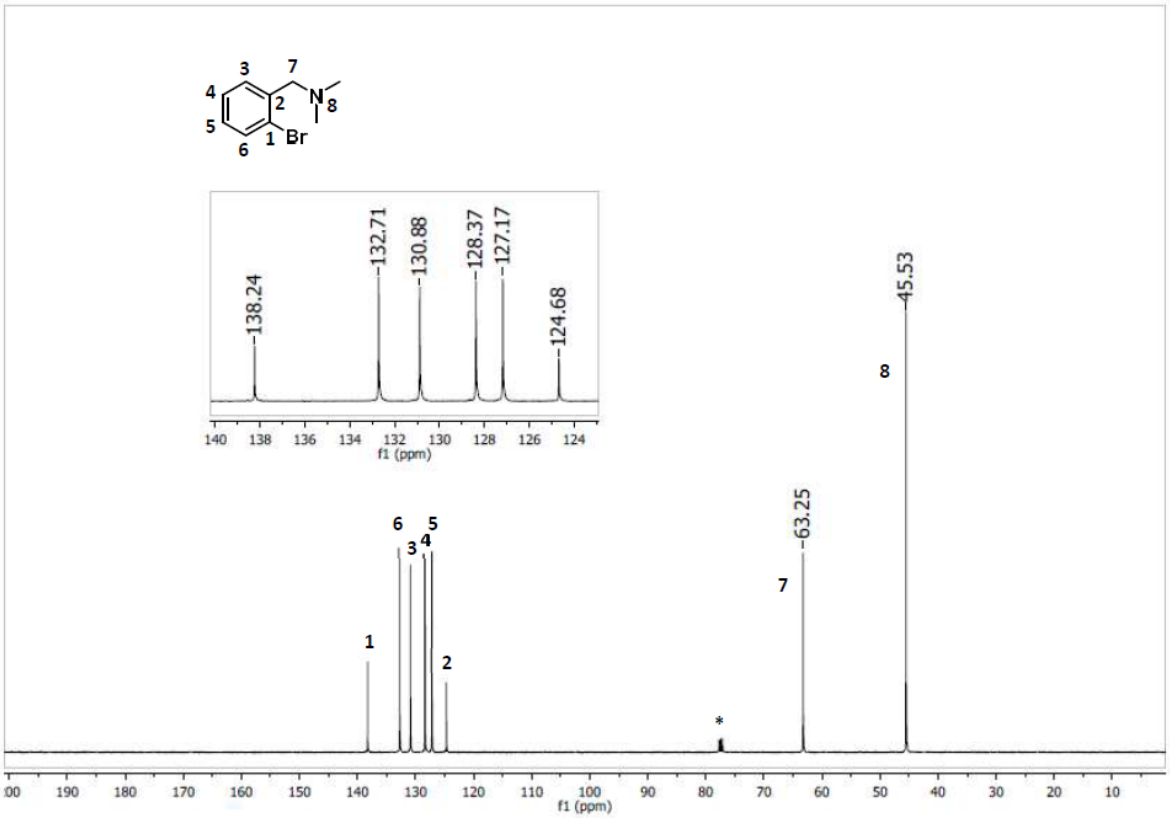

Figure S75. $^{13}C\{^{1}H\}$ NMR spectrum of **26** in $CDCl_3$

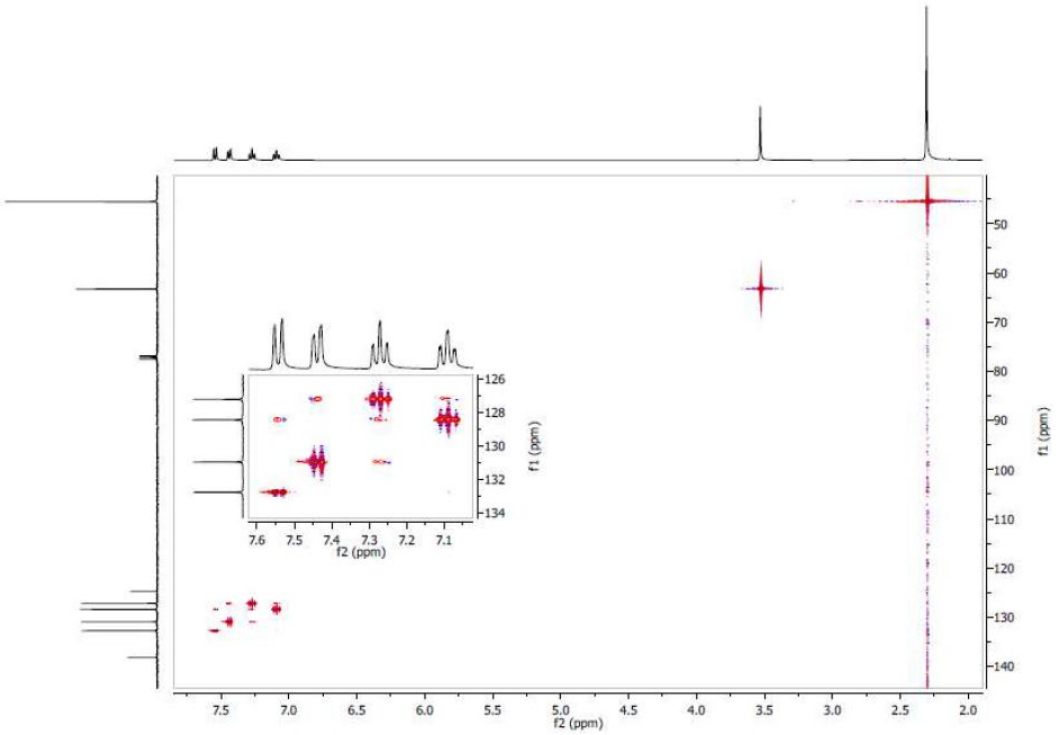

Figure S76. HSQC 2D-NMR spectrum of **26** in $CDCl_3$

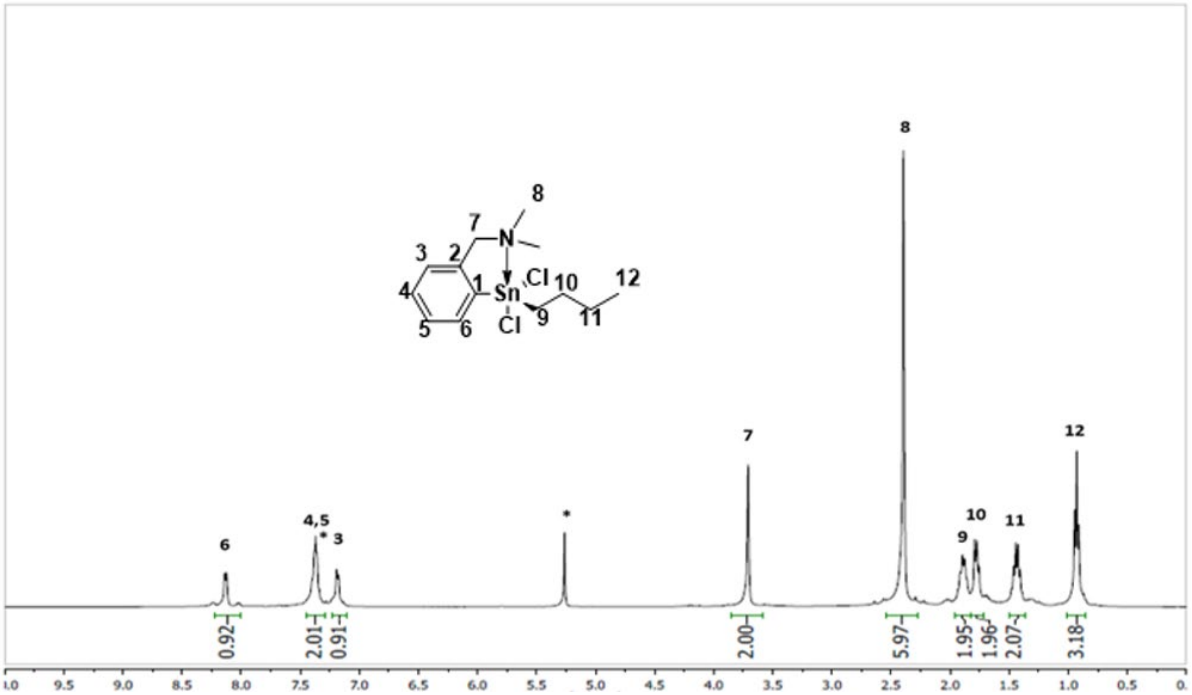

Figure S77. ^{1}H NMR spectrum of **28** in $CDCl_3$

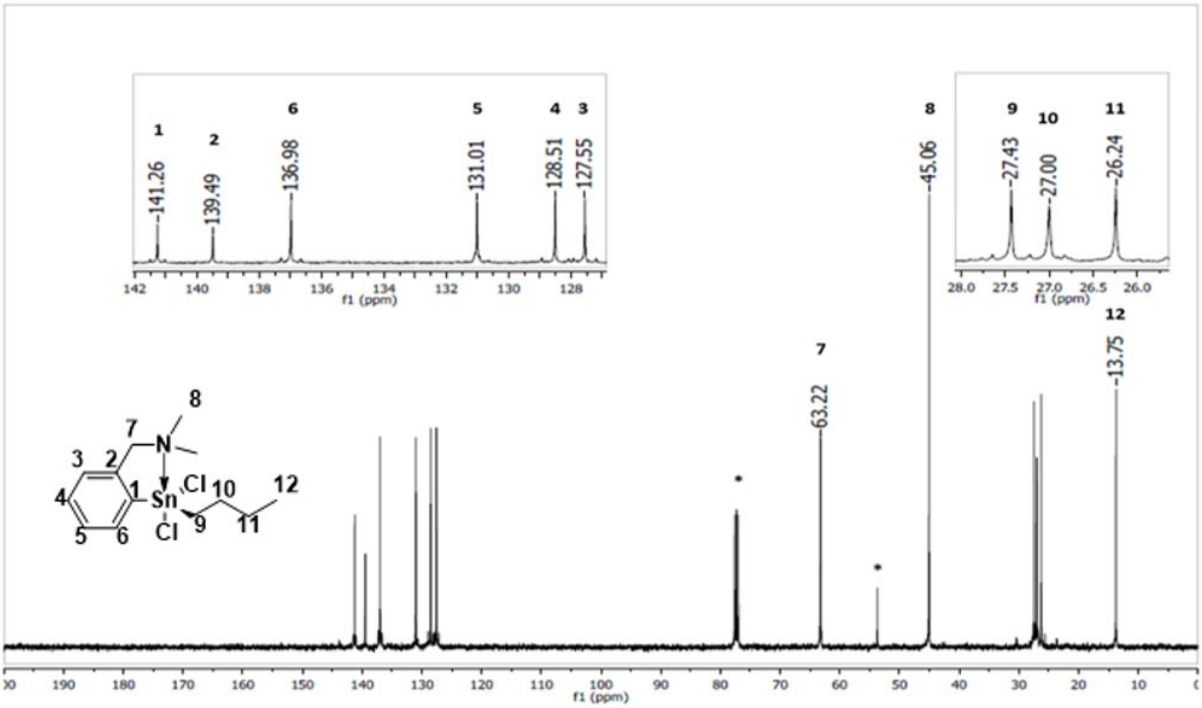

Figure S78. $^{13}C\{^{1}H\}$ NMR spectrum of **28** in $CDCl_3$

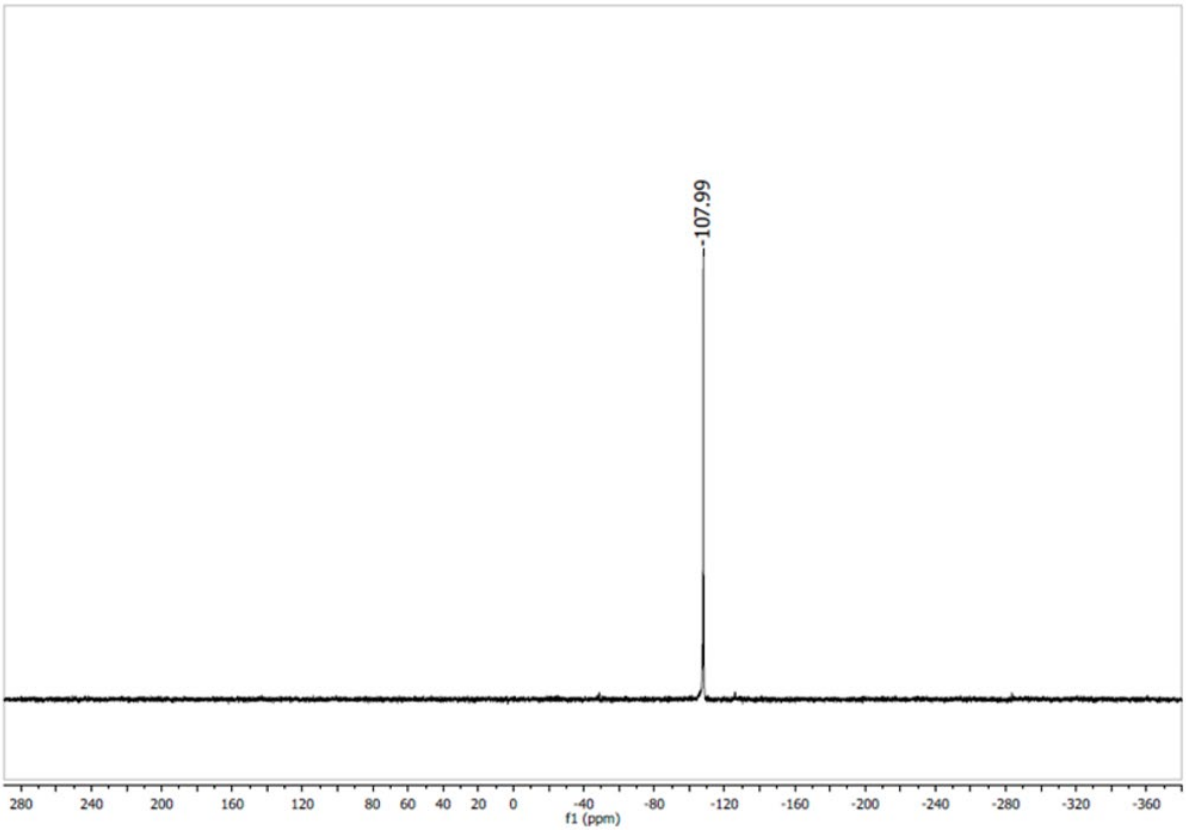

Figure S79. $^{119}Sn\{^{1}H\}$ NMR spectrum of **28** in $CDCl_3$

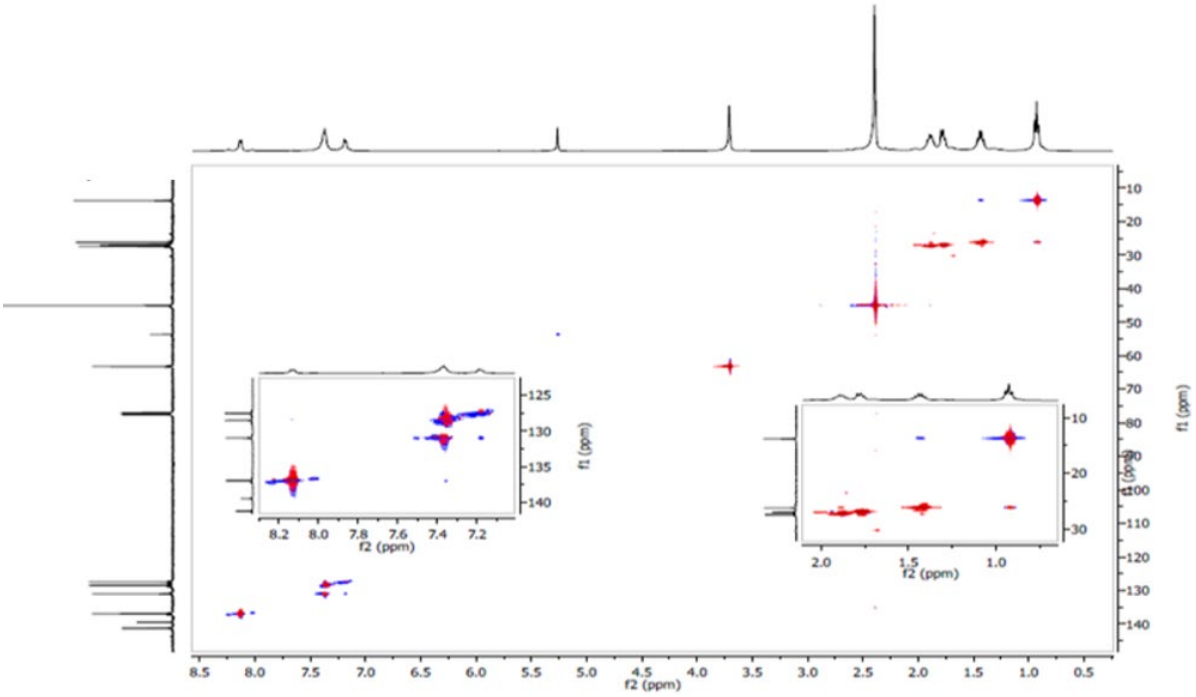

Figure S80. HSQC 2D-NMR spectrum of **28** in $CDCl_3$

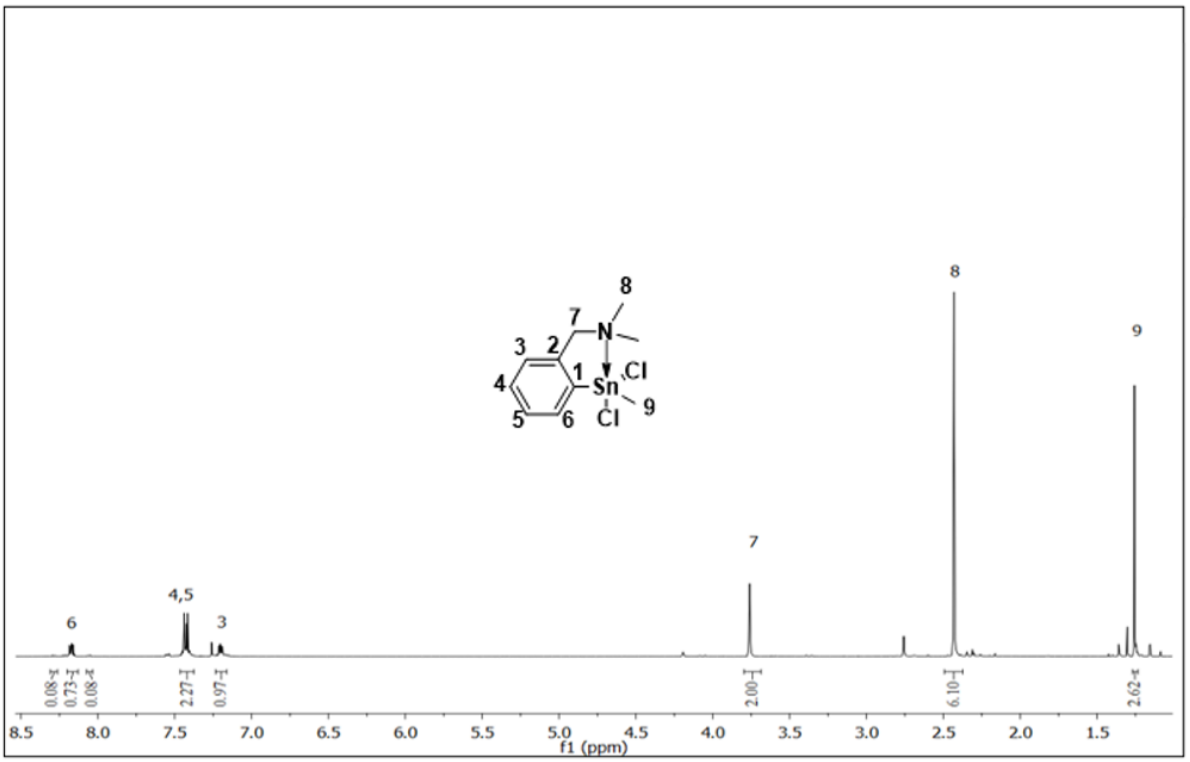

Figure S81. ^{1}H NMR spectrum of **29** in $CDCl_3$

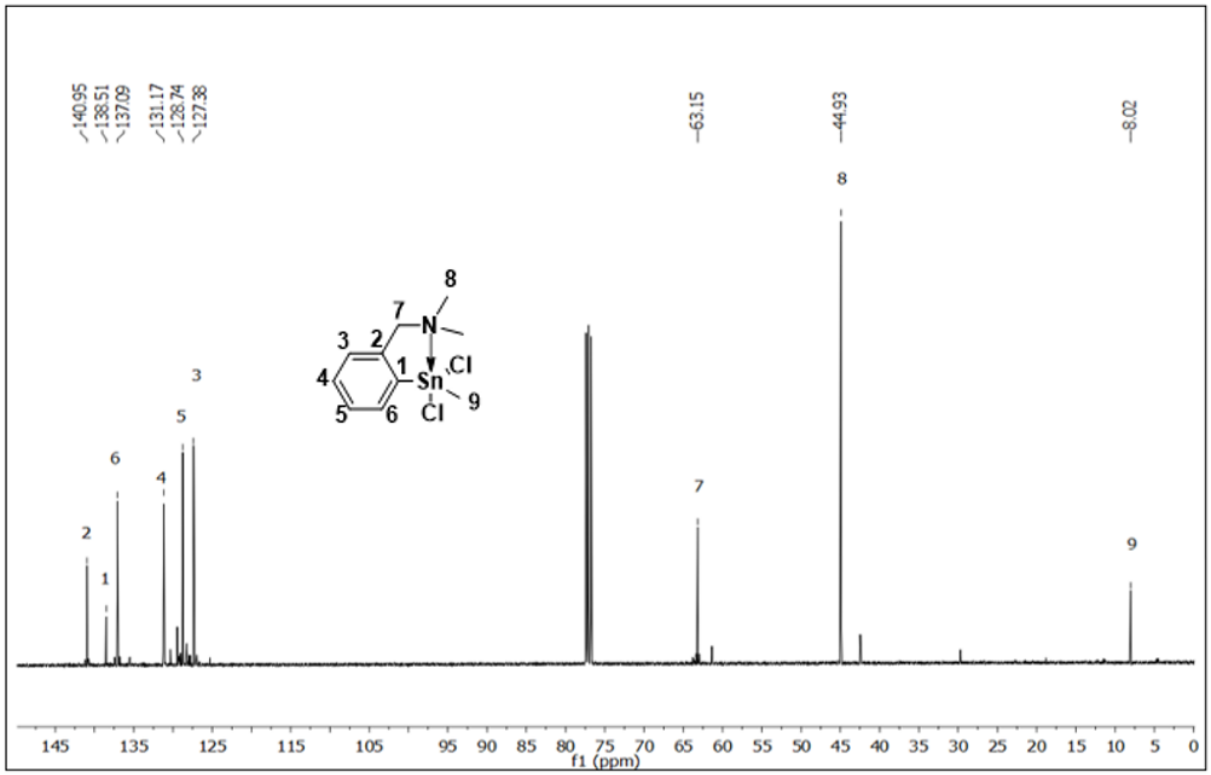

Figure S82. $^{13}C\{^{1}H\}$ NMR spectrum of **29** in $CDCl_3$

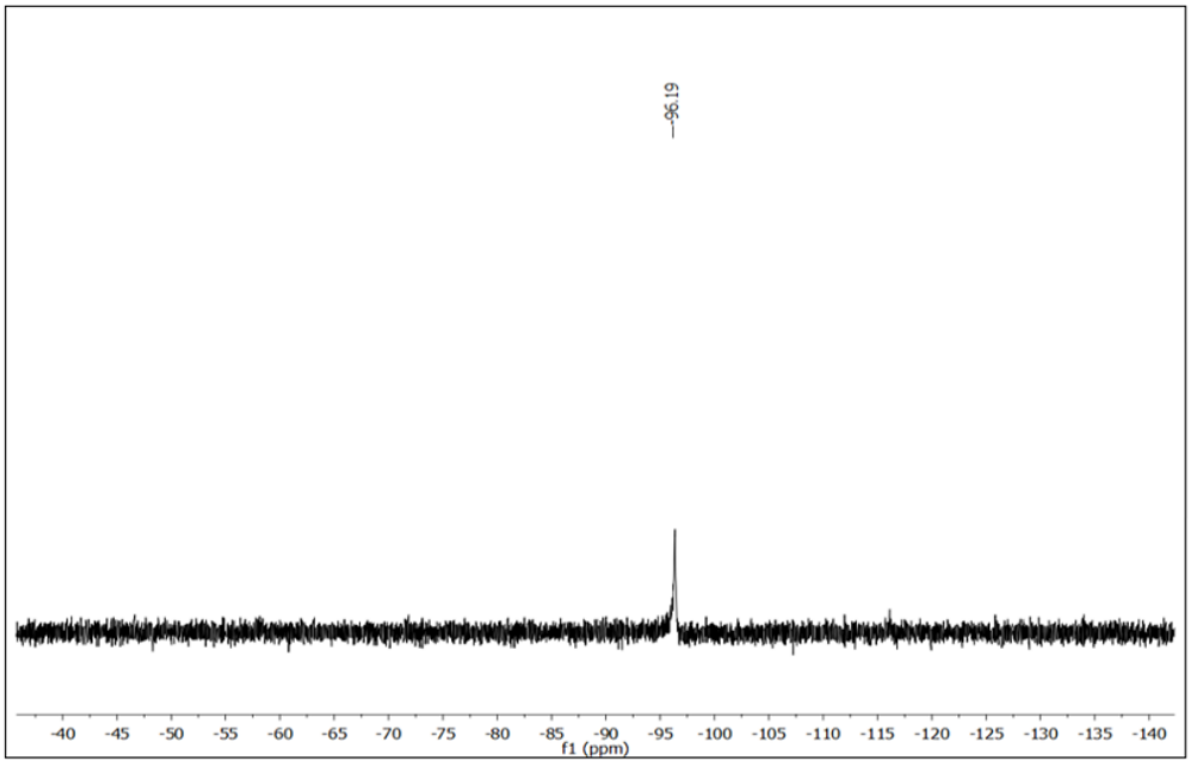

Figure S83. $^{119}Sn\{^{1}H\}$ NMR spectrum of **29** in $CDCl_3$

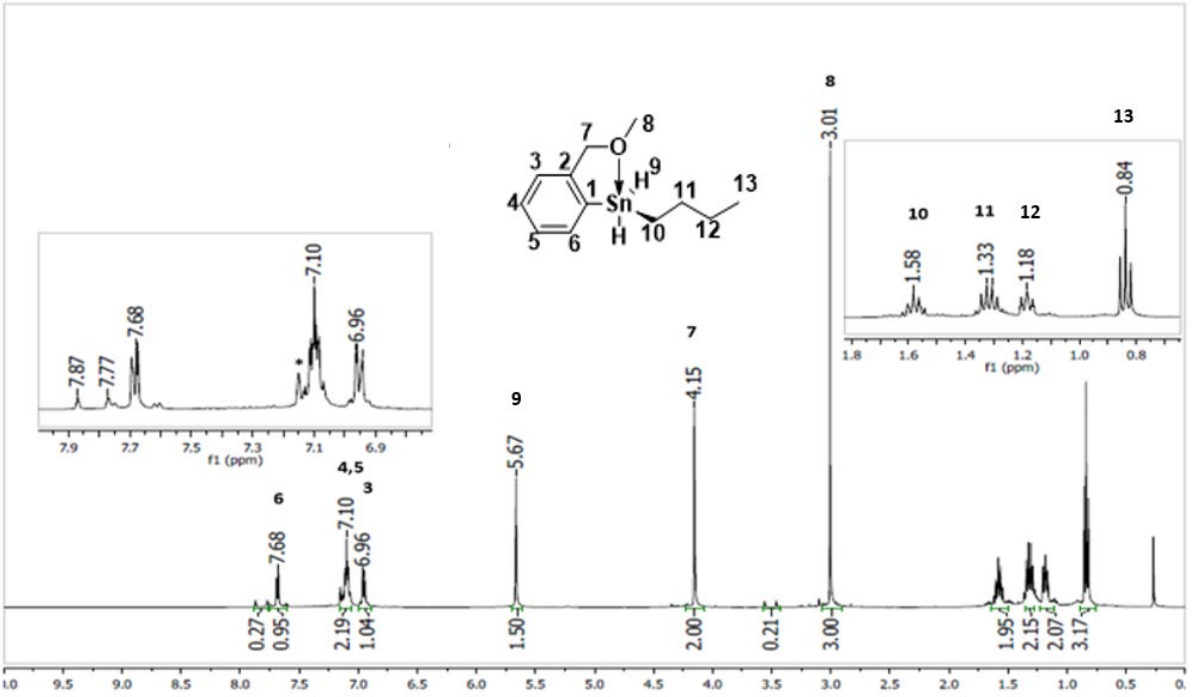

Figure S84. ^{1}H NMR spectrum of **30** in C_6D_6

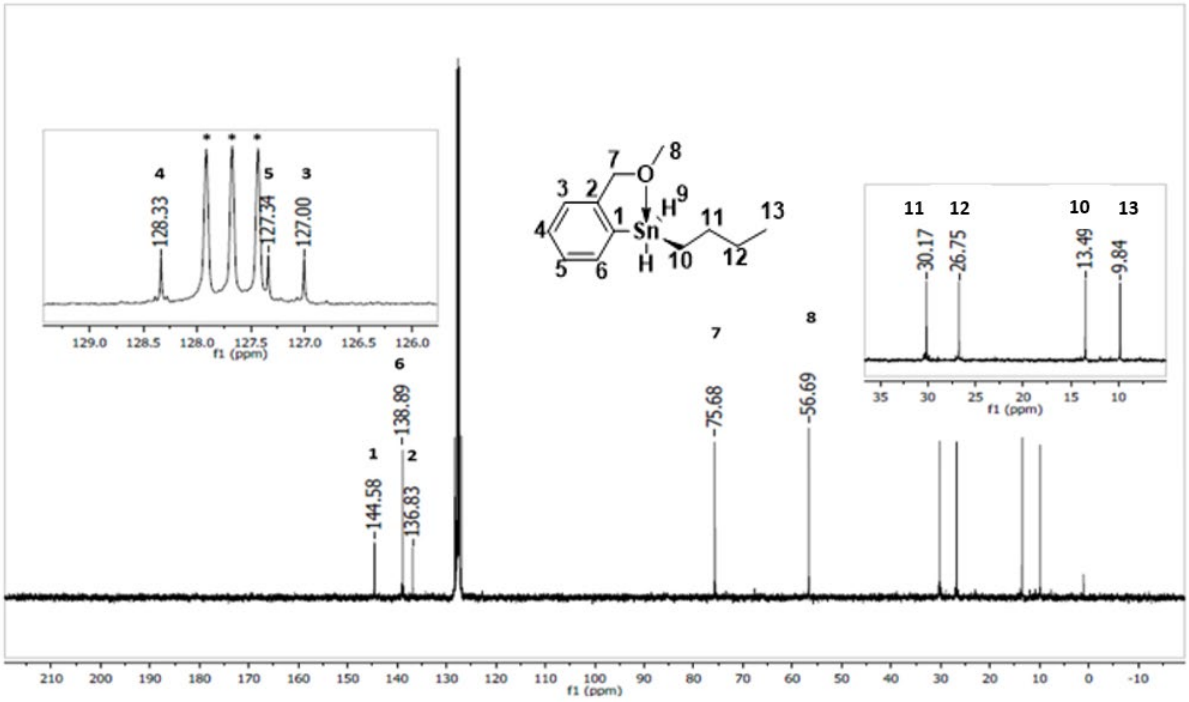

Figure S85. $^{13}C\{^{1}H\}$ NMR spectrum of **30** in C_6D_6

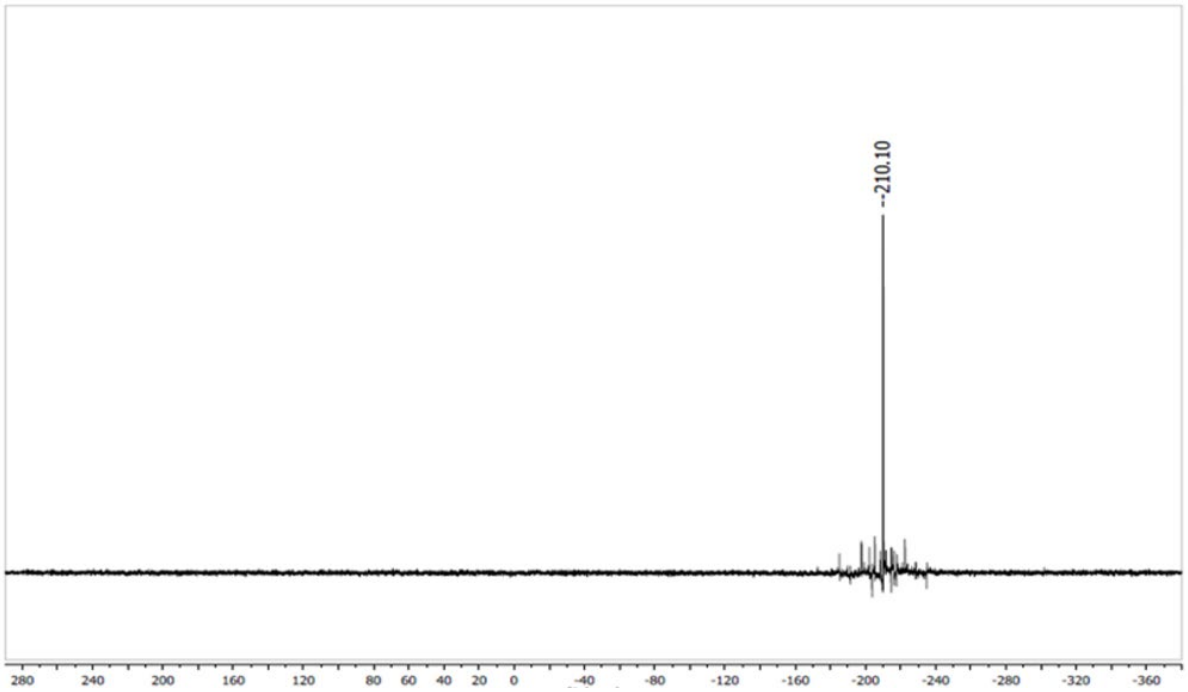

Figure S86. $^{119}Sn\{^{1}H\}$ NMR spectrum of **30** in C_6D_6

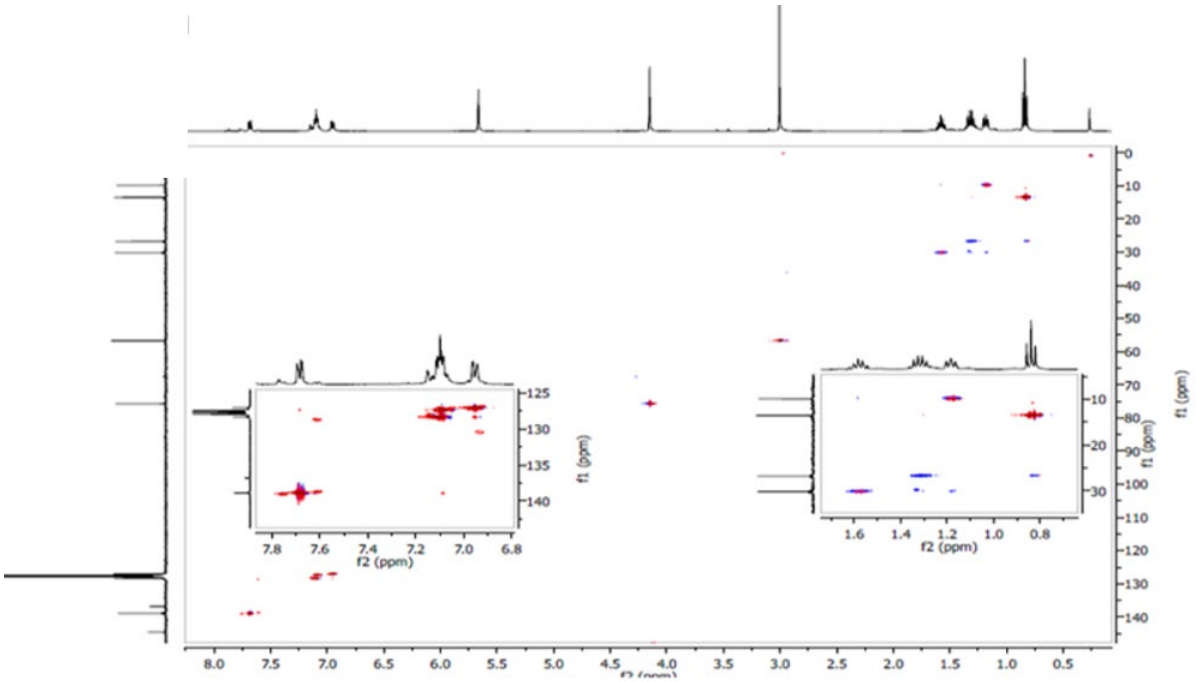

Figure S87. HSQC 2D-NMR spectrum of **30** in C_6D_6

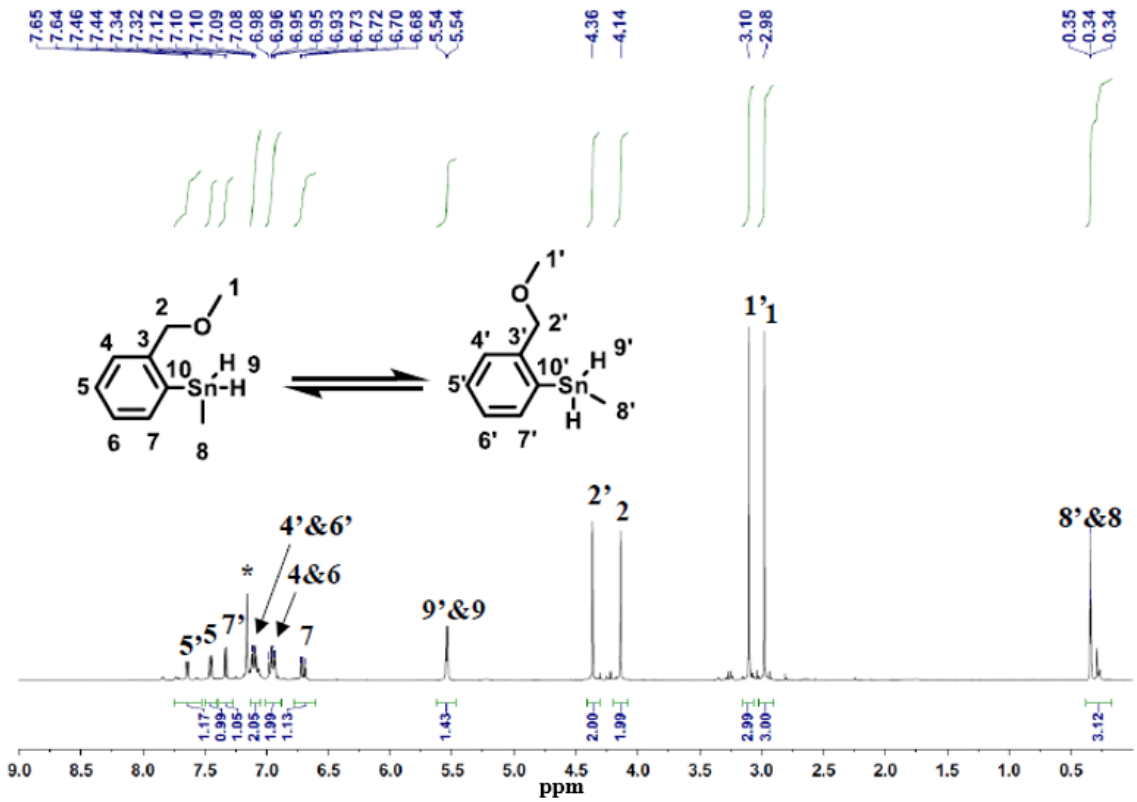

Figure S88. ^{1}H NMR spectrum of **31** in C_6D_6

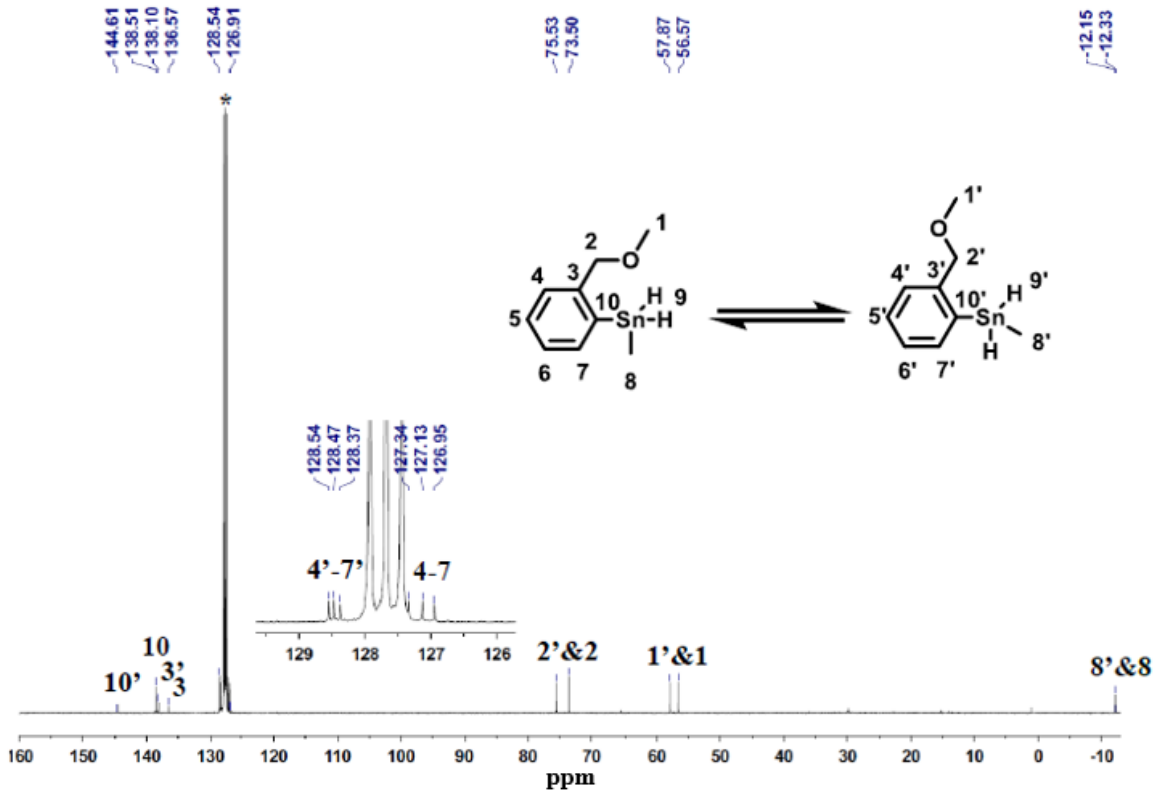

Figure S89. $^{13}C\{^{1}H\}$ NMR spectrum of **31** in C_6D_6

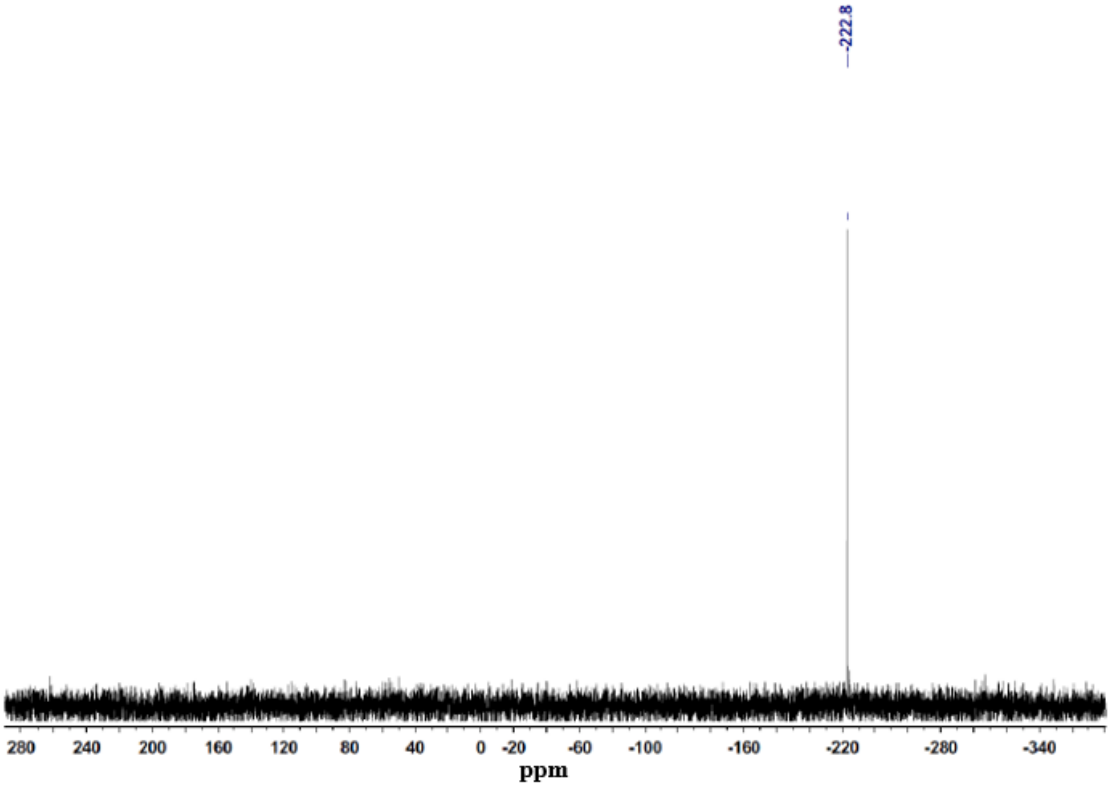

Figure S90. $^{119}Sn\{^{1}H\}$ NMR spectrum of **31** in C_6D_6

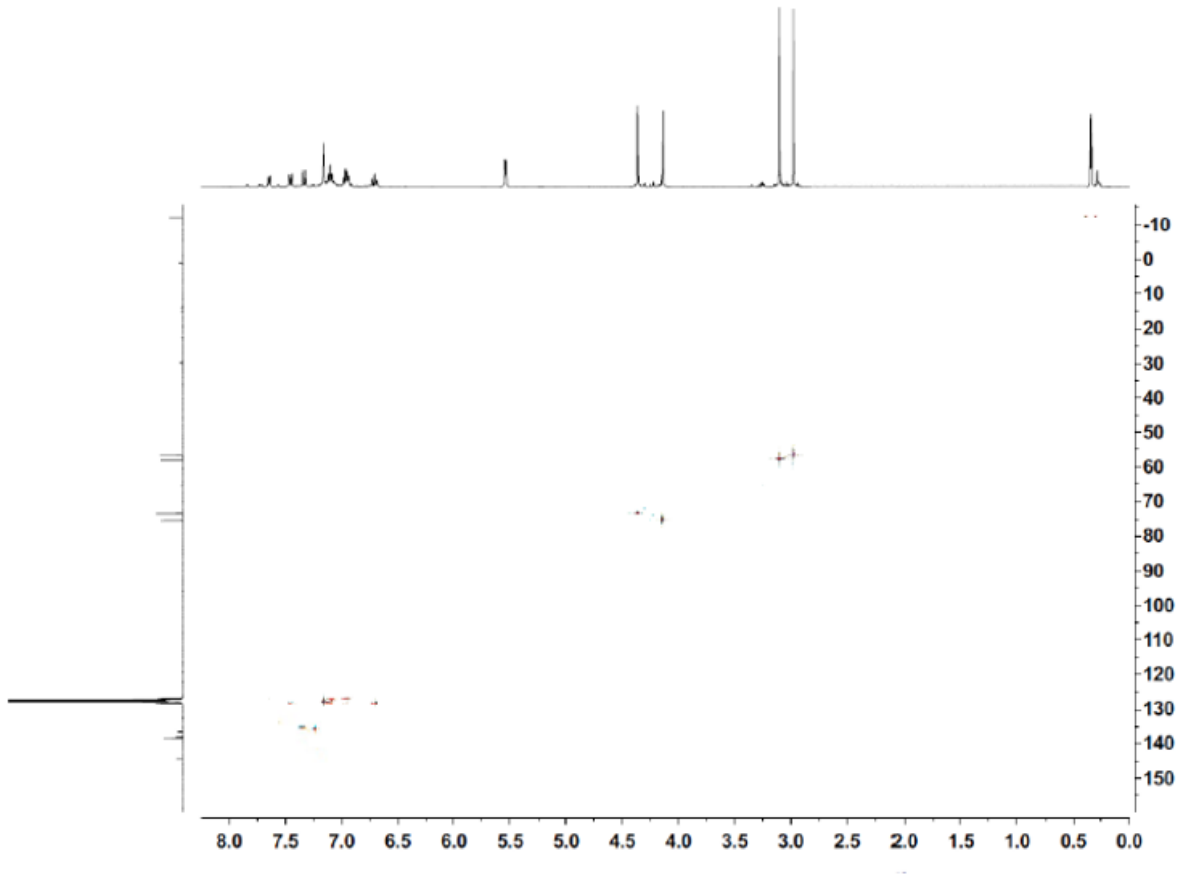

Figure S91. HSQC 2D-NMR spectrum of **31** in C_6D_6

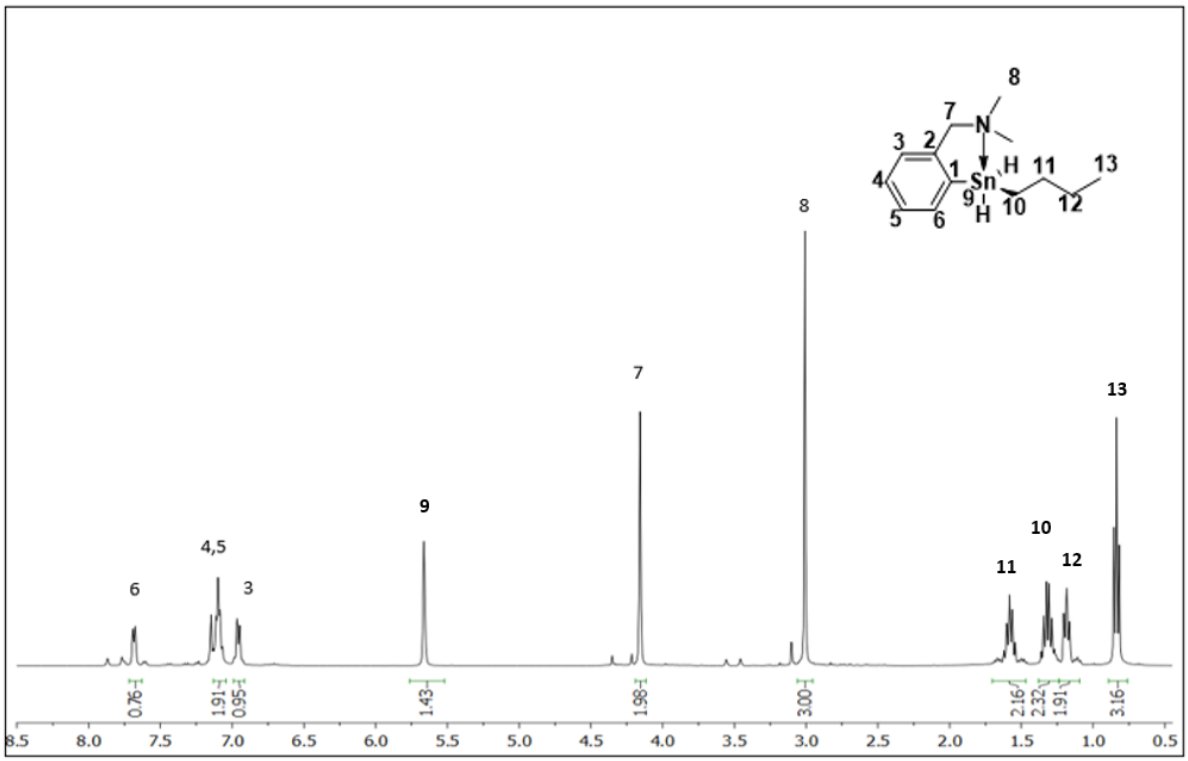

Figure S92. ^{1}H NMR spectrum of **32** in C_6D_6

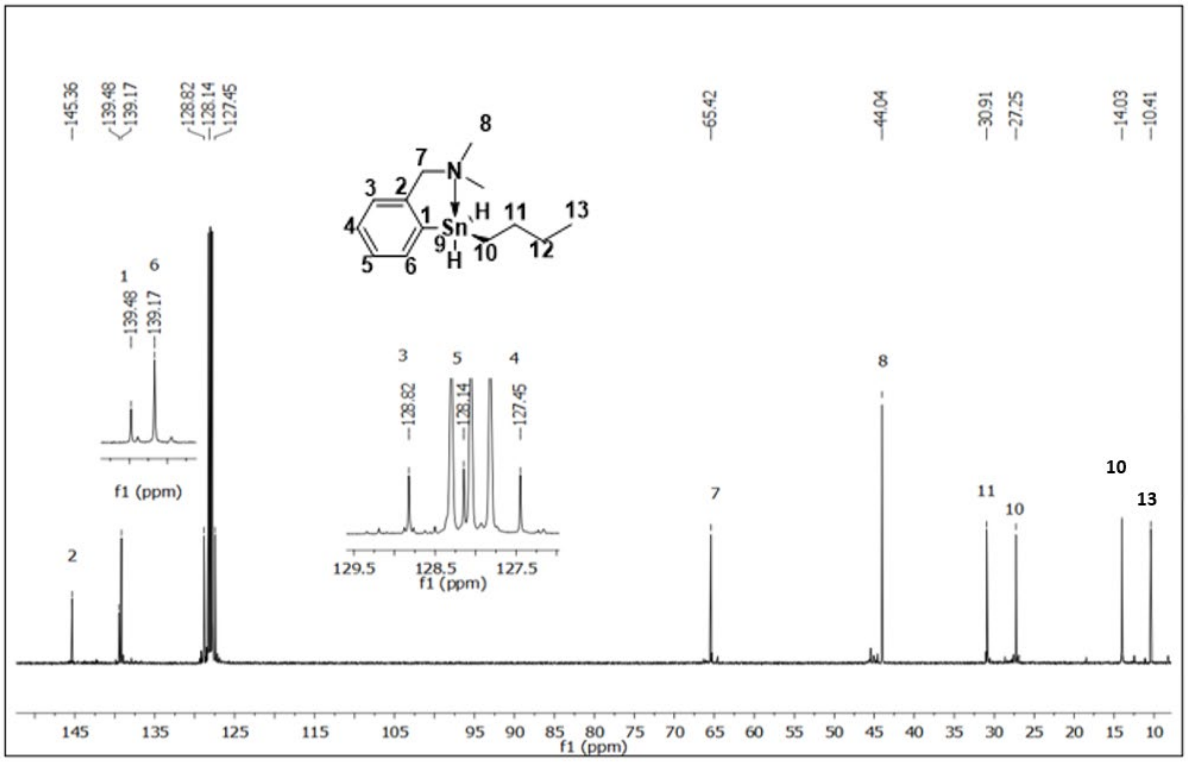

Figure S93. $^{13}C\{^{1}H\}$ NMR spectrum of **32** in C_6D_6

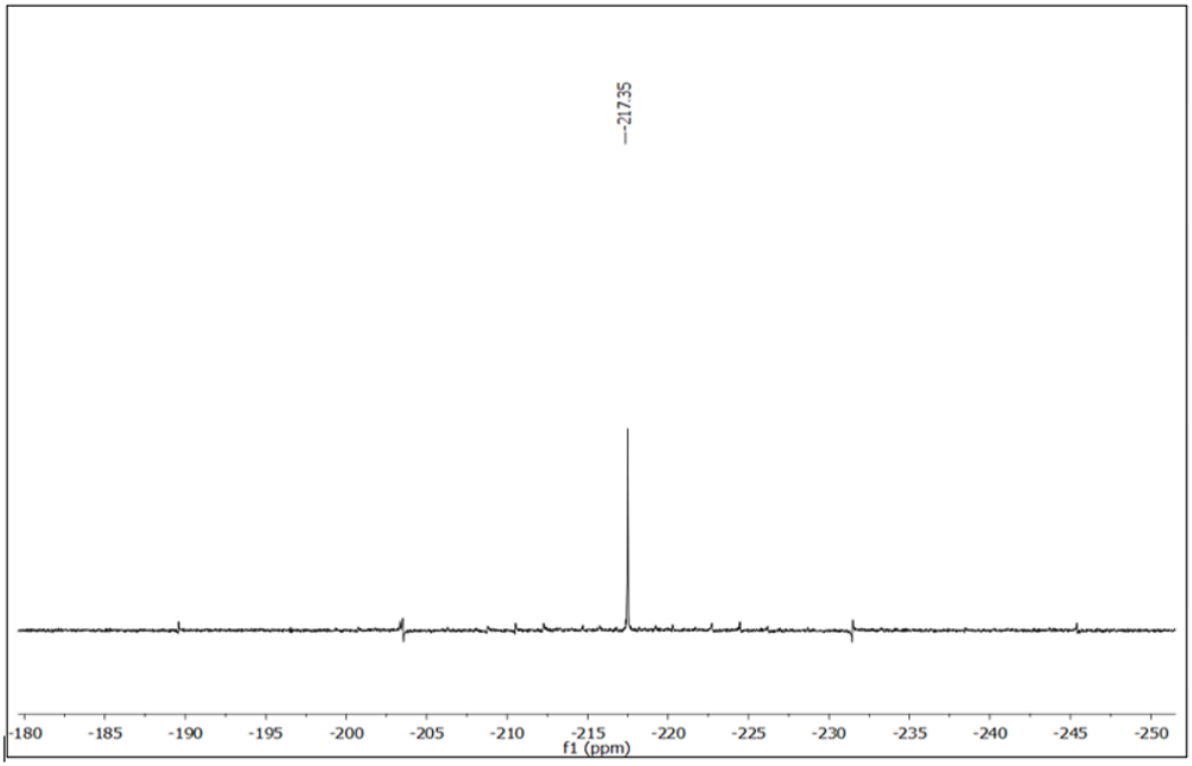

Figure S94. $^{119}Sn\{^{1}H\}$ NMR spectrum of **32** in C_6D_6

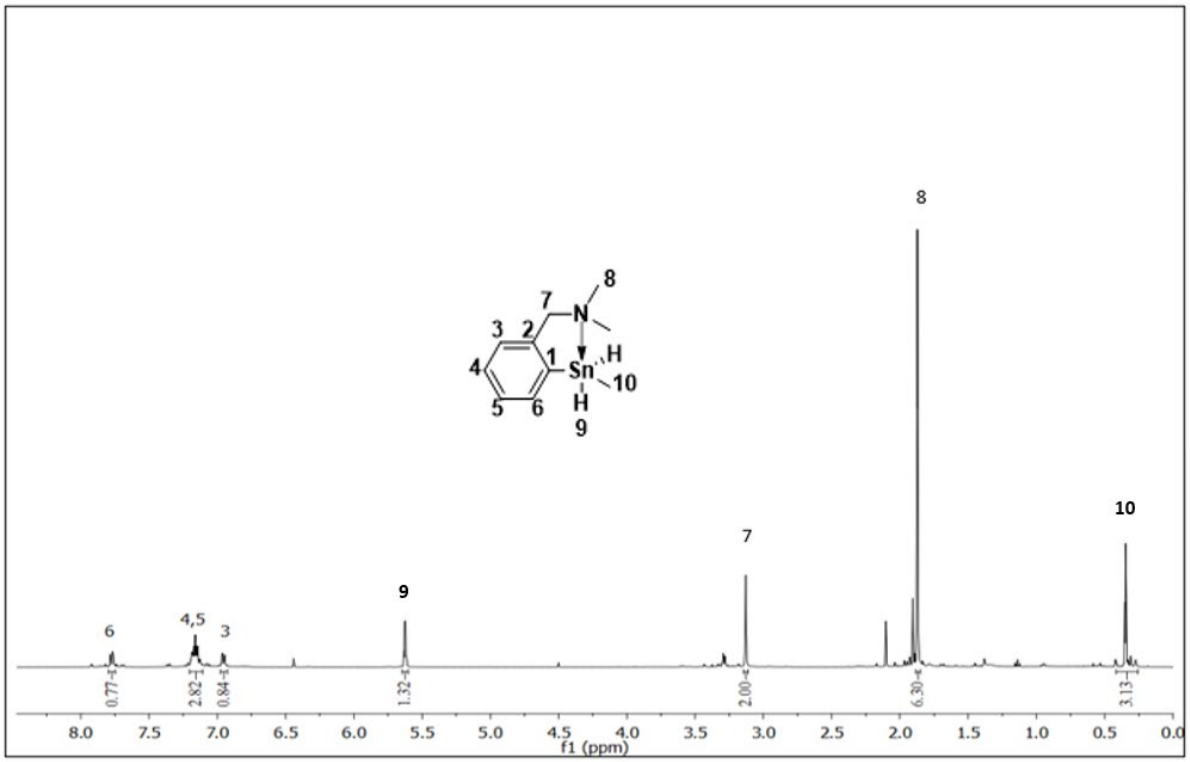

Figure S95. ^{1}H NMR spectrum of **33** in C_6D_6

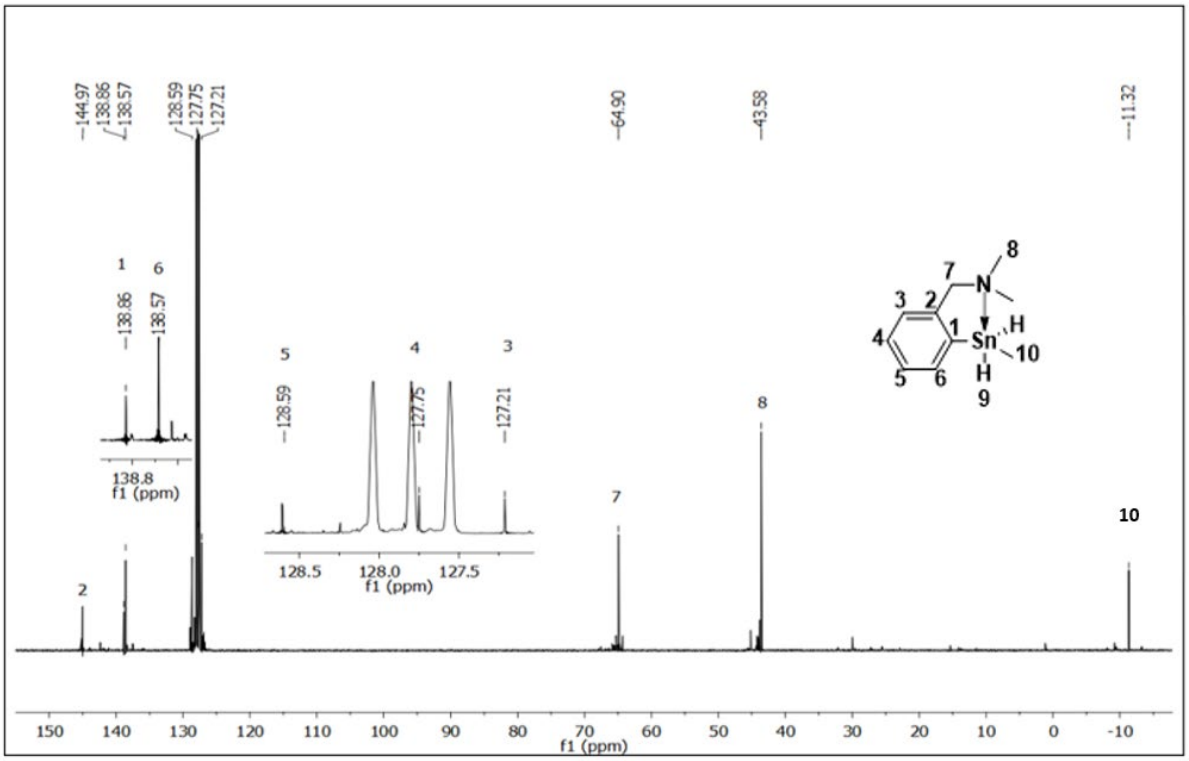

Figure S96. $^{13}C\{^{1}H\}$ NMR spectrum of **33** in C_6D_6

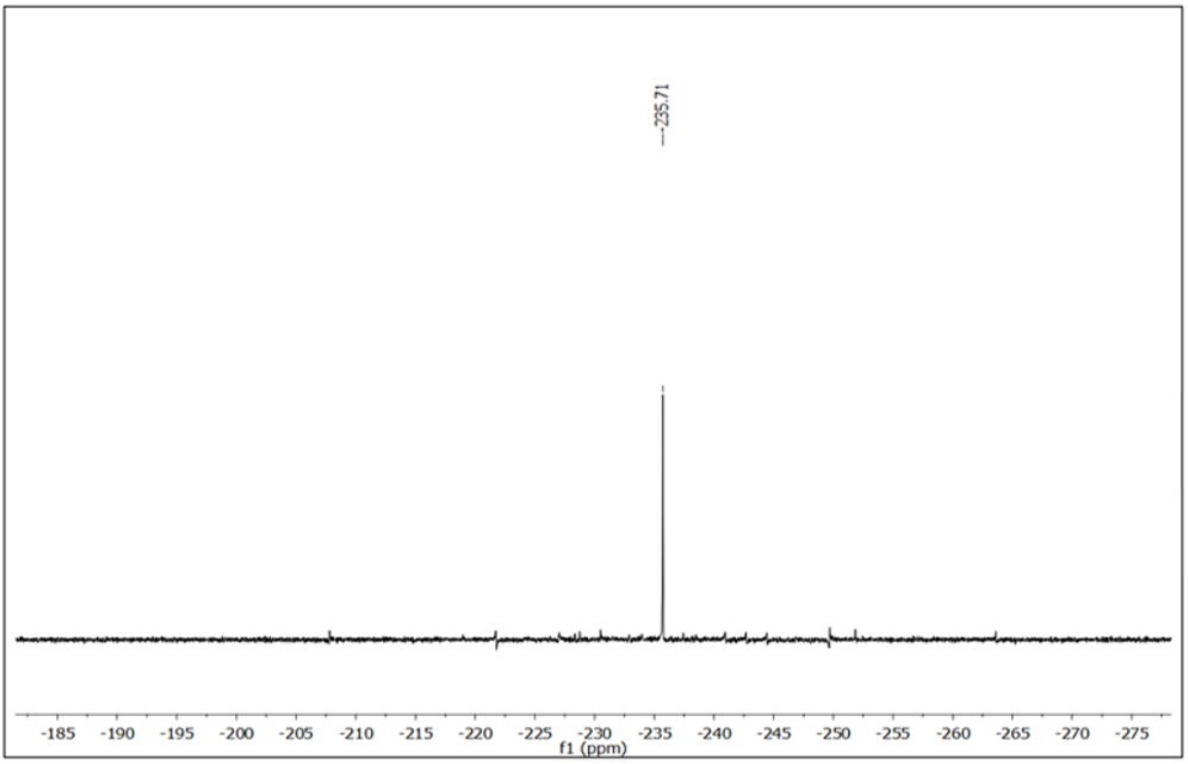

Figure S97. $^{119}Sn\{^{1}H\}$ NMR spectrum of **33** in C_6D_6

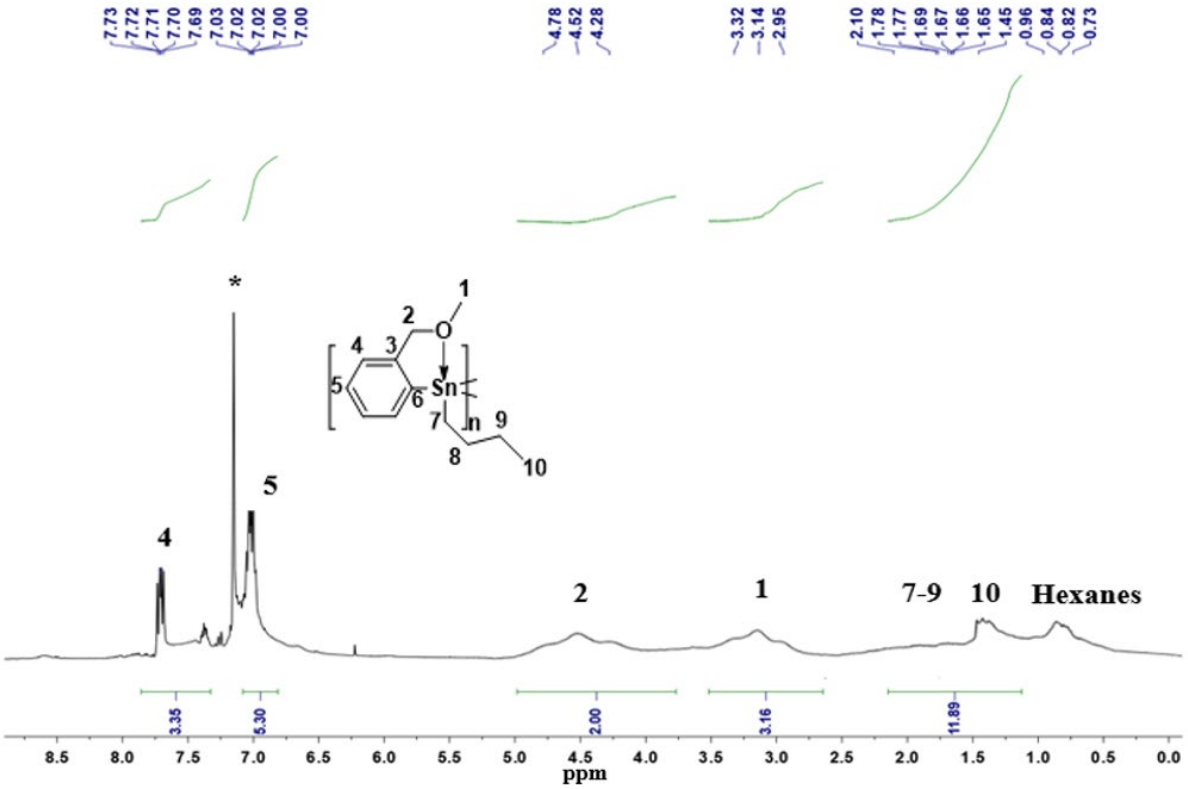

Figure S98. ^{1}H NMR spectrum of **34** in C_6D_6

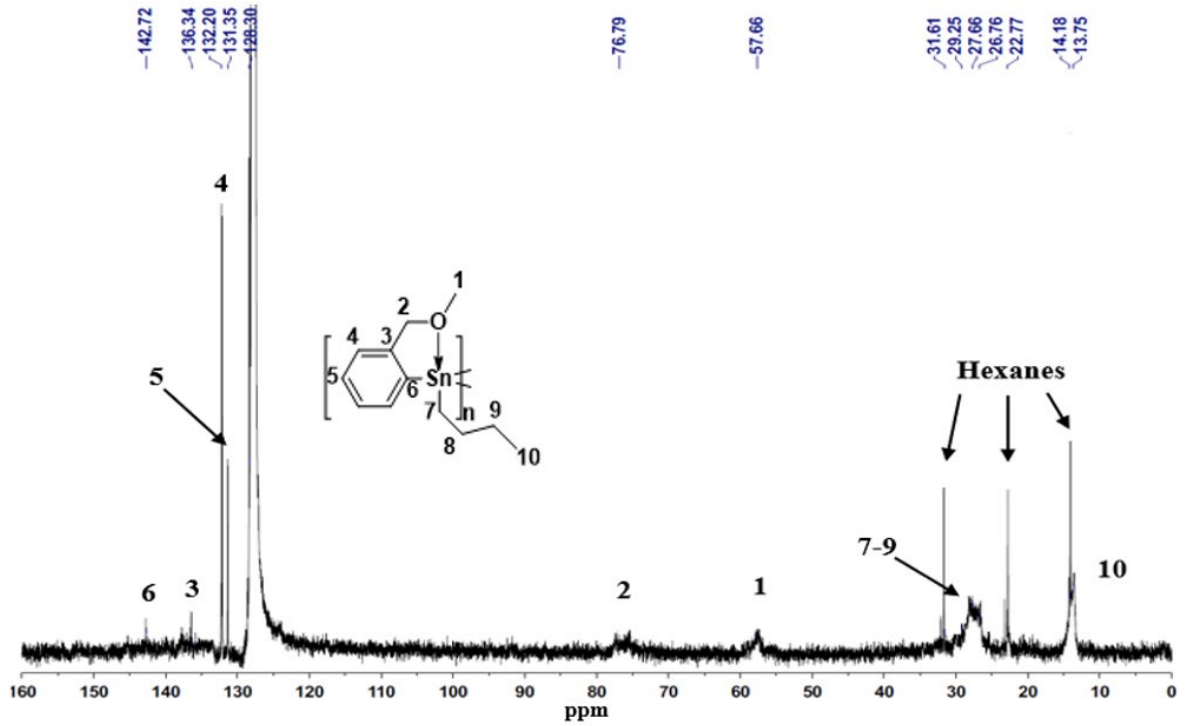

Figure S99. $^{13}C\{^{1}H\}$ NMR spectrum of **34** in C_6D_6

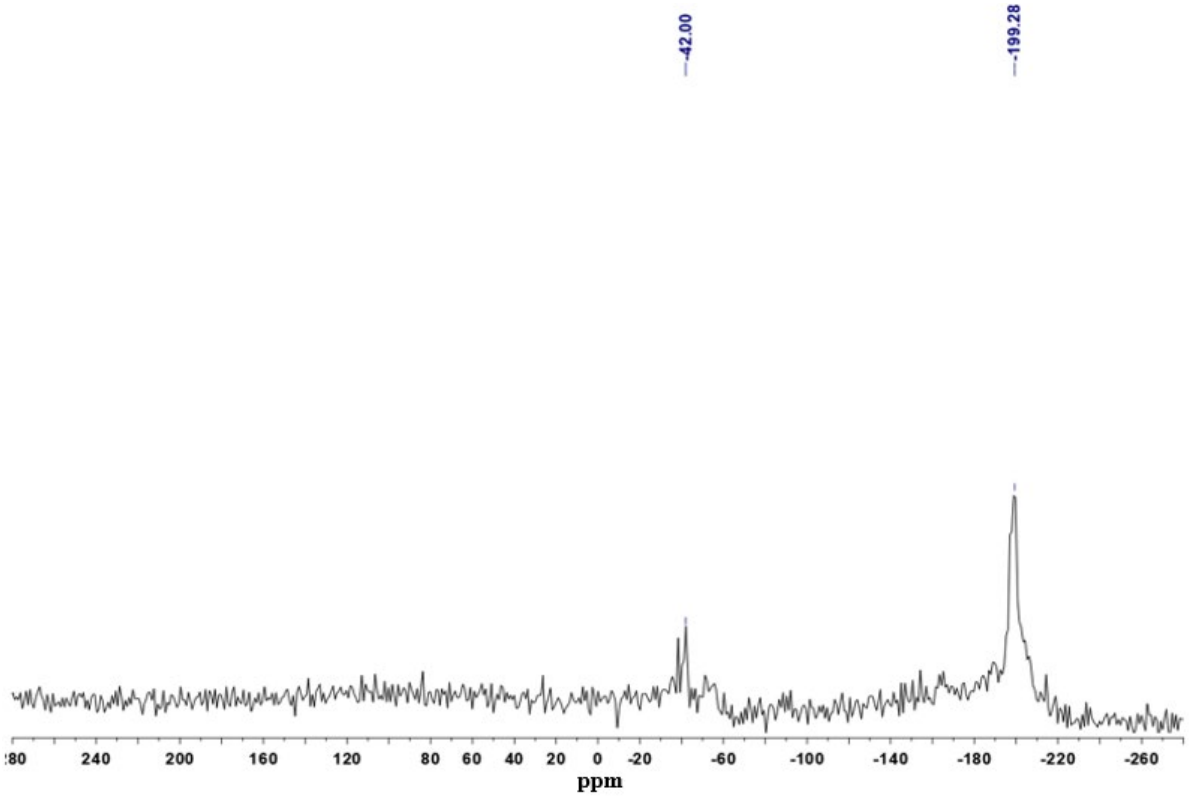

Figure S100. $^{119}Sn\{^{1}H\}$ NMR spectrum of **34** in C_6D_6

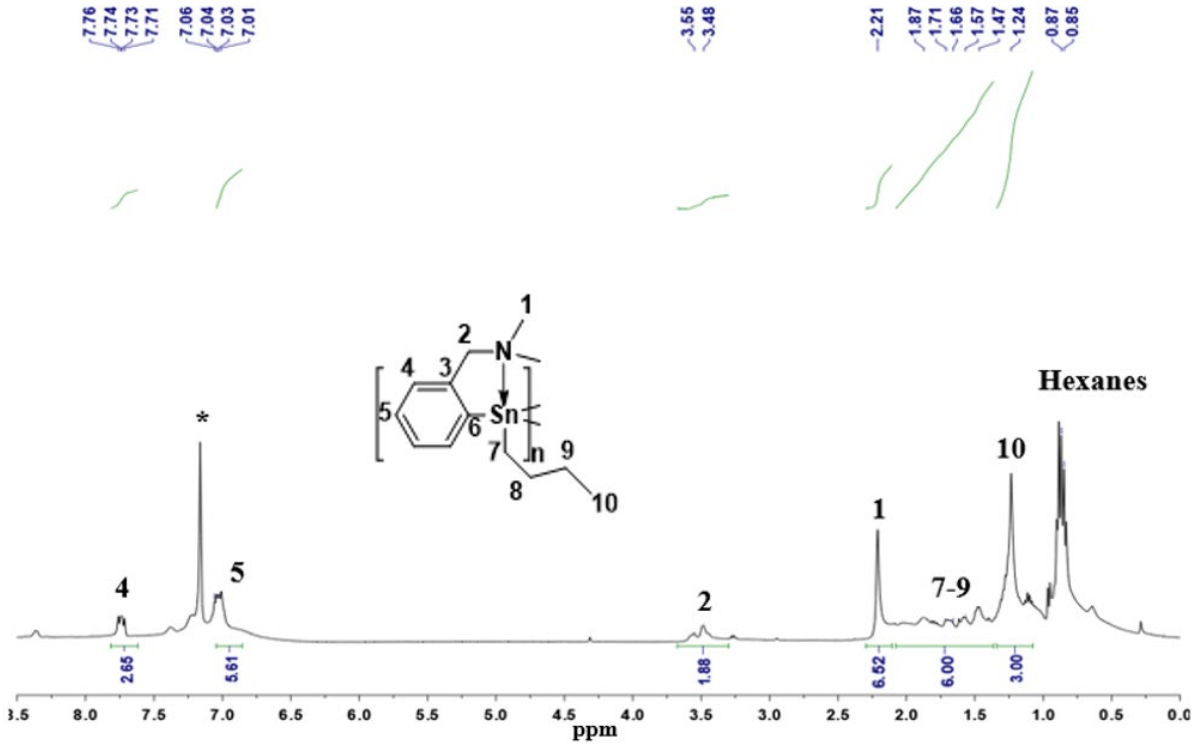

Figure S101. ^{1}H NMR spectrum of **35** in C_6D_6

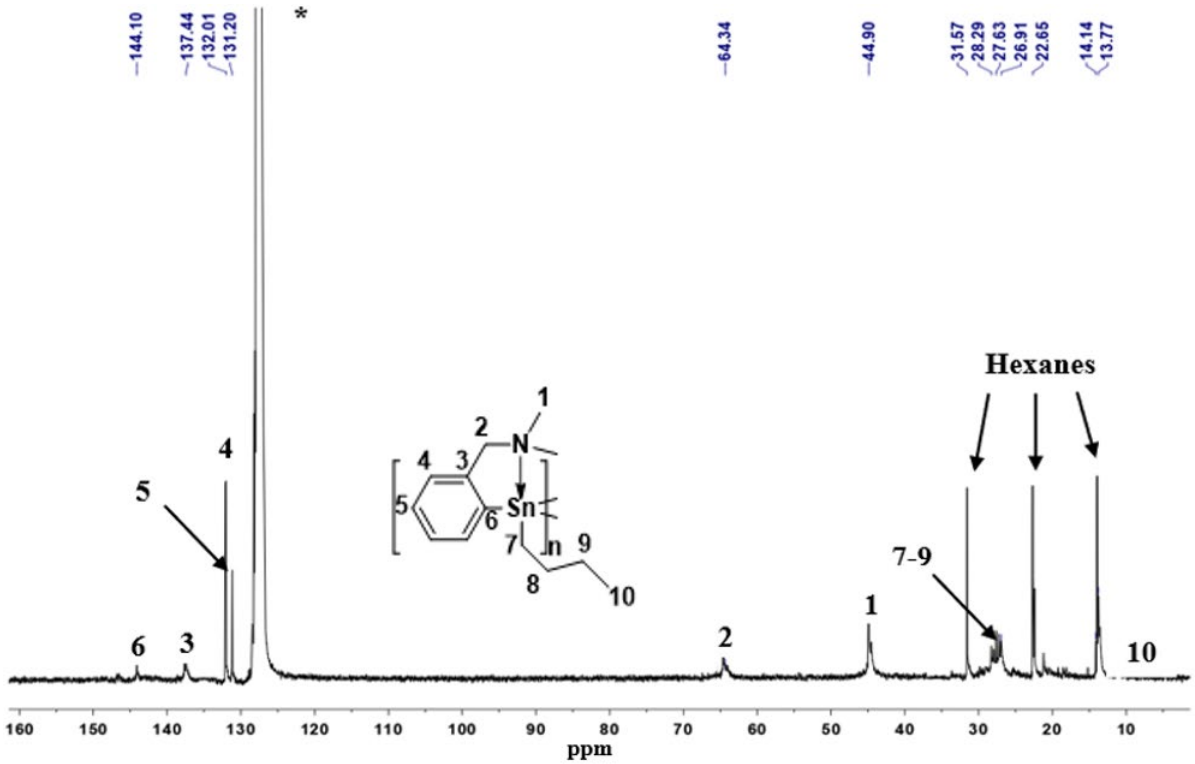

Figure S102. $^{13}C\{^{1}H\}$ NMR spectrum of **35** in C_6D_6

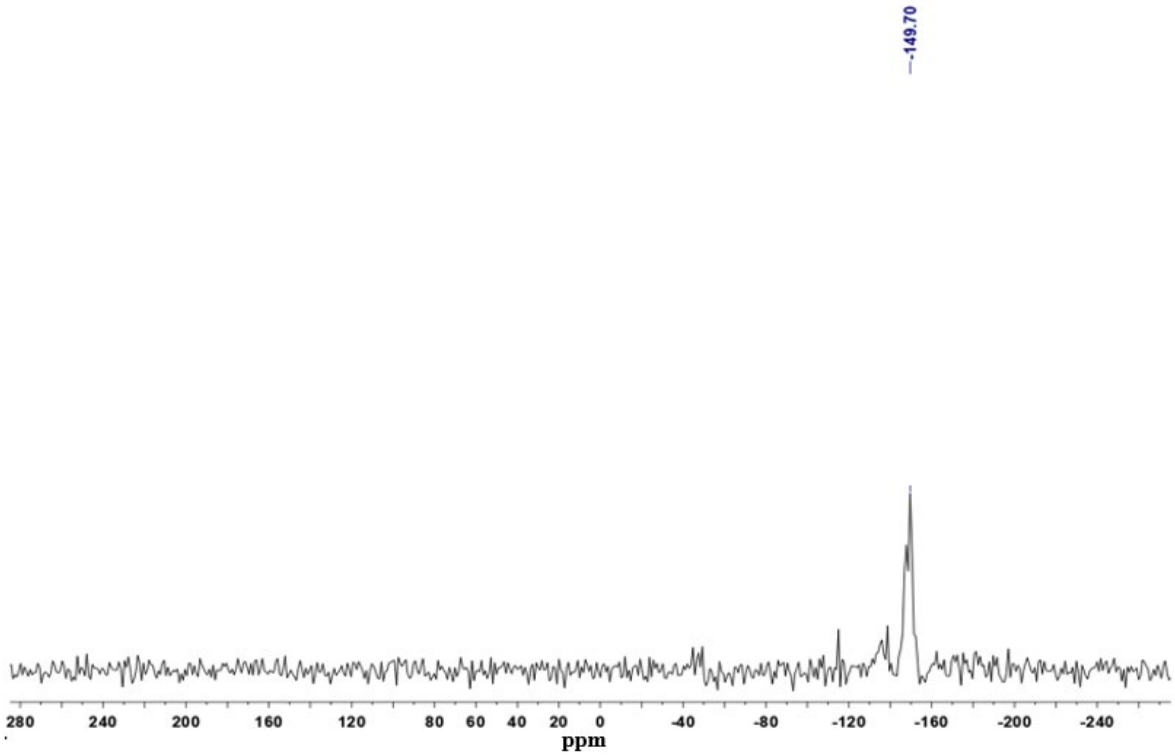

Figure S103. $^{119}Sn\{^{1}H\}$ NMR spectrum of **35** in C_6D_6

CHAPTER 3: DSC Traces

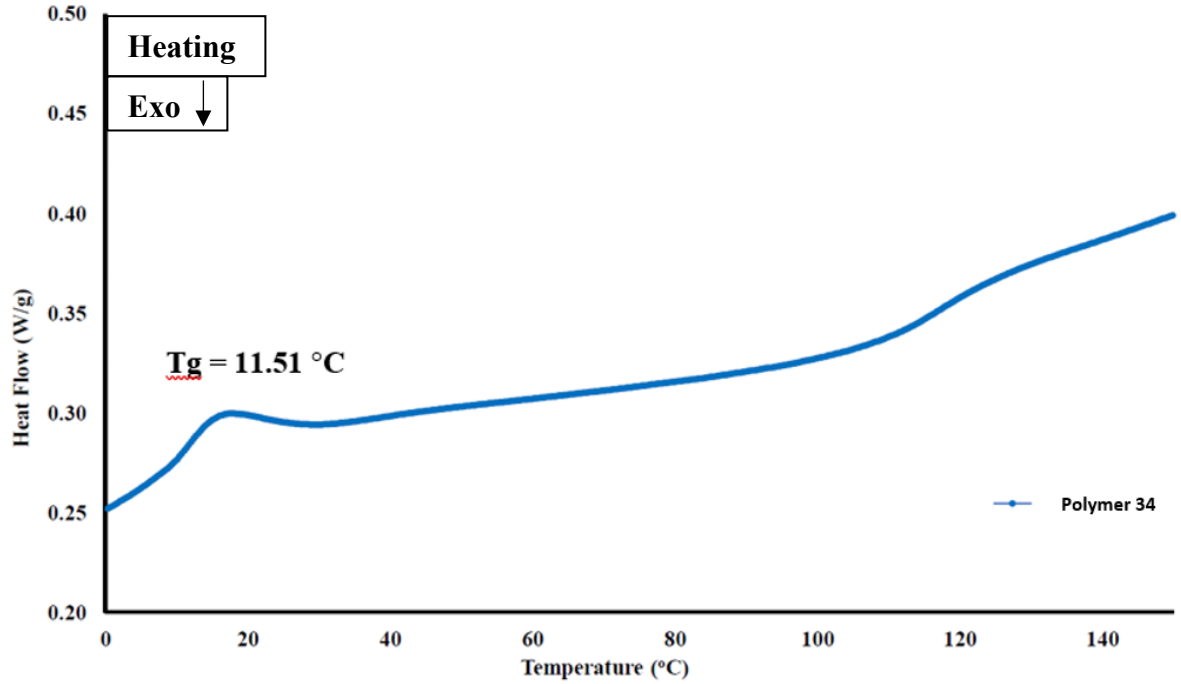

Figure S104. DSC spectra for polymer **34**

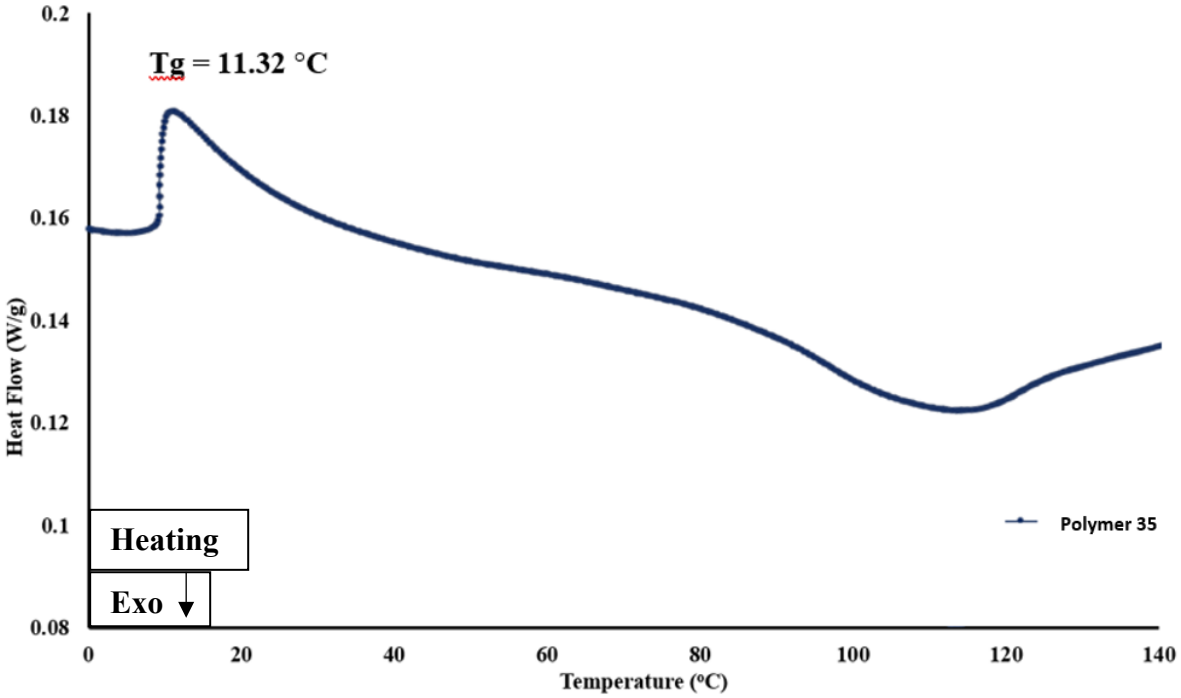

Figure S105. DSC spectra for polymer **35**

REFERENCES

(1) Koch, R.; Bruhn, T.; Weidenbruch, M. Theoretical Group 14 Chemistry.4. Cyclotriplumbanes : Relativistic and Substituents Effects. *J. Chem. Theory Comput.* **2005**, *1*, 1298–1303.

(2) Schoeller, W. W.; Sundermann, A.; Reiher, M.; Rozhenko, A. On the Bonding Properties of Diphosphanylmethanide Complexes with the Group-14 Elements Silicon, Germanium, Tin, and Lead in Their Divalent Oxidation States. *Eur. J. Inorg. Chem.* **1999**, *7*, 1155–1159.

(3) Bochkarev, L. N.; Begantsova, Y. E.; Shcherbakov, V. I.; Stolyarova, N. E.; Grigorieva, I. K.; Malysheva, I. P.; Basova, G. V; Bochkarev, A. L.; Barinova, Y. P.; Fukin, G. K.; et al. Synthesis and Some Properties of 14 Group Element-Containing Alkylidene Complexes of Molybdenum and Tungsten. *J. Organomet. Chem.* **2005**, *690*, 5720–5727.

(4) Giju, K. T.; Proft, F. De; Geerlings, P. Comprehensive Study of Density Functional Theory Based Properties for Group 14 Atoms and Functional Groups, - XY3 (X) C, Si, Ge, Sn, Pb, Element 114; (CH_3 , H, F, Cl, Br, I, At). *J. Phys. Chem. A.* **2005**, *3*, 2925–2936.

(5) Lidia, Ł.; Jakubowski, A. History of Semiconductors. *J. Telecommun. Inf. Technol.* **2010**, *1*, 1–9.

(6) DeRosa, T. F. Advances in Polymer Chemistry and Methods Reported in Recent US Patents. *Adv. Polym. Chem.* **2008**, *3*, 5361–5362.

(7) Inzelt, G. Conducting Polymers : Past , Present , Future. *J. Electrochem. Sci. Eng.* **2018**, *8*, 3–37.

(8) N, T.; S, H. Direct Synthesis Of Conducting Polymers From Simple Monomers. *Prog. Polym. Sci.* **1995**, *20*, 155–183.

(9) Qin, J.; Lin, F.; Hubble, D.; Wang, Y.; Li, Y.; Murphy, I. A.; Jang, S. H.; Yang, J.; Jen, A. K. Y. Tuning Self-Healing Properties of Stiff, Ion-Conductive Polymers. *J. Mater.*

Chem. A **2019**, *7*, 6773–6783.

(10) Lee, S. L.; Chang, C. J. Recent Developments about Conductive Polymer Based Composite Photocatalysts. *Polymers.* **2019**, *11*, 1–21.

(11) Sawatzky, A.; Zaanen, J. Band Gaps and Electronic Structure of Transition-Metal Compounds. *Am. Phys. Soc.* **1985**, *55*, 418–421.

(12) Vogl, P.; Hjalmarson, H. P.; Dow, J. D. A Semi-Empirical Tight-Binding Theory of the Electronic Structure of Semiconductors. *J. Phys. Chem. Solids* **1983**, *44*, 365–378.

(13) Munguia, T.; Pavel, I. S.; Kapoor, R. N.; Cervantes-Lee, F.; Párkányi, L.; Pannell, K. H. Lewis Acidity of Group 14 Elements toward Intramolecular Sulfur in Ortho-Aryl-Thioanisoles. *Can. J. Chem.* **2003**, *81*, 1388–1397.

(14) Choffat, F.; Wolfer, P.; Smith, P.; Caseri, W. Light-Stability of Poly(Dialkyl)Stannanes. *Macromol. Mater. Eng.* **2010**, *295*, 210–221.

(15) Imori, T.; Lu, V.; Cai, H.; Tilley, T. D. Metal-Catalyzed Dehydropolymerization of Secondary Stannanes to High Molecular Weight Polystannanes. *J. Am. Chem. Soc.* **1995**, *117*, 9931–9940.

(16) Bridgeman, A. J.; Nielsen, N. A. Multiple Bonding in Homonuclear Group 13 Ethene Analogues. *Inorg. Chim. Acta* **2000**, *303*, 107–115.

(17) Imori, T.; Lu, V.; Cai, H.; Tilley, T. D. Metal-Catalyzed Dehydropolymerization of Secondary Stannanes to High Molecular Weight Polystannanes. *J. Am. Chem. Soc.* **1995**, *117*, 9931–9940.

(18) Deacon, P. R.; Devylder, N.; Hill, M. S.; Mahon, M. F.; Molloy, K. C.; Price, G. J. Organotin Compounds Bearing Mesogenic Sidechains: Synthesis, X-Ray Structures and Polymerisation Chemistry. *J. Organomet. Chem.* **2003**, *687*, 46–56.

(19) Ciccioli, A.; Gigli, G.; Meloni, G. The Si-Sn Chemical Bond: An Integrated Thermochemical and Quantum Mechanical Study of the SiSn Diatomic Molecule and Small Si-Sn Clusters. *Chem. Eur. J.* **2009**, *15*, 9543–9560.

(20) Harrypersad, S.; Foucher, D. Alternating Polystannanes : Syntheses and Properties. *Chem. Commun.* **2015**, *51*, 7120–7123.

(21) Sita, L. R. A New Strategy for the Synthesis of Homologously Pure Linear Polystannane Oligomers. *Organometallics* **1992**, *11*, 1442–1444.

(22) Lu, V. Y.; Tilley, T. D. Poly(Diaryl)Stannanes: Influence of Substituents on the σ-Σ* Transition Energy. *Macromolecules* **2000**, *33*, 2403–2412.

(23) Choffat, F.; Käser, S.; Wolfer, P.; Schmid, D.; Mezzenga, R.; Smith, P.; Caseri, W. Synthesis and Characterization of Linear Poly(Dialkyl)Stannanes. *Macromolecules* **2007**, *40*, 7878–7889.

(24) Choffat, F.; Smith, P.; Caseri, W. Facile Synthesis of Linear Poly(Dibutyl)Stannane. *J. Mater. Chem.* **2005**, *15*, 1789–1792.

(25) Trummer, M.; Nauser, T.; Lechner, M. L.; Uhlig, F.; Caseri, W. Stability of Polystannanes towards Light. *Polym. Degrad. Stab.* **2011**, *96*, 1841–1846.

(26) Zhdankin, V. V. Chemistry of Hypervalent Compounds. *J. Am. Chem. Soc.* **1999**, *121*, 6971–6971.

(27) Gaspar, P. P. The Chemistry of Organic Germanium, Tin and Lead Compounds, Volume 2. Parts 1−2. *J. Am. Chem. Soc.* **2003**, *125*, 13620–13622.

(28) Pimentel, G. C. The Bonding of Trihalide and Bifluoride Ions by the Molecular Orbital Method. *J. Chem. Phys.* **1951**, *19*, 446–448.

(29) R. Hulme. The Crystal and Molecular Structure of Chloro(Trimethyl)Pyridinetin(V). *J. Chem. Soc.* **1963**, *287*, 1524–1527.

(30) Voronkov, M. G.; Trofimova, O. M.; Bolgova, Y. I.; Chernov, N. F. Hypervalent Silicon-Containing Organosilicon Derivatives of Nitrogen Heterocycles. *Russ. Chem. Rev.* **2007**, *76*, 825–845.

(31) Pukhnarevich, V. B.; Voronkov, M. G.; Kopylova, L. I. Dehydrocondensation of Organylsilanes Giving Si–Si Bonds. *Russ. Chem. Rev.* **2000**, *69*, 137–151.

(32) Reed, A. E.; Ragué Schleyer, P. Von. Chemical Bonding in Hypervalent Molecules. The Dominance of Ionic Bonding and Negative Hyperconjugation over d-Orbital Participation. *J. Am. Chem. Soc.* **1990**, *112*, 1434–1445.

(33) Ciccioli, A.; Gigli, G. Study of the Fundamental Units of Novel Semiconductor Materials: Structures, Energetics, and Thermodynamics of the Ge-Sn and Si-Ge-Sn Molecular Systems. *J. Phys. Chem. A* **2012**, *116*, 7107–7122.

(34) Molina, J.; Dobado, J. A. The Three-Center-Four-Electron (3c-4e$^-$) Bond Nature Revisited. An Atoms-in-Molecules Theory (AIM) and ELF Study. *Theor. Chem. Acc.* **2001**, *105*, 328–337.

(35) Cheung, Y. S.; Ng, C. Y.; Chiu, S. W.; Li, W. K. Application of Three-Center-Four-Electron Bonding for Structural and Stability Predictions of Main Group Hypervalent Molecules: The Fulfillment of Octet Shell Rule. *J. Mol. Struct.* **2003**, *623*, 1–10.

(36) Sun, X. The Three-Center, Four-Electron Bond in Hexacoordinated AB6-Type Main Group Molecules: An Alternative Model of Bonding without d-Orbital Participation in the Central Atom. *Chem. Educ.* **2002**, *7*, 261–264.

(37) Harrod, J. F.; Mu, Y.; Samuel, E. Catalytic Dehydrocoupling: A General Method for the Formation of Element-Element Bonds. *Polyhedron* **1991**, *10*, 1239–1245.

(38) Vidal, F.; Jäkle, F. Functional Polymeric Materials Based on Main-Group Elements. *Angew. Chemie. Int. Ed.* **2019**, *58*, 5846–5870.

(39) Choffat, F.; Buchmüller, Y.; Mensing, C.; Smith, P.; Caseri, W. Poly(Di(ω-Alkylphenyl))Stannanes. *J. Inorg. Organomet. Polym.* **2009**, *19*, 166–175.

(40) Pau, J.; Lough, A. J.; Wylie, R. S.; Gossage, R. A.; Foucher, D. A. Proof of Concept Studies Directed Towards Designed Molecular Wires: Property-Driven Synthesis of Air and Moisture-Stable Polystannanes. *Chem. Eur. J.* **2017**, *23*, 14367–14374.

(41) S., K. F. Organic Derivatives of Silicon. Part XXX. *J. Kyushu Dent. Soc.* **1978**, *32*, 2291–2297.

(42) Trefonas, P.; Djurovich, P. I.; Zhang, X. H.; West, R.; Miller, R. D.; Hofer, D. Organosilane High Polymers: Synthesis of Formable Homopolymers. *J. Polym. Sci. Polym. Lett. Ed.* **1983**, *21*, 819–822.

(43) Devylder, N.; Hill, M.; Molloy, K. C.; Price, G. J. Wurtz Synthesis of High Molecular Weight Poly(Dibutylstannane). *Chem. Commun.* **1996**, *6*, 711–712.

(44) Trummer, M.; Zemp, J.; Sax, C.; Smith, P.; Caseri, W. Reaction Products of Dichlorodiorganostannanes with Sodium in Liquid Ammonia: In-Situ Investigations with ^{119}Sn NMR Spectroscopy and Usage as Intermediates for the Synthesis of Tetraorganostannanes. *J. Organomet. Chem.* **2011**, *696*, 3041–3049.

(45) Trefonas, P.; Damewood, J. R.; West, R.; Miller, R. D. Organosilane High Polymers: Thermochromic Behavior In Solution. *Organometallics* **1985**, *4*, 1318–1319.

(46) Harrah, L. A.; Zeigler, J. M. Electronic Spectra of Polysilanes. *Macromolecules* **1987**, *20*, 601–608.

(47) Fujino, M.; Hisaki, T.; Fujiki, M.; Matsumoto, N. Preparation and Characterization of a Novel Organopolysilane. (3,3,3-Trifluoropropyl)Methylpolysilane. *Macromolecules* **1992**, *25*, 1079–1083.

(48) Johnson, P. S.; Huang, C.; Kim, M.; Safron, N. S.; Arnold, M. S.; Wong, B. M.; Gopalan, P.; Himpsel, F. J. Orientation of a Monolayer of Dipolar Molecules on Graphene from X-ray Absorption Spectroscopy. *Langmuir* **2014**, *30*, 2559–2565.

(49) Liao, M. S.; Scheiner, S. Electronic Structure and Bonding in Metal Porphyrins, Metal = Fe, Co, Ni, Cu, Zn. *J. Chem. Phys.* **2002**, *117*, 205–219.

(50) Merino, E.; Ribagorda, M. Control over Molecular Motion Using the Cis-Trans Photoisomerization of the Azo Group. *Beilstein J. Org. Chem.* **2012**, *8*, 1071–1090.

(51) Natansohn, A.; Rochon, P. Photoinduced Motions in Azo-Containing Polymers. *Chem. Rev.* **2002**, *102*, 4139–4175.

(52) Diau, E. W. G. A New Trans-to-Cis Photoisomerization Mechanism of Azobenzene on

the S1(n,Π*) Surface. *J. Phys. Chem. A* **2004**, *108*, 950–956.

(53) Riul, A.; Dos Santos, D. S.; Wohnrath, K.; Di Tommazo, R.; Carvalho, A. C. P. L. F.; Fonseca, F. J.; Oliveira, O. N.; Taylor, D. M.; Mattoso, L. H. C. Artificial Taste Sensor: Efficient Combination of Sensors Made from Langmuir-Blodgett Films of Conducting Polymers and a Ruthenium Complex and Self-Assembled Films of an Azobenzene-Containing Polymer. *Langmuir* **2002**, *18*, 239–245.

(54) Wardell, J. L.; Wigzell, J. M. Sulphur-Substituted Organotin Compounds. Part 8. Preparation and Reactions of 3-(*p*-Tolylthio)Propyl- and 4-(*p*-Tolylthio)Butyl-Triphenyltin. Interactions with Tetracyanoethylene. *Dalton. Trans.* **1982**, *12*, 2321–2326.

(55) Yoshihiro Yoshida; Sakakura, Y.; Aso, N.; Okada, S.; Tanabe, Y. Practical and Efficient Methods for Sulfonylation of Alcohols Using Ts(Ms)Cl/Et_3N and Catalytic Me_3NHCl Combined Base: Promising Alternative to Traditional Pyridine. *Tetrahedron* **1999**, *55*, 2183–2192.

(56) Munguia, T.; López-Cardoso, M.; Cervantes-Lee, F.; Pannell, K. H. Intramolecular Chalcogen-Tin Interactions in (*o*-MeE-C_6H_4)$CH_2SnPh_{3-n}Cl_n$ (E = S, O; n = 0, 1, 2), Characterized by X-Ray Diffraction and ^{119}Sn Solution and Solid-State NMR. *Inorg. Chem.* **2007**, *46*, 1305–1314.

(57) Khan, A.; Foucher, D. Hypercoordinate Compounds of the Group 14 Elements Containing K^n-*C,N*-, *C,O*-, *C,S*- and *C,P*-Ligands. *Coord. Chem. Rev.* **2016**, *312*, 41–66.

(58) Khan, A.; Komejan, S.; Patel, A.; Lombardi, C.; Lough, A. J.; Foucher, D. A. Reduction of *C,O*-Chelated Organotin(IV) Dichlorides and Dihydrides Leading to Protected Polystannanes. *J. Organomet. Chem.* **2015**, *776*, 180–191.

(59) Miles, D.; Burrow, T.; Lough, A.; Foucher, D. Wurtz Coupling of Perfluorinated Dichlorostannanes. *J. Inorg. Organomet. Polym. Mater.* **2010**, *20*, 544–553.

(60) Neale, N. R.; Tilley, T. D. A New Mechanism for Metal-Catalyzed Stannane

Dehydrocoupling Based on α-H-Elimination in a Hafnium Hydrostannyl Complex. *J. Am. Chem. Soc.* **2002**, *124*, 3802–3803.

(61) Champness, N. R. Coordinating Ability of Anions and Solvents towards Transition Metals and Lanthanides. *Dalt. Trans.* **2011**, *40*, 10742–10750.

(62) De Haas, M. P.; Choffat, F.; Caseri, W.; Smith, P.; Warman, J. M. Charge Mobility in the Room-Temperature Liquid-Crystalline Semiconductor Poly(Di-*n*-Butylstannane). *Adv. Mater.* **2006**, *18*, 44–47.

(63) Chuit, C.; Corriu, R. J. P.; Reye, C.; Young, J. C. Reactivity of Penta- and Hexacoordinate Silicon Compounds and Their Role as Reaction Intermediates. *Chem. Rev.* **1993**, *93*, 1371–1448.

(64) Chimicaacta, I.; Sciences, P.; Ponds, W. Tin-^{119}NMR Studies on Diorganoyltin(IV) Dihalides and Triorganotin(IV)Halides; Formation and Stereochemistry of Adducts. *Inorg. Chim. Acta* **1988**, *148*, 31–36.

(65) Van Koten, G. Crystal and Molecular Structure of *C,N*-[2-[(Dimethylamino)Methyl]Phenyl]Diphenyltin Bromide. *J. Organomet. Chem.,* **1976**, *118*, 183–189.

(66) Mahmud, T.; Iqbal, J.; Imran, M.; Mckee, V. Synthesis and Spectroscopic Studies of 2-Bromo *N, N*-Dimethylbenzylamine and Its Complexes with $Mo(CO)_6$ and $W(CO)_6$. *J. Appl. Sci.* **2007**, *7*, 1347–1350.

(67) Du, T.; Ma, S.; Pei, X.; Wang, S.; Zhou, F. Bio-Inspired Design and Fabrication of Micro/Nano-Brush Dual Structural Surfaces for Switchable Oil Adhesion and Antifouling. *Small*, **2017**, *13*, 1–10.

(68) Khan, A.; Pau, J.; Loungxay, J.; Magobenny, T.; Wylie, R. S.; Lough, A. J.; Foucher, D. Hypercoordinated Organotin (IV) Compounds Containing *C,O*- and *C,N*- Chelating Ligands : Synthesis , Characterisation , DFT Studies and Polymerization Behaviour. *J. Organomet. Chem.* **2019**, *900*, 120910.

(69) Pau, J.; D'Amaral, G. M.; Lough, A. J.; Wylie, R. S.; Foucher, D. A. Synthesis and Characterization of Readily Modified Poly(Aryl)(Alkoxy)Stannanes by Use of Hypercoordinated Sn Monomers. *Chem. Eur. J.* **2018**, *24*, 18762–18771.

(70) Reich, H. J.; Goldenberg, W. S.; Sanders, A. W.; Jantzi, K. L.; Tzschucke, C. C. Amine- and Ether-Chelated Aryllithium Reagents - Structure and Dynamics. *J. Am. Chem. Soc.* **2003**, *125*, 3509–3521.